MULTIDISCIPLINARY INSIGHTS: GEOTHERMAL WELLS, PRESERVATION, ENGINEERING, AND CHEMICAL PROCESSES

EDITOR
Assoc. Prof. Merivan Şaşmaz

İKSAD
Publishing House

MULTIDISCIPLINARY INSIGHTS: GEOTHERMAL WELLS, PRESERVATION, ENGINEERING, AND CHEMICAL PROCESSES

EDITOR

Assoc. Prof. Merivan Şaşmaz

AUTHORS

Betül TEMİZSOY

Büşra Selenay ÖNAL

Cem BALTACIOĞLU

Emrah ASLAN

Hasan DİLBAS

Hasan Üstün BAŞARAN

İbrahim Fadıl SOYKÖK

Kaan KOÇALİ

Mehmet OZCELIK

M. Maria SUDARWANI

Murat KIRANŞAN

Oguzhan DER

Yıldırım ÖZÜPAK

(The Licence Number of Publicator: 2014/31220)
TURKEY TR: +90 342 606 06 75
USA: +1 631 685 0 853
E mail: iksadyayinevi@gmail.com
www.iksadyayinevi.com

It is responsibility of the author to abide by the publishing ethics rules.
Iksad Publications – 2023©

ISBN: 978-625-367-156-3
Cover Design: İbrahim KAYA
JUNE / 2023
Ankara / Turkey
Size = 16x24 cm

CONTENTS

PREFACE

Within this compilation, esteemed experts have contributed their insights and expertise across nine comprehensive chapters that span various disciplines. Each chapter offers valuable perspectives and thoughtful analysis, representing the diligent work of the authors. The ten chapters in this compendium cover various disciplines and are authored by experts in their respective fields.

In the first chapter, we explore the properties of high-quality geothermal resources. We examine specific examples and potential risks associated with them. The chapter is titled "Investigation of the Risk of Brine Intrusion into Geothermal Boreholes Planned in Didim Plateau (Aydin/Turkiye)."

Moving on to the second chapter, we discuss a case study on the conservation and revitalization of the Ciliwung Riverbank in Manggarai, Jakarta. We explore ways to protect abused natural resources. This chapter is titled "The Conservation and Revitalization of The Ciliwung Riverbank in Manggarai, Jakarta."

In chapter three, we focus on finding efficient and cost-effective simulator options for robot design. We examine their applications and usefulness in this field. The chapter is titled "Simulators In Robot Design and Applications."

Chapters four and five provide an overview of engineering applications and introduce best practices. The topics covered include improving exhaust after-treatment thermal management to reduce emission rates in diesel-driven vehicles and reviewing the abrasive waterjet cutting of polymeric materials.

In chapters six and seven, we delve into research on high-performing materials. We explore the effects of surface treatment and fabric design on the mechanical properties of polymer matrix composites. Additionally, we analyze the setup and analysis of thermophotovoltaic systems using gallium antimonide (Gasb) cells in high temperatures.

Chapters eight and nine discuss chemical processes related to wastewater cleaning and food processing, respectively. We explore the fundamentals and applications of photocatalytic oxidation processes, as well as the use of ultrasound extraction in the food industry.

In chapter ten, prepare to embark on an enlightening journey into the realm of the Fuzzy HD Method, a revolutionary blend of high definition and fuzzy logic that challenges conventional approaches to data analysis, offering new insights into the complex interplay of precision and uncertainty.

The content presented in the aforementioned chapters is the responsibility of the respective authors and does not necessarily reflect the views or opinions of the ISPEC publising house and its editor. The information provided is based on the expertise and research of the authors up to the time of publication. Readers are encouraged to critically evaluate the material and consult additional sources for a comprehensive understanding of the subjects discussed.

Lastly, I would like to express my sincere gratitude to all the authors and the IKSAD publishing house for their invaluable contributions in compiling this insightful compendium. Their diligent work and expertise have brought together a diverse range of disciplines, providing readers with a wealth of knowledge and perspectives. I also extend my appreciation to the readers for their engagement and interest in this book. May this compilation serve as a catalyst for further exploration and scholarly discourse in the respective fields covered. Thank you for your time and dedication to expanding our understanding of these important subjects.

Assoc. Prof. Merivan ŞAŞMAZ

Editor, June 2023

CHAPTER 1

INVESTIGATION OF THE RISK OF BRINE INTRUSION INTO GEOTHERMAL BOREHOLES PLANNED IN DIDIM PLATEAU (AYDIN/TURKIYE)

Assoc. Prof. Dr. Mehmet OZCELIK[1]

[1] Süleyman Demirel University, Faculty of Engineering, Geological Engineering Department, 32260-Isparta, Turkey.e-mail: ozcelikmehmet@sdu.edu.tr
Orcid ID: 0000-0003-4511-1946

PREFACE

The plateau of Didim is located in the coastal zone of the geothermal field of Büyük Menderes on the Aegean Sea. For this reason, the construction of geothermal plants on the plateau is considered reasonable by the operators. However, in regions where a geothermal reservoir is located near the coast, geothermal drilling may result in brine freshwater intrusion. In addition, geothermal reservoirs near the coast are susceptible to saltwater intrusion from seawater. When cold seawater enters a hot geothermal reservoir, the temperature and pressure of the reservoir may decrease. However, overuse of geothermal reservoirs can lead to saltwater intrusion into freshwater regions. When geothermal fluid is withdrawn from the reservoir, the pressure in the reservoir may decrease, causing the water level to drop. This drop in water level can cause saltwater to enter the freshwater region. If the geothermal reservoir is located near a fault or fracture, there is a risk of saltwater intrusion into the freshwater region. High temperature gradients can also lead to saline intrusion. In regions with high temperature gradients, there may be a significant difference in water density between the hot geothermal fluid and the colder freshwater. This density difference can cause the two fluids to segregate, resulting in brine intrusion. Geological, hydrogeological, and geophysical measurements are being conducted in the potential geothermal areas on the Didim Plateau. This chapter aims to draw attention to the investigations that should be carried out in order to prevent the geothermal wells to be drilled in the coastal zone of Didim district from being affected by saltwater intrusion. In this sense, the present investigation aims to provide relevant data on the geothermal potential of Didim district and its surroundings in the westernmost part of the BMG region.

1. INTRODUCTION

Geothermal wells frequently experience brine intrusion. Geothermal resources in coastal areas are immediately impacted by any changes to the interactions between groundwater and seawater, which are the primary sources of energy for these systems (Hussein et al., 2013; Xing et al., 2022). When too much geothermal water is pumped in coastal areas, the saltwater-freshwater interface is disrupted (Motallebian et al., 2019). This triggers saltwater intrusion (Shin and Hwang, 2020). The mechanism of saltwater intrusion consists of vertical uplift and lateral intrusion (Costall et al., 2020). Excessive pumping in coastal areas results in vertical seawater uplift (Sebben et al. 2015; Rustadi et al., 2021). Reductions in groundwater recharge affect

groundwater flow rates and lateral recharge of seawater in the aquifer (Han & Currell, 2018). It may also be triggered by sea level rise due to global climate change. Changes in global sea level, particularly sea level rise, can affect the location of the saltwater-freshwater interface (Corniello et al., 2015; Costall et al., 2020). Simulations of the effects of sea level rise show a change in the saltwater-freshwater interface by up to several hundred meters toward land (Andrés Lloret, 2015).

Salinity may increase considerably as mixed seawater concentration increases, and geothermal water temperature may decrease (Wilopo et al., 2021). On the other hand, a decrease in mixed seawater results in a decrease in geothermal resources. In this case, high geothermal water use may cause seawater intrusion and considerable salinization of the geothermal water (Noorollahi et al., 2015). The water flow has salinized in many geothermal fields. The Geyser geothermal field in northern California is the largest geothermal field in the world and the best known example. The site has faced brine intrusion since the 1960s, which has reduced the productivity of some wells (Yuan et al., 2022). In the Reykjanes geothermal field on the Reykjanes Peninsula in Iceland, brine intrusion into the reservoir occurred because seawater was injected to increase productivity (Bjornsson & Palsson, 2013). The uncontrollable influx of brine has led to a deterioration in the quality of the geothermal fluid. Similarly, the Cerro Prieto geothermal field in Mexico is one of the largest geothermal fields in the world. At this site, brine intrusion occurred, resulting in the replacement of the freshwater aquifer with brine because the geothermal reservoir was over-pumped (González-Ramírez et al., 2019). However, in the Rotokawa geothermal field in New Zealand, brine intrusion occurred due to the hydraulic connection between the geothermal reservoir and the nearby Lake Rotokawa. The disturbance resulted in a degradation of the geothermal fluid quality and made it difficult to extract heat from the reservoir (Fariduddin & Ali, 2018; Karyono & Sulaeman, 2019).

The Büyük Menderes geothermal (BMG) field, one of the largest geothermal fields in Türkiye, is important for power generation (Rabet et al. 2017). 72% of geothermal power plants in Türkiye are located in the BMG field and 27% in the Gediz geothermal field (Aydın et al., 2020). According to the Energy Market Regulatory Authority (EMRA) report, 3.62% of the total electricity generated in Türkiye in November 2021 is provided by geothermal resources. The BMG field extends west to the Aegean Sea, and geothermal

energy is generated throughout the area outside the coastal zone. In order to evaluate the geothermal potential of the Didim Plateau, which is located west of the Büyük Menderes geothermal field, the studies to explore the geothermal resources have been increased. In recent years, geothermal resource exploration studies have been increased to evaluate the geothermal potential on the Didim Plateau. Current research largely focuses on calculating the temperature of geothermal reservoirs, hydrochemical isotopic characteristics of geothermal fields, and the creation of geothermal resources from regional structures. However, little is known about how geothermal resources are created and how geothermal fluids recharge, flow, and discharge. In particular, it is unknown how much seawater recharge contributes to the creation of geothermal resources. The objective of this study is to effectively prevent and control geothermal resources and environmental issues, such as potential mechanisms for replenishing the geothermal water cycle in coastal areas, the potential for salinization of geothermal water, seawater intrusion, and the potential reduction in geothermal water that may be caused by saline water.

2. MATERIALS AND METHODS

The methods used in this study provide clues to situations where brine intrusion from the sea may be a concern and provide tools for evaluating the significance of the problem. Brine inflow is the migration of saltwater into a freshwater aquifer. It occurs when freshwater loading and flow decrease at the interface with seawater. This usually occurs when a coastal aquifer is overpumped or there is insufficient groundwater available. No brine has yet been observed in the Didim Peninsula to infiltrate the nearshore aquifer in response to pumping, but this could become a problem for geothermal water production in coastal areas. Surface morphology, geology, hydrogeology, tectonics, climate, seismicity and geophysical measurements are being conducted in the potential geothermal areas on the Didim Plateau. In particular, AMT and MT are attracting attention as electromagnetic methods of natural or passive origin that use natural magnetotelluric fields in sound (10 Hz–10 kHz for AMT) or normal frequency bands (0.001–1000 Hz for MT) to probe the Earth's electrical conductivity structure.

2.1. Location of the geothermal field - Surface morphology

The study location is situated west of the BMG field in the Didim Peninsula's coastal region (Figure 1). The Didim Peninsula, in turn, extends southward from the Dilek Peninsula and has a very slight slope west of the Söke-Milas Highway. Elevations on this plateau vary between 0 and 240 m. The general slope is about 5%. The general slope is in the direction of WSW, N240°E. The Didim plateau consists of three levels. The high stage at 150-240 m extends in the north of the plateau, the middle stage at an altitude of 90-100 m includes wide plains in the south and the upper stage in the north. The low stage at 30-40 m covers a large area in the form of apartment sloping plains in the south and southwest and is represented by small plains and accumulation cones in the north. The Didim Plateau was formed on lake sediments of Pliocene age, consisting of conglomerate and sandstones in the lower part and limestone in the upper part. At the base of these sediments are the marbles of the Ilbir Mountains in the east.

Figure 1: Study area and selected geothermal fields (modified form https://www.wekeo.eu)

2.2. Geothermal geological conditions

The BMG is a tectonic depression formed in the late Miocene to Pliocene as a result of extensional tectonics and is filled with sediments of marine, fluvial and lacustrine origin. The geothermal field is located within a regional fault system consisting of several normal faults trending northeast to southwest and northwest to southeast (Ozcelik, 2021). The geothermal reservoir is located in fractured and permeable rock formations consisting mainly of altered

andesite, basalts, and tuffs of late Cretaceous to Eocene age. The reservoir is fed by hot water from a deep-seated magmatic source, which is believed to be located at a depth of 5-7 km. The geothermal fluids are produced from production wells with temperatures ranging from 110 to 270 °C, and the fluid chemistry is dominated by sodium chloride and sodium bicarbonate (Ozcelik, 2022a). Overall, the BMG field is a classic example of a geothermal system in an extensional tectonic setting where hot fluids are stored in fractured and permeable rocks within a fault system (Figure 2).

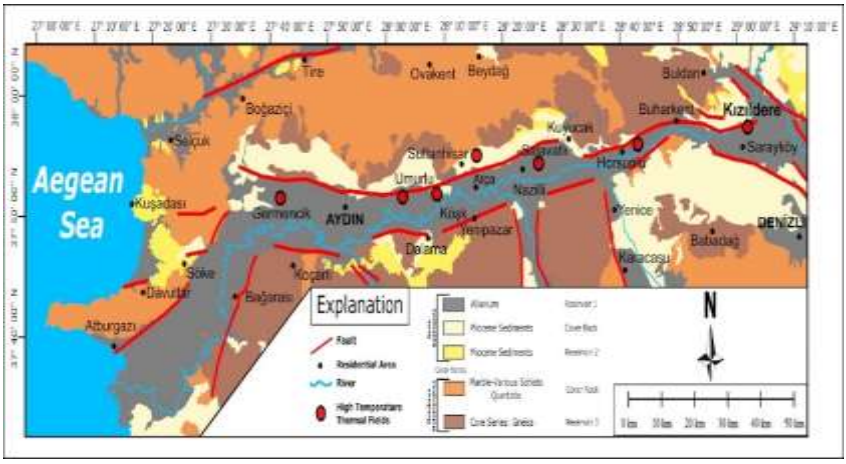

Figure 2: Geological setting of the BMG Field (Ozcelik, 2022b)

2.3. Site geology

Exploration and exploitation of geothermal resources is potentially very costly due to drilling costs. Therefore, the search for geothermal resources often relies on indirect exploration through geological and geophysical surveys that provide a general overview of subsurface conditions. Metamorphic rocks form the impermeable bedrock in Didim district and its surroundings. The metamorphic rocks are overlain by units of conglomerate and sandstones. At the top level, there are Pliocene lacustrine deposits consisting of limestone (Figure 3). The marbles alternating in the metamorphic rocks have karstic characteristics and are also considered a reservoir of geothermal water.

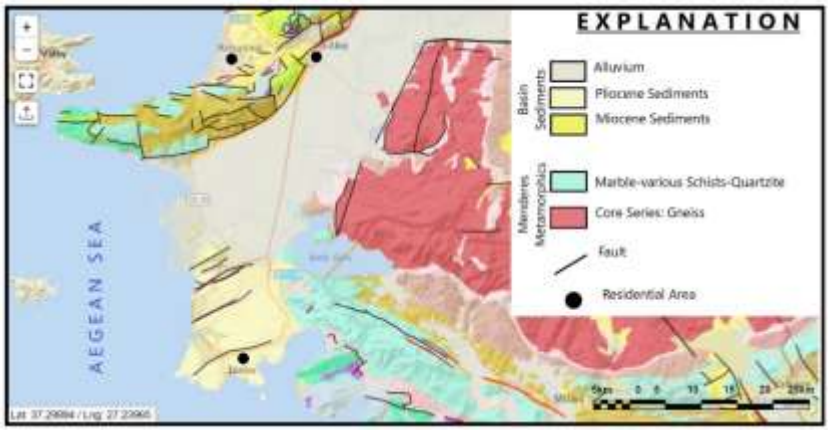

Figure 3: Geological map of the research area

2.4. Hydrogeology

The marbles of the Menderes Massif of Mesozoic age are karst aquifers for cold water. These units also form the reservoir rocks for the hot waters in the region. The pebble and thin limestone layers of the Kuşadası unit from the Neogene, which forms the caprock of the geothermal system due to the clayey layers it contains, are aquifers for cold water. The clayey layers of the Neogene Kuşadası unit form impermeable rocks for the cold-water aquifer. The presence of active tectonic lineations and basaltic volcanism from the Pliocene indicate a high heat flux and a geothermal gradient. The alluvium, on the other hand, is a good aquifer from which abundant groundwater can be extracted due to the width of the recharge area and its permeability.

2.5. Climate and hydrology

Heat flow in the Didim district and its environs as well as the land surface temperature map of the research area and surroundings (Figure 4) are utilized to locate and highlight areas with high geothermal potential. The southern expansion of the Akköy fault divides the distribution into two main regions. While the western section is distinguished by high values because of exposed magmatic rocks, the eastern sector is characterized by both low heat output and low heat flow rates. Higher average values for heat production and heat flow are anticipated due to the fact that the airborne measurements have a lesser resolution than the field data.

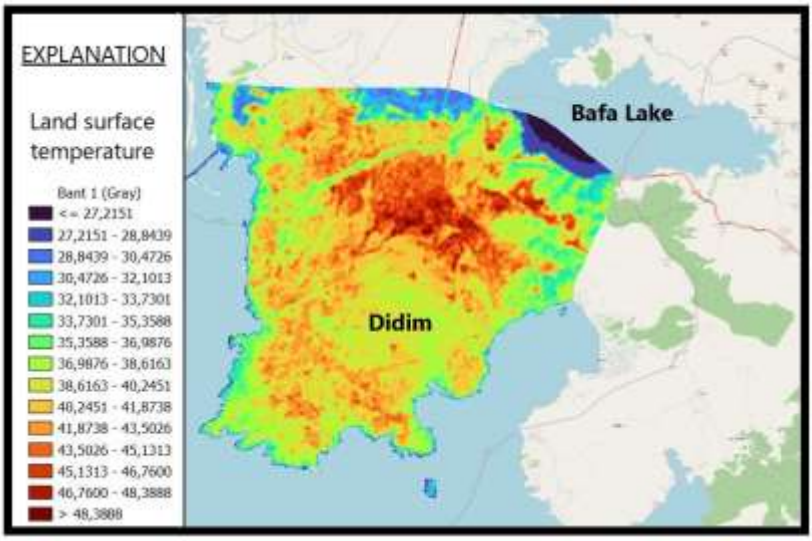

Figure 4: Land surface temperature map of the study area and surroundings

In order to estimate the reservoir temperatures of geothermal systems based on chemical analyses of the thermal waters, a variety of tools have been developed (Jeong et al., 2019; Bragin et al., 2021). These tools include silica and cation geothermometers, the Na-K-Mg ternary diagram, the silica-enthalpy model, and the thermodynamic equilibrium method. Within the scope of the study, the silica content was evaluated by taking samples from the thermal waters in the Didim plateau. High silica content in water samples is mostly associated with geothermal fluid. The value of Fedai thermal well from the thermal water samples taken from Didim plateau was measured as 79 mg/l SiO_2. The silica geothermometer results from the thermal water samples taken from the field are given in Table 1.

Table 1: Silica geothermometer results of thermal waters (Polat, 2020)

Thermal water	**Water temperature estimated by silica geothermometer (°C)**
E. Karst	38
Harabe Kaynak	68
Karstik Su	42
Karstik-2	70
Yörük-1	71
Yörük-2	65
Deniz Pansiyon	39
Fedai Kuyu	79
Orman Kampı	32

2.6. Drilling

Drilling is the most effective method for exploring geothermal resources. When planning geothermal drilling (slim hole, production and injection), it is very important to protect freshwater aquifers and not damage them. This is because reuse of freshwater resources contaminated by the geothermal fluid is impossible in most cases. Medium- and large-sized exploratory wells can also be drilled as exploration and confirmation wells, which can then be used as production and reinjection wells. Temperature gradients and other geothermal features are measured to provide information for determining and estimating geothermal potential. Pre-drilling surface reconnaissance activities such as resistivity measurements and seismic surveys will be conducted to establish an initial conceptual model of the geothermal reservoir and to identify the most appropriate target locations for exploratory drilling (Rosberg & Erlström, 2021). Impacts from the exploratory studies are expected to be minimal or nonexistent.

2.7. Geophysics

Geophysical surveys of the geothermal system are usually conducted to investigate the subsurface structure of the reservoir. By linking drilling data or combining different geophysical data sources, the geophysical survey can be used in some cases to determine reservoir properties such as temperature, porosity, and permeability (Bertaini, 2012). Its main purpose is to determine the depth and extent of the reservoir and the location of the heat source. The key to finding geothermal energy is geophysical research and monitoring of reservoirs with a depth of several kilometers. Due to the fact that subsurface

electrical conductivity is well known to be a very essential parameter for describing geothermal settings and resistivity is very sensitive to the presence of saline water, electromagnetic techniques (EM) are commonly utilized in geothermal exploration (Tsai & Lin, 2022). Due to changes in clay minerals brought on by hydrothermal processes, geothermal systems typically have higher electrical conductivity than the source rock. Additionally, the faults and geothermal fluids where the system is located also serve as conductors of electricity. Due to this, geothermal systems are excellent candidates for the application of EM techniques, such as the sonic magnetotellurics (AMT) and magnetotellurics (MT) natural resource-based approaches that are frequently used in volcanic regions for structural investigations, geothermal assessments, and hydrothermal determinations (Munoz, 2014). The lateral and vertical resistivity changes in the subsurface are usefully shown by the MT and AMT methods, which utilize the natural EM field surrounding the Earth as a source. According to Wu et al. (2012), the MT has an exploration depth that varies from a few meters to over 10 kilometers. The examination of near-surface geothermal reservoirs with depths less than 1000 m is typically done using AMT, which has a frequency range of 11.5-11.500 Hz and a relatively shallow depth of investigation (Alaydrus et al., 2022).

2.7.1. Data acquisition, and processing

AMT and MT are electromagnetic techniques of natural or passive origin that investigate the Earth's electrical conductivity structure by utilizing natural magnetotelluric fields in sonic (10 Hz–10 kHz for AMT) or regular frequency ranges (0.001–1000 Hz for MT). Tikhonov and Cagniard first proposed the MT approach in 1950 and 1953, respectively. Thunderstorms produce natural AMT and MT fields above around 1 Hz because the energy released by lightning creates EM fields that can travel across great distances. Most EM signals below 1 Hz come from systems already in the magnetosphere as a result of solar activity, according to He et al. (2016). Except for the frequency band and data acquisition time, the fundamental theory, field operation, and data processing of AMT and MT fields behave like plane waves on the Earth's surface. According to Pina-Varas et al. (2014), the AMT and MT methods specifically measure orthogonal electric (E) and magnetic (H or B) fields and create frequency-based impedance data in response to the electrical conductivity distribution in the subsurface. The commercial AMTU-5A equipment from Phoenix Geophysics (Toronto, ON, Canada) can be used to generate directional correlations between apparent

resistivity amplitude, impedance phase, and surface electric and magnetic fields from these data. The instrument consists of five main parts: 1) magnetic field sensors (coils), 2) sensor processors, 3) electric field sensors, 4) receiver, 5) computer. The AMTU-5A device used as a receiver has 5 channels. Two of these channels are used for measuring electric field components. The other three channels are used for magnetic field measurements. The magnetic sensors used were AMT AMTC-50H coils for the measurements and AMT AMTC30 coils for the measurements. Since the system has 5 channels, five principal components (Ex, Ey, Hx, Hy, Hz) can be measured at one AMT station. TE Mode (TE - Transverse Electric) and TM mode (TM - Transverse Magnetic) are two common electromagnetic wave modes. The TE mode occurs only when the electric field component of the electromagnetic wave is perpendicular to the wave propagation direction (z-axis). In this case, the magnetic field component moves along both the x and y axes. Therefore, the TE mode is also called the E-parallel mode. The TM mode, on the other hand, occurs only when the magnetic field component of the electromagnetic wave is perpendicular to the wave propagation direction. In this case, the electric field component moves in both the x and y axes. Therefore, the TM mode is also called the H-parallel mode. The TE and TM modes are only two of the many modes used in electromagnetic wave propagation. The other modes include several types such as TEM (transverse electromagnetic modes), TEM -like modes, HE, TE higher order and EH (TM higher order).

2.7.2. TE and TM modes

The apparent resistivity values measured in a layered medium do not depend on the directions of the electric and magnetic fields (Spichak & Manzella, 2009). In two- and three-dimensional environments, the situation is different compared to stratified environments. When the resistivity of the medium is constant along a horizontal axis (here the x-axis is taken), there are two electromagnetic modes separated from each other. These are the TE mode (TE - transverse-electric or E-parallel) and the TM mode (TM - transverse-magnetic or H-parallel). Within the scope of this study, 6 fields close to the coastal region of Didim plateau were selected and 8 measurements were made in each field. The TE and TM modes of each field were obtained separately. Models of TE and TM modes of area 3 are given below (Figure 5). As can be seen from these figures, the TE and TM modes are compatible with each other.

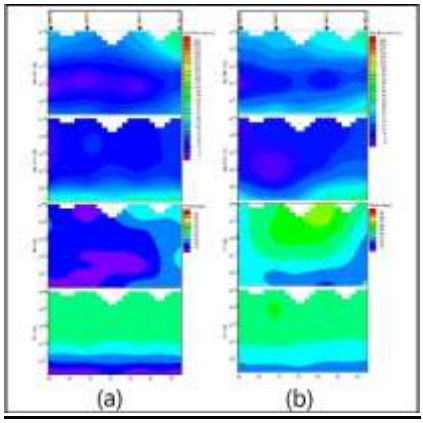

Figure 5: Models for (a) TE and (b) TM mode (HT Report, 2019)

2.7.3. Induction vectors

For the 2-D situation, the theoretical maximum amplitude of an induction vector is 1.0. It should be emphasized that the magnitude of the induction vector is a relative number that depends on the ratio of anomaly resistivity to background resistivity. The magnitude of the induction vector in a horizontally stratified soil is zero. Conductive environments and faults cause abnormalities in the magnitude of the induction vector. The amplitude and frequency of an anomaly are distributed according to the conductivity and depth of the conductive medium. The same is true for induction vector anomalies. The induction vector is unaffected by static drift. The "induction arrow" is formed from the vertical magnetic field to horizontal magnetic field ratio. The arrow in the middle of the polar diagram is drawn with its base and denotes the nearest conductor found at a certain frequency (following the "Parkinson" convention). As a result, at high frequencies, induction arrows point to nearby shallow conductors. Induction arrows indicate deeper and/or further conductors at low frequencies. The arrows will change direction with frequency if a deeper conductor is present. Almost all vectors in the inversion vector map created for the 1 Hz frequency depicting the deep areas are oriented north and northeast. This information suggests a probable fault in the north. The absence of a highly conductive medium is indicated by short vector lengths. As a result, the deep medium that offers conductivity is located on the north side (Figure 6).

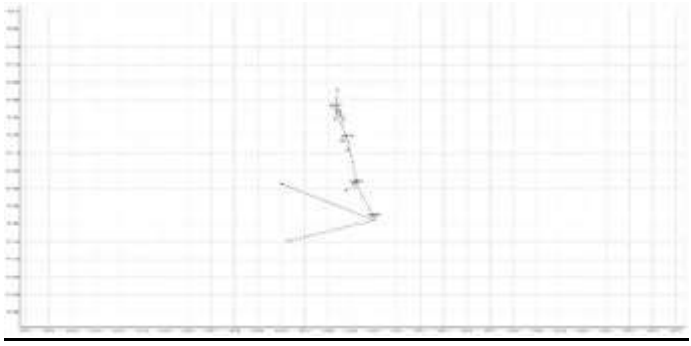

Figure 6: Induction Vectors (for 1000 Hz) (Ongor, 2019)

Vector lengths on the 1000 Hz vector map representing the surface are very short, except for the point in the south. The constant change of vector directions on the surface indicates the existence of a cracked-fractured environment. This suggests that the rocks may have been fragmented by the effect of a nearby fault.

2.7.4. 2 Dimensional AMT section

This section is located in a small part of the license area in the north-south direction. When the cross section is examined, we see that the resistivity increases regularly from top to bottom. At the top of the section (Figure 7), we see a zone of very low resistivity that thins from north to south. This zone, which is 200-250 meters thick in the north, thins towards the south of the section and ends completely or becomes very thin at the south end. Below the saline zone, an impermeable claystone marl level is observed. This level of resistivity between 10-20 Ωm prevents the transmission of surface salinity to depths. Below the claystone-marl level, which continues up to about 500 meters, there are sandstone-conglomerate or clayey limestone units with resistivity values between 20-70 Ωm. The base probably consists of gravelstone.

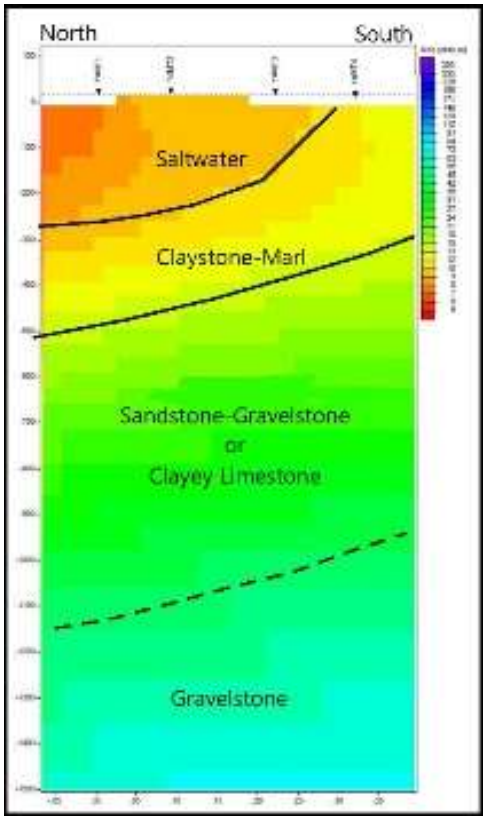

Figure 7: AMT section from the site (Ongor, 2019)

3. SEAWATER-FRESHWATER INTERFERENCE POTENTIAL

Under normal circumstances, the migration of freshwater towards the sea prevents saltwater from entering coastal aquifers, and the interface between freshwater and saltwater is maintained close to the beach or well below the land surface due to the difference in densities (Figure 8 a-c). This interface, where freshwater and saltwater combine, may be a sharp or a transition zone depending on the amount of seawater intrusion and aquifer characteristics (Costall et al., 2020). Resistance thermometers are used in drilling temperature records, which provide continuous temperature readings. In places where deep exploration wells enter the aquifer's effective bottom, temperature recording is the most popular way to measure aquifer thickness (Shin & Hwang, 2020). Due to the fact that the Didim plateau is located by

the sea, the salinization of the aquifers by the intrusion of sea water is one of the important hydrogeological problems. Although the marbles are a good aquifer due to their fractured and karstic structure, as mentioned above, it is the unit where sea water intrusion arising from this structure is quite common. The groundwater floor level is mostly determined by the sea level. For this reason, it is inconvenient to go below the sea level in the wells to be drilled in the marble unit close to the sea.

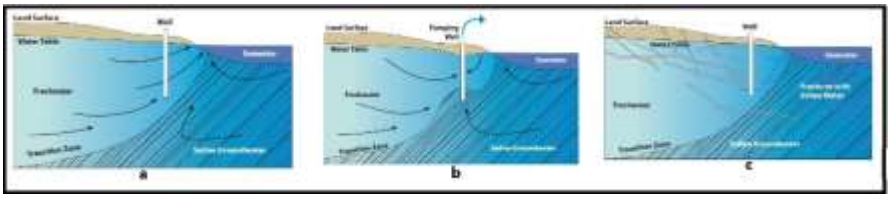

Figure 8: (a) In the absence of pumping, a depth-based equilibrium between fresh and salty groundwater exists**. (b)** Pumping or other disturbances, such as sea level rise or reduced recharge, can cause the freshwater-saltwater boundary to migrate upward or inland. A significant portion of the aquifer may be affected by salinity if a single well is overpumped or if numerous wells are pumping. **(c)** A single fracture in a bedrock aquifer can allow saltwater to enter a well (https://www2.gov.bc.ca).

4. RESULTS AND DISCUSSIONS

Surface morphology, geology, hydrogeology, tectonics, climate, seismicity, and geophysical measurements were taken for geothermal drilling wells planned in the coastal area of the Didim plateau, and geothermal potential was assessed. Within the scope of this study, 6 fields close to the coastal region of Didim plateau were selected and 8 geophysical measurements were made in each field. The TE and TM modes of each field were obtained separately. The results obtained were evaluated. However, suggestions for avoiding saltwater-freshwater interference in the geothermal wells to be drilled have been made. Some rules must be followed when drilling for geothermal purposes on the Didim plateau to prevent salt water intrusion. To begin with, the geothermal drilling well should be located at least 50 meters away from the shore, and drilling close to the shore geothermal well should be avoided. The depth of the freshwater-saltwater interface, on the other hand, is determined locally using the Ghyben-Herzberg formula. If bedrock is broken, special precautions must be taken. To avoid the risk of breakage in the open, hydro-fracturing should be avoided in areas less than 100 meters from the shore. When drilling geothermal, use the meter to

measure conductivity and stop drilling if it completely changes. To prevent salt water from entering, the well may need to be closed below a certain depth.

5. CONCLUSIONS

In recent years, more studies have been conducted to explore geothermal resources in order to evaluate the geothermal potential of the Didim Plateau. The possibility of salinization of geothermal water, seawater intrusion and geothermal water decline that may be caused by saline water is being evaluated to effectively prevent and control geothermal resources and environmental problems, such as potential mechanisms to recharge the geothermal water cycle in geothermal wells to be opened in areas near the Aegean coast of the BMG field. In order to prevent brine intrusion in geothermal wells in the coastal zone of Didim district, some standards for well operation should be observed. First and foremost, the position of the geothermal well should be at least 50 meters away from the coast, and deep wells near the coast should be avoided. Geophysical methods have been used to determine the possibility of brine intrusion into geothermal wells. The pumping depth for drilled wells must be decreased. A multi-well system requires coordinated pumping. Monitoring the following elements on a frequent basis is the best way to stop saltwater intrusion. Geothermal wells that are currently being drilled should have their electrical conductivity tested. Ionic mobility in an aqueous solution allows it to conduct electricity. Total dissolved solids, or TDS, increase in conductivity as salinity rises. Electrical conductivity can be used as a comparative indicator of chloride concentration because seawater has a higher chloride concentration (19,000 mg/L). TDS should be given in mg/L and micro-Siemens/centimeter (µS/cm) when conductivity is measured at 25°C. Following the drilling of the geothermal well, measurements of the groundwater level need to be made on a regular basis. The well's groundwater level is measured, and the pump should be configured to turn off automatically when the water level reaches a predetermined level. Geothermal water re-injection is anticipated to be successful in reducing brine influx.

Acknowledgements

The author would like to thank HT Animal Husbandry Tourism Construction and Foreign Trade Ltd. Company for their contribution to this study.

Author contributions The author confirms sole responsibility for the following: study conception and design, analysis and interpretation of results, and manuscript preparation.

Funding This research did not receive any specific grant from funding agencies in the public, commercial, or not-for-profit sectors.

Declarations

Conflict of interest The author declares that there are no conflicts of interest that should be disclosed.

REFERENCES

Alaydrus, A. T., Susilo, A., Minardi, S., Naba, A., & Mudyanto, A. (2022). Identification of seawater intrusion using geophysical methods in the Mandalika, Lombok, Indonesia. *International Journal of GEOMATE*, *23*(97), 12-21. https://doi.org/10.21660/2022.97.303

Andrés Lloret, C. (2015). *Use of geothermal energy for seawater desalination in the Galápagos Islands, Ecuador.* UNU-GTP Geothermal Training Programme. Reports 2015, Number 19, Reykjavik, Iceland

Bertani, R. (2012). Geothermal power generation in the world 2005–2010 update report, *Geothermics*, 41, 1-29, https://doi.org/10.1016/j.geothermics.2011.10.001

Bjornsson, G., & Palsson, O. P. (2013). Seawater intrusion in geothermal fields: A review. *Geothermics*, 48, 53-65

Bragin, I. V., Zippa, E. V., Chelnokov, G. A., & Kharitonova, N. A. (2021). Estimation of the Deep Geothermal Reservoir Temperature of the Thermal Waters of the Active Continental Margin (Okhotsk Sea Coast, Far East of Asia). *Water*, 13, 1140. https://doi.org/10.3390/w13091140

Cagniard, L., (1953). Basic theory of the magnetotelluric method of geophysical prospecting, *Geophysics*, 18, 605-635

Corniello, A., Cardellicchio, N., Cavuoto, G., Cuoco, E., Ducci, D., Minissale, A., Mussi, M., Petruccione, E., Pelosi, N., Rizzo, E., Polemio, M., Tamburino, S., Tedesco, D., Tiano, P., & Iorio, M. (2015). Hydrogeological Characterization of a Geothermal system: the case of the Thermo-mineral area of Mondragone (Campania, Italy). *International Journal of Environmental Research*, *9*(2):523-534, ISSN: 1735-6865

Costall, A. R, Harris, B. D., Teo, B., Schaa, R., Wagner. F. M., & Pigois, J. P. (2020). Groundwater throughflow and seawater intrusion in high quality coastal aquifers. *Scientific Reports*, 10, 9866. https://doi.org/10.1038/s41598-020-66516-6

Fariduddin, M., & Ali, M. (2018). Evaluation of potential impacts of seawater intrusion on geothermal reservoir at Pohang, Korea. *Geothermics*, 72, 88-98

Faulds, J. E., Hinz, N. H., Coolbaugh, M. F., Shevenell, L. A., Siler, D. L., dePolo, C. M., Hammond, W. C., Kreemer, C., Oppliger, G., Wannamaker, P., Queen, J. H., & Visser, C. (2015). Integrated

geologic and geophysical approach for establishing geothermal play fairways and discovering blind geothermal systems in the Great Basin Region, Western USA: A Progress Report. *GRC Transactions*, 39, 691-700

González-Ramírez, C., Carrasco, C., Sánchez-Camacho, E., & Suárez-Vidal, F. (2019). Seawater intrusion in a geothermal field in Baja California Sur, Mexico. *Environmental Earth Sciences*, 78(12), 1-13

Han, D., & Currell, M. J. (2018). Delineating multiple salinization processes in a coastal plain aquifer, northern China: hydrochemical and isotopic evidence. *Hydrology and Earth System Science*, 22, 3473–3491. https://doi.org/10.5194/hess-22-3473-2018

He, L., Chen, L., Dorji, X., Zhao, X., Chen, R., & Yao, H. (2016). Mapping the geothermal system using AMT and MT in the Mapamyum (QP) Field, Lake Manasarovar, Southwestern Tibet. *Energies*, 9, 855. https://doi:10.3390/en9100855

HT Report (HT Hayvancılık Turizm İnşaat ve Dış Ticaret Ltd Şti). (2019). Aydın, Didim (Balat, Yalıköy ve Fevzipaşa) jeotermal kaynak arama ruhsat alanları kaynak suları jeokimyasal değerlendirme raporu, 10 p.

http:www2.gov.bc.ca/assets/gov/environment/air-land-water/water/water-wells/saltwaterintrusion_ factsheet_flnro_web.pdf (accessed date 22/03/2023)

https://www.wekeo.eu (accessed date 24/04/2023)

Hussein, M. T., Lashin, A., Al Bassam, A., Al Arifi, N., & Al Zahrani, I. (2013). Geothermal power potential at the western coastal part of Saudi Arabia, *Renewable and Sustainable Energy Reviews*, 26, 668-684. https://doi.org/10.1016/j.rser.2013.05.073.

Jeong, C.-H., Lee, B.-D., Yang, J.-H., Nagao, K., Kim, K.-H., Ahn, S.-W., Lee, Y.-C., Lee, Y.-J., & Jang, H.-W. (2019). Geochemical and Isotopic Compositions and Geothermometry of Thermal Waters in the Magumsan Area, South Korea. *Water*, 11, 1774

Karyono, K., & Sulaeman, C. (2019). Seawater intrusion to geothermal reservoir in Lahendong geothermal field, Indonesia. *Geothermics*, 81, 232-242

Motallebian, M., Ahmadi, H., Raoof, A., & Cartwright, N. (2019). An alternative approach to control saltwater intrusion in coastal aquifers using a freshwater surface recharge canal. *Journal of Contaminant Hydrology*, 222, 56-64. https://doi.org/10.1016/j.jconhyd.2019.02.007.

Munoz, G. (2014). Exploring for geothermal resources with electromagnetic methods. *Survey Geophysics*, 35, 101–122

Noorollahi, Y., Ghasempour, R., & Jalilinasrabady, S. (2015). A GIS based integration method for geothermal resources exploration and site selection. *Energy Exploration & Exploitation*, *33*(2), 243–258

Ongur, T. (2019). HT Hayvancılık Turizm İnşaat ve Dış Ticaret Ltd Şti' ne ait, Aydın, Didim (Balat, Yalıköy ve Fevzipaşa) jeotermal kaynak arama ruhsat alanlarında jeofizik incelemeler sonrasinda sera ısıtma amaçlı akışkan elde etme olanaklarının değerlendirilmesi ve öneriler, 20 p. (Unpublished Report)

Ozcelik, M. (2021). Sustainable management to prevent seismic risks in the Büyük Menderes geothermal province (SW Turkey). *International Journal Energ and Water Resources*, 5, 371–378. https://doi.org/10.1007/s42108-021-00131-7

Ozcelik, M. (2022a). Induced seismic risk assessment of geothermal energy production, Büyük Menderes Graben, Turkey. *Arabian Journal of Geosciences*, 15, 1114. https://doi.org/10.1007/s12517-022-10033-5

Ozcelik, M. (2022b). Environmental and social impacts of the increasing number of geothermal power plants (Büyük Menderes Graben—Turkey). *Environmental Science and Pollution Research*, 29, 15526–15538

Pina-Varas, P., Ledo, J., Queralt, P., Marcuello, A., Bellmunt, F., Hidalgo, R., & Messeiller, M. (2014). 3-D Magnetotelluric exploration of Tenerife geothermal system (Canary Islands, Spain). *Survey Geophysics*, 35, 1045–1064

Polat, F. (2020). HT Hayvancılık Turizm İnşaat ve Dış Ticaret Ltd Şti, Aydin Didim (Balat, Yalıköy ve Fevzipaşa) jeotermal kaynak arama ruhsat alanları, kaynak sulari jeokimyasal dğerlendirme raporu, 10 p.

Rabet, R. S., Simsek, C., Baba, A., & Murathan, A. (2017). Blowout mechanism of Alasehir (Turkey) geothermal field and its effects on groundwater chemistry. *Environmental Earth Science*, 76, 49. https://doi.org/10.1007/s12665-016-6334-6

Rustadi, R., Darmawan, I. G. B., Nandi, H., Suharno, S., & Setiawan, A. (2021). *Geophysical approach for assessment of seawater intrusion in the coastal aquifer of Bandar Lampung, Indonesia*. IOP Conference Series: Materials Science and Engineering. 1173. 012007. 10.1088/1757-899X/1173/1/012007

Rosberg, J-E. & Erlström, M. (2021). Evaluation of deep geothermal exploration drillings in the crystalline basement of the Fennoscandian Shield Border Zone in south Sweden. *Geothermal Energy*, 9, 20. https://doi.org/10.1186/s40517-021-00203-1

Sebben M. L, Werner, A. G., & Graf, T. (2015). Seawater intrusion in fractured coastal aquifers: A preliminary numerical investigation using a fractured Henry problem. *Advances in Water Resources*, 85, 2015, 93-108. https://doi.org/10.1016/j.advwatres.2015.09.013.

Shin, J., & Hwang, S. (2020). A borehole-based approach for seawater ıntrusion in heterogeneous coastal aquifers, eastern part of Jeju Island, Korea. *Water*, 12. 609. 10.3390/w12020609

Spichak, V., & Manzella, A. (2009). Electromagnetic sounding of geothermal zones. *Journal of Applied Geophysics*, 68, 459–478

Tikhonov, A. N., (1950). *On determining electrical characteristics of the deep layers of the Earth's crust, Doklady*, 73, 295-297.

Tsai, C-C., & Lin, C-H. (2022). Review and future perspective of geophysical methods applied in nearshore site characterization. *Journal of Marine Science Engineering*, 10: 344. https://doi.org/10.3390/jmse10030344

Xing, Y., Yu, H., Liu, Z., Li, J., Liu, S., Han, S., & Wang, G. (2022). Study on chemical genesis of deep geothermal fluid in Gaoyang Geothermal Field. *Frontiers Earth Science*, 9, 787222. doi: 10.3389/feart.2021.787222

Wilopo, W., Risanti, Susatio, R., & Putra, D. P. E. (2021). Seawater intrusion assessment and prediction of sea-freshwater interface in Parangtritis coastal aquifer, South of Yogyakarta Special Province, Indonesia. *Journal of Degraded and Mining Lands Management*, 8(3), 2709-2718, doi: 10.15243/jdmlm. 2021.083.2709

Wu, G. J., Hu, X. Y., Huo, G. P., & Zhou, X. C. (2012). Geophysical exploration for geothermal resources: An application of MT and CSAMT in Jiangxia, Wuhan, China. *Journal of Earth Science*, 23, 757–767

Yuan, J., Xu, F., & Zheng, T. (2022). The genesis of saline geothermal groundwater in the coastal area of Guangdong Province: Insight from hydrochemical and isotopic analysis, *Journal of Hydrology*, 605, 127345, ISSN 0022-1694, https://doi.org/10.1016/j.jhydrol.2021.127345

CHAPTER 2

THE CONSERVATION AND REVITALIZATION OF THE CILIWUNG RIVERBANK IN MANGGARAI, JAKARTA[1]

Dr. M. Maria SUDARWANI, S.T., M.T.

[1]Faculty of Engineering, Universitas Kristen Indonesia, Jakarta, Indonesia
Email: margareta.sudarwani@uki.ac.id

INTRODUCTION

Jakarta city is the center of the economy, from regional to international, because 65% of national money circulates in the capital region, so that nearly 80% of economic activity in Indonesia is centered in the city of Jakarta. Centers for science and technology, as well as socio-cultural activities are also based in Jakarta. This is the main attraction, making the growth and development of the population in Jakarta more rapid (Rahmatulloh, 2017). However, this also results in an unequal ratio between the population and the availability of land (especially the need for agriculture and settlements), so that many residents turn the riparian area into a residential and agricultural area (Diva, 2019). Based on the Government Regulation of the Republic of Indonesia Number 38 of 2011 concerning Rivers, trends that have a negative impact on rivers need to be controlled so that a harmonious and sustainable state can be achieved between river functions and human life, for the benefit of the future. If this trend is not addressed immediately, then in the future, it is likely that rivers will become increasingly polluted, floods will become uncontrollable, and the life of the people living along the river will become increasingly uncontrollable with a low quality of life. Even these things have started to happen now.

The Ciliwung River is one of the historic rivers in the city of Jakarta, which stretches from Bogor (upstream), covers the areas of Mount Pangrango, Mount Gede and Cisarua, then flows downstream on the north coast of Jakarta. The length of this river reaches 120 kilometers and the area of the watershed (DAS) is 387 square kilometers. The Ciliwung River is divided into 3 (three) sub-watersheds, namely; The upstream Ciliwung with an area of 15,251 hectares (located in the Regency and City of Bogor area), the middle Ciliwung with an area of 16,706 hectares (in the Depok, Bekasi, Regency and Bogor City areas), and the downstream Ciliwung with an area of 6,295 hectares (in the DKI Jakarta area). At the end of 2020, it is estimated that only 9.7 percent/3,693 hectares of forest area will remain, which is the natural regulator of water management, remaining in the Ciliwung Watershed. While the ideal area of green open space is around 30 percent of the area of the river (Rahmad, 2020). Based on the results of research conducted by LIPI, it revealed that there was another problem that occurred, namely the threat of extinction of fish in the Ciliwung river, around 92.5 percent of fish species in the Ciliwung river had become extinct, caused by continued pollution (Hadiaty, 2017).

One of the first steps to be able to control this tendency is to provide

socialization to the community, especially those living in the river border areas, so that awareness and concern for the current condition of the river arises. But to restore the function of the river and preserve it for future generations, it is not enough just to socialize, a long-term solution is needed in the form of area planning along the river border. One of them is by establishing clear and firm river demarcation lines and watersheds (watersheds), as well as creating green lanes and green open spaces (RTH) along rivers. This will reduce runoff by 30 percent, by making the river 50-70 meters wide, 2-3 meters deep, 2 meters wide bank, 2-3 meters wide embankment, one meters high embankment with bare stone material, filled with grass plants, which are able to control flooding in the rainy season, when the river water level is still -0.5 to -1 below the embankment (Purwono & Mustika, 2018).

Another thing that can be done is to conserve and revitalize the Ciliwung river area. River conservation is an effort to use, protect, restore river functions, and maintain rivers for now and in the future (Setyowati et al., 2018). Meanwhile, revitalization of rivers will increase the quality and value of the area, by improving and creating spaces that are beneficial for social, cultural and economic activities (Purwantiasning, 2015). The purpose of this study is to provide a systematic description or description of the facts in the field, based on the results of an analysis of the case study of the Ciliwung, Manggarai, Tebet, South Jakarta riverbank areas, and describe the design efforts that have been carried out in the framework of conservation and revitalization.

THE RESEARCH METHODS

The planned research location is located on the banks of the Ciliwung River, Manggarai Village, Tebet District, South Jakarta. The location map can be seen in Figure 1. This research was carried out for approximately 5 (five) months and started in November 2021 until March 2022. Based on the results of a survey from the sub-district regarding future plans to become the location of the manggarai station as a city station, so we decided to widen the site from the research area so that there is continuity and alignment of environmental functions around the central station area in Jakarta. Designation: city forest, city park, billboards, strategic mining (conditional). Data was collected through photos and videos observing the location of the Ciliwung Riverbanks.

Figure 1. The Research Location

THE HISTORY OF CILIWUNG RIVER

The Ciliwung River was originally the place where the Dutch first built a castle on the east bank of the estuary. Meanwhile, there is the Culemborg Building and Jalan Pakin Customs office on the west bank of the estuary. Kali Besar is a straight stream of the Ciliwung River to the south, Weltervreden to the west, Sunda Kalapa Harbor at the mouth of the river, and there is a private house that was once the office of Sultan Hamengkubuwono IX of Yogyakarta to the east, Prapatan area. Small boats sailed along the Ciliwung river to transport goods from warehouses near the Kali Besar to ships that anchored at sea in the early Batavia period. The boat entrance from the canal to Waterpoort is via a branch of the Ciliwung River which empties into the ocean (See Figure 2).

Figure 2. a) Raft with cargo on the Ciliwung river in Batavia;
b) Crossing on the Ciliwung River in Batavia
(Source: konservasidasciliwung.wordpress.com)

In addition, Ciliwung river water was originally used as a source of drinking water for local residents, but this river water has been considered unhealthy since 1740, because of the discharge of hospital waste water and all the garbage that flows directly into the river. This caused many patients to

suffer from dysentery and cholera, and even caused a very high death rate among residents of Batavia/Jakarta (Hasits, 2021), because there were shops, hotels, and luxury villas which were the residences of VOC officials along the canals built by the VOC (Arby, 2020) (See Figure 3).

Figure 3. Aerial photo of Batavia with the Ciliwung River (Source: konservasidasciliwung.wordpress.com)

The Ciliwung River Basin in Indonesia has a very strategic value. This is evident in terms of topography, the Ciliwung watershed is divided into 3 (three) parts, namely the upstream, middle and downstream. Changes in the upstream part of the watershed will affect all other parts as a watershed ecosystem. The city of Jakarta has a strategic value in its development and management because it is located in the downstream part of the Ciliwung watershed (Ruspendi et al., 2013). However, there is an increase in the need for space such as settlements, public facilities, and other built-up land due to the rapid development activities in the Ciliwung watershed area. An increase in population also causes dynamics/changes in space requirements from time to time (Saridewi et al., 2014).

Another thing that happens in the Ciliwung watershed is disturbance to the surface of the water bodies around and within it, as a result of land change and reclamation, as well as the pollution that occurs. Based on the results of research conducted by Arifin et al. (2014), regarding Blue Open Space, distance from the main road, slope, city, population density, and soil type are factors that influence changes in Blue Open Space in the Ciliwung Watershed. 11 (eleven) strategic alternatives based on Strengths Weaknesses Opportunities Threats (SWOT) analysis were obtained, and five of them were: 1) Required to provide Blue Open Space as environmental service providers, when creating residential areas, and making special rules for (private)

property developers, 2) Provide socialization to the community about the important role of Blue Open Space, 3) Complete the Blue Open Space infrastructure to protect against siltation, 4) The regional government makes a Blue Open Space management plan by providing a reward and punishment mechanism for the community, and 5) Develop local community-based tourism areas in Blue Open Space that are considered potential.

THE RIVERBANK AREA DESIGN

In designing riverbank areas, guidelines are needed to serve as a basis or benchmark, so that they can be carried out systematically. Republic of Indonesia Government Regulation Number 38 of 2011 concerning rivers and river management is the guideline used in this research.

In Article 5 regulations, riverbeds and riverbanks are part of a river. The function of the riverbed is as a space for flowing water and as a place for river ecosystem life to take place. While the function of the river border is as a buffer space between the land and the river ecosystem, so that the function of the river and human activities are not mutually disturbed. River border lines are very important in river design, in article 8 it is explained that river border lines are determined at: a) rivers without embankments within urban areas; b) rivers without embankments outside urban areas; c) river embankments within urban areas; d) embankment rivers outside urban areas; e) rivers affected by tides; f) flood exposure lakes; and g) water springs.

The Ciliwung River as the object of this research is included in the non-banked river in urban areas. So, the boundary line is determined by: a) the depth of the river is less than or equal to 3 m (three meters), and has a minimum distance of 10 m (ten meters) from the right and left banks of the riverbed along the river channel; b) the depth of the river is more than 3 m (three meters) up to 20 m (twenty meters), and has a minimum distance of 15 m (fifteen meters) from the right and left banks of the riverbed along the river channel; c) the depth of the river is more than 20 m (twenty meters), and has a minimum distance of 30 m (thirty meters) from the right and left banks of the riverbed along the river channel. River conservation, river development, and controlling the destructive power of river water are part of river management. River management is usually carried out by involving technical agencies and related community elements, which is carried out based on standards, guidelines, norms and criteria set by the Minister.

River protection (flood lakes and floodplains, riverbeds, riverbanks,

stream maintenance of rivers, and river restoration sections), and prevention of river water pollution are activities that are usually carried out in the context of river conservation.

THE RIVERBANK AREA COMPARATIVE STUDY

This comparative study will explain the results of several studies on riverbank housing. What are the factors that trigger the emergence of housing in riverbank areas, and what solutions are provided by researchers for any problems that arise due to the development of housing in riverbank areas. See Table 1.

Table 1. Comparative Study Results

Aspect	Surabaya River	Riverbanks Kahayan in Palangkaraya	Kalimas River (Dinoyo Tenun area)	Riverbanks Martapura Banjarmasin
Areas	Close to the Joyoboyo bus terminal (north side), market and train station Wonokromo (South side).	The river functions as a water transportation route (main function), a source of drinking water, and for daily needs.	Many stalls have sprung up selling daily necessities.	The riverbanks functioned as open public spaces (siring) and became water transportation routes for the people of South Kalimantan to go inland.
Residents/users	Work in terminal, market and station areas.	1. The majority are of productive age, 2. The majority work as shrimp and fish fishermen.	1. Low-income groups, and immigrants from outside the city of Surabaya 2. Only a small proportion of the population has a permanent job, 3. Most of the population has elementary school education, 4. Public awareness to protect the environment is quite good, as evidenced by visitors from around the location and from afar.	Visitors from around the site and from afar.
Problems	1. Network infrastructure 2. Water pollution	1. Water pollution 2. Sanitation 3. Danger of wild animals 4. Building strengt	The use of rivers to support daily activities is still high (for defecating and for making a living with activities 'mining' or catching	

			fish).	
Solution	Local people expect compensation in the form of funds, land for relocation or both	1. Create new settlements for relocation that are still close to rivers, 2. Counseling and training from the local government. 1. The government and the private sector must also build hospitals, health centers, schools, mosques and other facilities	1. Create a center of economic activity, 2. Create 3. city recreation.	1. Front edge approach, to add more value to the riverside area, 2. Techno-economic approach, 3. The affordability of the location in the development of an open space. 4. Interesting design or shape.

THE CITY PLANNING INFORMATION DATA

The planned research location is located on the banks of the Ciliwung River, Manggarai Village, Tebet District, South Jakarta. Location map can be seen in the following figure Designation: City Forest, city park, billboards, strategic mining (conditional) (See Figure 4).

Figure 4. The City Plan Information

At the front of the settlement, the pedestrian area has not been fully constructed, where the pedestrian area that is made stops until opposite Manggarai Station. While other parts have not been made pedestrian areas so that the settlement is directly adjacent to the main road which has relatively fast traffic (See Figure 5).

Figure 5. The Pedestrian Area

From direct observation, the condition of the Ciliwung River and the housing on its banks are not well organized and rundown. Housing along the Ciliwung River does not have easy access to clean water. There is no domestic waste disposal system, so some people dispose of household waste directly into the river without being treated first. The provision of electricity for housing along the Ciliwung River is also not well organized (See Figure 6).

Figure 6. a) Ciliwung River; and b) Housing Highway of Ciliwung Riverbank

Due to the absence of a playground or RPTRA, many children living along the Ciliwung River do activities and play on the side of the main road which has relatively fast traffic. Data on the number of residents of each RW, residents' occupation, residents' education, and religion can be found from population data collected by the Manggarai ward every year. The research scope data consists of three RWs located on the banks of the Ciliwung River, namely RW 01, RW 04 and RW 010. The total population consisting of RW

01, RW 04, and RW 010 is 9,177 people, while the number of residents who are right on the banks of the Ciliwung River is approximately 2,500 after deducting the residents of RW 01 and 010 who are not on the banks of the Ciliwung River and residents who live in TNI housing that cannot be moved.

According the land analysis, the land is located along the banks of the Ciliwung River in the Manggarai sub-district area, it is included in the RW 1 – 4 – 10 area. In fact, the land is an area along the banks of dense and slum residential areas. The area on the land is divided into 4 areas, namely the commercial flat area, the commercial and lodging area, TNI housing, and the park area (See Figure 7). Manggarai Station will become Jakarta's central station, and the park area will be used to accommodate social and children's needs to play and interact, which so far have not been accommodated in that area, causing children to often play on the main road which is of course very dangerous. Based on Schematic Drawing of Area Division, it is found that the size of the existing area is divided into 4 types, namely commercial flats, commercial lodging, TNI housing, and park areas, the following is the calculation of the area per area: a) Commercial Flat Area: 8915m^2; b) Lodging Commercial Area: 8,708m^2; c) TNI Residential Area: 7308m^2; d) Park Area: 13.420m^2; e) Total: 38,351m^2; and Total area designed: 31.043m^2. The area that is designed includes the area of commercial flats, commercial and lodging, and the garden area, in the TNI housing area, is not an area that is included in the area designed in the research project.

Figure 7. Schematic Drawing of Area Division

THE REVITALIZATION OF THE CILIWUNG RIVERBANK

Here is the overall concept that we can suggest for the benefit of revitalizing the Ciliwung riverbank area so that it can function properly:

1. Site Plan

The site design concept is taken from the elements and principles of landscape design, the pattern can be adapted and applied to the site as an allotment of spatial patterns that take the form of curved lines and round pattern shapes which in their application are combined with straight lines as a form reference, in the park area there is a green field area to accommodate the main needs, namely an outdoor children's play area as well as a place to exercise because a jogging track is provided that surrounds the green field area, and there is also a water pool area for ventilation functions in this hot area so that in addition to being a tourist spot and social interaction it can also answer needs environment and increase the temperature around the area, there is also a parking area that is provided to avoid illegal parking around the riverbank area, and there is also a trader's area for selling so that economic functions can still be carried out around the area (See Figure 8).

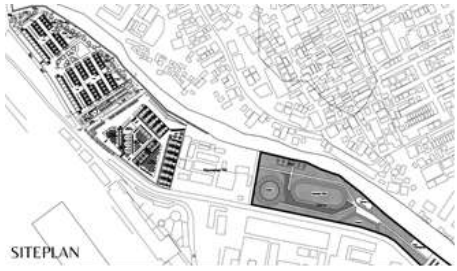

Figure 8. Site Plan

The site plan area is divided into 4 areas, namely the Commercial Flats area, Commercial and Lodging Area, TNI Housing, and the Park area, each area is designed to meet the needs of the environment so that there is a reversal of the function from what was previously only a slum housing which polluted the environment, to areas that can be utilized can even produce good economic value and social interaction.

2. The Commercial Flats Area

There are 12 flats with a capacity of around 115 heads of households, to accommodate residents who previously lived in slum settlements and owned businesses so that they could still get decent housing with good sanitation while still being able to open businesses. On the part directly adjacent to the road, commercial flats are made where the first floor is a shop

area and the second floor is a residential area. While on the inside is a flat area where the first floor and second floor are residential areas. In addition to the low tide unit, there is an outdoor space provided for social interaction so that the impression of a residential house is not lost and also so that social interaction can continue to occur thereby increasing the economic value around the commercial flat area (See Figure 9).

Figure 9. The Commercial Flats Area

3. The Commercial and Lodging Areas

The commercial area is designed for commercial and lodging needs, because to accommodate the mobility of the Central Jakarta Station at Manggarai Station later, therefore the commercial area will later become a culinary tourism spot with existing tenants as well as a place for capsule lodging, so as to be able to accommodate the large number of people who will come and stay, because of its strategic location, namely on the opposite side of the direct station, the commercial area connects the commercial area with the station area with a special JPO designed for pedestrian transportation from the commercial area to the station area (See Figure 10).

Figure 10. The Commercial and Lodging Area

4. Environmental Park Area

Figure 11. The Environmental Park Area

The Environmental Park Area is designed not with tall buildings and prioritizes outdoor spatial planning which will later be used for activities such as playing sports, and carrying out social interactions, the greenery pattern around the park area is regulated so as to protect and separate the main road from the park area (See Figure 11).

CONCLUSION

In a research project around the Ciliwung riverbank area in the Manggarai sub-district, South Jakarta, we found that the Manggarai station was planned by the government to change its function to become the largest central station in Jakarta, the unavailability of adequate infrastructure to accommodate the Manggarai central station is one of the focuses of the research. this, still needs a lot of improvement and also government policies to fix around the banks which have now become slums that pollute the river, of course this is a bad thing if it is maintained for a prolonged period, it will cause environmental damage, the population density will continue to soar, and the squalid areas around the riverbanks so that the water in the Ciliwung river is polluted and brings disease to both humans - river biota - and the surrounding environment, therefore some of what we can conclude, among others, is the need for system improvements em population, changes in the layout and function of the land for flat areas, commercial areas and lodging as well as a playground area for children, so that the circulation and needs of local residents can be met.

The result of the research is planning suggestions as well as design outputs for the design of areas around the riverbank area by looking at the

changes in function in the area to become the central station area in Jakarta, and also to meet the standards of human needs for activities, land use, and the surrounding environment when viewed from the field of architectural science.

REFERENCES

Arbi, I. A. 2020. "Menyusuri Riwayat Sungai Ciliwung, Sempat Berdamai dengan Ibu Kota di Zaman VOC," (*Tracing the History of the Ciliwung River, Had Peace with the Capital City during the VOC Era*) Kompas.com, pp. 1–2, 2020.

Arifin, N.H.S., & Kaswanto. 2014. "Manajemen Lanskap Ruang Terbuka Biru di Daerah Aliran Sungai Ciliwung," (*Landscape Management of Blue Open Spaces in the Ciliwung River Basin*). IPB Repository, 2014. [Online]. Available: https://repository.ipb.ac.id/handle/123456789/70806.

Diva, I.H. "Konduksi: Konservasi Sempadan Sungai Berbasis Edukasi Spasial," (*Conduction: Spatial Education-Based River Border Conservation*), pp. 2–7, 2019.

E. Setiawan, 2021 "Kamus Besar Bahasa Indonesia" (*Indonesia Dictionary*).

Hadiaty, D. R. K. 2021. "Ini Tujuh Spesies Ikan Baru Hasil Temuan Peneliti LIPI dan Prancis," (*These are Seven New Fish Species Findings by LIPI and French Researchers*). [Online]. http://lipi.go.id/berita/ini-tujuh-spesies-ikan-baru-hasil-temuanpeneliti-lipi-dan-prancis/17993. [Accessed: 27-Feb-2021].

Hasits, M. 2021. "Sejarah Ciliwung, sumber air minum yang kini jadi tempat sampah." (*The history of Ciliwung, a source of drinking water which is now a trash can*) [Online]. Available: https://www.merdeka.com/peristiwa/sejarah-ciliwung-sumber-air minumyang-kini-jadi-tempat-sampah.html#:~:text=Dahulu Sungai Ciliwung airnya digunakan,1699%2C mengakibatkan kenaikan tingkat pengendapan. [Accessed: 28-Feb2021].

Peraturan Pemerintah Republik Indonesia Nomor 38 Tahun 2011 Tentang Sungai" (*Government Regulation of the Republic of Indonesia Number 38 of 2011 concerning Rivers*) pp. 1–21, 2011.

Purwantiasning, A.W. 2015. "Kajian Revitalisasi Pada Bantaran Sungai Sebagai Upaya Pelestarian Bangunan Tua Bersejarah, Studi Kasus : Kawasan Malaka," (*Revitalization Study on Riverbanks as an Effort to Preserve Old Historical Buildings, Case Study: Malacca Region).* Pros. SNTT FGDT 2015, no. July 2015.

Purwono, R. and Mustika, L. 2018. "Rekayasa Lansekap Untuk Penanganan Banjir (Studi Kasus: Bukit Duri, Kampung Pulo, Kampung Melayu dan Kali Bata Jakarta)" (*Landscape Engineering for Flood Handling,*

Case Study: Bukit Duri, Kampung Pulo, Kampung Melayu and Kali Bata Jakarta) Sabua J. Lingkungan Binaan, vol. 8, no. 3, pp. 32–39, 2018.

Rahmatulloh. 2017. "Dinamika Kependudukan di Ibukota Jakarta, Deskripsi Perkembangan Kuantitas, Kualitas dan Kesejahteraan Penduduk di DKI Jakarta" (*Population Dynamics in the Capital City of Jakarta, Description of Population Quantity, Quality and Welfare Developments in DKI Jakarta*), Genta Mulia, vol. VIII, no. 2, pp. 54–67, 2017.

Ruspendi, D., Hadi, S., & Rusdiana, O. 2013. "Kajian Perubahan Penutupan Lahan Pada Das Ciliwung Hulu Dengan Pendekatan Spasial Dinamik," (*Study of Land Cover Changes in the Upstream Ciliwung Watershed Using a Spatial Dynamic Approach).* J. Lanskap Indonesia, vol. 5, no. 2, pp. 1–5, 2013.

Saridewi, T. R., Hadi, S., Fauzi, A. and Rusastra, I. W. 2014. "Penataan Ruang Daerah Aliran Sungai Ciliwung dengan Pendekatan Kelembagaan dalam Perspektif Pemantapan Pengelolaan Usahatani," (*Spatial Planning of the Ciliwung River Basin with an Institutional Approach in the Perspective of Consolidating Farming Management*) Forum Peneliti Agro Ekonomi, vol. 32, no. 2, p. 87, 2014.

Setyowati, D.L., Hardati, P. and Arsal, T. 2018. "Konservasi Sungai Berbasis Masyarakat di Desa Lerep Das Garang Hulu" (*Community Based River Conservation in Lerep Das Garang Hulu Village*), Pros. Semin. Nas. Geogr. UMS IX 2018, pp. 401–410, 2018.

CHAPTER 3

SIMULATORS IN ROBOT DESIGN AND APPLICATIONS

Lecturer Emrah ASLAN[1]

Dr. Yıldırım ÖZÜPAK[2]

[1] Dicle University, Silvan Vocational School, Diyarbakır, Türkiye, emrah.aslan@dicle.edu.tr ORCID : 0000-0002-0181-3658

[2] Dicle University, Silvan Vocational School, Diyarbakır, Türkiye, yildirim.ozupak@dicle.edu.tr ORCID: 0000-0001-8461-8702

INTRODUCTION

In humans and animals, learning takes place along with growth. As the body and brain grow in these creatures, movements such as crawling, standing, walking, running, jumping and eating are learned in parallel. However, the learning action in robots does not proceed in this way. Robots are a system consisting of mechanical, electronic and software components designed to perform the desired tasks. Robots have an advanced infrastructure like humans. Thanks to the sensors and motors on them, the ability to use the body efficiently is taught later (Aslan, 2023).

Robots according to the operations to be performed; They can be designed as fixed, mobile or mobile robots. These robots can work in different environments such as air, land and water. Some robots can work in only one of these environments, while others can work in all environments. Robots have motors that provide movement. These motors are controlled by controllers and the desired movement is made to the robot. In order for robot movements to be smooth and efficient, it must receive signals from the external environment. For this, various sensors are added to the robots in accordance with the intended use. Thanks to these sensors, various information such as the robot's position, direction, speed, detection of surrounding objects, acceleration, etc. are obtained. The data received from the sensors are processed by the controller on the robot, allowing the motors to move appropriately (Aslan et al., 2023; Güllü 2017).

One of the biggest challenges in robots is real-world testing. Artificial intelligence systems that direct robot movements require very long training in order to imitate human movements. When testing robots in the real world, there may be a need to test a skill thousands of times or years on the tracks in order to acquire a skill. After a robot is damaged during real-world testing, it may need to be repaired on a regular basis. Repairing the damage to the robot after each test both increases the cost and slows down the training.

Robotics; It is a platform where advanced technological studies where mechanical, electronic and software systems are combined. The development, implementation and improvement of these studies is both costly and time consuming. In robotic studies, the mechanical model can be defined in the computer environment before the applications are run in the real world. Algorithm tests can be performed in the computer environment of the robot

whose mechanical model is defined. Robotic simulators are used to perform these operations in the computer environment.

Robotic simulators are computer programs used to test embedded software applications to be installed on robots, physically independent of the robot. This saves both time and money. The application developed in the simulation environment can be loaded onto the real robot without making any changes. For example; the program developed on the Robotis-OP2 humanoid robot in the Webots simulation environment can be loaded and run on the real robot.

An alternative method to real-world tests is to perform operations on simulation. Thanks to the simulation software, it is possible to test the programs to be loaded on the robot in a virtual environment independent of the real robot. Simulation software, a 3-D virtual version of the robot, can be trained quickly in a computer environment and without the cost of physical infrastructure to be created in the real world.

PURPOSE

In this study, our aim is to give information about simulators that will enable robots to be designed and implemented in a computer environment before performing their work in real life. Robot systems are expensive and sensitive systems. Tests to be carried out directly in the real world can cause damage to the robot hardware and additional costs. Therefore, virtual tests are needed before real-world tests. These virtual tests are carried out with robotic simulators.

ROBOTIC SIMULATION PLATFORMS

A robotics simulator is used to create an application for a physical robot without being tied to the real machine. Thus, cost and time savings are achieved. In some cases, these applications can be transferred to the physical robot without any changes.

In robotic simulators, robots and working environments can be modeled in three dimensions. In this way, thanks to the three-dimensional modeling opportunity, it is possible to test it close to the real environment. In simulators, the sensors and motors on the real robot are designed and created with exactly the same features. Robotic simulators are designed as user-friendly applications. In terms of convenience during robot programming,

they allow application development with more than one programming language.

In the selection of simulation programs used in robot programming, the support of the robot to be used by simulation should be considered. With simulation programs, it provides the opportunity to design and program the robot from scratch, as well as to develop an existing robot.

There are many robotic simulators for robot development or programming. Some of these simulators are open source and some are licensed robotic simulators. Examples of open source simulators are software such as Gazebo, ARS, Breve, Moby, OpenHRP3, MORSE, SimRobot. Software such as Webots, V-REP, Microsoft Robotics, Developer Studio, Workspace5 can be given as examples of licensed robotics simulators.

V-Rep

V-Rep (Virtual Robot Experimentation Platform) is a virtual experiment platform in which a physical and software model of a robot system is realized. V-Rep program is a licensed product developed by Coppelia Robotics as a general purpose robot simulation.

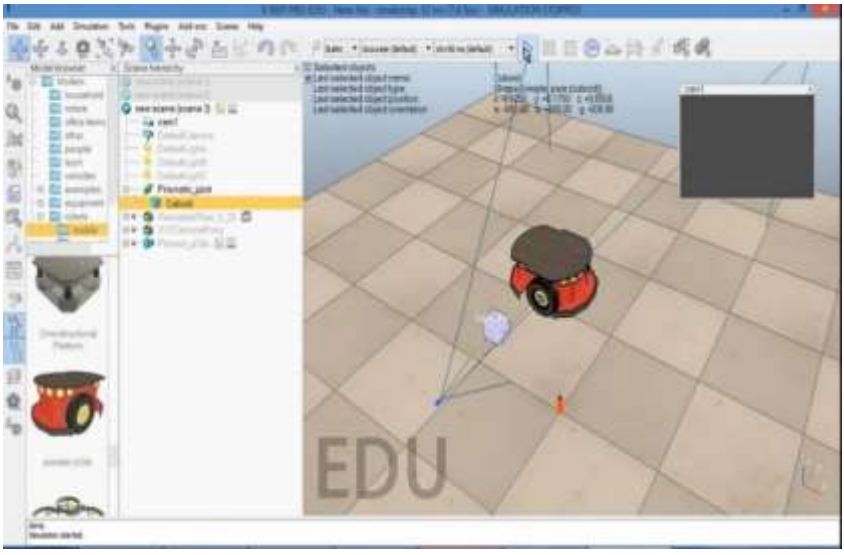

Figure 1: V-Rep Simulator

This simulator runs on Windows, Linux and MAC operating systems. The V-Rep simulator allows the programmer to program in seven different languages such as C/C++, Java, Python, Matlab, Lua, Urbi and Octave.

Thanks to its user-friendly interface, the simulator allows easy use, rapid prototyping and coding. The V-Rep simulator allows creating real-world environments as it allows three-dimensional designs. With V-Rep, robots moving on land, sea and air can be simulated. The three main functions of V-Rep can be listed as follows;

- Scene objects
- Calculation modules
- Control mechanisms

In the V-Rep simulator; objects such as shapes, joints, distance sensors, image sensors, force and torque sensors, graphics, cameras, lights, roads, reference objects, cutters. This scene allows modeling of various functional robots using different objects and sensors (eg accelerometer, gyroscope, GPS, Torque etc.). There are large libraries of sensors and robot models that can be easily added to the environment created in the V-Rep simulator by dragging them. The fact that these model libraries can be customized according to the project to be used makes V-Rep attractive for researchers. An example of the interface screenshot of the V-Rep simulator is given in Figure 1 (Yolal, 2015).

With the V-Rep simulator, users can read and process data from various sensors on the robots they work with. In addition, video recordings of the simulation can be created against the request of visually displaying the applications.

Ready-made robot libraries and sensors in V-Rep can be used, as well as the researcher can create his own functional robot from the design tools tab and add the necessary sensors to the robot. During the simulation, the data of the robot can be exported with graphics. For example; the torque value in a joint of a robot can be exported instantly via graphics.

Webots

Cyberbotics developmented the free robot creation simulator Webots. The Khpera Simulator was created using free source software.

It is a development environment for modeling, programming, and simulating robots. Webots, which enable 3D design, are used in academic studies. It is a simulation software that offers the opportunity to design the physical properties of objects such as mass, joints, friction, shape, texture

close to the real world. Webots has an easy-to-use UI and is a straightforward simulator. An example of the interface screenshot of the Webots simulator is given in Figure 2.

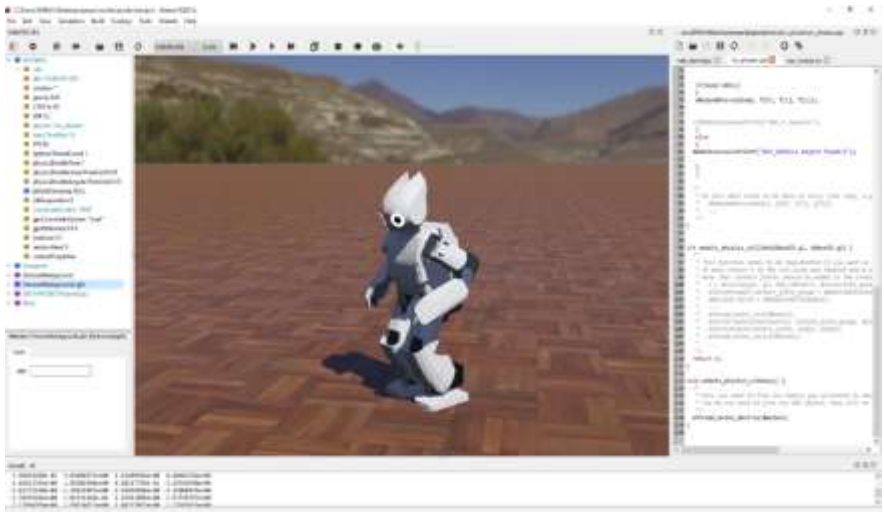

Figure 2: Webots Simulator

The libraries it contains enable for the programming and creation of a wide variety of robots. In the Webots environment, learning and processing sensor data is extremely easy. It can read and quickly process data from sensors such as accelerometer, gyroscope, force/torque sensor, pressure/touch sensor, light sensor, camera, GPS on the robot. It has various functions that can process the data it receives from the sensors because of its libraries.

It allows the robots in Webots to be programmed to work in the real world. With Webots, four-legged, bipedal, wheeled, flying, floating and stationary robots can be programmed and simulated. In the real world, data is noisy.

Webots allows researchers to add the desired noises in the simulation environment through the sensors in the physics libraries it contains. For example; with a physics library, an external force can be applied to the robot.

To conduct robot controls, it can compile programming languages including C/C++, Java, and Python in its own editor. Additionally, it offers the chance to compile the codes here owing to the established MATLAB interface.

With Webots, more than one robot can be programmed and simulated in the same environment. Apart from the robots available in their libraries, the researcher can design his own robot. He can integrate all the sensors he needs into this robot he designed.

The fact that Webots works independently of the operating system provides benefit from to the developers. It is possible to visualize the simulation or create a video recording. Webots is very useful compared to other simulation software with its libraries, powerful sensor and plug-in support, architecture, simple interface, functionality, and ability to compile codes within itself.

Robot Operating System

Robot Operating System (ROS) is an open source software framework for controlling robots. It was developed by the company named Willow Garage after the first studies started at Stanford University. Even though its name says operating system, ROS is not actually an operating system. In order to use the ROS structure, it is necessary to use a Linux-based operating system. It supports many programming languages such as C/C++, Java, Python, Lua, Lisp. In addition to the standard libraries it contains and also incorporates with many libraries created by robot developers and becomes a standard in robot research and development studies.

ROS aims to make the robot do the desired job by making small changes on the codes in an application. In order to make the robot do a job, it is desired to create ready-made code structures in the form of load and use. Instead of rewriting the written code for each robot, ROS aims that the code written once can be run on all similar robots. For example; a standard structure is created, such as being able to access the position information of another robot's engine with the code that we receive the position information of any motor of a robot. The main purpose of ROS is to establish a standard between the programmer and the robot. ROS is fully compatible with Gazebo.

Gazebo

Gazebo software is a three-dimensional dynamic simulation program that allows to develop robotic applications. It is developed as an open source software project by the Open Source Robotics Foundation (OSRF), a non-commercial purpose. Due to its open source code, there is a large community that has developed various tools to develop Gazebo for different purposes.

Since Gazebo uses high quality graphics and interfaces, it allows to create three-dimensional designs that are very similar to the real world. It is possible to design the simulation environment to be built according to the problem we need in the real world. With Gazebo, realistic interior and exterior designs can be made. Creating environments similar to the real world environment allows us to simulate robots more accurately and efficiently. An example of the interface screenshot of the Gazebo simulator is given in Figure 3.

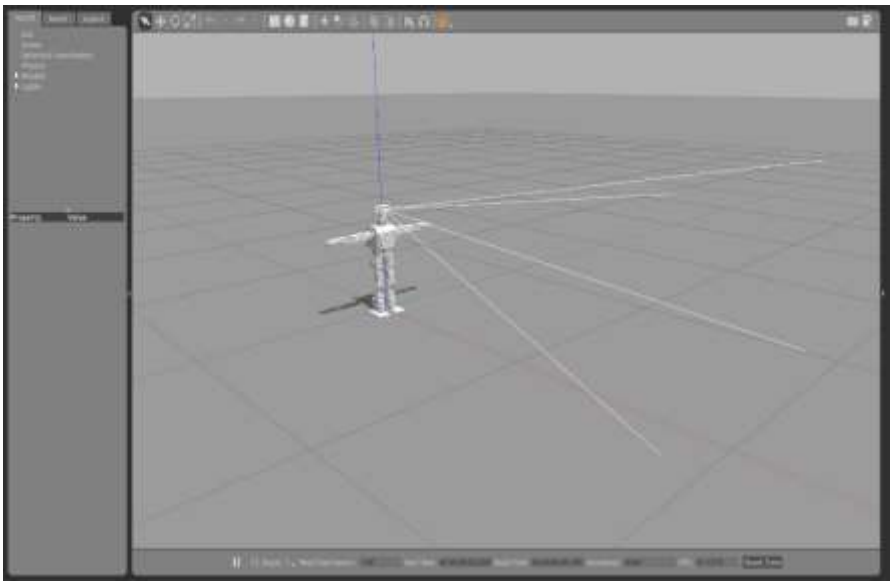

Figure 3: Gazebo Simulator

More than one robot can be simulated at the same time with Gazebo. Gazebo can simulate us with many sensor data such as camera, accelerometer, distance sensor, GPS, LIDAR. Gazebo is a versatile simulator and has plug-in support for significant modifiability.

Gazebo is very fast in creating and testing various robot programs. It is also a very useful simulator in terms of designing robots and performing artificial intelligence applications.

In simulation environments, data is calculated without noise. But in the real world, data is often noisy. Before testing the applications in the real world, tests should be carried out in the simulation environment, taking this into account. Gazebo offers researchers the opportunity to add noises that they may encounter in the physical environment through sensors. Thus, a realistic

simulation can be realized by minimizing the differences between the simulation environment and the real world.

It is also compatible with Robot Operating System (ROS). The connection between Gazebo and ROS is provided through the application programming interface.

MobileSim

It was developed by Active Media company as open source mobile robot development and simulation software. The MobileSim simulator was developed for Pionner robots. Robot control and communication is provided via TCP with ARIA interface. ARIA is an open source library developed with C++ that runs on Linux and Windows operating systems.

Barriers in the simulation environment are defined by lines. These lines can be created with MapperBasic, a free map-based software. The environment created with MapperBasic is saved as a .map file. This saved file is opened with the MobileSim simulator. In Figure 4, an example of the interface screenshot of the MobileSim simulator is given.

MobileSim LIDAR can process many sensor data such as GPS, gyroscope, accelerometer, distance sensor. In the simulation, more than one robot can be simulated at the same time.

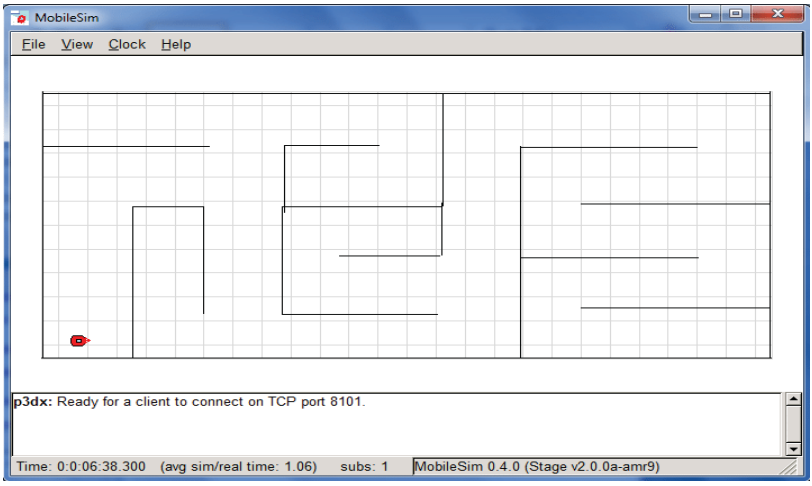

Figure 4: MobileSim Simulator

MATLAB Simulink

MATLAB provides the user with various ready-made algorithms and functions for robotic coding. Robots can be simulated quickly using deep learning algorithms on MATLAB.

MATLAB Simulink offers Model-Based Design and pre-built blocks to use modeling and simulation to program robots. In addition, simulations are created by using Robotics System Toolbox, Navigation Toolbox, ROS Toolbox and many advanced robot tools in MATLAB.

MATLAB Robotics System Toolbox provides tools and algorithms for designing, simulating and testing mobile robots. It contains many ready-made algorithms such as path planning, collision control, mapping, and motion control. MATLAB Navigation Toolbox mapping operations, performing two- and three-dimensional designs. IMU is a tool used to access sensor data such as GPS, distance sensor, accelerometer, gyroscope. It is used in automated driving, robotics, and consumer electronics applications.

It is compatible with MATLAB RIS. Thanks to the ROS blocks in Simulink, the user can access the sensor data and perform operations. Since it contains many ready-made ROS blocks, many operations can be performed with very little code. An example of a simulation screenshot performed with MATLAB Simulink is given in Figure 5.

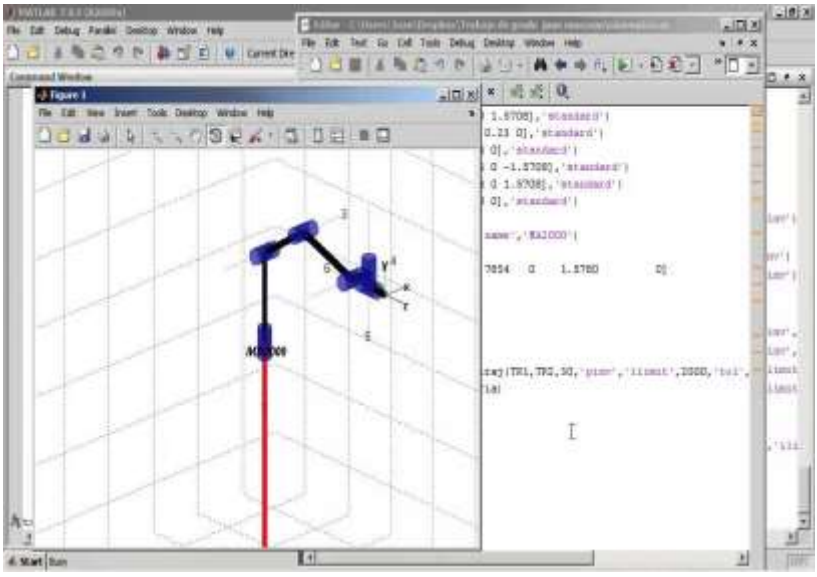

Figure 5: A screenshot example of robot programming in MATLAB Simulink

Robot simulation processes such as prototyping, testing concept models, and robot programming are created via MATLAB. By creating an RIS network over MATLAB Simulink, access to RIS blocks is provided and simulation is performed.

Anykode Simülâtör

Anykode is a commercial 3D robot simulator. Three-dimensional environmental design can be made in the program and it can give real-life responses during the study. In the program, which is offered free of charge for limited software and time for students, there are three commercially available licensing options: Pro, Project and Edu.

Mobile robot design can be done flexibly in the program. In the 3D drawing environment, the motor positions and body structure of the mobile robot can be determined. There are many sensors in the program to provide data flow between the mobile robot and the environment. Robot control software can be developed by adding sensors such as gyroscope, GPS and Lidar to a designed mobile robot. An example of the interface screenshot of the Anykode simulator is given in Figure 6.

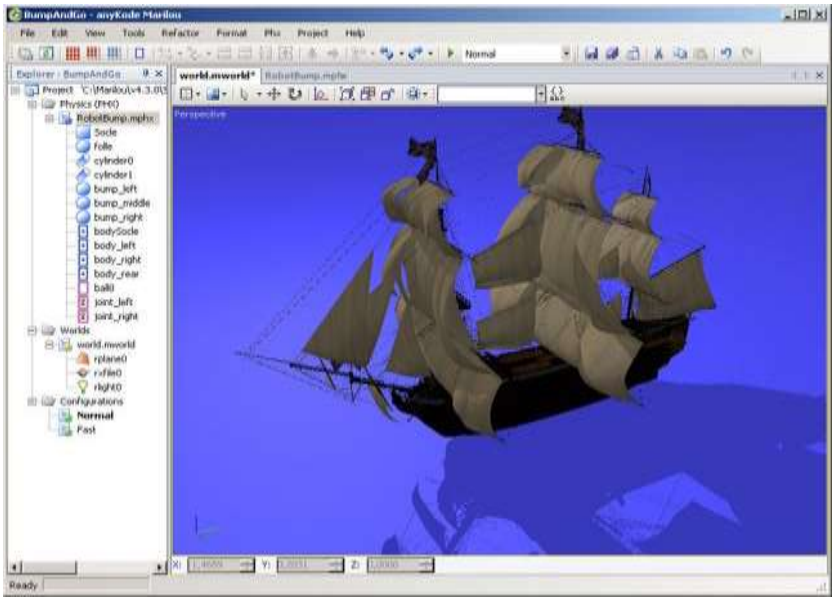

Figure 6: Anycode Simulator

It supports programming languages such as C, C++, C++ CLI, C#, VB# and J#. This mobile robot provides many conveniences for the designer.

In addition, the development of the program with software such as MATLAB, Bonavision iRSP will enable different algorithms to be tested in different software environments. After the development of the control software, the behavior of the robot can be observed in the 3D environment with the compiled program. The program also offers a feature such as sending and receiving physical data from the real world. In this way, real-time studies can be performed.

Simbad 3D Robot Simülâtör

Simbad is a Java-based 3D free robot simulator developed for academic and educational studies. Although 3D designs are not very similar to the real world, it allows the development of artificial intelligence-based autonomous robots with the libraries it contains. There are predefined libraries for many sensors in the simulator. It is necessary to have a good level of Java programming knowledge for robot control. In Figure 7, an example of a simulation screenshot performed with Simbad 3D Robot Simulator is given. The main features of Simbad can be listed as follows.

- 3D design
- Simultaneous programming of one or more robots
- Vision sensors
- Distance sensors
- Contact Sensors
- Swing User interface for control

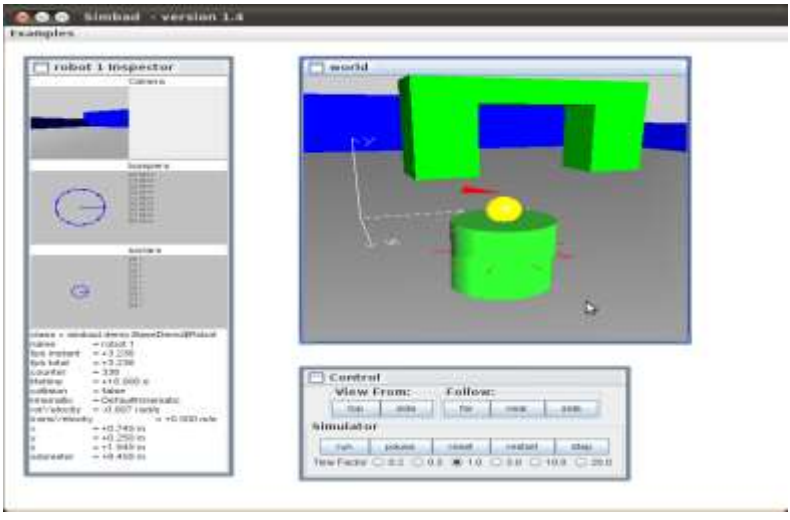

Figure 7: Simbad 3D Robot Simulator

Simbad 3D robot simulator offers developers a simple interface. For users, there are sample codes and documents on the Simbad simulator's own website.

STDR Simulator

It is a free open source robot development simulator based on Linux. 2D designs can be realized with STDR Simulator. It allows programming of multiple robots at the same time. In the software, where a graphical environment is not presented, experiments such as object detection such as maze, wall, and more than one robot simulation can be made. STDR Simulator is compatible with ROS libraries. It uses a ROS-based compiler to compile programs.

It has a simple user-friendly interface. Creating mazes and adding robots can be done easily. In order to perform robot control on this platform, a good degree of programming knowledge is required. It allows users working in a Linux environment to perform operations such as one or more robot communication, control, and collaboration with a simple interface. An example of a screenshot for the STDR Simulator is shown in Figure 8.

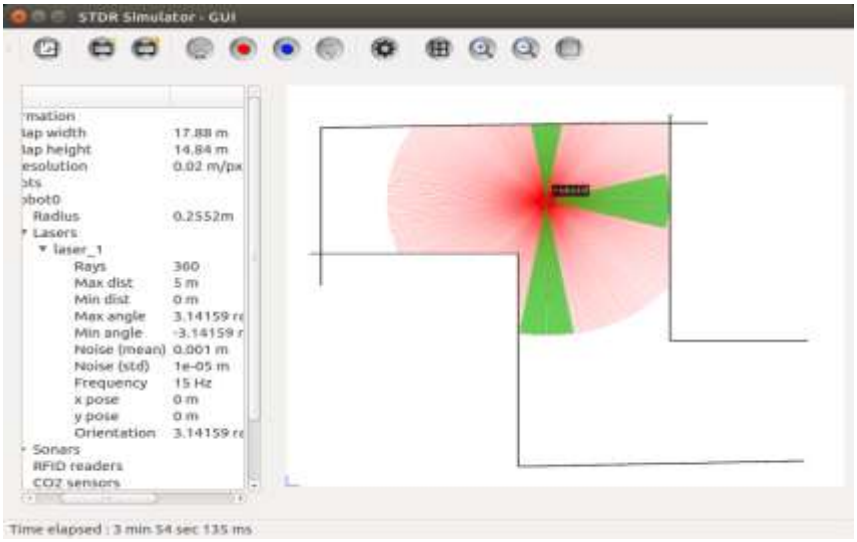

Figure 8: STDR Simulator

Microsoft Robotics Developer Studio

It is a Windows-based robot control simulator developed by Microsoft in 2006. It is developed based on .NET as block programming. This

language, which is created by pre-defining various blocks, is called Visual Programming Language. Contrary to known programming languages, it imposes some limits on environment creation and robot control. This simulator has a ready-made library of many robots. Although the sensor libraries are limited compared to other software, they contain many important sensors. In Figure 9, an example of the interface screenshot of the Microsoft Robotics Developer Studio simulator is given.

Figure 9: Microsoft Robotics Developer Studio

Microsoft Robotics Developer Studio enables 3D design. This simulator, developed by Microsoft, is offered to robot developers free of charge.

CONCLUSION

Thanks to robotic simulators, we can perform preliminary work on robots in a virtual environment. This saves both time and money. Although simulation software offers conveniences in terms of time and cost, these are only an estimate of the real world. These softwares do not completely eliminate the need for real-world testing. Real-world tests are required for environments or unexpected situations that cannot be created in simulations.

REFERENCES

E. Aslan, (2023). "Derin Pekiştirmeli Öğrenme Kullanarak İnsansı Robotlar İçin İtme Kurtarma Kontrol Sisteminin Geliştirilmesi", PhD thesis, Dicle University, Diyarbakır Türkiye

E. Aslan, M. A. Arserim, A. Uçar (2023) "Development Of Push-Recovery Control System For Humanoid Robots Using Deep Reinforcement Learning" Ain Shams Engineering Journal, doi: https://doi.org/10.1016/j.asej.2023.102167

A. Güllü, (2017). "Labirentlerde Yapay Zeka Tabanlı Yön Bulma Algoritmaları Kullanan Bir Gezgin Robot Geliştirilmesi," PhD thesis, Trakya University, Edirne Türkiye

E. Yolal, (2015). "Mobil Robot Simülatörleri Ve İleri Seviyeli Simülasyonlar", Yüksek lisans tezi, İstanbul Teknik Üniversitesi, İstanbul Türkiye

V-Rep Robotic Simulator Testing, Erişim: https://www.youtube.com/watch?v= qPkUhDGXVoY (Erişim Tarihi: 30.03.2023)

Coppelia Robotics, Erişim: https://coppeliarobotics.com/features (Erişim Tarihi: 04.04.2023)

Webots User Guide, Erişim: https://cyberbotics.com/doc/guide/index (Erişim Tarihi: 30.03.2023)

T. Terzimehic, S.Silajdzic, V. Vajnberger, J. Velagic, N. Osmic, (2011). "Path Finding Simulator for Mobile Robot Navigation", 2011 XXIII International Symposium on Information, Communication and Automation Technologies, 27-29 October 2011.

Using Matlab for hardware-in-the-loop prototyping#1: Message passing system, Erişim: https://robohub.org/using-matlab-for-hardware-in-the-loop-prototyping-1-message-passing-systems/ (Erişim Tarihi: 2.04.2023)

AnyKode Simülatör, Erişim: http://www.anykode.com/index.php (Erişim Tarihi: 4.04.2023)

Simbad 3D Robot Simülator, Erişim: https://simbad.sourceforge.net/ (Erişim Tarihi: 4.04.2023)

STDR Simülâtör, Erişim: https://stdr-simulator-ros-pkg.github.io/# (Erişim Tarihi: 4.04.2023)

CHAPTER 4

AN OVERVIEW OF AIRFLOW-BASED MEASURES TO IMPROVE EXHAUST AFTER-TREATMENT THERMAL MANAGEMENT TO REDUCE EMISSION RATES IN DIESEL-DRIVEN VEHICLES

Assist. Prof. Hasan Üstün BAŞARAN[1]

[1] Izmir Katip Celebi University, Faculty of Naval Architecture and Maritime, Naval Architecture and Marine Engineering Department, Izmir, TURKEY.
hustun.basaran@ikcu.edu.tr, 0000-0002-1491-0465.

INTRODUCTION

Currently, highway and marine vessels mostly prefer diesel engines due to low fuel consumption and reliable performance during transportation. Experts estimate that many heavy-duty (HD) vehicles will keep using diesel engines at least in the near future (Lešnik et al., 2020). Many customers tend to use hybrid or electric vehicles year after year due to environmentally friendly performance (Muratori et al., 2021). However, those vehicles are still cost ineffective and diesel engines are predicted to attain over 50% thermal efficiency in a not very distant future (Conway et al., 2021). Therefore, it is undeniable that they will still be favorable for transport. Notwithstanding the considerable efforts for improved fuel economy, at present diesel engines are threatened due to unavoidable tailpipe pollutant rates. Particularly, the engine-out emission rates of nitrogen oxide (NOx) and particulate matter (PM) are accepted as highly dangerous to human health and thus, many environmental bodies around the world such as Environmental Protection Agency (EPA) and European Union (EU) specified stringent restrictions for those contaminants (Dieselnet, US standards, 2023; Dieselnet, EU standards, 2023). Figure 1 depicts explicitly how emission limits for HD engines have lowered from Euro 1 to Euro 6 (Mohan & Badra, 2023). As shown, not only NOx and PM, but also carbon monoxide (CO) and hydrocarbon (HC) emission rates are demanded to be minimized by HD engines. However, limits for NOx and PM rates are especially tightened from Euro 3 to Euro 6 in Figure 1. Future Euro 7 standards can be estimated to demand almost zero NOx and PM rates for HD vehicles.

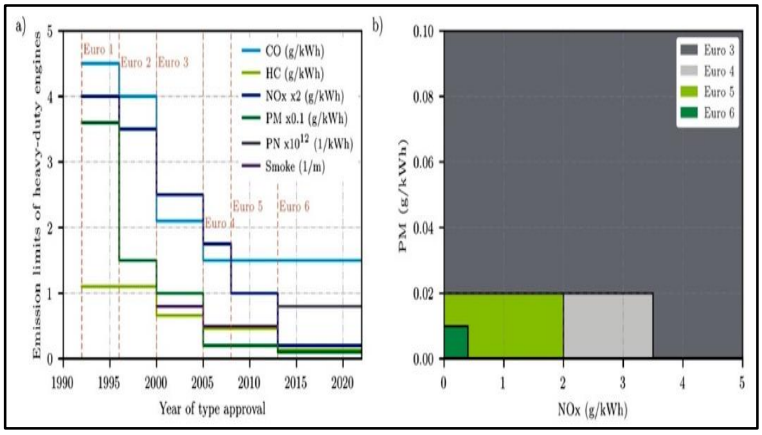

Figure 1: (a) Evolution of European emission standards for heavy-duty engines under steady-state testing, (b) Evolution in NOx and PM emission standards. (Mohan & Badra, 2023)

Given the ever-stricter limits in Figure 1, engine producers and researchers continue to devise new strategies to minimize the engine-out emission rates in diesel vehicles (Joshi, 2022; Xu et al., 2023). Circulating exhaust gas back to the cylinders is one effective technology to curb particularly harmful NOx rates in diesel-driven vehicles (Abd-Alla, 2002). This method is known as exhaust gas recirculation (EGR) as it restricts partially the release of the whole in-cylinder exhaust gas and directs some portion of it back to the engine cylinders. As fresh air is mixed with the recirculated exhaust gas, the temperature inside the cylinders decreases and therefore, NOx rate, which is sensitive to the temperature, is reduced (Agarwal et al., 2011). Another significant and popular method is to utilize alternative fuels for internal combustion engines (Stančin et al., 2020). Hydrogen, ammonia, liquefied natural gas (LNG) and methanol appear to be effective alternative fuels to improve ship carbon reduction in maritime transport (Wang et al., 2023). These non-diesel and non-gasoline fuels are investigated in HD highway vehicles to fulfill the strict emission norms as well (Chen et al., 2018; Geng et al., 2017; Jeyaseelan et al., 2022). In addition to non-conventional fuels, advanced in-cylinder combustion methods are applied to on-road vehicles to constrain the discharge of harmful contaminants into the environment (Imtenan et al., 2014; Bobi et al., 2022). Replacing diesel and gasoline engines in HD vehicles with battery-based driving sources, namely electric or hybrid vehicles, also enables significant reductions in unhealthy emission rates (Bastida-Molina et al., 2020; Shafique et al., 2022). Battery-dependent transport is effective to decrease emission rates. However, currently electric vehicles are cost-ineffective, problematic about long range transport and do not have adequate infrastructure for reliable and steady operation of vehicles (Scrosati et al., 2015). At present, diesel vehicles do not acquire none of those drawbacks. Thus, there is still considerable time for a complete replacement of diesel vehicles with battery-based electric or hybrid vehicles.

The improvement achieved in emission rates via aforementioned strategies is undeniable. However, these methods are generally effective at some definite vehicle operation zones and are in some cases quite insufficient to sustain emission rates within the limits specified in the regulations. Thus, producers predominantly place an exhaust after-treatment (EAT) system in modern HD vehicles to meet highly tight emission norms (Votsmeier et al., 2009). Those systems are normally placed at the outlet of exhaust units in HD

vehicles. EAT systems has the objective of filtering the contaminants inside the engine-exit flow and enable the release of non-hazard exhaust flow to the surrounding. Those systems are generally named as Three-Way Catalytic (TWC) converters since they utilize internal catalysts to complete the filtering process and typically include three main specific units as illustrated in Figure 2 (Papagianni et al., 2022). Those Selective Catalytic Reduction (SCR), Diesel Particulate Filter (DPF) and Diesel Oxidation Catalyst (DOC) units, placed in order from the end of the exhaust system to the very beginning, function to provide under limit carbon monoxide (CO), unburned hydrocarbon (UHC), PM and NOx rates in different types of HD vehicles.

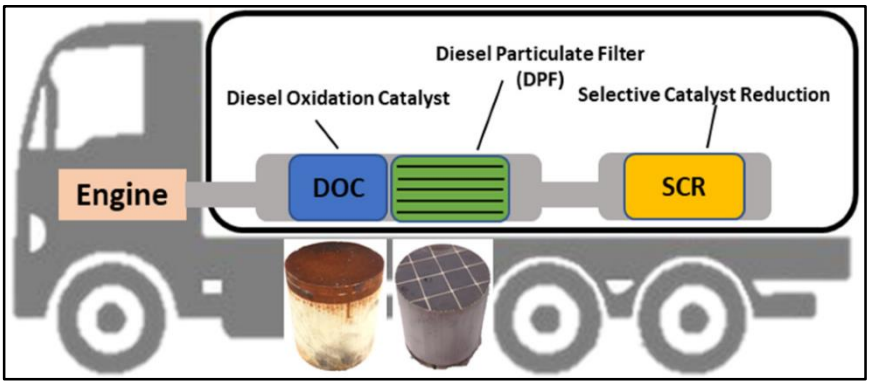

Figure 2: A typical catalytic system in a HD vehicle (Papagianni et al., 2022)

EAT systems are usually competent to bring down the emission rates and meet the strict regulations for current vehicles. However, they are not 100% effective for the entire operation zone of an on-road vehicle or a marine vessel. In order to attain sufficient and steady cleaning of the turbo-out exhaust flow in diesel vehicles, the catalysts inside those components are required to be retained within a definite temperature range (mostly between 250^{o}C – 450^{o}C) (Ye et al., 2012). When different types of selective catalysts are examined in Figure 3, it is explicitly noticed that the temperature at SCR upstream owns a direct impact on the NOx conversion effectiveness of a SCR system (Marathe et al., 2022). The most notable result from the plot is that SCR unit performs extremely poorly, especially as upstream temperature falls below 250^{o}C. Similarly, the poor conversion efficiency is seen when temperature is maintained particularly above 450^{o}C, although not as poor as the one at low temperature. Between those points, the efficiency remains above 90%, which is decent to keep minimized NOx rates in a light-duty (LD)

or a HD vehicle. Considering the different cruise conditions of a vehicle, the upstream temperature may change and go out of this conversion-suitable optimum zone. Therefore, in such cases, harmful pollutants cannot be reduced in a tolerable manner through the EAT systems (Robinson et al., 2013; Wardana & Lim, 2022).

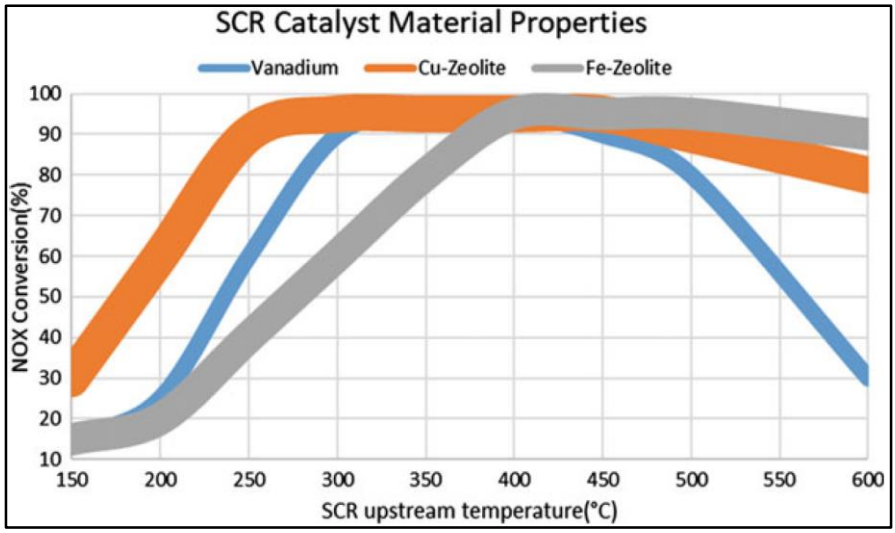

Figure 3: Comparison of operational characteristics selective catalysts (Marathe et al., 2022)

Upstream temperature on a typical EAT system is in most cases directly affected by warmness of engine-out or turbo-out of exhaust gas in diesel powered vehicles. As the hotness of turbo-exit does not exceed 250^{o}C, EAT unit is maintained at low temperature and thus, the system suffers the poor emission conversion, as Figure 3 vividly presents. When the exhaust temperature variation for a typical compression-ignition engine is examined in Figure 4, it is observed that engine-out temperature is not always held at high levels (Garg, 2013). At speeds above 1500 RPM and at relatively high loads, exhaust temperature is reasonably ideal for successful EAT operation. At those cases, the system can maintain low emission rates through a reliable EAT unit. However, particularly at light loads and at speeds below 1500 RPM, the system produces relatively cold exhaust temperatures (< 250^{o}C), and thus, EAT unit is forced to work ineffectively, leading to high emission rates. In this zone, it is difficult to achieve active EAT system unless exhaust temperature is increased in a proper manner.

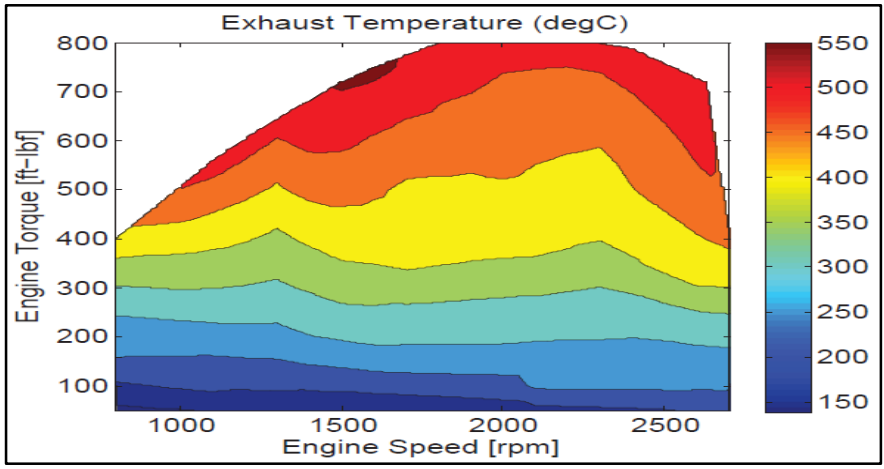

Figure 4: Exhaust temperatures (°C) for Cummins ISB 2010 6.7L engine (Garg, 2013)

When HD vehicles do not have any particular heat-up component such as an afterburner or an electrical heating device near the exhaust unit (Kim et al., 2012; McCarthy Jr et al., 2022), the sole energy source to warm up the EAT system is the exhaust flow heat. Therefore, exhaust temperature at EAT inlet has a paramount role to realize effective EAT units in highway vehicles (Hu et al., 2023; Basaran, 2023).

This study particularly focuses on current airflow-based inner-engine measures to rise exhaust temperature and enhance EAT thermal control in HD diesel vehicles. Those methods are relatively easy to implement in automotive vehicles, as they do not need any external item to be put on the system. The next section goes over briefly those techniques and then, in the following section, positive and negative effects of each method on the engine system are examined in an explicit manner.

1. OVERVIEW OF STRATEGIES

The inner-engine techniques for improved EAT heat management are generally grouped under two main categories: air-based measures and fuel-based measures. At first, it is intended to mention the main characteristics of those techniques in the leading subsections. Although fuel-based methods are briefly revised and mentioned in the text, this study addresses particularly the overview of air-dependent techniques to achieve better EAT thermal control in diesel vehicles.

1.1. Air-Based Methods

Those techniques concentrate on the modulation of airflow in diesel and gasoline engines. Considering the exhaust flow is formed through total air charged into the cylinders and total fuel injected prior to combustion, it is directly affected by the actuation of the airflow in an engine system. The modulation for airflow is mostly achieved via using throttle valves at inlet or exhaust or modifying the intake and exhaust valve timings or disabling some of the active cylinders in the system. Particularly, intake components in an engine system mainly control how high or low the airflow is maintained during operation. They also control the percentage of engine volumetric efficiency, which is directly related to the exhaust temperature. Overall, those throttling-dependent or valve-dependent strategies achieve increased exhaust temperatures through altering the airflow (in most cases decreasing the intake charge flow) in HD engine systems (Mayer et al., 2003; Betz & Eilts, 2019).

1.2. Fuel-Based Methods

The aim of fuel-based methods is similar to those air-based methods mentioned in the previous subsection, namely to improve the exhaust temperature. However, the path they follow is different from air-based measures. Contrary to airflow-dependent methods, fuel-based measures focus on the combustion in compression-ignition or spark-ignition engines. These techniques generally adjust the nominal combustion process to attain high exhaust temperatures. Considering the in-cylinder combustion occurs close to the exhaust phase in a four-stroke diesel engine, it is inevitable that exhaust temperature is influenced by the combustion regulation during operation. It is typically applied delayed fuel injection timing, close or late post-fuel injection to raise exhaust temperature in engine systems (Honardar et al., 2011; Wu et al., 2021). Those strategies usually result in impaired combustion and increased fuel need in the system, thus contributing to an increase in engine-out temperature (Zhang et al., 2022; Ozel et al., 2018). Rising load and speed at idling is also an option to increase fuel consumption and boost exhaust temperature (Gong et al., 2011).

2. AIR-BASED INNER-ENGINE MEASURES

Airflow-dependent measures aim to increase exhaust temperature through adjusting the total air charge into the cylinders. These measures generally need throttling valve opening control or the modulation of engine

valve opening & closing timings or in some cases, appropriate deactivation of certain cylinders of the engine. The airflow-modulating techniques concerning those requirements are mainly examined below.

2.1. Throttle Valve Opening Modulation

One easy-to-implement method for increased exhaust temperature is to actuate the throttle valve opening in diesel and gasoline engine systems. The technique mainly depends on the actuation of either intake throttle or exhaust throttle valve openings. While intake throttle valve is usually positioned right before the inlet ports, exhaust throttle valve is generally put at the downstream of outlet ports in a HD engine system. Opening percentage of those throttle valves has a significant effect on the behavior of in-cylinder airflow (Lyu et al., 2022).

Wu et al. (2020) achieves one of the recent research concerning the impact of intake throttling in a four-stroke six-cylinder compression-ignition engine (Wu et al., 2020). In this work, the researchers examine the influence of intake throttling on engine-out temperature for various engine speeds and loads. It is observed that the rise on exhaust temperature seems to be very slight at low throttling degrees (percentage). However, after a certain degree, the temperature rise accelerates, and up to 123.3^{o}C exhaust temperature increase is possible via using only intake throttling (as illustrated in (a) and (b) of Figure 5). In addition, engine performance at high loads and speeds are generally found to affect exhaust temperature in a positive manner. In most of the cases, exhaust temperature gets higher whenever either load or speed is increased in the system. There is a certain temperature difference between 50 N.m and 600 N.m in Figure 5 (a), which is due to the system's need for extra fuel at high loads compared to low loads. This additional fuel requirement is valid for Figure 5 (b) too. Other researchers find similar results, namely exhaust temperature improvement via intake throttling at different load and speeds, as well (Mayer et al., 2003; Bai et al., 2018).

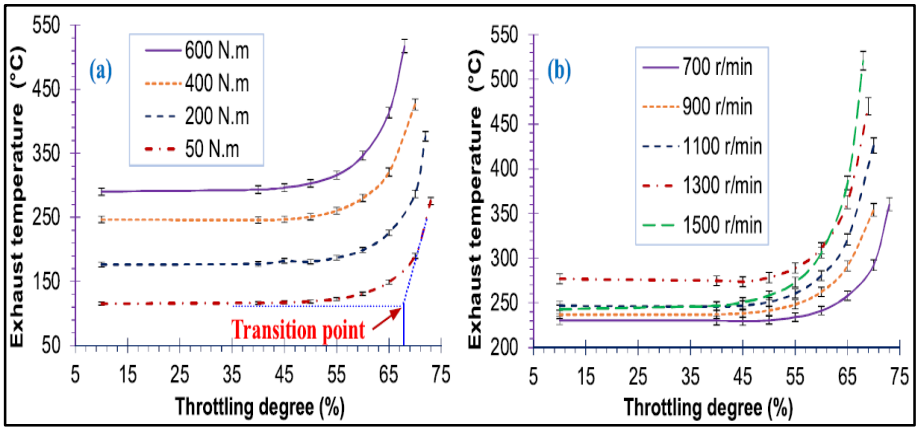

Figure 5: The exhaust temperature dependency on intake throttling degree: (a) under various loads (1100 r/min), (b) under various speeds (400 N.m) (Wu et al., 2020)

In addition to intake throttling, exhaust throttling is investigated to enhance exhaust temperature in compression-ignition engines (Bawache et al., 2020). Nie et al. (2022) explores the potential of different thermal management measures, including exhaust throttling, on exhaust temperature, fuel consumption and also SCR NOx conversion efficiency in a four-stroke inline four-cylinder diesel engine (Nie et al., 2022). In this work, it is observed that exhaust throttling causes fuel consumption penalty. However, it also results in significant exhaust temperature rise, as indicated in Figure 6 (a) and (b). As turbine outlet pressure is raised up to 25 kPa in increments of 5 kPa, that is, exhaust flow is throttled at turbine inlet, exhaust temperature is seen to be steadily rising both for 1400 RPM and 2200 RPM engine speeds. Not only does the study examine exhaust throttling, but also effect of altitude on exhaust temperature, as seen in Figure 6. At high altitudes (both 1000 m and 2000 m), exhaust temperature is higher than the nominal altitude level (0 m) since engine air flow rate decreases at high altitudes and causes relatively richer mixtures inside the cylinders.

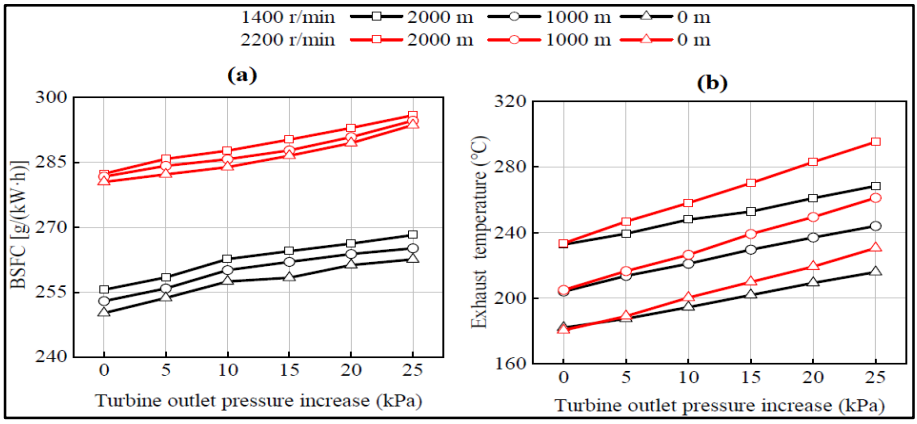

Figure 6: The effect of exhaust throttling on (a) fuel consumption and (b) exhaust temperature at different speeds and altitudes (Nie et al., 2022)

It is derived from the results that both intake and exhaust throttling can noticeably elevate exhaust temperature in diesel engines at several speeds and loads. However, both methods also lead to fuel consumption penalty, which generally restricts the application at particularly low speeds and low loads due to high exhaust temperature rise need at those cases. As such, high fuel inefficiency is inevitable at low loads. Intake & exhaust throttling seems to be proper to use at medium speeds and loads, as relatively low temperature rise and thus, low fuel penalty is required at those cases.

2.2. Variable Valve Timing (VVT)

VVT is already an effective strategy in automotive vehicles for enhanced fuel economy and improved emission rates (De Ojeda, 2010). However, it is recently used in diesel engines, as a successful alternative method, to improve the EAT thermal management (Maniatis et al., 2019). VVT is mostly implemented via actuating the on and off timings of engine valves. Obviously, there are certain opening and closure timings for both intake and exhaust valves in an engine system. Normally those timings are kept constant in a traditional cam system. However, those opening and closing timings can be either delayed or advanced in a modern variable valve actuation system. Thus, it is possible to modulate the fresh airflow at intake ports or engine-out flow at exhaust ports or the fraction of in-cylinder residual exhaust gas through altering the nominal valve timings. Exhaust temperature is highly sensitive to those in and out of cylinder flow modulations and can be determined via reasonable control of valves. As such, VVT is currently a

reliable technology to elevate exhaust temperature in compression-ignition engines (Shipp & Dane, 2021).

One effective VVT technique to boost exhaust temperature is to implement delayed intake valve closure (DIVC) (Basaran & Ozsoysal, 2017). In this mode, nominal intake closure is moderately or aggressively retarded to lower the total charged intake air and thus, obtain fuel-rich in-cylinder mixture. Garg et al. (2016) explores the impact of DIVC and early intake closure through experiments in a 4-stroke 6-cylinder HD diesel engine (Garg et al., 2016). As seen in Figure 7, EAT inlet temperature, namely turbine out temperature (TOT), can exceed 250^{o}C at a light load condition when either late or early valve closure (LIVC or EIVC) is maintained in the system. That temperature rise is essential to keep active EAT unit and thus, low NOx rates. The study also mentions that this particular VVT method leads to minimized pumping losses and thus, fuel efficiency in the system, which can enable further reduction in NOx rates at low loads.

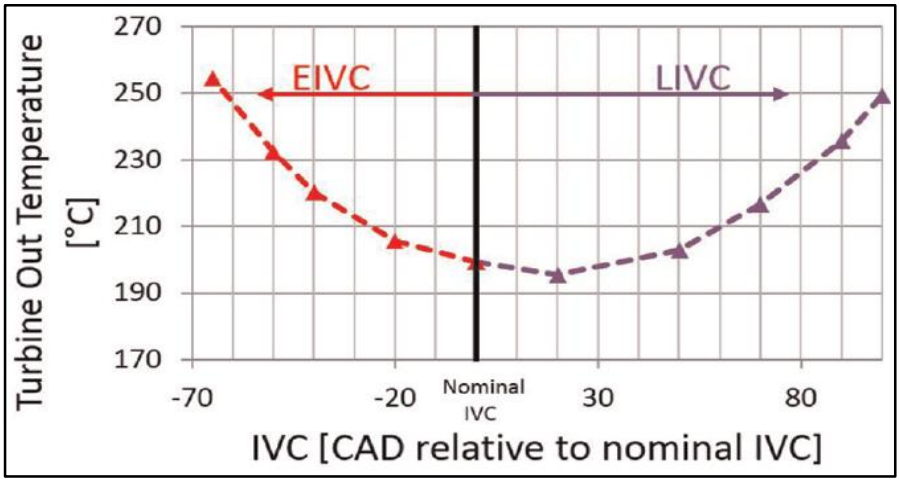

Figure 7: Exhaust gas temperatures along EIVC and LIVC sweeps at 1200 RPM, 2.5 bar BMEP (Garg et al., 2016)

Another successful VVT technique, early exhaust valve opening (EEVO), can be adopted to yield high exhaust temperature in diesel engines. This strategy does not directly affect the intake flow; however, it has a significant effect on exhaust flow. As exhaust is released earlier, that is, the nominal EVO timing is advanced, there is generally seen a decrease on the useful expansion work produced in the engine system (Piano et al., 2017). Thus, it is inevitable that more waste work (as exhaust energy) is allowed to

leave the system in EEVO mode.

In most cases of EEVO application, fuel consumption is raised to sustain constant engine load, which further rises the exhaust temperature. The improved engine-out temperature is generally attributed to the fuel-rich mixture due to high fuel inefficiency and high fuel-to-air ratio (FAR) during the combustion process in the cylinders (Arnau et al., 2021). Increased FAR, particularly through extra fuel injection, is prone to induce high exhaust temperature.

Basaran (2020) implements not only EEVO and but also late EVO (LEVO) in a simulation work and achieves exhaust temperature above 250°C at a low-loaded diesel engine (Basaran, 2020). It is indicated in this study, as shown in Figure 8, that it is possible to accelerate the exhaust temperature via either advanced or delayed exhaust opening. Although both approaches are helpful to stimulate the EAT warm up, the operation is faced with increased fuel penalty (up to 20%), which is likely to rise CO and PM rates. Thus, further research is required for this technology to limit the high fuel penalty.

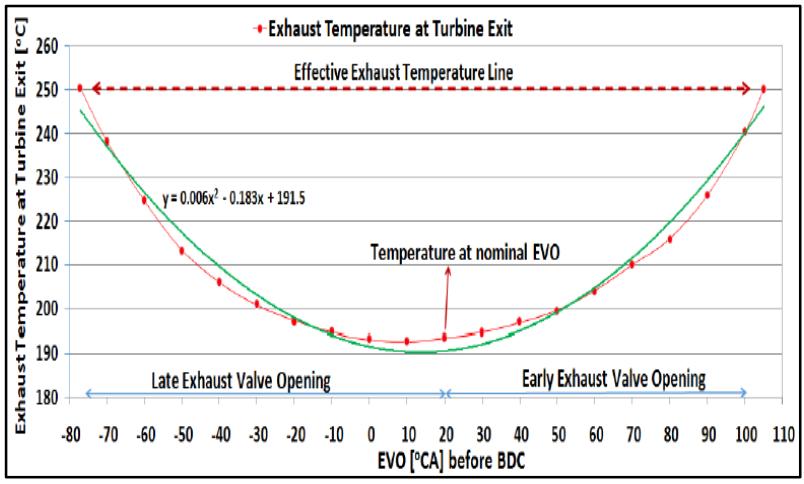

Figure 8: Effect of EVO modulation on exhaust temperature at 1200 RPM engine speed and 2.5 bar BMEP engine load (Basaran, 2020)

Aside from the aforementioned VVT-alone methods, combining VVT with other techniques, such as delayed fuel injection, is investigated to obtain high exhaust temperature (Basaran, 2022). VVT is certainly practical to increase the temperature before the EAT inlet; however, it cannot alone satisfy the required temperature rise at all loads. Guan et al. (2020) quantifies

the potential of the joined application of LIVC, EGR and post-fuel injection on engine emission rates and exhaust gas temperature (EGT) (Guan et al., 2020). In essence, multiple inner-engine methods are implemented to further increase engine-out temperature and improve emission rates. Figure 9 points out that much higher EGT and thus, much lower NOx can be maintained as long as Miller cycle through LIVC is co-applied properly with late start of injection (SOI) and EGR. It is seen that EGR is slightly effective on EGT; however, it enables much lower NOx rates compared to that achieved in non-EGR mode. Thus, it is vital to combine EGR with an inner-engine thermal management measure to minimize emission rates.

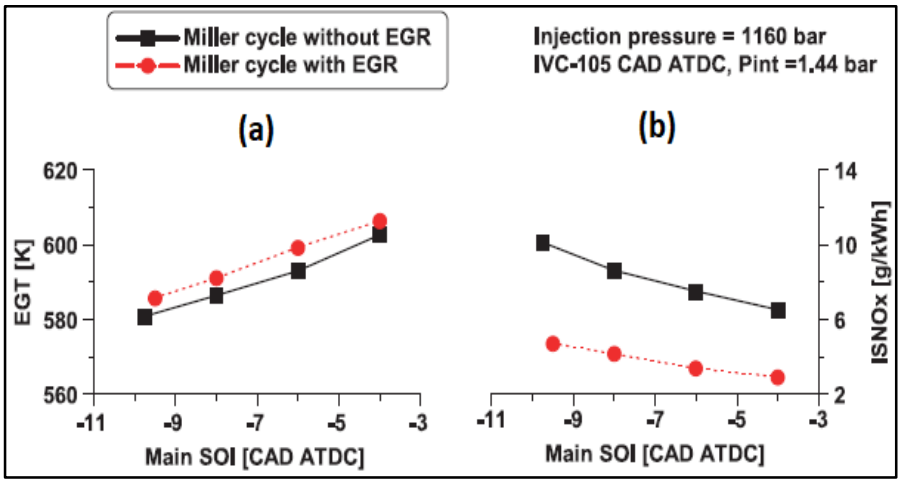

Figure 9: The effect of Miller cycle combined with delayed SOI and EGR on (a) EGT and (b) ISNOx rates (Guan et al., 2020)

2.3. Cylinder Deactivation

Another effective air path technique to control exhaust temperature is to utilize cylinder deactivation (CDA) in engine systems (Hushion et al., 2022). In fact, this strategy can be seen as a particular version of VVT method. Rather than modulating valve timings in all cylinders, engine valves are completely switched off for some of the cylinders of a multi-cylinder diesel engine. CDA also requires the fuel injection cut off in those cylinders. The objective is to reduce air-to-fuel ratio (AFR) through higher fuel injection in active cylinders, and thus, elevate exhaust temperature at low loads (Basaran, 2018). Overall, the engine system is performed with the similar power output, but with lower active cylinders compared to the baseline

condition. The piston still moves up and down inside the passive cylinders. However, it does not transmit any power to crankshaft since there is not a considerable pressure rise inside those disabled cylinders to produce any useful work.

McCarthy (2017) implements CDA in a six-cylinder compression-ignition engine system with the primary objective of improving EAT thermal management (McCarthy, 2017). The experiments are achieved at different speeds & loads for both nominal, namely full engine (6-cylinder active), and CDA, namely half engine (3-cylinder active), operation modes. Figure 10 demonstrates the benefit of CDA for both after-treatment and brake specific fuel consumption (BSFC) at 1000 rpm engine speed.

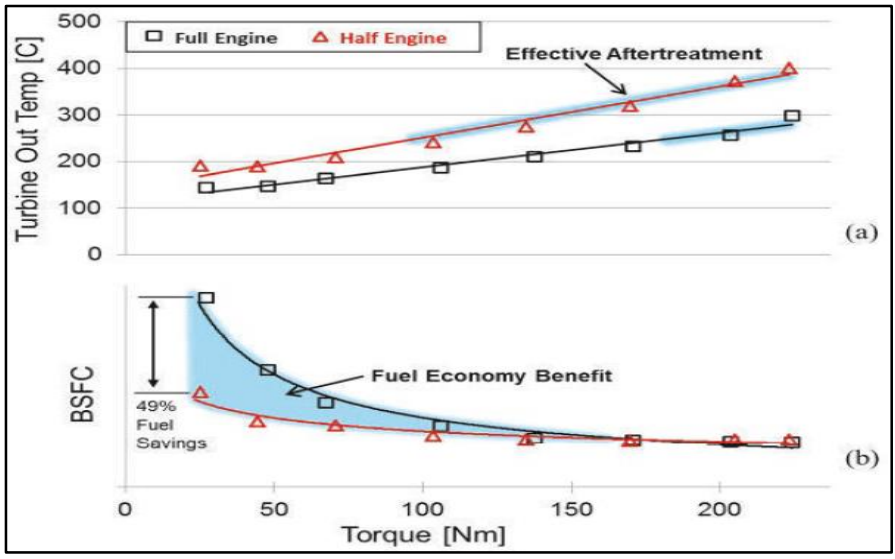

Figure 10: Effect of CDA on (a) Turbine Out Temperature and (b) BSFC as a function of Torque (Nm) at 1000 rpm (McCarthy, 2017)

It is seen in Figure 10 that at full engine case, effective EAT (250^{o}C turbine out temperature) can only be attained at engine loads (as torque) above 190 Nm, which is unfortunate since a high portion of engine load zone is prone to ineffective EAT performance. However, in CDA case, the turbine out temperature is held above 200^{o}C almost at all loads and more importantly, EAT is effective (250^{o}C turbine out temperature) for loads above 90 Nm, which is much lower than the one achieved in full engine case. It is derived that CDA mode can limit the ineffective operation of EAT unit to a lower engine loading range compared to nominal engine mode. Moreover, BSFC is

enhanced up to 49% via CDA at particularly low loads, as seen in Figure 10. That decreased fuel consumption is no doubt highly useful to improve NOx and CO rates even more at those loads, along with elevated exhaust temperatures.

CDA not only has positive effects on the maintenance of exhaust unit at high temperature, but it also significantly contributes to fuel efficiency. Thus, it seems to be a perfect practical solution for inefficient EAT at low loads. However, it is generally difficult to implement CDA in an engine system. It requires transition from full engine mode to CDA mode and vice versa, probably through a controller maintaining valves and fuel injection in disabled cylinders (Gosala et al., 2017; Joshi et al., 2018). Those complicated systems certainly rise the cost in engine production, which is not desirable for both customers and manufacturers. Also, when some cylinders are deactivated, the cylinder combustion order is altered and the engine system is mostly faced with noise, vibration and harshness (NVH). Those obstacles are not easy to handle and can worsen the comfortability in HD vehicles. Overall, every technology comes with some drawbacks. Therefore, researchers continue to overcome the high cost and undesired NVH in CDA operation (Fridrichova et al., 2021).

2.4. Internal Exhaust Gas Recirculation

An effective method to maintain the in-cylinder temperature in diesel engines is to control the amount of recirculated exhaust gas into the cylinders. That is normally applied through either external or internal EGR. External EGR needs the flow of exhaust gas through pipes and thus, some heat is inevitably lost to the surrounding during the process. However, internal EGR (IEGR) is also possible in diesel engines. IEGR is enabled via reasonable control of valve overlap (duration in which intake and exhaust valves are both open) during operation. To retain greater amounts of residual in-cylinder exhaust gas before the next engine cycle, intake opening is delayed and exhaust release is advanced, corresponding to negative valve overlap (NVO), through multi-VVT operation (Basaran, 2019). It is usually feasible to yield high exhaust temperature via NVO since it induces the mixture of residual hot gas with the fresh charge and improves the in-cylinder temperature. Particularly when it is combined with EEVO, it not only achieves much higher EAT inlet temperatures, but also provides fuel-saving performance

compared to EEVO-alone mode through reducing the in-cylinder mass to be heated (Gosala et al., 2018).

Joshi et al. (2022) specifically examines how effective the IEGR method is for improving EAT heat-up and thermal control at idle state in a diesel engine system (Joshi et al., 2022). IEGR is attained in two different manners in this work: using NVO via controlled VVT and using exhaust gas reinduction via reopening of exhaust valves during intake process of the engine. In fact, one of the objective of the study is to compare those particular IEGR strategies. Figure 11 shows how those specific IEGR modes affect turbine out temperature (TOT) and exhaust flow rate considering the fuel penalty suffered in the system.

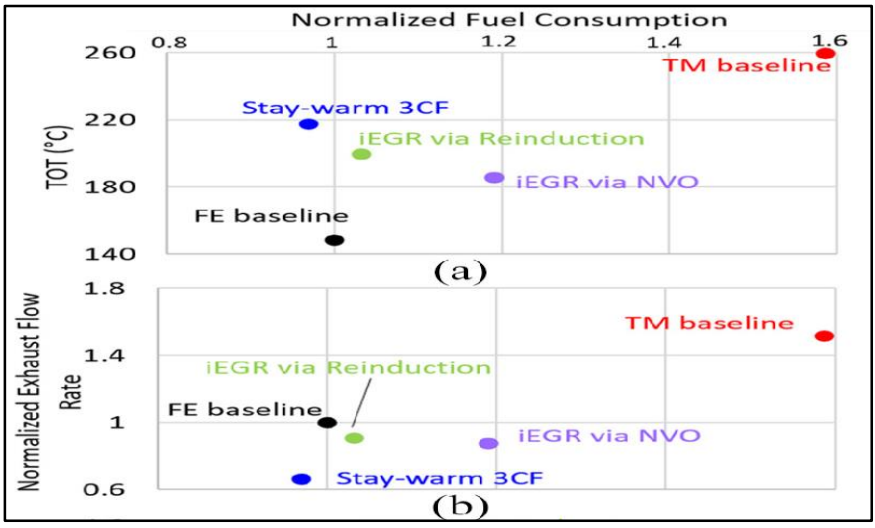

Figure 11: Effect of different IEGR techniques on (a) TOT and (b) Normalized exhaust flow rate at 800 RPM and 1.3 bar BMEP (Joshi et al., 2022)

IEGR via reinduction seems to be superior to IEGR via NVO as it causes lower fuel penalty and can keep TOT above 200°C, which IEGR via NVO fails to achieve. It also has similar exhaust flow rate compared to both baseline and IEGR via NVO conditions. Conventional thermal management (TM baseline) and stay-warm 3CF (3-cylinder active operation) is more effective at rising TOT. Nevertheless, those methods either cause undesirable fuel penalty or a significant reduction in exhaust rate, which mostly worsens the EAT unit get-warm period. Also, it is derived that IEGR via reinduction decreases NOx rates with better fuel efficiency in comparison to other methods due to decreased airflow and heat loss and thus, it is a favorable

option to maintain high EAT temperature at idling conditions (Joshi et al., 2022).

2.5. Cylinder Cutout

Another alternative air path strategy for active EAT thermal management is to provide cylinder cutout (CCO) in an engine system (Gosala et al., 2021). CCO is actually very similar to CDA technique in operation. However, there are some differences as well. CDA closes all valves completely at passive cylinders, along with a complete cut off of the fuel injection. Unlike CDA operation, in CCO mode, valves are not switched off at passive cylinders; they still perform similar to the baseline condition. The system only halts the fuel injection in passive cylinders. In those cylinders, the piston goes upward and downward without any combustion. Only fresh air is compressed and released inside the cylinders and eventually discharged into the exhaust unit at the end of the cycle. A comparison of those two methods is indicated in a six-cylinder diesel engine in Figure 12 (Vos et al., 2019).

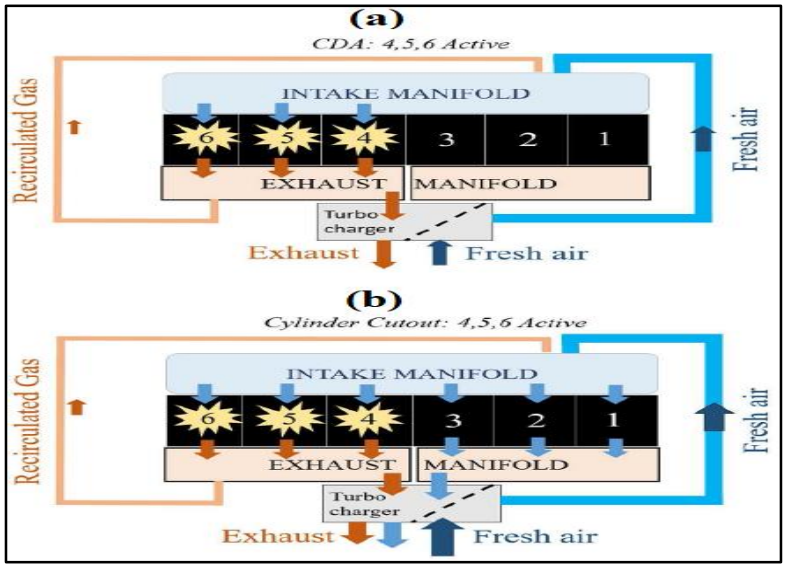

Figure 12: Comparison of the processes of (a) CDA and (b) Cylinder Cutout in a six-cylinder turbocharged diesel engine system (Vos et al., 2019)

As seen in Figure 12, unlike CDA, CCO allows mass flow in and out of the passive cylinders (1, 2, and 3), in which no combustion takes place. One can predict that CCO is relatively less complex compared to CDA as it does not need to modulate either intake or exhaust valves in passive cylinders,

which is one of the requirements of CDA mode. However, a similar advantage cannot be considered for fuel consumption since fresh air charging and discharging in passive cylinders during CCO operation rises the pumping loss, which is not valid for CDA mode. It seems that CCO is prone to increase fuel penalty, but also is likely to reduce the technical difficulty and cost compared to CDA method.

Vos et al. (2019) quantifies the particular benefits of CDA and CCO methods for EAT thermal management in a diesel engine at curb idle (Vos et al., 2019). As illustrated in Figure 13, various CDA and CCO techniques are implemented to raise TOT while exhaust flow and BSFC are considered. It is shown that conventional thermal management (TM Baseline) has the highest fuel penalty and thus, is disadvantageous. However, CDA and CCO modes are able to yield comparable TOT rise with improved fuel penalty. CDA mode is particularly attractive as it can elevate TOT more than 100^{o}C with the minimum fuel consumption. However, it also significantly decreases exhaust flow rates and thus, is prone to decelerate EAT get-warm process. Unlike CDA mode, CCO mode reduces exhaust flow rates moderately while it can still keep TOT above 220^{o}C, which is more helpful to improve EAT get-hot process. Overall, passivating the cylinders (2, 3 or even 4 cylinders) in a multi-cylinder diesel engine has certain benefits for rapid EAT warm up through increased TOTs.

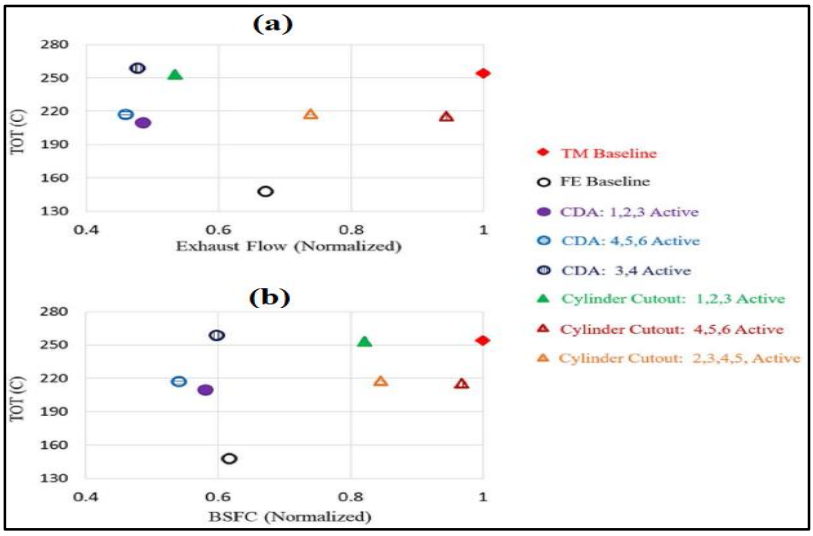

Figure 13: Impact of different CDA and CCO techniques on (a) TOT and exhaust flow and (b) TOT and BSFC at 800 RPM and 1.3 bar BMEP (Vos et al., 2019)

CONCLUSIONS

In this study, some current engine-dependent methods to improve diesel after-treatment thermal management are investigated. Those techniques are generally placed under two basic groups: airflow-dependent and fuel-dependent techniques. This survey mainly provides an overview of airflow-dependent techniques; but fuel-dependent methods are concisely mentioned as well.

Intake and exhaust throttling can be simply applied to attain high exhaust temperatures via controlling the opening area of throttling valves. However, those strategies mostly induce high fuel penalty and reduce the exhaust rates, which adversely affects EAT unit warm up.

VVT is hard to produce, yet it is highly promising to boost EAT inlet temperature. Particular VVT modes, namely EIVC and LIVC, improve engine fuel economy via enhanced pumping loss as well. However, they impair the EAT get-warm process due to decreased exhaust rates. Also, other VVT methods such as EEVO and LEVO require undesirable fuel consumption rise (above 20%) to improve the temperature at turbine-exit. However, those two methods are preferable to EIVC and LIVC as they indirectly affect airflow (in some cases slight, but generally no significant effect) and are able to produce both high TOTs and high exhaust flow rates. Thus, they certainly have the highest potential to enhance EAT get-hot process within all VVT techniques.

IEGR through NVO and IEGR through exhaust valve reopening can be seen as alternative VVT methods to keep exhaust temperatures at high levels. Both methods are preferable to external EGR due to low exhaust heat loss during recirculation and thus, high temperature rise potential. Particularly, IEGR via exhaust valve reopening is favorable since it raises TOT with lower fuel penalty compared to IEGR via NVO.

CDA and CCO are technically difficult to maintain yet have notable potential to elevate TOTs. In most cases (particularly at low loads), they are fuel saving as well. Those techniques are found to be favorable for the improvement of EAT stay-warm process due to high exhaust temperatures (> 250^{o}C). However, similar to EIVC, LIVC and intake throttling, they highly diminish exhaust rates and thus, are mostly inadequate to enhance EAT get-warm process. They need to be combined with other techniques such as EEVO, LEVO or IEGR in order to improve both EAT get-hot and EAT stay-hot processes in a diesel engine system.

REFERENCES

Abd-Alla, G. H. (2002). Using exhaust gas recirculation in internal combustion engines: a review. Energy Conversion and Management, Vol. 43(8), pp. 1027-1042.

Agarwal, D., Singh, S. K., & Agarwal, A. K. (2011). Effect of Exhaust Gas Recirculation (EGR) on performance, emissions, deposits and durability of a constant speed compression ignition engine. Applied energy, Vol. 88(8), pp. 2900-2907.

Arnau, F. J., Martin, J., Pla, B., & Aunon, A. (2021). Diesel engine optimization and exhaust thermal management by means of variable valve train strategies. Int. J. Eng. Res., Vol. 22(4), pp. 1196-1213.

Bai, S., Han, J., Liu, M., Qin, S., Wang, G. & Li, G. X. (2018). Experimental investigation of exhaust thermal management on NOx emissions of heavy-duty diesel engine under the world Harmonized transient cycle (WHTC). Appl. Therm. Eng., Vol. 142, pp. 421-432.

Basaran, H. U. & Ozsoysal, O. A. (2017). Effects of application of variable valve timing on the exhaust gas temperature improvement in a low-loaded diesel engine. Appl. Therm. Eng., Vol. 122, pp. 758-767.

Basaran, H. U. (2018). FUEL-SAVING EXHAUST AFTER-TREATMENT MANAGEMENT ON A SPARKIGNITION ENGINE SYSTEM VIA CYLINDER DEACTIVATION METHOD. Isı Bilimi ve Tekniği Dergisi, Vol. 38(2), pp. 87-98.

Basaran, H. U. (2019). Improving exhaust temperature management at low-loaded diesel engine operations via internal exhaust gas recirculation. Dokuz Eylül Üniversitesi Mühendislik Fakültesi Fen ve Mühendislik Dergisi, Vol. 21(61), pp. 125-135.

Basaran, H. U. (2020). Utilizing exhaust valve opening modulation for fast warm-up of exhaust after-treatment systems on highway diesel vehicles. International Journal of Automotive Science and Technology, Vol. 4, No. 1, pp. 10-22.

Basaran, H. U. (2022). Late Fuel Injection Combined with Retarded Intake Valve Closure for Improved Exhaust System Warm-up in Diesel Automotive Vehicles. Sustainability of Natural Resources' Efficiency, pp. 33-60.

Basaran, H. U. (2023). Enhanced Exhaust After-treatment Warmup in a Heavy-Duty Diesel Engine System via Miller Cycle and Delayed

Exhaust Valve Opening. Energies, Vol. 16(12), p. 4542. DOI: 10.3390/en16124542

Bastida-Molina, P., Hurtado-Perez, E., Penalvo-Lopez, E. & Moros-Gomez, M. C. (2020). Assessing transport emissions reduction while increasing electric vehicles and renewable generation levels. Transportation Research Part D: Transport and Environment, Vol. 88, p. 102560.

Bawache, K.,Chila, S., Balasubramanian, K. & Rohokale, D. (2020). Selection of Different Strategies of Exhaust Gas Thermal Management for Optimum Fuel Economy. SAE Technical Paper No. 2020-28-0339.

Betz, M. & Eilts, P. (2019). Optimization of the Exhaust Aftertreatment System of a Heavy Duty Diesel Engine by Means of Variable Valve Timing. SAE Technical Paper No. 2019-24-0143.

Bobi, S., Kashif, M., & Laoonual, Y. (2022). Combustion and emission control strategies for partially-premixed charge compression ignition engines. A review. Fuel, Vol. 310, 122272.

Chen, Y., Ma, J., Han, B., Zhang, P., Hua, H., Chen, H. and Su, X. (2018). Emissions of automobiles fueled with alternative fuels based on engine technology: A review. Journal of Traffic and Transportation Engineering (English Edition). Vol. 5(4), pp. 318-334.

Conway, G., Joshi, A., Leach, F., Garcia, A. & Senecal, P. K. (2021). A review of current and future powertrain technologies and trends in 2020. Transportation Engineering, Vol. 5, p. 100080.

De Ojeda, W. (2010). Effect of variable valve timing on diesel combustion characteristics. SAE Technical Paper No. 2010-01-1124.

Dieselnet, EU standards. http://www.dieselnet.com/standards/eu/hd.php#stds (Retrieved: 11.04.2023)

Dieselnet, US standards. http://www.dieselnet.com/standards/us/hd.php#stds (Retrieved: 11.04.2023)

Fridrichova, K., Drapal, L., Voparil, J. & Dlugos, J. (2021). Overview of the potential and limitations of cylinder deactivation. Renewable and Sustainable Energy Reviews, Vol. 146, p. 111196.

Garg, A. (2013). Exhaust thermal management using intake valve closing modulation. PhD dissertation, Purdue University.

Garg, A., Maggee, M., Ding, C., Roberts, L., Shaver, G., Koeberlein, E., Shute, R., Koeberlein, D., McCarthy Jr, J. & Nielsen, D. (2016). Fuel-efficient exhaust thermal management using cylinder throttling via

intake valve closing timing modulation. Proceedings of the Institution of Mechanical Engineers, Part D: Journal of Automobile Engineering, Vol. 71, pp. 470-478.

Geng, P., Cao, E., Tan, Q. and Wei, L. (2017). Effects of alternative fuels on the combustion characteristics and emission products from diesel engines: A review. Renewable and Sustainable Energy Reviews, Vol. 71, pp. 523-534.

Gong, C., Huang, K., Deng, B. & Liu, X. (2011). Catalyst light-off behavior of a spark-ignition LPG (liquefied petroleum gas) engine during cold start. Energy, Vol. 36(1), pp. 53-59.

Gosala, D. B., Allen, C. M., Ramesh, A. K., Shaver, G. M., McCarthy Jr, J., Stretch, D., Koeberlein, E. & Farrell, L. (2017). Cylinder deactivation during dynamic diesel engine operation. Int. J. Eng. Res., Vol. 18(10), pp. 991-1004.

Gosala, D. B., Ramesh, A. K., Allen, C. M., Joshi, M. C., Taylor, A. H., Van Voorhis, M., Shaver, G. M., Farrell, L., Koeberlein, E., McCarthy Jr, J. & Stretch, D. (2018). Diesel engine aftertreatment warm-up through early exhaust valve opening and internal exhaust gas recirculation during idle operation. Int. J. Eng. Res., Vol. 19(7), pp. 758-773.

Gosala, D. B., Shaver, G. M., McCarthy Jr, J. E. & Lutz, T. P. (2021). Fuel-efficient thermal management in diesel engines via valvetrain-enabled cylinder ventilation strategies. Int. J. Eng. Res., Vol. 22(2), pp. 430-442.

Guan, W., Pedrozo, V. B., Zhao, H., Ban, Z. & Lin, T. (2020). Miller cycle combined with exhaust gas recirculation and post-fuel injection for emissions and exhaust gas temperature control of a heavy-duty diesel engine. Int. J. Eng. Res., Vol. 21(8), pp. 1381-1397.

Honardar, S., Busch, H., Schnorbus, T., Severin, C., Kolbeck, A. F. & Korfer, T. (2011). Exhaust temperature management for diesel engines assessment of engine concepts and calibration strategies with regard to fuel penalty. SAE Technical Paper No. 2011-24-0176.

Hu, J., Wu, Y., Liao, J., Cai, Z. & Yu, Q. (2023). Heating and storage: A review on exhaust thermal management applications for a better trade-off between environment and economy in ICEs. Appl. Therm. Eng., Vol. 220, 119782.

Hushion, C., Thiruvengadam, A., Pondicherry, R., Thompson, G., Baltrucki, J., Janak, R., Lee, J. & Farrell, L. (2022). Investigating cylinder deactivation as a low fuel-penalty thermal management strategy for

heavy-duty diesel engines. Frontiers in Mechanical Engineering, Vol. 8, p. 987170.

Imtenan, S., Varman, M., Masjuki, H. H., Kalam, M. A., Sajjad, H., Arbab, M. I. & Fattah, I. R. (2014). Impact of low temperature combustion attaining strategies on diesel engine emissions for diesel and biodiesels: A review. Energy Conversion and Management, Vol. 80, pp. 329-356.

Jeyaseelan, T., Ekambaram, P., Subramanian, J., & Shamim, T. (2022). A comprehensive review on the current trends, challenges and future prospects for sustainable mobility. Renewable and Sustainable Energy Reviews, Vol. 157, 112073.

Joshi, M., Gosala, D., Allen, C., Srinivasan, S., Ramesh, A., VanVoorhis, M., Taylor, A., Vos, K., Shaver, G., McCarthy Jr, J., Farrell, L. & Koeberlein, D. (2018). Diesel engine cylinder deactivation for improved system performance over transient real-world drive cycles. SAE Technical Paper No. 2018-01-0880.

Joshi, M. C., Shaver, G. M., Vos, K., McCarthy Jr, J. & Farrell, L. (2022). Internal exhaust gas recirculation via reinduction and negative valve overlap for fuel-efficient aftertreatment thermal management at curb idle in a diesel engine. Int. J. Eng. Res., Vol. 23(3), pp. 369-379.

Joshi, A. (2022). A Review of Emissions Control Technologies for On-Road Vehicles. Engines and Fuels for Future Transport, pp. 39-56.

Kim, C. H., Paratore, M., Gonze, E., Solbrig, C. & Smith, S. (2012). Electrically heated catalysts for cold-start emissions in diesel aftertreatment. SAE Technical Paper No. 2012-01-1092.

Lešnik, L., Kegl, B., Torres-Jimenez, E. and Cruz-Peragon, F. (2020). Why we should invest further in the development of internal combustion engines for road applications. Oil & Gas Science and Technology-Revue d'IFP Energies nouvelles, Vol. 75, p. 56.

Lyu, M., Alsulaiman, Y., Hall. M. J. & Matthews, R. D. (2022). Impacts of Intake Throttling on the Combustion Characteristics and Emissions of a Light-Duty Diesel Engine under the Idle Mode. Energies, Vol. 15(23), p. 8846.

Maniatis, P., Wagner, U. & Koch, T. A. (2019). A model-based and experimental approach for the determination of suitable variable valve timings for cold start in partial load operation of a passenger car single-cylinder diesel engine. Int. J. Eng. Res., Vol. 20(1), pp. 141-154.

Marathe, N. V., Walke, N. H., Juttu, S., Chaudhari, H. B., Dev, S. & Samant, M. P. (2022). Introduction to Thermal Management Techniques. Handbook of Thermal Management of Engines, pp. 3-27.

Mayer, A., Lutz, T. & Lammle, C., Wyser, M. & Legerer, F. (2003). Engine intake throttling for active regeneration of diesel particle filters. SAE Technical Paper No. 2003-01-0381.

McCarthy, J. (2017). Cylinder deactivation improves diesel aftertreatment and fuel economy for commercial vehicles. In 17. Internationales Stuttgarter Symposium Automobil-und Motorentechnik, pp. 1013-1039. Wiesbaden: Springer Fachmedien Wiesbaden.

McCarthy Jr, J., Matheaus, A., Zavala, B., Sharp, C. & Harris, T. (2022). Meeting Future NOx Emissions Over Various Cycles Using a Fuel Burner and Conventional Aftertreatment System. SAE International Journal of Advances and Current Practices in Mobility, 4(2022-01-0539), pp. 2220-2234.

Mohan, B. & Badra, J. (2023). An automated machine learning framework for piston engine optimization. Applications in Energy and Combustion Science, Vol. 13, p. 100106.

Muratori, M., Alexander, M., Arent, D., Bazilian, M., Cazzola, P., Dede, E.M., Farrell, J., Gearhart, C., Greene, D., Jenn, A. and Keyser, M. (2021). The rise of electric vehicles – 2020 status and future expectations. Progress in Energy, Vol. 3, No. 2, p. 022002.

Nie, X., Bi, Y., Liu, S., Shen, L. & Wan, M. (2022). Impacts of different exhaust thermal management methods on diesel engine and SCR performance at different altitude levels. Fuel, Vol. 324, p. 124747.

Ozel, C., Hall, M. J. & Matthews, R. (2018). Increasing Exhaust Temperature of an Idling Light-Duty Diesel Engine through Post-Injection and Intake Throttling. SAE Technical Paper No. 2018-01-0223.

Piano, A., Millo, F., Di Nunno, D. & Gallone, A. (2017). Numerical analysis on the potential of different variable valve actuation strategies on a light duty diesel engine for improving exhaust system warm up. SAE Technical Paper No. 2017-24-0024.

Papagianni, S., Moschovi, A. M., Polyzou, E. & Yakoumis, I. (2022). Platinum Recovered from Automotive Heavy-Duty Diesel Engine Exhaust Systems in Hydrometallurgical Operation, Metals, Vol. 12(1), p. 31.

Robinson, K., Ye, S., Yap, Y. & Kolaczkowski, S. T. (2013). Application of a methodology to assess the performance of a full-scale diesel oxidation

catalyst during cold and hot start NEDC drive cycles, Chemical Engineering Research and Design, Vol. 91(7), pp. 1292-1306.

Scrosati, B., Garche, J. & Tillmetz, W. (2015). Advances in battery technologies for electric vehicles. Woodhead Publishing, pp. 8-11.

Shafique, M., Azam, A., Rafiq, M. & Luo, X. (2022). Life cycle assessment of electric vehicles and internal combustion engine vehicles: A case study of Hong Kong. Research in Transportation Economics, Vol. 91, p. 101112.

Shipp, T. & Dane, M. H. (2021). Combustion and Thermal Management Strategies Using Variable Valve Timing. United States Patent, Patent No. US 10,920,644 B2.

Stančin, H., Mikulcic, H., Wang, X. and Duic, N. (2020). A review on alternative fuels in future energy system. Renewable and Sustainable Energy Reviews, Vol. 128, p. 109927.

Vos, K. R., Shaver, G. M., Ramesh, A. K. & McCarthy Jr, J. (2019). Impact of cylinder deactivation and cylinder cutout via flexible valve actuation on fuel efficient aftertreatment thermal management at curb idle. Frontiers in Mechanical Engineering, Vol. 5, p. 52.

Votsmeier, M., Kreuzer, T., Gieshoff, J. & Lepperhoff, G. (2009). Automobile exhaust control. Ullmann's Encyclopedia of Industrial Chemistry, Vol. 4, pp. 407-424.

Wang, Q., Zhang, H., Huang, J. and Zhang, P. (2023). The use of alternative fuels for maritime decarbonization: Special marine environmental risks and solutions from an international law perspective. Frontiers in Marine Science, Vol. 9, p. 2625.

Wardana, M. K. A. & Lim, O. (2022). Review of Improving the NOx Conversion Efficiency in Various Diesel Engines fitted with SCR System Technology. Catalysts, Vol. 13(1), p. 67.

Wu, D., Deng, B., Li, M., Fu, J. & Hou, K. (2020). Improvements on performance and emissions of a heavy duty diesel engine by throttling degree optimization: A steady-state and transient experimental study, Chemical Engineering and Processing – Process Intensification, Vol. 157, 108132.

Wu, B., Jia, Z., guo Li, Z., yi Liu, G. & lin Zhong, X. (2021). Different exhaust temperature management technologies for heavy-duty diesel engines with regard to thermal efficiency. Appl. Therm. Eng., Vol. 186, p. 116495

Xu, G. et al. (2023). Advances in emission control of diesel vehicles in China. Journal of Environmental Sciences, Vol. (123), pp. 15-29.

Ye, S., Yap, Y. H., Kolaczkowski, S. T., Robinson, K. & Lukyanov, D. (2012). Catalyst 'light-off' experiments on a diesel oxidation catalyst connected to a diesel engine – Methodology and techniques. Chemical Engineering Research and Design, Vol. (90)6, pp. 834-845.

Zhang, X., Zhu, J., Zhang, Z. & Bai, S. (2022). Study on the Effect of Exhaust Thermal Management on SCR of Euro VI Diesel Engine, FEB – Fresenius Environmental Bulletin, 11678.

CHAPTER 5

ABRASIVE WATERJET CUTTING OF POLYMERIC MATERIALS: A REVIEW

Assistant Professor Dr. Oguzhan DER[1]

[1] Bandırma Onyedi Eylul University, Faculty of Maritime, Department of Marine Vehicles Management Engineering, Balıkesir, Türkiye, oder@bandirma.edu.tr. ORCID: 0000-0001-5679-2594

INTRODUCTION

Abrasive waterjet cutting (AWC) is a machining technique that utilizes a high-pressure water jet mixed with abrasive particles to cut through various materials, including polymeric materials. In AWC, a high-velocity stream of pressurized water is forced through a small orifice, creating a focused jet. This jet is then combined with abrasive particles, such as garnet or aluminum oxide, which are added to enhance the cutting efficiency. The combination of high-pressure water and abrasive particles allows AWC to overcome the challenges associated with cutting polymers, such as their tendency to melt, deform, or generate heat during traditional cutting methods like sawing or milling. AWC offers several advantages in the context of polymeric materials. These are as follows; cold cutting, precision and complex shapes, minimal material waste, versatility, and reduced post-processing (Sadasivam et al., 2009).

AWC is a cold-cutting process that does not generate significant heat, minimizing the risk of thermal damage to the polymer. This is particularly important for heat-sensitive polymers or materials prone to melting. AWC enables the cutting of intricate shapes and precise contours, making it suitable for applications where high precision is required, such as in the fabrication of complex parts or components. AWC is a non-contact process that produces narrow kerf widths, resulting in minimal material wastage. This is advantageous when working with expensive or scarce polymeric materials. Thermoplastics, thermosets, elastomers, and composites are just a few of the many polymeric materials that can be treated with AWC. It offers flexibility in terms of material selection, making it suitable for diverse industrial applications. AWC often produces smooth and finished edges, reducing the need for additional post-processing steps, such as sanding or polishing, which can save time and costs (Wang & Guo, 2002).

The relevance of AWC in the context of polymeric materials lies in its ability to provide precise, clean, and efficient cutting without compromising the integrity of the material. It has found applications in various industries, including aerospace, automotive, electronics, and manufacturing, where precise cutting of polymers is crucial for the production of components, parts, gaskets, seals, and other specialized products (Wang, 1999).

The motivation behind using AWC for cutting polymers stems from the unique advantages it offers compared to traditional cutting methods. Here are some key motivations and benefits of using AWC for cutting polymers:

Non-Thermal Cutting: AWC is a non-thermal cutting process, which means it does not generate significant heat during cutting. This is particularly important for polymers, as they can melt, deform, or suffer from thermal damage when exposed to high temperatures. AWC allows for clean, precise cutting without altering the material properties or causing thermal effects.

Precision and Complex Shapes: AWC enables the cutting of intricate shapes and precise contours in polymeric materials. The high-pressure water jet combined with abrasive particles can accurately cut complex geometries, sharp corners, and fine details. This precision is beneficial for applications that require intricate shapes, such as in the production of automotive components, gaskets, or custom-designed parts.

Minimal Material Waste: AWC produces narrow kerf widths, resulting in minimal material wastage. The ability to achieve narrow cuts reduces material loss, making AWC cost-effective and efficient, especially when working with expensive or limited-availability polymers.

Versatility: AWC is a versatile cutting method suitable for a wide range of polymeric materials. It can effectively cut various types of polymers, including thermoplastics, thermosets, elastomers, and composite materials. This versatility makes AWC a valuable tool across different industries that work with polymers.

Clean and Finished Edges: AWC typically produces clean and finished cutting edges, eliminating the need for additional post-processing steps like sanding or polishing. The cut edges are often smooth and of high quality, reducing the time and effort required for finishing work.

Material Compatibility: AWC is compatible with both soft and hard polymeric materials, allowing for efficient cutting regardless of the polymer's hardness or flexibility. It can handle materials ranging from soft elastomers to rigid thermoplastics or composites, expanding its applicability across a wide spectrum of polymeric materials (Ashok Kumar et al., 2020).

Potential applications of AWC for cutting polymers include aerospace, automotive, manufacturing, construction, medical also prototyping and rapid manufacturing. AWC is utilized in aerospace industries for cutting

polymer components such as gaskets, seals, insulation materials, and composite parts. AWC finds application in the automotive sector for cutting polymer-based components like interior trim, gaskets, seals, and custom-shaped parts. AWC is employed in various manufacturing processes where precise cutting of polymers is required, such as in the production of electronics, packaging materials, and industrial components. AWC can be used for cutting polymer-based construction materials, including pipes, tubes, panels, and insulation. AWC is employed in the medical field for cutting polymer components used in surgical instruments, implants, medical devices, and prosthetics. AWC enables quick and accurate cutting of polymer prototypes and small-scale production runs, facilitating rapid manufacturing processes (Trzepieciński et al., 2022).

In general, AWC offers numerous advantages for cutting polymers, making it a valuable technique in various industries that rely on the precise, clean, and efficient cutting of polymeric materials.

PRINCIPLES of ABRASIVE WATERJET CUTTING

The fundamental principles of abrasive waterjet cutting (AWC) involve the use of a high-pressure water jet combined with abrasive particles to cut through materials. A schematic representation of the abrasive waterjet cutting is illustrated in Figure 1. The equipment used in AWC typically consists of the following components:

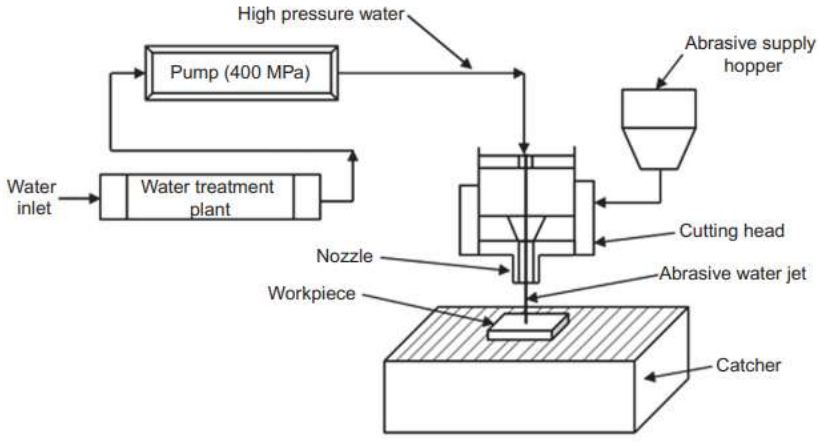

Figure 1: Sketch of abrasive-waterjet machining setup(Saxena et al., 2018).

Water Supply System: A high-pressure water supply system is essential for AWC. It includes a water pump capable of generating pressures ranging from 30,000 to 90,000 pounds per square inch (psi) or even higher. The water supply system ensures a continuous and pressurized water flow to the cutting nozzle (Potom et al., 2019).

Cutting Nozzle: The cutting nozzle is a critical component in AWC. It is designed to focus and control the high-pressure water jet. The nozzle typically has a small orifice, typically between 0.003 to 0.020 inches in diameter, through which the water jet passes. The nozzle may also include an additional orifice for introducing the abrasive particles into the water jet.

Abrasive Delivery System: Abrasive particles, such as garnet or aluminum oxide, are introduced into the water jet to enhance the cutting efficiency. The abrasive particles are typically stored in a hopper and fed into the water stream using a mixing chamber or a venturi effect. The abrasive particles are entrained and accelerated by the high-velocity water jet, creating an abrasive water mixture.

High-Pressure Control System: AWC requires precise control of the water pressure to optimize cutting performance. The high-pressure control system regulates and maintains the desired pressure level. It usually includes pressure gauges, valves, and a control panel for adjusting and monitoring the water pressure (Potom et al., 2019).

The basic setup for AWC involves the following steps. The water supply system pressurizes the water to the desired level, typically within the range of 30,000 to 90,000 psi (water pressurization). The abrasive particles are introduced into the water stream. This can be done by mixing the particles with the water in a mixing chamber or using a venturi effect to create a vacuum that draws the abrasive particles into the water stream (abrasive introduction). The high-pressure water jet passes through the cutting nozzle, which has a small orifice that helps focus and concentrate the jet (nozzle focusing). The focused water jet, now combined with abrasive particles, is directed toward the material to be cut. The high-velocity water jet, along with the abrasive particles, erodes and removes material, resulting in a cutting action. The nozzle is moved along the desired cutting path to achieve the desired shape or contour (cutting process). During the cutting process, the water jet acts as a coolant, dissipating heat and minimizing thermal effects on

the material. The water also flushes away the eroded particles and debris from the cutting zone (cooling and flushing) (Potom et al., 2019).

The setup may also include additional components such as motion control systems, robotic arms, or CNC (Computer Numerical Control) systems to automate and control the cutting process with precision. By combining high-pressure water and abrasive particles, AWC allows for the efficient cutting of various materials, including polymeric materials, while minimizing heat generation and achieving precise and clean cuts.

High-pressure water jets and abrasive particles play crucial roles in the cutting process in AWC. Here's a detailed explanation of their respective roles:

High-Pressure Water Jets: High-pressure water jets serve as the primary cutting tool in AWC. They possess several important functions:

Cutting Force: The high-pressure water jet exerts a significant cutting force on the material, enabling the removal of particles and inducing material separation. The force is generated by the high kinetic energy of the water jet (Shakouri & Abbasi, 2018).

Erosion: The high-velocity water jet causes erosion on the material's surface by wearing away the material through impingement. The constant impact of the water stream weakens and erodes the material, facilitating the cutting process.

Cooling: As the water jet interacts with the material, it absorbs heat generated during the cutting process, acting as a cooling agent. This cooling effect helps prevent thermal damage to the material, particularly important for heat-sensitive polymers.

Kinematic Energy: By speeding the abrasive particles and facilitating their impact on the material, the high velocity of the water jet contributes to the cutting action. The kinetic energy of the water stream enhances the effectiveness of the cutting process (Shakouri & Abbasi, 2018).

Confinement: The focused and concentrated nature of the high-pressure water jet allows for precise cutting. By directing the water jet through a small orifice, the cutting nozzle controls and confines the cutting action to a specific area, achieving accurate and controlled cuts.

Abrasive Particles: Abrasive particles, such as garnet or aluminum oxide, are introduced into the high-pressure water jet to enhance the cutting efficiency. They fulfil several important functions:

Material Removal: The abrasive particles, entrained by the high-velocity water jet, act as cutting agents that physically abrade the material. As the water jet impacts the material, the abrasive particles help to dislodge and remove material particles, enhancing the cutting action.

Material Weakening: The abrasive particles contribute to the weakening and erosion of the material by initiating micro-fractures and dislodging particles from the material surface. This assists in breaking down the material structure and facilitating efficient cutting.

Abrasiveness: The abrasive particles possess hardness and sharp edges, which aid in the abrasion and cutting process. They effectively remove material by scratching, grinding, and wearing away the material surface.

Kinetic Energy Transfer: The high-velocity water jet transfers kinetic energy to the abrasive particles, propelling them with force against the material. This increases their cutting effectiveness by increasing their impact energy on the material.

Particle Interaction: The abrasive particles in the water jet also contribute to the erosion of the material surface by colliding with and breaking apart particles within the material, aiding in material removal (Shakouri & Abbasi, 2018).

By combining high-pressure water jets and abrasive particles, AWC achieves efficient cutting of various materials, including polymeric materials. The high-pressure water jet exerts cutting force, erosion, and cooling effects, while the abrasive particles enhance material removal and weakening. The synergy between these elements results in precise, controlled, and efficient cutting processes.

Several parameters significantly influence the performance and outcomes of AWC. Understanding and optimizing these parameters are crucial for achieving desired cutting results. Here are key parameters that affect AWC:

Water Pressure: Water pressure plays a vital role in AWC as it determines the velocity and cutting power of the water jet. Higher water pressure generally leads to increased cutting speed and improved material

removal. However, excessively high pressures may result in erosion of the cutting nozzle or cause material damage. The optimal water pressure depends on the specific material being cut, its thickness, and the desired cutting speed and precision (S. Zhang & Li, 2010).

Abrasive Particle Size: The size of abrasive particles affects the cutting performance and surface quality in AWC. Smaller particle sizes result in finer cutting action, enabling more precise cuts and smoother surface finishes. Larger particles, on the other hand, contribute to faster material removal but may produce rougher cut surfaces. The selection of the appropriate abrasive particle size depends on the material type, thickness, and desired cutting outcome (L. Zhang et al., 2019).

Abrasive Particle Concentration: Cutting effectiveness and material removal rate is influenced by the abrasive particle concentration in the water jet. Higher abrasive particle concentrations generally lead to faster cutting speeds due to increased cutting power. However, excessively high concentrations may cause nozzle clogging or result in abrasive particle clustering, reducing cutting performance. It is important to optimize the particle concentration based on the material being cut and the desired cutting speed and surface quality (L. Zhang et al., 2019).

Standoff Distance: The standoff distance refers to the distance between the cutting nozzle and the material surface. It affects the cutting performance and the quality of the cut edges. A shorter standoff distance typically results in faster cutting speeds and greater cutting power, but it may also lead to rougher surface finishes. A longer standoff distance allows for smoother cuts but may reduce cutting speed. The optimal standoff distance depends on the material properties, nozzle geometry, and desired cutting outcomes (Madhu & Balasubramanian, 2021).

Traverse Speed: Traverse speed refers to the speed at which the cutting nozzle moves along the cutting path. It influences cutting efficiency and surface quality. Higher traverse speeds generally result in faster cutting, but they may impact the precision and quality of the cut edges. Slower traverse speeds can improve cutting precision but may increase the overall cutting time. The appropriate traverse speed depends on the material being cut, its thickness, and the desired cutting precision and productivity (Madhu & Balasubramanian, 2021).

Nozzle Design: The design of the cutting nozzle, including the shape, size, and orifice diameter, affects the characteristics of the water jet and the cutting performance. The nozzle design determines the focus, concentration, and direction of the water jet, influencing cutting precision and power. Optimal nozzle design depends on factors such as material type, thickness, and desired cutting results (Madhu & Balasubramanian, 2021).

It is crucial to remember that these factors are interconnected, and that improving one parameter may have an impact on how well the others work. Therefore, experimentation, testing, and parameter adjustments are often necessary to achieve the desired cutting outcomes for specific materials and applications in AWC (Momber et al., 1997).

MATERIAL CONSIDERATIONS

Abrasive waterjet cutting (AWC) is a versatile cutting method that can be applied to various types of polymeric materials. Here is an overview of the different categories of polymeric materials commonly cut using AWC:

Thermoplastics: Thermoplastics are a broad class of polymers that can be melted and reformed multiple times without undergoing significant degradation. AWC is commonly used to cut thermoplastics due to its ability to achieve precise and clean cuts without causing thermal damage. Examples of thermoplastics that are frequently cut using AWC include (Sambruno et al., 2019):

- Polyethylene (PE)
- Polypropylene (PP)
- Polycarbonate (PC)
- Acrylic (PMMA)
- Polyvinyl Chloride (PVC)
- Nylon (PA)

Thermosetting Plastics: Unlike thermoplastics, thermosetting plastics undergo irreversible chemical cross-linking upon curing, resulting in a rigid and heat-resistant material. AWC is well-suited for cutting thermosetting plastics due to its non-thermal cutting process. Common thermosetting plastics cut using AWC include (Shanmugam et al., 2002):

- Epoxy resins
- Phenolic resins

- Polyurethane (PU)
- Melamine formaldehyde (MF)
- Urea formaldehyde (UF)

Elastomers: Elastomers are polymers that possess rubber-like elasticity, allowing them to stretch and return to their original shape. Cutting elastomers using conventional methods can be challenging due to their flexibility and tendency to deform. AWC offers an effective solution for precise cutting of elastomers. Some commonly cut elastomers include (Maurya et al., 2023):

- Natural rubber (NR)
- Synthetic rubber (SBR, NBR, EPDM)
- Silicone rubber
- Polyurethane elastomers

Composite Materials: Composite materials are engineered materials composed of a matrix material (often a polymer) reinforced with fibers or particles. AWC can cut through composite materials, providing precise cutting without damaging the reinforcing fibers. Common composite materials cut using AWC include (Popan et al., 2017):

- Fiber-reinforced plastics (FRP)
- Carbon fiber-reinforced polymers (CFRP)
- Glass fiber-reinforced polymers (GFRP)
- Aramid fiber-reinforced polymers (AFRP)

Specialty Polymers: AWC is also used to cut various specialty polymers with specific properties and applications. These specialty polymers may have unique characteristics, such as high temperature resistance, chemical resistance, or biocompatibility. Examples of specialty polymers cut using AWC include (Parvin & Brighton, 2014):

- Polyetheretherketone (PEEK)
- Polyimide (PI)
- Polyetherimide (PEI)
- Polytetrafluoroethylene (PTFE)
- Polyether block amide (PEBA)
- Biodegradable polymers (PLA, PHA)

It is worth noting that the suitability of AWC for cutting specific polymeric materials may vary based on their properties, thickness, and specific cutting requirements. Optimization of cutting parameters and proper

selection of abrasives may be necessary to achieve desired cutting results for different polymeric materials. Polymers exhibit a wide range of properties, and these properties can influence their suitability or pose challenges when it comes to AWC. Here, we discuss the specific properties of polymers that impact their behavior in AWC:

Melting and Thermal Properties: AWC is advantageous for cutting polymers due to its non-thermal cutting process. However, some polymers have low melting points, and excessive heat generated during cutting can lead to melting or thermal degradation. Thermally sensitive polymers, such as polystyrene (PS) or polyvinyl chloride (PVC), may require careful control of cutting parameters to prevent heat-related issues (Larson, 2015).

Hardness and Abrasion Resistance: Polymers vary in hardness and abrasion resistance, which affects their response to abrasive particles in AWC. Harder polymers, like polyetheretherketone (PEEK) or polyimide (PI), generally require more abrasive particles or higher cutting pressures to achieve efficient material removal. Softer polymers, such as polyethylene (PE) or polypropylene (PP), are more easily cut, but their lower abrasion resistance may result in faster nozzle wear.

Elasticity and Flexibility: Elasticity and flexibility of polymers, particularly elastomers, can make them challenging to cut with conventional methods. However, AWC offers a solution by utilizing the high-pressure water jet to provide the necessary cutting force. The flexibility of elastomers allows them to deform under the water jet, but AWC can still achieve precise cuts by combining high-pressure water with abrasive particles (Larson, 2015).

Fiber Reinforcement: Polymer composites, reinforced with fibers such as carbon, glass, or aramid, pose unique challenges for cutting. The reinforcing fibers are typically harder and more abrasion-resistant than the polymer matrix. AWC can effectively cut through composite materials while minimizing damage to the fibers. However, the cutting process may vary depending on the fiber type, orientation, and volume fraction within the composite.

Chemical Resistance: Some polymers exhibit high chemical resistance, which can affect their response to the abrasive particles used in AWC. Certain polymers, such as polytetrafluoroethylene (PTFE) or polyvinylidene fluoride (PVDF), have excellent chemical resistance but can be more challenging to cut due to their low surface energy and non-reactivity

with abrasives. Special considerations may be required to optimize cutting parameters for chemically resistant polymers (Biron, 2018).

Thickness and Structural Integrity: The thickness and structural integrity of polymers can impact the cutting process. Thicker polymers may require longer cutting times or adjustments in cutting parameters to ensure complete material removal without excessive cutting forces. Delicate or thin-walled polymer structures can be susceptible to deformation or damage during cutting, necessitating careful control of cutting parameters to maintain structural integrity (Biron, 2018).

It is significant to note that the specific properties and behavior of polymers can vary widely, even within the same polymer family. It is recommended to conduct thorough testing and experimentation to determine the optimal cutting parameters for each specific polymer, taking into account its unique properties and requirements. Cutting specific polymer types using AWC may present unique considerations or challenges due to their specific properties. Here are some examples:

Polyvinyl Chloride (PVC): PVC is a common thermoplastic used in various applications. However, cutting PVC using AWC can be challenging due to its high chlorine content, which makes it prone to thermal degradation and the release of corrosive gases. Special attention should be given to controlling cutting parameters to prevent excessive heat and the potential release of harmful fumes (Maros, 2018).

Polycarbonate (PC): Polycarbonate is a transparent thermoplastic known for its impact resistance and clarity. When cutting PC using AWC, care must be taken to prevent the formation of cracks or surface defects, as PC can be susceptible to stress concentration. Optimizing cutting parameters such as water pressure, abrasive concentration, and standoff distance can help minimize the risk of damage (Monno & Ravasio, n.d.).

Polypropylene (PP): PP is a widely used thermoplastic with excellent chemical resistance and low density. However, PP can be challenging to cut using AWC due to its low melting point and tendency to deform under high temperatures. It is important to carefully control cutting parameters, including water pressure and traverse speed, to avoid excessive heat generation and ensure clean cuts (Chen & Siores, 2001).

Polyethylene (PE): PE is another commonly used thermoplastic known for its toughness and chemical resistance. While PE is generally easier to cut compared to other polymers, it is important to consider the selection of abrasive particles. Softer abrasive particles or lower concentrations may be preferred to prevent excessive wear on the cutting nozzle, as PE has lower abrasion resistance compared to some other polymers (Maros, 2018).

Polyurethane (PU): PU is a versatile polymer known for its resilience, flexibility, and excellent abrasion resistance. However, PU can present challenges in AWC due to its elastomeric nature. The flexible nature of PU may cause it to deform under the high-pressure water jet, requiring careful control of cutting parameters to achieve clean and precise cuts (Maros, 2018).

Fiberglass Reinforced Plastics (FRP): FRP, consisting of a polymer matrix reinforced with glass fibers, presents unique challenges in AWC. The cutting process must consider the interaction between the abrasive particles and the glass fibers. Careful selection of cutting parameters, including water pressure and abrasive particle size, is necessary to ensure efficient material removal while minimizing damage to the reinforcing fibers (Maros, 2018).

CUTTING PERFORMANCE AND QUALITY

The cutting performance of abrasive waterjet cutting (AWC) on polymeric materials can be evaluated based on factors such as cutting speed, accuracy, and surface finish. Here is an assessment of these performance aspects. AWC can achieve relatively high cutting speeds on polymeric materials, especially compared to other conventional cutting methods. The cutting speed depends on various factors, including water pressure, abrasive particle size, standoff distance, and traverse speed. By optimizing these parameters, AWC can achieve efficient material removal rates, resulting in faster cutting speeds (Rozario Jegaraj & Ramesh Babu, 2007).

AWC offers good cutting accuracy and precision on polymeric materials. The non-thermal cutting process minimizes the occurrence of heat-related distortions or thermal damage to the workpiece. Additionally, the focused and controlled nature of the water jet allows for precise cutting along complex shapes and intricate details. However, achieving high accuracy may require careful parameter adjustments and optimization, particularly for thin or delicate polymeric structures. The surface finish achieved by AWC on polymeric materials can vary depending on several factors. Generally, AWC

produces a relatively smooth surface finish, especially when compared to some other cutting methods that may cause heat-induced deformations or mechanical stresses. However, the choice of abrasive particle size, concentration, and cutting parameters can influence the surface roughness. Finer abrasive particles and optimized cutting parameters can result in smoother surface finishes, while coarser abrasives may produce slightly rougher surfaces (Radovanovic, 2020).

AWC can provide clean and sharp cutting edges on polymeric materials. The non-contact nature of the cutting process minimizes mechanical stress, burrs, or deformations that can be associated with other cutting methods. However, it is crucial to note that certain polymeric materials may have specific characteristics, such as brittleness or stress concentration, which can impact the edge quality. Careful parameter selection and optimization are necessary to achieve high-quality, smooth, and precise edges. Thermoplastics, thermosetting plastics, elastomers, composite materials, and specialized polymers are just a few of the numerous polymeric materials that AWC is often appropriate for. However, the cutting performance may vary depending on the specific properties of each material. Factors such as hardness, abrasion resistance, chemical resistance, and fiber reinforcement can influence the cutting process and may require specific parameter adjustments or considerations (Radovanovic, 2020).

Overall, AWC demonstrates favorable cutting performance on polymeric materials, offering high cutting speeds, good accuracy, and smooth surface finishes. However, achieving optimal results requires careful parameter selection, material characterization, and optimization based on the specific polymeric material being cut and the desired cutting outcomes. Conducting tests and experimentation is recommended to determine the optimal cutting parameters for each application.

APPLICATIONS

Abrasive waterjet cutting (AWC) is widely employed for cutting polymeric materials in various industries due to its versatility and advantages. Here is a comprehensive overview of the applications of AWC in different sectors:

Aerospace Industry: AWC is extensively used in the aerospace industry to cut composite materials, such as fiber-reinforced plastics (FRP), carbon fiber-reinforced polymers (CFRP), and glass fiber-reinforced polymers

(GFRP). AWC enables precise and efficient cutting of composite structures for aerospace components like fuselages, wings, and interior parts (Khan et al., 2021).

Automotive Industry: AWC is utilized for cutting polymeric materials in the production of automotive interior components. This includes cutting door panels, instrument panels, dashboard components, and other interior trim materials made from thermoplastics or composites. AWC is employed for cutting elastomeric materials to create gaskets and seals used in automotive applications. Elastomers such as rubber or silicone can be accurately cut with AWC to achieve the desired shape and fit (Khan et al., 2021).

Manufacturing Industry: AWC is utilized in the manufacturing sector for rapid prototyping and manufacturing of polymeric parts. AWC allows for quick and precise cutting of various polymeric materials, enabling efficient production of prototypes or small-scale production runs. AWC is also employed in die cutting applications where it offers advantages over traditional die-cutting methods. AWC can cut complex shapes and intricate patterns in polymeric materials, providing greater flexibility and precision compared to mechanical die-cutting processes (Khan et al., 2021).

Electronics Industry: AWC is used to cut polymeric materials used in the production of circuit boards. It enables accurate and efficient cutting of materials such as epoxy resins or laminates, allowing for the creation of circuit board components with precise dimensions. AWC is employed to cut polymeric materials used for insulation and packaging in the electronics industry. This includes cutting materials like polyethylene foam, polycarbonate sheets, or polypropylene for creating insulation components or protective packaging (Khan et al., 2021).

Medical and Healthcare Industry: AWC is utilized in the manufacturing of various medical devices made from polymeric materials. It enables precise cutting of materials used in surgical instruments, implants, prosthetics, and medical equipment components. AWC can be applied to cut biocompatible polymers used in medical and healthcare applications. It allows for the creation of intricate shapes and custom designs required for medical implants, drug delivery systems, and surgical tools (Khan et al., 2021).

Packaging Industry: AWC is employed for cutting flexible packaging materials, including films and laminates made from polymeric materials. It

enables efficient cutting of packaging materials for food, consumer goods, and industrial products (Khan et al., 2021).

The applications of AWC for cutting polymeric materials extend beyond these industries, with its versatility allowing for a wide range of applications in other sectors as well, such as consumer goods, construction, and textiles. The ability to achieve precise cuts, accommodate various polymeric materials, and handle complex shapes makes AWC a valuable cutting method in many industries.

CHALLENGES AND FUTURE PERSPECTIVES

While abrasive waterjet cutting (AWC) offers numerous advantages for cutting polymeric materials, there are still some challenges and limitations that exist. Here are some of the current challenges and limitations associated with AWC.

Thermal Effects: AWC can generate heat during the cutting process, which can potentially lead to thermal effects on certain polymeric materials. Thermally sensitive polymers may experience melting, degradation, or changes in material properties due to the heat generated by the high-pressure water jet. This can affect the quality of cut edges and overall cutting performance (Hirsch et al., 2019).

Delamination: Delamination refers to the separation or splitting of layers in laminated or composite polymeric materials. AWC can sometimes cause delamination due to the high-pressure water jet impacting the interface between layers or the presence of abrasive particles. Delamination can compromise the structural integrity of the material and result in lower-quality cut edges (Hirsch et al., 2019).

Surface Roughness: While AWC generally produces relatively smooth surface finishes, achieving a high-quality surface finish may be challenging for some polymeric materials. The selection of abrasive particle size, concentration, and cutting parameters can influence surface roughness. Coarser abrasive particles or suboptimal parameter settings may result in rougher surface finishes that require additional post-processing.

Edge Quality: Achieving high-quality, clean-cut edges can be challenging with AWC, especially for certain polymeric materials. Factors such as material properties, cutting parameters, and nozzle design can influence the sharpness, precision, and smoothness of cut edges. Brittle or

stress-sensitive polymers may be prone to edge chipping or cracking, requiring careful parameter optimization and nozzle design (Barone et al., 2017).

Material Integrity: AWC can potentially impact the integrity of certain polymeric materials. Softer or low-density polymers may experience deformation or distortion due to the high-pressure water jet, resulting in irregularities or compromised dimensional accuracy. Careful parameter selection and optimization are necessary to minimize material deformation and maintain the structural integrity of the workpiece (Barone et al., 2017).

Abrasive Particle Wear: The use of abrasive particles in AWC introduces the issue of abrasive particle wear over time. High-velocity water jets can cause erosion of the abrasive particles, leading to changes in their size and cutting effectiveness. As the abrasive particles wear, the cutting performance may decline, requiring periodic replenishment or adjustment of the abrasive concentration.

Process Cost: AWC can be more expensive compared to some other cutting methods, primarily due to the costs associated with high-pressure water systems, abrasive materials, and maintenance of equipment. The initial setup costs and ongoing operational expenses may pose challenges for smaller-scale operations or industries with strict cost constraints.

It is important to note that advancements in technology, nozzle design, and process optimization are continuously addressing these challenges and expanding the capabilities of AWC for cutting polymeric materials. Through careful parameter control, material characterization, and process refinement, many of these limitations can be mitigated or overcome to achieve improved cutting performance on a wide range of polymeric materials (Barone et al., 2017).

CONCLUSION

This review provides a comprehensive overview of abrasive waterjet cutting (AWC) of polymeric materials. It covers various aspects related to AWC, its advantages, and its applications in different industries. The main points discussed in the chapter are as follows.

AWC is a cutting method that utilizes a high-pressure water jet containing abrasive particles to cut polymeric materials. AWC offers several advantages for cutting polymers, including non-thermal process, high cutting

speed, accuracy, and the ability to cut complex shapes and intricate details. The fundamental principles of AWC involve high-pressure water jets that accelerate abrasive particles, which assist in the cutting process by enhancing material removal. Parameters such as water pressure, abrasive particle size, and concentration have a significant influence on AWC. Optimizing these parameters is crucial for achieving desired cutting outcomes. AWC is suitable for cutting various polymeric materials, including thermoplastics, thermosetting plastics, elastomers, composites, and specialty polymers. Polymeric materials have properties that make them suitable for AWC, such as their non-conductivity, non-reflectivity, and ability to withstand water and abrasive forces. However, certain challenges arise due to their thermal sensitivity, brittleness, or stress concentration (Kalla et al., 2012).

The cutting performance of AWC on polymeric materials is evaluated based on factors such as cutting speed, accuracy, surface finish, and edge quality. AWC demonstrates favorable cutting performance but requires parameter optimization for optimal results. Specific considerations and challenges may arise when cutting different types of polymers, such as fiber-reinforced composites, brittle polymers, or highly filled materials. Process parameters, such as water pressure, abrasive particle size, concentration, standoff distance, and traverse speed, influence the quality of cut edges and can lead to issues like thermal effects or delamination. AWC finds applications in various industries, including aerospace, automotive, manufacturing, electronics, medical, healthcare, and packaging, due to its versatility in cutting polymeric materials.

Despite its advantages, AWC has some limitations and challenges, including thermal effects, delamination, surface roughness, edge quality, material integrity, abrasive particle wear, and process cost. By considering these points, researchers, engineers, and practitioners can gain insights into the use of AWC for cutting polymeric materials and make informed decisions regarding its application in different industries. Unlike a normal review, this work aims to provide users with information about the process rather than a review of the existing literature. For many researchers, this book chapter aims to be a starting resource for AWC of polymeric materials.

REFERENCES

Ashok Kumar, U., Mehtab Alam, S., & Laxminarayana, P. (2020). Influence of Abrasive Water Jet Cutting on Glass Fibre Reinforced Polymer (GFRP) Composites. Materials Today: Proceedings, 27, 1651–1654. https://doi.prg/10.1016/J.Matpr.2020.03.554

Barone, S., Paoli, A., Neri, P., Razionale, A. V., & Giannese, M. (2017). Mechanical and Geometrical Properties Assessment of Thermoplastic Materials for Biomedical Application (pp. 437–446). https://doi.org/10.1007/978-3-319-45781-9_44

Biron, M. (2018). Thermoplastics and Thermoplastic Composites. In Thermoplastics and Thermoplastic Composites. https://doi.org/10.1016/C2017-0-01099-6

Chen, F. L., & Siores, E. (2001). The Effect of Cutting Jet Variation on Striation Formation in Abrasive Water Jet Cutting. International Journal of Machine Tools and Manufacture, 41(10), 1479–1486. https://doi.org/10.1016/S0890-6955(01)00013-X

Hirsch, P., Bastick, S., Jaeschke, P., Van Den Aker, R., Geyer, A., Zscheyge, M., & Michel, P. (2019). Effect of Thermal Properties on Laser Cutting of Continuous Glass and Carbon Fiber-Reinforced Polyamide 6 Composites. Machining Science and Technology, 23(1), 1–18. https://doi.org/10.1080/10910344.2018.1449216

Kalla, D. K., Dhanasekaran, P. S., Zhang, B., & Asmatulu, R. (2012). Abrasive Waterjet Machining of Fiber Reinforced Composites: A Review. 535–542. https://doi.org/10.1063/1.4707606

Khan, M. A., Soni, H., Mashinini, P., & Uthayakumar, M. (2021). Abrasive Water Jet Cutting Process Form Machining Metals and Composites for Engineering Applications: A Review. Engineering Research Express, 3(2), 022004. https://doi.org/10.1088/2631-8695/Abfe98

Larson, E. R. (2015). An Overview of Thermoplastic Materials. Thermoplastic Material Selection, 97–143. https://doi.org/10.1016/B978-0-323-31299-8.00004-0

Madhu, S., & Balasubramanian, M. (2021). Challenges in Abrasive Jet Machining of Fiber-Reinforced Polymeric Composites – A Review. World Journal of Engineering, 18(2), 251–268. https://doi.org/10.1108/WJE-05-2020-0190

Maros, Z. (2018). Machining of Different Materials with Abrasive Waterjet Cutting. IOP Conference Series: Materials Science and Engineering, 448, 012009. https://doi.org/10.1088/1757-899X/448/1/012009

Maurya, P., Kamath, R. C., & Gaddale Srinivas, V. (2023). Experimental Investigation of Suspension-Type Abrasive Water Jet Machining of Nitrile Rubber for Positive Displacement Motor Applications. International Journal of Lightweight Materials and Manufacture, 6(3), 367–378. https://doi.org/10.1016/J.Ijlmm.2023.03.002

Momber, A. W., Kovacevic, R., & Kwak, H. (1997). Alternative Method for the Evaluation of the Abrasive Water-Jet Cutting of Grey Cast Iron. Journal of Materials Processing Technology, 65(1–3), 65–72. https://doi.org/10.1016/0924-0136(95)02243-0

Monno, M., & Ravasio, C. (n.d.). The Effect of Pressure on the Surfaces Generated by Waterjet: Preliminary Analysis. In AMST'05 Advanced Manufacturing Systems and Technology (pp. 413–425). Springer Vienna. https://doi.org/10.1007/3-211-38053-1_40

Parvin, A., & Brighton, D. (2014). FRP Composites Strengthening of Concrete Columns Under Various Loading Conditions. Polymers, 6(4), 1040–1056. https://doi.org/10.3390/Polym6041040

Popan, I. A., Contiu, G., & Campbell, I. (2017). Investigation on Standoff Distance Influence on Kerf Characteristics in Abrasive Water Jet Cutting of Composite Materials. MATEC Web of Conferences, 137, 01009. https://doi.org/10.1051/Matecconf/201713701009

Potom, B., Madhu, S., Kannan, S., & Prathap, P. (2019). Performance Analysis of Abrasive Water Jet Cutting Process in Carbon Fiber Epoxy Polymer Composite. IOP Conference Series: Materials Science and Engineering, 574(1), 012014. https://doi.org/10.1088/1757-899X/574/1/012014

Radovanovic, M. (2020). Multi-Objective Optimization of Abrasive Water Jet Cutting Using MOGA. Procedia Manufacturing, 47, 781–787. https://doi.org/10.1016/J.Promfg.2020.04.241

Rozario Jegaraj, J. J., & Ramesh Babu, N. (2007). A Soft Computing Approach for Controlling the Quality of Cut with Abrasive Waterjet Cutting System Experiencing Orifice and Focusing Tube Wear. Journal of Materials Processing Technology, 185(1–3), 217–227. https://doi.org/10.1016/J.Jmatprotec.2006.03.124

Sadasivam, B., Hizal, A., & Arola, D. (2009). Abrasive Waterjet Peening with Elastic Prestress: A Parametric Evaluation. International Journal of

Machine Tools and Manufacture, 49(2), 134–141. https://doi.org/10.1016/J.Ijmachtools.2008.10.001

Sambruno, A., Bañon, F., Salguero, J., Simonet, B., & Batista, M. (2019). Kerf Taper Defect Minimization Based on Abrasive Waterjet Machining of Low Thickness Thermoplastic Carbon Fiber Composites C/TPU. Materials, 12(24), 4192. https://doi.org/10.3390/Ma12244192

Saxena, K. K., Bellotti, M., Qian, J., Reynaerts, D., Lauwers, B., & Luo, X. (2018). Overview of Hybrid Machining Processes. In Hybrid Machining (pp. 21–41). Elsevier. https://doi.org/10.1016/B978-0-12-813059-9.00002-6

Shakouri, E., & Abbasi, M. (2018). Investigation Of Cutting Quality and Surface Roughness in Abrasive Water Jet Machining of Bone. Proceedings of the Institution of Mechanical Engineers, Part H: Journal of Engineering in Medicine, 232(9), 850–861. https://doi.org/10.1177/0954411918790777

Shanmugam, D. K., Chen, F. L., Siores, E., & Brandt, M. (2002). Comparative Study of Jetting Machining Technologies Over Laser Machining Technology for Cutting Composite Materials. Composite Structures, 57(1–4), 289–296. https://doi.org/10.1016/S0263-8223(02)00096-X

Trzepieciński, T., Najm, S. M., & Lemu, H. G. (2022). Current Concepts for Cutting Metal-Based and Polymer-Based Composite Materials. Journal Of Composites Science, 6(5), 150. https://doi.org/10.3390/Jcs6050150

Wang, J. (1999). A Machinability Study of Polymer Matrix Composites Using Abrasive Waterjet Cutting Technology. Journal of Materials Processing Technology, 94(1), 30–35. https://doi.org/10.1016/S0924-0136(98)00443-9

Wang, J., & Guo, D. M. (2002). A Predictive Depth of Penetration Model for Abrasive Waterjet Cutting of Polymer Matrix Composites. Journal of Materials Processing Technology, 121(2–3), 390–394. https://doi.org/10.1016/S0924-0136(01)01246-8

Zhang, L., Huang, Y., Chen, G., Xu, M., Xia, W., & Fu, Y. (2019). Experimental Study of Coverage Constraint Abrasive Flow Machining of Titanium Alloy Artificial Joint Surface. Proceedings of the Institution of Mechanical Engineers, Part B: Journal of

Engineering Manufacture, 233(13), 2399–2409. https://doi.org/10.1177/0954405419840553

Zhang, S., & Li, X. (2010). Theoretical Analysis of Piercing Delicate Materials with Abrasive Water-Jet. Journal of the Chinese Institute of Engineers, 33(7), 1015–1019. https://doi.org/10.1080/02533839.2010.9671690

CHAPTER 6

HEMP FIBERS AS REINFORCEMENT MATERIAL IN POLYMER MATRIX COMPOSITES: EFFECTS OF SURFACE TREATMENT AND FABRIC DESIGN ON MECHANICAL PROPERTIES

Assoc. Prof. Dr. İbrahim Fadıl SOYKÖK[1]

[1] Manisa Celal Bayar University, Hasan Ferdi Turgutlu Faculty of Technology, Department of Mechatronics Engineering, 45400 Turgutlu, Manisa, Turkey
E-mail: ifsoykok@gmail.com, ibrahim.soykok@cbu.edu.tr
Tel: +90 236 314 10 10, ORCID ID: 0000-0001-8392-4505

1. INTRODUCTION

Due to the environmental concerns like efforts to reduce carbon emissions and to prevent the use of non-biodegradable petroleum products, bio-based composite production is gaining increasing importance and the studies to find the most suitable and efficient bio-compounds are continuously extended. Bio-composites can be made of both biopolymers and natural fiber reinforced petroleum oil-based polymers namely synthetic based polymers (Mirițoiu et al., 2019). Besides eco-friendly natures, natural fibers have a great potential to subrogate their synthetic counterparts because of reasonable cost, low specific weight, good thermal and acoustic insulating properties etc. (Chandramohan et al., 2011). There are many different types of natural fiber reinforcements that can be produced from animal products like wool/hair, silk, and feather. Also, plants are an important source of natural fiber as a rich and wide range origin of raw materials. Flax, jute, bamboo, pineapple leaf and oil palm fibers, kenaf, and industrial hemp are regarded as the most prominent plant based natural fibers (Mohanty et al., 2005). Mineral fibers which are mainly produced from asbestos, a natural mineral found usually in a crystalline structure in nature can be also regarded the third type of natural fibers (Figure 1). Nevertheless, using asbestos as a structural element have been avoided long since due to the inhalation of fibers is critically harmful to human and animal health.

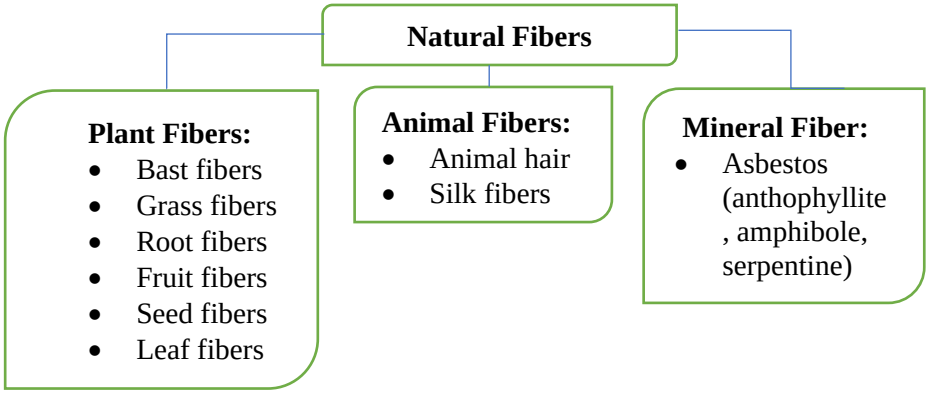

Figure 1: Classification of Natural Fibres (Lee et al. 2020)

Unfortunately, natural fibers employed as reinforcement in composites usually fail to satisfy some desirable features at which synthetic fibers are comparatively better. These include high strength and modulus of elasticity, resistance to moisture and heat, and compatibility with matrix material. Therefore, despite its forementioned advantages, the application area of natural fiber composites has remained at a very limited degree. Nevertheless, there are already applications in various fields, primarily in the automotive and construction sectors, which proves that natural fiber composites can be an alternative to ones with synthetic fibers. In fact, the use of jute, flax and hemp fibers in automobile door panels dates to the 90s (Fogorasi & Barbu, 2017). Natural fiber composites have now become an indispensable structural element used by leading automotive manufacturers in the construction of various parts of new model products, such as door panels, panel trays, trunk and boot linings, molded foot well linings, door trim panels, foot well linings, spare wheel compartment covers, engine or transmission covers and so on (Brett, 2008, Kozłowski & Mackiewicz-Talarczyk, 2020).

Natural plant fibers can be classified into many types of products according to their extracting techniques from plants. One of them is bast fibers which are extracted from inner part of fibrous plant stems such as papyrus, jute, ramie, roselle, kenaf, and hemp. As chemical content, lignin, pectin, and hemicelluloses are also present in the main cellulosic structure of the bast fibers. A bast layer is the secondary part in plants and surrounds the core layer. With its helically wounded micro-fibrils made of long cellulose molecules and containing less amount of waxes, oils, bast layer constitutes a prominent part of plants governing the mechanical features. Another plant-based reinforcing elements are the core fibers made of mostly porous structure and having short fibers. Those are primarily extracted from sisal, abaca, and raffia plant stems. Grass fibers are made of usually bamboo, banana stalk, rice, corn, sugarcane, napier grass, and bagasse are also utilized as stiffener member in composites. The grass fibers have a vascular bundle embedded parenchymatous texture generating hollow and cylindrical stem. Although, the fibers of grasses are resistant to mechanical loads, its widespread industrial use is inhibited by difficulties of processing and availability (Supa'at, 2012).

Among the natural fibers, due to superior mechanical properties, hemp (Cannabis sativa L.) fibers which belongs to the cannabis family are currently used in production of bio-composite parts in automotive components, insulating and packaging materials (Alawar et al., 2009). Due to its durable and strong fiber content, hemp has attracted a considerable

attention as the earliest developed known source of bast fiber (Kymäläinen, 2004). Regions having at least 650 mm annual rainfall, moist soil, humid atmosphere, and mild climate are preferable for hemp production. The total world hemp market supply is met nearly 70% by Russia, China, South Korea. Although its production was limited for being a source to make narcotic drag in 1948 in the US, several countries still produce hemp for textile and composite industry (Thygesen, 2006). Bio-composite applications account for nearly 14 %, whereas insulating material account for about 26 % of the total usage of hemp fibers (Carus et al., 2013). Hemp fiber with high strength, stiffness, tolerate solvent and creep resistance is regarded as one of the most available and convenient composite reinforcement (Väisänen et al. 2017).

Composites reinforced with hemp fibers can be a great alternative to synthetic fiber composites thanks to some chemical treatments or other innovative preparation techniques (Karri et al., 2022). In this review, the main reason for investigating particularly hemp plant fibers as a natural reinforcement is that the contribution of this plant to nature, ecological balance and economy is much more prominent compared to its rivals used for similar purposes. First, it is very important for the agricultural lands where hemp plantation is realized. As it covers the soil widely, it does not require the use of any chemicals to prevent harmful worms or pests and the growth of weeds. It is reported that hemp does not diminish the mineral structure of the soil, instead positively affects it. In fact, it is known that the soil productivity increases by 10-20% in lands planted with grain after hemp cultivation. In addition, thanks to the ability of hemp plant to absorb heavy metals from soil, it is an effective method for reintroducing lands contaminated due to industrial wastes to agriculture (Jonaitienė et al., 2016). It has varied sorts of hemp plants and each type of crop contributes directly or indirectly to the environment, economy, and human health. Up to a widespread prohibition in the 20th century due to its use in drugs, it had been a long history with human being. However, this ancient crop is gaining a renewed interest with changing perceptions (Phipps & Schluttenhofer, 2022). In this sense, in terms of its mechanical properties, it will be examined how competitive the cannabis plant, which has so many benefits to the nature as a reinforcing element in composite industry.

2. EXTRACTION AND MODIFICATION OF HEMP FIBERS (CANNABIS SATIVA L.) FOR COMPOSITE PRODUCTION

To make the hemp plant fibers functional in the production of composites, the harvested plants need to be passed through a series of processing stages. The first of these is named as the retting process, which means a separation action of plant fiber bundles from pectic ingredients and other substances like oil and waxes. In the retting process, it is possible to apply different methods separately or successively. However, each method has its own advantages and possible drawbacks, which will be discussed in the relevant sections. Afterwards, hemp fibers are subjected to some specific surface treatments using various chemical agents to be able form a good interfacial bond with the matrix material in composite structure. The type of treatment chemical has significant effects on the mechanical features of the composite structure to be produced. In this section, the retting and the surface treatment processes applied to convert cannabis sativa plants into reinforcement for composite production will be discussed in detail, including mechanical impacts on the final product.

2.1. Derivation of Fiber Bundles from Hemp Plant (Retting Process)

The stem diameters of original cannabis (hemp) plants are measured as between 5 – 15 mm while the plants can reach up to 2.5 m high (Liu et al., 2015). A hemp stem may comprise of 30-40% bast fibers by weight in the entire stem. A schematic full cross-section view of a hemp stem is given in Figure 2. It is also illustrated a macroscopic partial section of a typical hemp stem and its locally magnified partial section views showing primary and secondary fibers on a microscopic scale. The primary wall of the fiber is composed of tightly rolled cellulose micro fibrils constituting an irregular interwoven network (Ali et al., 2018). The secondary wall consists of crystalline cellulosic micro fibrils which are arranged helically. The micro fibrils are embedded into an amorphous matrix made of hemi-cellulose and pectin which provide them a binding medium. Additionally, the secondary wall has three individual sublayers, called inner, middle, and outer layers which are coded as S3, S2, and S1, respectively, in Figure 2. The middle layer S2 constitutes nearly 80% of the total sectional fiber area. So, S2 can be considered as the most responsible component for determining load bearing capacity and other mechanical features of a single fiber (Rong et al., 2001).

The bast fibers derived from hemp plant is of 15-55 mm length, 17-22.8 μm fiber diameter and 310-750 MPa tensile strength (Paridah et al., 2011). The hemp fibers predominantly composed of cellulose and hemicellulose constituents by nearly 74 % and 14 %, respectively. The substances like lignin, pectin, and other materials (oil and waxes) make up the remaining 12% of the bast fibers (Väisänen et al., 2018). A process separating the bast fibers from the woody core (xylem) is named as retting in which hemp stems are degraded. Retting is an important process that removes cementing materials from the fiber bundles for obtaining cellulose-rich hemp fibers with as little damage as possible, because removing effectively nonfibrous and woody matters from cellulosic fibers considerably affects chemical and physical properties of bast fibers (Fernando et al., 2019; Manimekalai & Kavitha, 2017). Separating long bast fibers from nonfibrous impurities is traditionally accomplished by using dew or water retting methods. However, several alternative degradation processes are also reported such as enzymatic, chemical, mechanical decortication and heat treatments (Paridah et al., 2011).

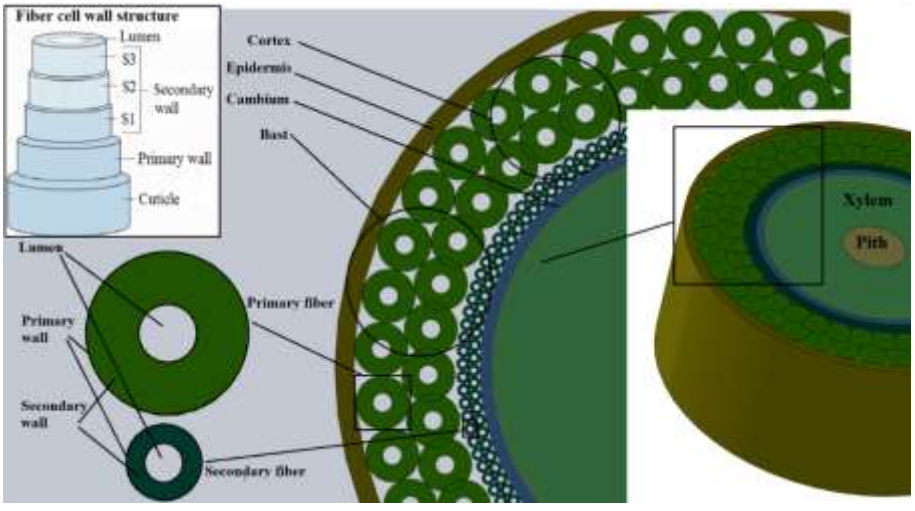

Figure 2: Simulated Transverse Section of Hemp Stem (Ramesh, 2018; Gedik & Avinc, 2020)

2.1.1. Dew Retting

Dew retting is based on leaving the plants in the field uniformly after harvesting, so microorganisms can separate fibers from the core. During the dew retting process plants are subjected to moisty atmosphere so pectins are

disintegrated by the aid of the formation of H_2 and CO_2 gases as well as the aerobic bacteria. The process enables bundles of bast fibers are easily separated by machines. The retting process should be stopped at the right time in order not to cause a possible over retting which may cause microorganisms to degrade cellulose fibers and reduce mechanical performance. Dew retting is a low labor cost and sustainable process; however, it has limitations such as relatively poor fiber quality, dark fiber color and dependence on uncontrollable weather conditions (Ramesh, 2018; Yusriah & Sapuan, 2018; Tulaphol et al., 2021).

2.1.2. Water Retting

Cold water retting and hot water retting are also conventional methods in which fiber sections of plants are immersed in running water of rivers or streams prior to be transferred to water tanks in which pectin is broken by anaerobic bacteria. In case the tanks are heated up to 40 ºC, it is possible to achieve cleaner and higher quality fibers. The water retting process enables better and easily controlled quality product in comparison to dew retting. The process doesn't require high technology machines and weather conditions are not determinant as opposed to dew retting process. Nevertheless, the method has also some drawbacks, like high water consumption, high cost of post-retting fiber drying process, and polluting wastewater (Ramesh, 2018; Gedik & Avinc, 2020; Horne, 2020).

2.1.3. Enzymatic Retting

In enzymatic retting process which enables to produce consistent high-quality fibers, special enzymes are utilized for separating basts fibers from plants. The enzymes are properly activated only at an optimum temperature at which denaturation starts (Foulk et al., 2001). The fibers treated by this way are more convenient to be employed as reinforcement in bio composites. This technique stands out with having low environmental impact, shorter duration, and good controllability (Hemmati et al., 2021). The activity and efficiency of the enzymes can be increased by some pretreatments such as mechanical procedures and chelating agents (Foulk et al., 2001; Henriksson et al., 1997; Akin et al., 2000).

2.1.4. Chemical Retting

Chemical retting process is commenced by submerging plants into sulfuric acid, sodium-potassium hydroxide, chlorinated lime, and soda ash solutions in hot water for dissolving pectin. Then fibers are depurated from remaining non-cellulosic matters by some surface-active agents. The cost of

chemical method is usually higher compared to traditional methods; however, it enables to get premium quality fibers as well as considerably reduce long processing time (Ramesh, 2018; Sanjay et al., 2019).

2.1.5. Mechanical Decortication

Mechanical extraction of fibers from dried straw is performed (sometimes after retting process) by scutching with shives. After that, the fibers are pulled through pin sets to remove any woody tissues and align the bundles in the same direction (Hänninen et al., 2012). In comparison of the alternative retting processes, mechanical decortication was found to be a simple and quick process giving high quantity of fibers (Lee et al., 2020).

2.2. Surface Treatments of Hemp Fibers for Composite Production

One of the prominent challenges of utilizing natural fibers in composite fabrication is known as poor wetting ability of the matrix material on fibers at interface prior to curing. Consequently, the poor wetting brings about a low strength interaction between the hydrophilic natural fibers and hydrophobic polymeric matrix. Modifying natural fiber surfaces with some physical, chemical, or mechanical techniques prior to manufacturing composite parts are well-accepted and valid methods to overcome this common obstacle (Narayana & Rao, 2021; Rong et al., 2001; Bledzki et al., 1996; Lu et al., 1999). The structure of natural fibers is known as a chemically complex natural composite itself, composed of lignin and hemicellulose matrix reinforced by helically arranged hard cellulose micro-fibrils. The content of hemp fiber structure is significantly altered by treatment processes, so lignin, cellulose and hemicellulose components are reduced to some extent (Moudood et al., 2019). So, each treatment method has distinctive impacts on natural fibers in terms of structural and functional properties. Such that, even in the chemical treatment method, the property changes could be quite different according to the type of the applied chemical, as can be seen in Table 1. The property changes also differ according to the type of the natural fiber treated or the concentration of alkali used for the process. Therefore, each kind of natural fiber has its own optimum concentration of chemical and distinctive change in property. For example, the increase in tensile strength of Abaca is measured as 8% with applying 5% optimum alkali solution, whereas Sisal exhibits 28% increase in tensile strength with the application of 5% optimum alkali solution (Narayana & Rao, 2021).

Table 1: Effects of Different Chemical Treatments on the General Properties of Natural Fibers (Ali et al., 2018; Peças et al., 2018; Kalia et al., 2009)

Treatment	Improve Tensile strength	Improve Tensile Modulus	Improve Flexural strength	Improve Flexural Modulus	Improve hydrophobicity	Reduce lignin content	Reduce moisture regain
Alkali	-	+	+	+	-	+	-
Acetylation	+	+	+	+	-	-	+
Benzoylation	+	-	-	-	+	-	-
Enzyme	-	-	-	-	-	+	-
Grafting	+	-	-	-	+	-	-
Isocyanate	-	-	-	-	+	-	-
Mercerization	+	-	-	-	+	-	+
Methacrylate	+	+	+	+	-	-	-
Ozone	-	-	-	-	+	-	-
Peroxide	-	-	-	-	-	-	+
Plasma	-	-	-	-	+	-	-
Silane	-	+	+	+	+	-	-
Sodium chlorite	+	+	+	+	-	-	-

2.2.1. Effect of Surface Treatment on Mechanical Properties

The Effects of treatment with different chemicals and their specific concentrations on tensile and flexural properties of hemp fiber composites are noteworthy (Sepe et al., 2018). As seen in Table 2, tensile strengths of hemp fiber composites are adversely affected by both NaOH and Silane treatments to some certain extents depending on the concentration of chemical solution. However, the situation appears to be different for tensile modulus. Such that, as a treatment chemical, the use of Silane contributes to improve the tensile modulus considerably depending on the concentration, whereas the application of NaOH solution plays even an adverse role on tensile modulus. As for the flexural strength, hemp fiber composite is badly affected again by NaOH treatment. When the solution chemical is switched to silane, however, the chemical treatment especially those with low concentrations exerts a

significant impact on increasing flexural strength of hemp fiber composites. The variation in flexural stiffness of hemp fiber composite according to the chemical type and concentration occurs nearly in a similar manner as flexural strength. Briefly, 1 % the optimum concentration of silane treatment improves mechanical properties (tensile modulus, flexural strength, and flexural stiffness) of hemp fiber composites except for tensile strength. Regardless of the concentration, the treatments made with the chemical NaOH reflect negatively on the mechanical properties of hemp fiber composites.

As listed in Table 2, the flexural strength and flexural modulus of alkali treated fiber are both 27% higher than the composite made with untreated hemp fibers. The possible reasons of these property enhancements are removal of constituents like lignin and hemicelluloses from fiber bundles. Similar but slightly lover degree improvements are also observed in silane treated hemp fiber composites compared to untreated ones. These increments (16% and 23% in respectively flexural strength and flexural modulus) can be attributed to that silane molecules are reacted with reactive OH molecules causing to form siloxane bridges in fiber-matrix interface bonding faces (Kabir et al., 2012; Abdelmouleh et al., 2007). The acetylation treatment contributes the flexural properties presumably by removing hemicelluloses and lignin matters thanks to acetic anhydride reactions on the fiber surface. Among the tested UPR matrix composites, the acetylation process turns out to be the less effective technique and enables the lowest rates of increase in flexural strength and flexural modulus by 12% and 14%, respectively.

Table 2: Mechanical Properties of Treated Hemp Fiber Reinforced Composites (Epoxy Resin "Er" Unsaturated Polyester Resin "UPR", Polypropylene "PP") ([1]Sepe et al., 2018; [2]Kabir et al., 2012; [3]Ragoubi et al., 2010).

Treatment	Concentration of chemical %	Fiber Weight fraction (%w)	Matrix material	Tensile strength (MPa)	Tensile Modulus (MPa)	Flexural strength (MPa)	Flexural Modulus (MPa)	Reference
Untreated	-	42	ER	80.74	5336	118.35	3999	[1]
NaOH	1	42	ER	69.24	5270	114.27	3773	[1]
NaOH	5	42	ER	60.89	4947	114.02	3695	[1]
Silane	1	42	ER	71.55	5847	124.52	4145	[1]

Silane	5	42	ER	72.16	5828	122.54	4186	[1]
Silane	20	42	ER	73.24	5543	113.75	4032	[1]
Untreated	-	10	UPR	-	-	47.50	3500	[2]
Alkali	8	10	UPR	-	-	60.51	4440	[2]
Silane	8	10	UPR	-	-	54.95	4310	[2]
Acetylation	8	10	UPR	-	-	53.31	4000	[2]
Untreated	-	20	PP	28.60	1079	-	-	[3]
Corona discharge	-	20	PP	37.80	1215	-	-	[3]

Corona discharge treatment (CDT) is a physical treatment method applied on fibers or polymer matrix to improve mutual surface compatibility and bondability properties (Park & Seo, 2011). The process utilizes high voltage electrodes to perform a plasma process and affects loose fibers on textiles (Kulkarni, 2019). Corona discharge treatment improve fiber-matrix interactions by inducing surface oxidation (Belgacem & Gandini, 2005). The effect of CDT is very remarkable on tensile properties of hemp fiber reinforced polypropylene matrix composites as seen in Table 2. The increases in tensile strength as 32%, and tensile modulus 13% are mainly attributed to mechanical ablation effect of oxygen plasma bombardment on the fiber surface (Kabir et al., 2012; Sun et al., 2006).

2.2.2. Effect of Surface Treatment on Thermal Properties

The sort of treatment chemical is also effective on thermal properties of hemp fiber composites as seen in Table 3. The obtained Glass Transition Temperature (T_g) increased from 181 ºC to 214 ºC as the material is changed from neat resin to silane treated hemp fiber reinforced composite. Remaining cyclohexane/ethanol and alkali-treated hemp fiber reinforced samples take intermediate T_g values which are also superior to that of neat resin. The values such as 5 % weight loss decomposition temperature (T_5), 10 % weight loss decomposition temperature (T_{10}), and char yield (Y_c) are essential for measuring the thermal stability. The neat poly-benzoxazine resin exhibits the highest T_5, T_{10}, and Y_c thermal stability indicators recorded as 338 ºC, 365 ºC, and 28.7%, respectively. Also, reinforcement with hemp fibers is observed to reduce the thermal stability values. Nevertheless, the significance of treatment chemical on the thermal stability is clearly read from Table 3. The treatment of hemp fibers with the solution of silane is found to cause the lowest decrease in thermal stability values (T_5, T_{10}, and Y_c) of poly-benzoxazine based material (Dayo et al., 2018).

Table 3: Thermal parameters of hemp fiber/poly-benzoxazine composites on different treatments of fibers (Dayo et al., 2018)

Fiber treatment chemical	E' (GPa, 50ºC)	T_g (ºC)	T_5 (ºC)	T_{10}(ºC)	Y_c (%, at 800 ºC)
Neat Resin	2.31	181	338	365	28.7
Cyclohexane/ ethanol	2.98	195	313	337	28.2
Alkali	3.18	211	321	342	28.3
Silane	3.41	214	324	346	28.5

2.2.3. Effect of Surface Treatment on Water Absorption

Susceptibility to moisture is one of the most delicate issues in designing natural fiber composites (Alshahrani et al., 2022). Especially after surface treatment in water based chemical solutions, the plant based bast fibers may contain some moisture inside reaching up to 15% in hemp fibers, 20% in Jute fiber, 2.3% in flax fibers, and 21% in kenaf fibers (Paridah et al., 2011). This moisture should be then removed by vaporizing in vacuum driers or similar devices. Up-taking excessive moisture from humid medium may be quite harmful for fiber-matrix interface of which quality is of critical importance for the mechanical properties of composite. Besides, natural fibers such as hemp fibers admit of the moisture to be soaked up which break hydrogen bonds at the amorphous region. For this reason, inter-molecular spaces are formed between the cellulose chains resulting in swollen natural fibers (Moudood et al., 2019). However, whether caused by immersion in water or by the humidity of the surrounding environment, swelling is usually not a case for the synthetic counterparts of natural fibers (Zhai et al., 2016).

The poly-benzoxazine neat resin has a very low water absorption property, so the calculated diffusion coefficient is only $5.05x10^{-9}$ m^2/s and 0.58% water uptake observed in one-week immersing time (Table 4). On the other hand, when reinforced with natural fibers the hydrophobic poly-benzoxazine resin couldn't bear against water uptake. The water absorption phenomenon in a natural fiber composite is dependent on various factors including fiber-matrix volume fraction, fiber type, fiber orientation, water temperature. When these parameters are kept constant, it is clear from Table 4 that the surface treatment chemical applied on hemp fibers has a dramatical impact on water diffusion rate as well as saturated % moisture uptake of

composites. Here, the surface treatment of hemp fibers with the chemical silane brings about a top-quality fiber/matrix interface which also imply reduced polar functional OH groups in the composite body. So, the most reduced amount of water uptake saturation content and minimum diffusion velocity is observed in those reinforced by silane-treated hemp fibers.

Table 4: The water absorption parameters for the hemp fibre composites at ambiance temperature (Dayo et al., 2018; Bollino et al., 2023)

Matrix material	**Chemical treatment**	**Saturation content %**	**Diffusion coefficient (10^{-9} m^2/s)**
Neat poly-benzoxazine	-	0.76	5.05
Poly-benzoxazine	Cyclohexane/ethanol (1:1, v/v)	7.06	11.67
Poly-benzoxazine	Alkaline NaOH 10%	5.33	10.26
Poly-benzoxazine	Silane/ethanol-water mixture (1g/100ml)	4.47	9.71
Epoxy	Untreated	7.74	1850
Epoxy	Alkaline NaOH 1%	7.86	1850
Epoxy	Alkaline NaOH 5%	6.46	1260
Epoxy	Silane 1%	6.76	1350
Epoxy	Silane 5%	5.58	1210
Epoxy	Silane 20%	7.24	1300

3. THE TEXTILE STRUCTURES OF HEMP FIBRES FOR COMPOSITE PRODUCTION

For ensuring high mechanical performance, it is more desirable to utilize fully aligned fiber bundles. However, the length of bast fibers is restricted and therefore to achieve an effective load transmission is a more challenging issue than continuous synthetic fibers. Spinning of natural fibers into yarns is known as a useful technique to create continuous fibers from bast fibers having limited lengths (Lu et al., 2022; Yang et al., 2021). Both the efficiency of fiber length and optimal angle of orientation have been primary focused parameters for improving mechanical performance of composites produced by using bast fibers. The textile technology provides a wide range design alternatives for composite production (Lu et al., 2022). There are various types of designed natural fiber reinforcing textures such as twill, satin, and plain-woven hemp fabrics as illustrated in Figure 3 (Corbin et al., 2020a, 2020b). Although using these woven fabrics brings in composite material

superior mechanical features in both two fiber directions, there are also some unavoidable drawbacks such as the adverse effect of yarn twist angle causing to reduce the fiber strength in the final composite and misalignment of fibers due to interleaving yarns (Lu et al., 2022; Madsen et al., 2009). Alternative natural fiber-based textiles having unidirectional fibers are also produced for producing effective green composites. To visualize the refenced semi-products, macro photos of reinforcing elements composed of diverse type woven hemp fabrics and alternative unidirectional hemp fibers are given in Figure 4. In fact, the tensile strengths of unidirectional hemp fiber reinforced composites are very close and sometimes even relatively higher than those made by weaved fabrics although having lover fiber mass fraction as seen in Table 5. It also consists of special strength ratio ($R_{\sigma/F}$) of composites produced using different forms of hemp reinforcements which is derived by dividing maximum tensile strengths (σ_{max}) to fiber mass fractions (F_{fm}). $R_{\sigma/F}$ stands for the comparison value free from the effect of the fiber mass fraction of the maximum strength values. In the reviewed literature, the highest $R_{\sigma/F}$ are observed at unidirectional hemp roving and unidirectional hemp felt reinforced epoxy resin matrix composites as 5.91 MPa and 5.22 MPa, respectively. It proves higher mechanical features of hemp fiber composites composed of fully aligned fiber bundles in comparison to woven fabric reinforced composites at equivalent fiber mass fractions. The Studies have revealed that randomly oriented hemp fiber composites exhibit relatively the lowest strength values in case fiber weight ratios are considered.

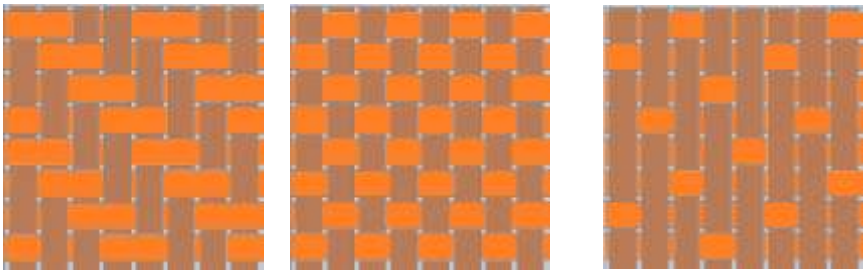

(a) (b) (c)

Figure 3: Types of fabric weaves a) twill, b) satin, c) plain

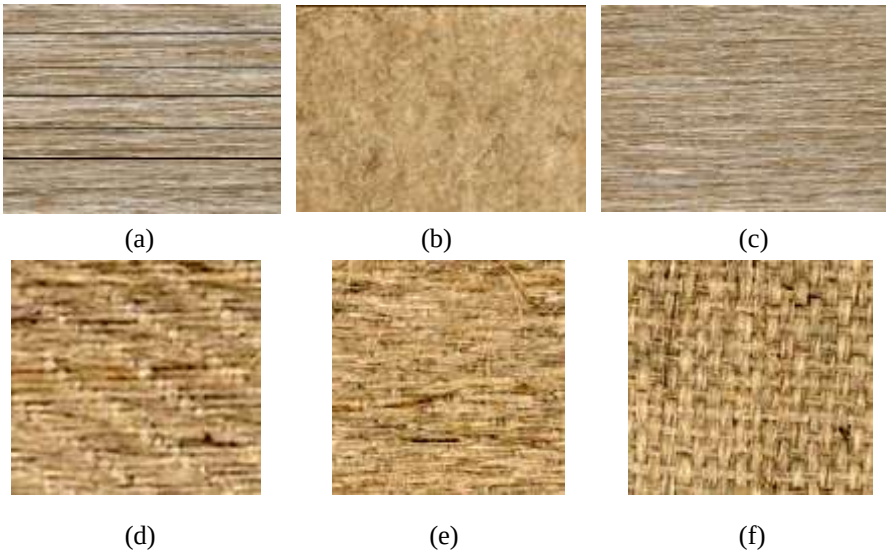

Figure 4: Pictures of a) Unidirectional hemp felt, b) Randomly orientated hemp felt, c) Hemp roving d) twill 6 weft, e) Satin 6 weft, f) Plain woven hemp fabrics (Corbin et al., 2020)

Table 5 also illustrates that, the plain woven, basket and twill hemp fabric reinforced composites reach moderate tensile strengths, where twill fabrics, among them, reach slightly more satisfactory strength value of which $R_{\sigma/F}$ was calculated as 4.53 MPa, the closest value to those of the unidirectional hemp fiber composites. The elastic properties of unidirectional reinforced hemp composites appear to be also superior to those of their alternatives. So, the highest tensile modulus encountered in the reviewed literature is 19.00 GPa value of a unidirectional hemp roving reinforced epoxy resin composite with only 33% fiber mass ratio.

Table 5: Relevant research results regarding tensile strength of different fabric tissued hemp fibre composites in the literature ([1]Lu et al., 2022, [2]Liu et al., 2015, [3]Gouanve et al., 2006; [4]Shah et al., 2014; [5]Karaduman, 2022; [6]Corbin et al., 2020).

Reinforcement	Matrix	Fiber mass fraction F_{fm} (%)	Molding Method	Special strength ratio (MPa) " $R_{\sigma/F}= \sigma_{max}/$	Tensile strength σ_{max} (MPa)	Tensile modulus E (GPa)	Reference
U.D. hemp felt	Unsaturated polyester resin	32	Hot press molding	5.22	166.9	10.48	[1]
Randomly orientated hemp felt	Unsaturated polyester resin	50	Hot press molding	1.68	84.0	-	[2]
Randomly orientated hemp felt	Unsaturated polyester resin	50	Hot press molding	2.30	115.0	11.50	[3]
Hemp roving fabric with twill 6 weft effect	Epoxy resin	45	Hot press molding	4.53	203.8	-	[4]
Hemp roving	Epoxy resin	33	Vacuum assisted resin infusion	5.91	195.0	19.00	[5]
Hemp roving	Unsaturated polyester resin	35	Vacuum assisted resin infusion	4.89	171.0	15.60	[5]
Plain woven hemp	Unsaturated polyester resin	30	Hot press molding	1.88	56.52	5.62	[1]

Quasi-U.D hemp felt	Unsaturated polyester resin	30	Hot press molding	4.61	138.19	8.95	[1]
U.D. hemp	Epoxy resin	39	Compression molding	3.79	147.77	8.02	[6]
Plain woven 1/1 hemp	Epoxy resin	31	Compression molding	2.72	84.27	4.73	[6]
Basket 2/2 hemp	Epoxy resin	33	Compression molding	2.23	73.49	4.52	[6]
Twill 2/2 hemp	Epoxy resin	32	Compression molding	2.08	66.56	4.18	[6]

4. CONCLUSION

With eco-friendly natures, hemp fiber reinforced composites as well as other natural fiber added counterparts are currently becoming more competing products and gaining gradually a potential to substitute synthetic fiber composites owing to extensive investigations and innovative scientific efforts. The most leading challenges to achieve the replacement of synthetic fibers with organic substitutes are poor fiber-matrix interfacial bonding, hydrophilic nature of natural fibers, susceptibility to moisture uptake, and a relatively more pronounced cutback effect of twist angles on ultimate strengths of some woven natural fiber fabrics. The current paper has given a review on studies addressing to evaluate mechanical, thermomechanical, and sensitiveness to moisture features of hemp fiber composites which can be controlled by some parameters like fiber surface treatment methods and fabric design etc. It can be concluded from the research that surface treatments applied on hemp fibers with only the concentration in some certain ranges gives produced composites extra stiffness and strength as well as durability to

humid conditions. The studies also reveal that fabrics with fully aligned fiber bundles offers to composites consisting of hemp fibers higher mechanical performance in comparison to weaved and randomly oriented fiber fabrics.

REFERENCES

Abdelmouleh, M., Boufi, S., Belgacem, M. N., & Dufresne, A. (2007). Short natural-fibre reinforced polyethylene and natural rubber composites: Effect of silane coupling agents and fibres loading. *Composites Science and Technology*, *67*(7–8), 1627-1639. https://doi.org/10.1016/j.compscitech.2006.07.003

Akin, D.E., Dodd, R.B., Perkins. W., Henriksson. G., & Eriksson. K-EL. (2000). Spray Enzymatic Retting: A New Method for Processing Flax Fibers. *Textile Research Journal*, *70*(6), 486-494. https://doi:10.1177/004051750007000604

Alawar, A., Hamed, A. M., & Al-Kaabi, K. (2009). Characterization of treated date palm tree fiber as composite reinforcement. *Composites Part B: Engineering*, *40*(7), 601-606. https://doi.org/10.1016/j.compositesb.2009.04.018

Ali, A., Shaker, K., Nawab , Y., Jabbar, M., Hussain, T., Militky, J., & Baheti, V. (2018). Hydrophobic treatment of natural fibers and their composites—A review. *Journal of Industrial Textiles, 47*(8), 2153-2183. https://doi.org/10.1177/1528083716654468

Alshahrani, H., Alshammari, B. A., Shah, A. H., & Dayo, A. Q. (2022). Development of Hybrid Composite Utilizing Micro-Cellulose Fibers Extracted from Date Palm Rachis in the Najran Region. *Polymers*, *14*(21), 4687. https://doi.org/10.3390/polym14214687

Belgacem, M. N., & Gandini, A. (2005). The surface modification of cellulose fibres for use as reinforcing elements in composite materials. *Composite Interfaces*, *12*(1-2), 41-75. https://doi.org/10.1163/1568554053542188

Bledzki, A.K., Reihmane, S., & Gassan, J. (1996). Properties and modification methods for vegetable fibers for natural fiber composites. *J. Appl. Polym. Sci.*, *59*, 1329-1336. https://doi.org/10.1002/(SICI)1097-4628(19960222)59:8<1329::AID-APP17>3.0.CO;2-0

Bollino, F., Giannella, V., Armentani, E., & Sepe, R. (2023). Mechanical behavior of chemically-treated hemp fibers reinforced composites subjected to moisture absorption. *Journal of Materials Research and Technology*, *22*, 762-775. https://doi.org/10.1016/j.jmrt.2022.11.152

Brett, C. S. (2008). Industrial Fibres: Recent and Current Developments. *Proceedings of the Symposium on Natural Fibres (Rome). i0709e10*. https://www.fao.org/3/i0709e/i0709e10.pdf

Carus, M. C., Karst, S., Kauffmann, A., Hobson, J., & Bertucelli, S. (2013). The european hemp industry: Cultivation, processing and applications for fibres, shives and seeds. *European Industrial Hemp Association*, *1*(9).

Chandramohan, D., & Marimuthu, K. (2011). A Review on Natural Fibers. *International Journal of Research and Reviews in Applied Sciences*, *8*, 194-206.

Corbin, A. C., Ferreira, M., Labanieh, A. R., & Soulat, D. (2020). Natural fiber composite manufacture using wrapped hemp roving with PA12. *Materials Today: Proceedings*, *31*(2), 329-334. https://doi.org/10.1016/j.matpr.2020.02.307

Corbin, A. C., Soulat, D., Ferreira, M., Labanieh, A. R., Gabrion, X., Malécot, P., & Placet, V. (2020). Towards hemp fabrics for high-performance composites: Influence of weave pattern and features. *Composites Part B: Engineering*, *181*, 107582. https://doi.org/10.1016/j.compositesb.2019.107582

Dayo, A. Q., Zegaoui, A., Nizamani, A. A., Kiran, S., Wang, J., Derradji, M., Cai, W. A., & Liu, W. B. (2018). The influence of different chemical treatments on the hemp fiber/polybenzoxazine based green composites: Mechanical, thermal and water absorption properties. *Materials Chemistry and Physics*, *217*, 270-277. https://doi.org/10.1016/j.matchemphys.2018.06.040

Fernando, D., Thygesen, A., Meyer, A. S., & Daniel, G. (2019). Elucidating field retting mechanisms of hemp fibres for biocomposites: Effects of microbial actions and interactions on the cellular micro-morphology and ultrastructure of hemp stems and bast fibres, *BioRes*. 14(2), 4047-4084.

Fogorasi, M.S., Barbu, I. (2017). The potential of natural fibres for automotive sector – review. *IOP Conf. Ser.: Mater. Sci. Eng. 252*, 012044. https://doi.org/10.1088/1757-899X/252/1/012044

Foulk, J. A., Akin, D. E., & Dodd, R. B. (2001). Processing techniques for improving enzyme-retting of flax. *Industrial Crops and Products*, *13*(3), 239-248. https://doi.org/10.1016/S0926-6690(00)00081-9

Gedik, G., & Avinc, O. (2020). Hemp Fiber as a Sustainable Raw Material Source for Textile Industry: Can We Use Its Potential for More Eco-

Friendly Production?, In: S. Muthu, & M. Gardetti (Eds.), *Sustainability in the Textile and Apparel Industries. Sustainable Textiles: Production, Processing, Manufacturing & Chemistry*. Springer, Cham. https://doi.org/10.1007/978-3-030-38541-5_4

Gouanve, F., Meyer, M., Grenet, J., Marais, S., Poncin-Epaillard , F., & Saiter, J. M. (2006). Unsaturated polyester resin (UPR) reinforced with flax fibers, untreated and cold He plasma-treated: Thermal, mechanical and DMA studies. *Composite Interfaces*, *13*(4-6), 355-364. https://doi.org/10.1163/156855406777408548

Hänninen, T., Thygesen, A., Mehmood, S., Madsen, B., & Hughes, M. (2011). Mechanical processing of bast fibres: The occurrence of damage and its effect on fibre structure. *Industrial Crops and Products*, *39*, 7-11. https://doi.org/10.1016/j.indcrop.2012.01.025

Hemmati, F., Farizeh, T., & Mohammadi-Roshandeh, J. (2021). Lignocellulosic Fiber-Reinforced PLA Green Composites: Effects of Chemical Fiber Treatment. In: M.T. Hameed Sultan, M.S.A. Majid, M.R.M. Jamir, A.I. Azmi, & N. Saba, (Eds.), *Biocomposite Materials. Composites Science and Technology* (pp.97-204) Springer, Singapore. https://doi.org/10.1007/978-981-33-4091-6_5

Henriksson, G., Akin, D. E., Rigsby, L. L., Patel , N., & Eriksson , K. E. (1997). Influence of Chelating Agents and Mechanical Pretreatment on Enzymatic Retting of Flax. *Textile Research Journal*, *67*(11), 829-836. https://doi.org/10.1177/004051759706701107

Horne, M.R.L. (2020). 5 - Bast fibres: hemp cultivation and production, In: R.M. Kozłowski, & M. Mackiewicz-Talarczyk (Eds.), *In Woodhead Publishing Series in Textiles, Handbook of Natural Fibres* (2nd ed.), (pp. 163-196). Woodhead Publishing. https://doi.org/10.1016/B978-0-12-818398-4.00007-4

Jonaitienė, V., Jankauskienė, Z., Stuogė, I. (2016). Hemp Cultivation Opportunities and Perspectives in Lithuania. In: Fangueiro, R., Rana, S. (eds) Natural Fibres: Advances in Science and Technology Towards Industrial Applications. RILEM Bookseries, vol 12. Springer, Dordrecht. https://doi.org/10.1007/978-94-017-7515-1_32

Kabir, M. M., Wang, H., Lau, K. T., Cardona, F., & Aravinthan, T. (2012). Mechanical properties of chemically-treated hemp fibre reinforced sandwich composites. *Composites Part B: Engineering*, *43*(2), 159-169. https://doi.org/10.1016/j.compositesb.2011.06.003

Kalia, S., Kaith, B. S., & Kaur, I. (2009). Pretreatments of natural fibers and their application as reinforcing material in polymer composites—A review. *Polym Eng Sci*, *49*, 1253-1272. https://doi.org/10.1002/pen.21328

Karri, R., Lappalainen, R., Tomppo, L., & Yadav, R. (2022). Bond quality of poplar plywood reinforced with hemp fibers and lignin-phenolic adhesives. *Composites Part C: Open Access*, *9*, 100299. https://doi.org/10.1016/j.jcomc.2022.100299

Kozłowski, R. M., & Mackiewicz-Talarczyk, M. (2020). *Handbook of natural fibres: Processing and applications* (2nd ed.). Woodhead Publishing Limited.

Kulkarni, S. (2019) 3 - Plasma Assisted Polymer Synthesis and Processing. In S. Thomas, M. Mozetič, U. Cvelbar, P. Špatenka, & K.M. Praveen (Eds.), *Non Thermal Plasma Technology for Polymeric Materials* (pp. 67-93). Elsevier. https://doi.org/10.1016/B978-0-12-813152-7.00003-2.

Kymäläinen, H. R. (2004). *Quality of Linum usitatissimum L. (flax and linseed) and Cannabis sativa L. (fibre hemp) during the production chain of fibre raw material for thermal insulations* [Doctoral dissertation, University of Helsinki].

Lee, C. H., Khalina, A., Lee, S., & Ming Liu (2020). A Comprehensive Review on Bast Fibre Retting Process for Optimal Performance in Fibre-Reinforced Polymer Composites. *Advances in Materials Science and Engineering*, *Article ID 6074063*. https://doi.org/10.1155/2020/6074063

Liu, M., Fernando, D., Daniel, G., Madsen, B., Meyer, A. S., Ale, M. T., & Thygesen, A. (2015). Effect of harvest time and field retting duration on the chemical composition, morphology and mechanical properties of hemp fibers. *Industrial Crops and Products*, *69*, 29-39. https://doi.org/10.1016/j.indcrop.2015.02.010

Liu, W., Xie, T., & Qiu, R. (2015). Styrene-free unsaturated polyesters for hemp fibre composites. *Composites Science and Technology*, *120*, 66-72. https://doi.org/10.1016/j.compscitech.2015.10.017

Lu, C., Wang, C., Liu, S., Zhang, H., Tong, J., Yi, X., & Zhang, Y. (2022). Towards high-performance textile-structure composite: Unidirectional hemp fiber tape and their composite. *Industrial Crops and Products*, *189*, 115821. https://doi.org/10.1016/j.indcrop.2022.115821

Lu, X., Zhang, M.Q., Rong, M.Z., Shi, G., Yang, G.C., & Zeng, H.M. (1999). Natural Vegetable Fibre / Plasticised Natural Vegetable Fibre - a Candidate for Low Cost and Fully Biodegradable Composite. *Advanced Composites Letters*, *8*(5). https://doi:10.1177/096369359900800505

Madsen, B., Thygesen, A., & Lilholt, H. (2009). Plant fibre composites – porosity and stiffness. *Composites Science and Technology*, *69*(7–8), 1057-1069. https://doi.org/10.1016/j.compscitech.2009.01.016

Manimekalai, G., & Kavitha, S. (2017). A review on application of retting techniques for natural fiber extraction. *Int. Journal of Creative Research Thoughts*, *5*(4), 372-377.

Miriţoiu, C. M. M., Stănescu, M. M., Burada, C. O., Bolcu, D., Pădeanu, A., & Bolcu, A. (2019). Comparisons between some composite materials reinforced with hemp fibers. *Materials Today: Proceedings*, *12*(2), 499-507. https://doi.org/10.1016/j.matpr.2019.03.155

Mohanty, A.K., Misra, M., & Drzal, L.T. (Eds.). (2005). Natural Fibers, Biopolymers, and Biocomposites (1st ed.). CRC Press. https://doi.org/10.1201/9780203508206

Moudood, A., Rahman, A., Öchsner, A., Islam, M., & Francucci, G. (2019). Flax fiber and its composites: An overview of water and moisture absorption impact on their performance. *Journal of Reinforced Plastics and Composites*, *38*(7), 323-339. https://doi:10.1177/0731684418818893

Narayana, V. L., & Rao, L. B. (2021). A brief review on the effect of alkali treatment on mechanical properties of various natural fiber reinforced polymer composites. *Materials Today: Proceedings*, *44*(1), 1988-1994. https://doi.org/10.1016/j.matpr.2020.12.117

Paridah, M. T., Ahmed, A. B., SaifulAzry, S. O. A., & Ahmed, Z. (2011). Retting process of some bast plant fibers and its effect on fibre quality: A review. *BioRes.* 6(4), 5260-5281.

Park, S.J., & Seo, M.K. (2011) 3 - Solid-Liquid Interface, In S.J. Park, & M.K. Seo (Eds.), *Interface Science and Technology*, (pp. 147-252). Elsevier. https://doi.org/10.1016/B978-0-12-375049-5.00003-7.

Peças, P., Carvalho, H., Salman, H., & Leite, M. (2018). Natural Fibre Composites and Their Applications: A Review. *Journal of Composites Science*, *2*(4), 66. https://doi.org/10.3390/jcs2040066

Phipps, B., Schluttenhofer, C. (2022). Chapter 1 - Perspectives of industrial hemp cultivation. In M. Pojić, B. K. Tiwari (Ed.). Industrial Hemp

(pp. 1-36). Academic Press. https://doi.org/10.1016/B978-0-323-90910-5.00002-6

Ragoubi, M., Bienaimé, D., Molina, S., George, B., & Merlin, A. (2010). Impact of corona treated hemp fibres onto mechanical properties of polypropylene composites made thereof. *Industrial Crops and Products*, *31*(2), 344-349. https://doi.org/10.1016/j.indcrop.2009.12.004

Ramesh, M. (2018). 9 - Hemp, jute, banana, kenaf, ramie, sisal fibers, In A. R. Bunsell (Eds.), *The Textile Institute Book Series, Handbook of Properties of Textile and Technical Fibres* (2nd ed.) (pp. 301-325). Woodhead Publishing. https://doi.org/10.1016/B978-0-08-101272-7.00009-2.

Rong, M. Z., Zhang, M. Q., Liu, Y., Yang, G. C., & Zeng, H. M. (2001). The effect of fiber treatment on the mechanical properties of unidirectional sisal-reinforced epoxy composites. *Composites Science and Technology*, *61*(10), 1437-1447. https://doi.org/10.1016/S0266-3538(01)00046-X

Sahbaz Karaduman , N. (2021). Experimental investigation of the effect of weave type on the mechanical properties of woven hemp fabric/epoxy composites. *Journal of Composite Materials*, *56*(8), 1255-1265. https://doi.org/10.1177/00219983221075416

Sanjay, M. R., Siengchin, S., Parameswaranpillai, J., Jawaid, M., Pruncu, C. I., & Khan, A. (2019). A comprehensive review of techniques for natural fibers as reinforcement in composites: Preparation, processing and characterization. *Carbohydrate Polymers*, *207*, 108-121. https://doi.org/10.1016/j.carbpol.2018.11.083

Sepe, R., Bollino, F., Boccarusso, L., & Caputo, F. (2018). Influence of chemical treatments on mechanical properties of hemp fiber reinforced composites. *Composites Part B: Engineering*, *133*, 210-217. https://doi.org/10.1016/j.compositesb.2017.09.030

Shah, D. U., Schubel, P. J., Clifford, M. J., & Licence, P. (2014). Mechanical Property Characterization of Aligned Plant Yarn Reinforced Thermoset Matrix Composites Manufactured via Vacuum Infusion. *Polymer-Plastics Technology and Engineering*, *53*(3), 239-253. https://doi.org/10.1080/03602559.2013.843710

Sun, D., & Stylios, G. K. (2006). Fabric surface properties affected by low temperature plasma treatment. *Journal of Materials Processing*

Technology, *173*(2), 172-177. https://doi.org/10.1016/j.jmatprotec.2005.11.022

Supa'at, I. (2012). *Preparation and characterization of biocomposites prepared from polyvinyl alcohol, starches and fibers* [Doctoral dissertation, University of Malaya].

Thygesen, A. (2006). *Properties of hemp fibre polymer composites - An optimization of fibre properties using novel defibration methods and detailed fibre characterization* [Doctoral dissertation, Risø National Laboratory, Denmark].

Tulaphol, S., Sun, Z., & Sathitsuksanoh, N. (2021). 6 - Biofuels and bioproducts from industrial hemp, In: Y. Li & W. Zhou (Eds.), *Advances in Bioenergy*, 6(1) (pp. 301-338). Elsevier. https://doi.org/10.1016/bs.aibe.2021.06.003

Väisänen, T., Batello, P., Lappalainen, R., & Tomppo, L. (2018). Modification of hemp fibers (Cannabis Sativa L.) for composite applications. *Ind. Crops Prod.*, *111*, 422-429. https://doi.org/10.1016/j.indcrop.2017.10.049

Yang, X., Fan, W., Ge, S., Gao, X., Wang, S., Zhang, Y., Foong, S. Y., Liew, R. K., Lam, S. S., & Xia, C. (2021). Advanced textile technology for fabrication of ramie fiber PLA composites with enhanced mechanical properties. *Industrial Crops and Products*, *162*, 113312. https://doi.org/10.1016/j.indcrop.2021.113312

Yusriah, L., & Sapuan, S.M. (2018). 6 - Properties of Betel Nut Husk Reinforced Vinyl Ester Composites, In S.M. Sapuan, H. Ismail & E.S. Zainudin (Eds.), *In Woodhead Publishing Series in Composites Science and Engineering, Natural Fibre Reinforced Vinyl Ester and Vinyl Polymer Composites* (pp. 129-155). Woodhead Publishing. https://doi.org/10.1016/B978-0-08-102160-6.00006-8

Zhai, Z., Feng, L., Liu, Z., & Li, G. (2016). Water absorption test for carbon fiber epoxy resin composite based on electrical resistance. *Polymer Testing*, *56*, 394-397. https://doi.org/10.1016/j.polymertesting.2016.10.020

CHAPTER 7

THERMOPHOTOVOLTAIC SYSTEM SETUP AND ANALYSIS WITH USING GALLIUM ANTIMONIDE (GaSb) CELL IN HIGH TEMPERATURE

Research Assistant Büşra Selenay ÖNAL [1]*

Assist. Prof. Dr., Kaan KOÇALİ [2,3]

[1] Research Assistant, Istanbul Aydin University, Engineering Faculty, Department of Mechanical Engineering, Kucukcekmece, Istanbul, Turkey, bselenayonal@aydin.edu.tr, ORCID: 0000-0002-4856-9816

[2] Assist. Prof. Dr., Istanbul Gelisim University, Istanbul Gelisim Vocational School, Occupational Health and Safety Program, Avcilar, Istanbul, Turkey, kkocali@gelisim.edu.tr

[3] CEO & Occupational Health and Safety Specialist (A Class), Kampus Mining Consulting Mac. Ind. Dom. and For. Trade Co. Ltd., Kucukcekmece, Istanbul, Turkey, kaan.kocali@kampusmadencilik.com.tr, ORCID: 0000-0002-1329-6176

INTRODUCTION

Energy is one of the most important consumption items and an indispensable civilization tool in our age. Energy consumption, which is one of the most important needs of countries with a high level of development, is constantly increasing. We have consumed energy in order for the opportunities offered by technological developments to continue in our lives (Koçali, 2016; Le & Nguyen, 2019; Wen et al., 2021; Lee et al., 2022). Energy is one of the cornerstones of civilization we have today and has been an indicator of the development (Zhang, 2021).

The most current energy production and consumption techniques, however, use energy sources that cannot be replaced by new ones. Research and development require the use of renewable and ecologically friendly energy sources (Ishaq et al, 2020; Salim & Alsyouf, 2020). The use of fossil resources in energy production is not preferred today in terms of harming the environment (Lou & Li, 2016). In this case, the fact that the use of renewable energy sources, which is the natural product of our environment, is increased day by day, instead of these energy sources, which were ignored before, and the use of which is gradually increasing with the development of the industry, the damages it causes in the way of development and industrialization are better understood day by day (Li et al, 2021; Koçali & Erçetin, 2021; Agyekum, 2021).

The principle put forward for the operation of thermophotovoltaic batteries dates to the Photovoltaic Event. The origins of TPV date back to the early 1960s. In 1839, Becquerel, for the first time, observed that the angerylum formed between electrodes immersed in electrolyte changed according to the light coming on the electrolyte and explained the Photovoltaic Phenomenon. In 1876, selenium crystals were first tested in accordance with the photovoltaic phenomenon by G. W. Adams and R. E. Day. Studies carried out in the following years enabled the use of photo diodes based on copper oxide and selenium in light meters for photography (Aigrain, 1961; White et al, 1961; Guazzoni et al, 1968; Yerebakan, 2010).

The discovery of TPV trace back to about 1956. An article is given by Nelso Un and Kolmar about TPV system that solar cells power supply (Wedlock, 1963; National Research Council, 2001; Bauer, 2011). TPV has attracted praiseworthy interest as a possible participant in a combustion-driven power generation system. Work on TPV energy generation began

irregularly in the 1960s, but because high efficiency converters are now widely available, a number of projects have noticeably advanced in the past ten years (Coutts, 1999; Coutts, 2001).

Until the mid-1970s, three main heat sources (nuclear, solar and combustion) and spectral control options (PV cell front, filter, eluent radiator, and rear surface reflector) were defined in line with research conducted in the USA (Bauer, 2011; Önal & Utlu, 2017). Due to the emergence of high-performance converters, TPV technology underwent a period of hibernation in the 1980s but has recently experienced exceptional growth (White & Hottel, 1994; Yamaguchi & Yamaguchi, 1999). Applications for TPV have been used in a wide range of fields, such as in glass processing (Bauer et al, 2003) extreme industrial temperatures (Coutts, 2001) integrated TPV and TE power system (Qui & Hayden, 2012), co-generation systems (Bianchi et al, 2012), space exploration (Teofilo et al, 2006), military devices (Nelson, 2003). The key features of TPV technology have greatly benefited continued interest in the disciplines described above. The inherent advantages of TPV systems, such as their high-power density, mobility, lightweight design, maintenance-free operation, and fuel adaptability, have boosted their acceptance in a variety of energy sectors (Coutts, 1999; Coutts, 2001). Despite not having a significant market share, the TPV power system represents a favorable environment for research and development. The discussion that follows quickly examines the fundamental ideas behind the TPV power system before presenting a thorough analysis of the technical features to guide and captivate the reader on this fascinating topic (Fraas et al, 1998; Kruger et al, 1998; Colangelo et al, 2003). High power density, fuel flexibility, mobility, silent operation, sun-independent operation, and minimal maintenance costs are some of the potential benefits of TPV. Other potential uses include large-scale recovery of high-temperature waste heat from industrial processes like the production of glass; stand-alone domestic gas furnaces; power systems for sailing boats; silent power supplies on recreational vehicles; co-generation of electricity and heat; and many others (Fraas et al, 2003; Qui & Hayden, 2003; Aicher et al, 2004).

Electrical energy can be produced from thermal infrared radiation using thermophotovoltaic (TPV) cells. Due to its many benefits and the development of low bandgap (0.50-0.74 eV) TPV cells like GaSb, GaInAs, and GaInAsSb cells, TPV energy generation is gaining technical interest (Qui & Hayden, 2003; Qui et al, 2006). In industrial systems with high temperature

waste heat recycling thermophotovoltaic applications an example of theoretical modeling has been made, and in line with the study by Utlu and Önal (2017), the efficiency of In0.2 Ga0.8 As0.18 Sb0.82 cell was higher when compared to the GaSb cell at the same source temperature. The system was divided into three low, medium and high temperature regions by Önal and Utlu (2018), and the thermodynamic analysis of the system was made.

MATERIAL AND METHODS

It is important to examine the structure of the thermophotovoltaic system within the scope of the study and to clearly reveal the formulas required for the analysis. Because the study will be among the main studies for the system installation in Turkey with the GaSb cells used in the experimental installation. For this reason, system setup for simple system setup and experimentation should be in accordance with scientific rules and international regulations.

Structure of Thermophotovoltaic System

Thermal radiation from terrestrial heat sources is converted into electricity by thermophotovoltaics (TPVs). A TPV device is made up of three major parts: a TPV cell that turns incident photons into electricity; a vacuum gap between the emitter and the cell; and an emitter that radiates photons by absorbing thermal energy from a heat source (Akhtar et al, 2015; Mustafa et al, 2016). The heat source, selective emitter, cooling system, filter, and photovoltaic cell are all included in the system. The thermal energy from the heat source is transferred to the solar cells after passing via the selective emitter and filters. In photovoltaic cells, thermal energy is transformed into electricity (Andreev et al, 2004; Andreev et al, 2005; Ferrari et al, 2014). A standard TPV setup includes a heat source (such as a flame, radiative isotope, or the sun), a radiator, a semiconductor converter, a way to recycle sub-bandgap photons to save energy, and a power conditioning system that operates at temperatures between 1000 and 1500 °C (Coutts, 1999; Coutts, 2001). Thermal energy is transformed into electrical energy as the TPV's primary operating mechanism. Thermophotovoltaic systems used for central heating have an operating temperature of 1000–1300 °C (Önal, 2017).

In thermophotovoltaic systems, not only the sun can be used as a heat source, but also the waste heat from the combustion system, fuels, and industrial processes during the production phase. In TPV systems, the heat source is utilized to produce photons, and the selective emitter is used to boost

system effectiveness. The filter reflects insufficiently energetic radiation and sends it back to the selective emitter. As opposed to this, photovoltaic cells transform the photon energy from the emitter into electrical energy. Photovoltaic cells convert solar energy into electrical and thermal energy. The obtained linear current can be converted into alternating current and electrical energy can be used in different areas (Datas & Algora, 2010; Utlu et al, 2017; Utlu & Önal, 2017; Önal, 2017; Utlu & Önal, 2018). Thermophotovoltaic systems are being investigated as an alternative to the way electricity is now produced since they produce electrical energy from heat and reuse waste heat (Fraas et al, 1998; Home et al, 2000) in Figure 1.

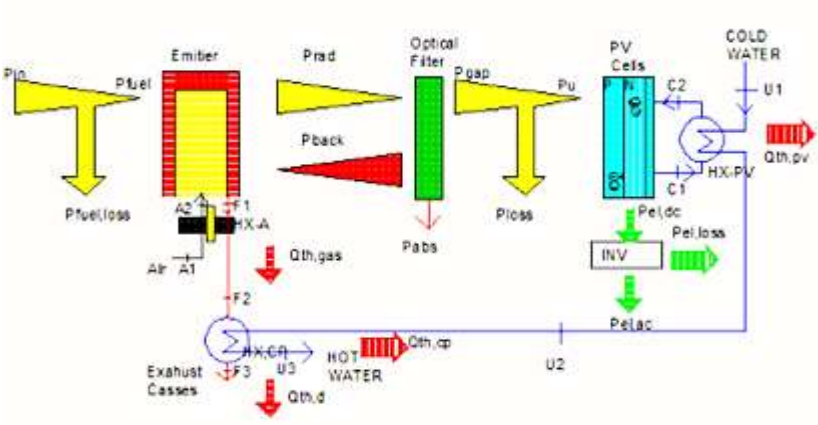

Figure 1: Schematic Representation of the TPV System

The reflector on the rear of the TPV cells, which is used to reflect low-energy photons to reheat the emitter, is how the best photon recycling technology works. In actuality, the low-energy photons are absorbed by the TPV cell material before they reach the back reflector since TPV cells are often made to a thickness of several hundred microns (Li & Xuan, 2022). The fuel enters the selective emitter and mixing with the air. The system discharges exhaust gas. Photons from the selective emitter travel with radiation to the optical filter, and low-energy photons are reflected from the filter to the selective emitter. The photovoltaic cell is reached by photons with a suitable band gap in terms of energy (Amin, 2022; Xue et al, 2022). Direct current is the type of electricity that the solar cell produces. Direct current (DC) is changed into alternating current (AC) via an inverter (converter) (AC). The system's cooler regulates the temperature of the solar cell and

keeps it from overheating. The filter also stops the cell from overheating (Ouremchi et al, 2022; Hasan et al, 2021).

The behavior of values has been compared between real and theoretical analyses of thermophotovoltaic systems using GaSb cells. These values are fill factor (FF), short circuit current (Jsc), energy conversion efficiency value (η) and open circuit voltage (Vc); which are fundamental parameters versus cell temperature. These values vary linked in the radiation source temperature (Green, 1981; Fentahun et al, 2021; Herterich et al, 2022; Khaledi et al, 2022; Talbi et al, 2022):

- Fill factor (FF); It is the value found by dividing the maximum power obtained from the panel by the theoretical power found by multiplying the open-circuit voltage by the short circuit current.
- Short-circuit current (Jsc); during the short-circuit at the short-circuit point is the flowing current. It is a time-varying function in alternating current systems.
- Energy conversion efficiency (η) is the energy expression of the ratio between the useful output and input of the energy conversion. The useful output can be electrical power, mechanical power, or heat.
- Open circuit voltage (Vc); It is the voltage value of the thermophotovoltaic panel when there is no electrical load, that is when it is not producing current. This value is the voltage value used when calculating the inverter and battery. According to this value, the panels are connected in series or parallel to make them suitable for the system voltage.

In the literature, it was observed that the effect of the change in the energy efficiency of the cell temperature at different source temperatures decreased, and the cell temperature increased the energy efficiency (Utlu & Önal, 2017; Utlu & Önal, 2018). The equations used for the analysis of the thermophotovoltaic system are as follows in Table 1 (Fraas et al, 1998; Coutts, 2001; Fraas et al, 2003; Colangelo et al, 2003; Lee et al, 2005; Qui & Hayden, 2006; Qui et al, 2006; Butcher et al, 2011; Ferrari et al, 2013; Önal, 2017).

Table 1: The Equations for the Analysis

Incoming energy into the photovoltaic cell	$P_U = P_{GAP} - P_{loss} = P'_{GAP} - P_{loss} - P_{abs}$ P_{abs} is frequently ignored. P_{loss} is the term for the power lost from the photovoltaic cell to the optical filter.	(1)
Electrical power is the definition of the solar cell's power	$P_{el,dc} = V_{OC}$ x I_{SC} x FF $V_{OC} = (kbT_{em} / e)$ x ln $(I_L / I_O + 1)$ I_{SC} = e. $\int\Phi(\lambda)\, EQE(\lambda)\, d\lambda$ EQE (λ) is the external quantum efficiency of the wavelength absorbed by the cell and the photon probability value. Φ (λ) is the photon flux.	(2) (3) (4)
The overall electrical efficiency of the TPV system is equal to the multiplication of the below-mentioned efficiencies	$\eta_{EL,} = \eta_{CC}.\ \eta_{RAD}.\ \eta_{GAP}.\ \eta_{F}.\ \eta_{VF}.\ \eta_{PV}.\ \eta_{dc/ac}$	(5)
η_{CC}, the system's fuel efficiency is determined by the proportion of fuel power to heat source power entering the system.	$\eta_{CC} = P_{fuel} / P_{in}$	(6)
The ratio of radiant energy to fuel power is known as η_{RAD}, or radiant efficiency entering the optical filter.	$\eta_{RAD} = P_{RAD} / P_{fuel}$	(7)
η_{GAP} spectral efficiency	$\eta_{GAP} = P_{GAP} / P_{RAD}$	(8)
η_{F} efficiency of the filter	$\eta_{F} = P_{GAP} / P'_{RAD}$	(9)
The ratio of the power entering the solar cell to the spectral power is known as the visibility factor efficiency.	$\eta_{VF} = P_U / P_{GAP}$	(10)
The ratio of electrical energy to the power entering the solar cell is known as the photovoltaic cell efficiency.	$\eta_{PV} = P_{el,dc} / P_U$	(11)
Direct current is the type of electricity produced by the solar cell. A current inverter is used to change direct current to alternating current.	$\eta_{dc/ac} = P_{el,ac} / P_{el,dc}$	(12)

System Setup

The usage areas of GaSb cells in Turkey are quite limited and experimental studies are generally carried out. For this reason, besides the experimental and real application comparisons mentioned above, it is of great importance to specify the points to be considered during the installation of the system. Sunlight is converted using a wide range of methods, most of which are based on semiconductors. The National Renewable Energy Laboratory (NREL) tests the efficiency of various solar cell and module designs to guarantee the reliability and consistency of measurements of photovoltaic performance. While the experimental set was being set up, the user manual of the GaSb cell manufacturer was examined and compared with the manuals of other companies producing similar products in the market. Published standards regarding the established experimental set were also examined. There are 203 standards in 2018, 331 standards in 2019, and 261 standards in 2020. When the countries that published standards are examined, it is seen that China published 203, United Kingdom 164, Iran 129, Denmark 125, Netherlands 124 standards (Nanotechnology Standards, 2023).

Most of the national standards like International Labor Organization (ILO) conventions, OHSAS 18001 Occupational Health and Safety Management System (2023) are consisting of five main title which are policy, planning, implementation and operation, control and corrective action and management review. There is no specific standard published on TPV systems and nanotechnology in Turkey.

In Turkey, there are the Occupational Health and Safety Law numbered 6331 which came into force in 2012 to take Occupational Health and Safety, and the TS-18001 Occupational Health and Safety Management Systems Requirements standards by the Turkish Standards Institute. In the regulations mentioned above information about the obligations of the employer and employees, definitions about risk assessment and the responsibilities of the safety council are given. The purpose of risk assessment is to pre-determine and record the hazards that may arise from risks in the workplace, and to take precautions and work with current methods. With the works done, it is ensured that the hazards that may arise from the risks are determined in advance and Occupational Health and Occupational Safety measures are taken, and that the damages that may occur are at the minimum level or that the damage does not occur and while the risk assessment is being prepared, the identified risks are determined to be responsible for and control. Risk assessment analysis is carried out in many projects application and it

purpose is to determine in advance the negativities that may arise from the risks that may arise during the execution of the project. Aim of the identified risks is ensuring that the cost of the invested project is kept at a determined level. In addition, thanks to the risk assessment analysis prepared, taking safety measures in terms of occupational health and safety ensures that the reliability of the security measures taken is checked. Risk assessment analysis is important in the installation of energy systems. Because there are many unexpected factors during installation. The reliability of the risk assessment analysis ensures that the plant installation is completed on time and that the employees work in a healthy environment. Risk assessment analysis should be done in accordance with national and international standards and legal framework. The most important step in energy systems risk assessment analysis is the selection and calculation of the energy panels and inverters to be used in the planning phase. Because if the panel and the inverters are not compatible, even if high voltage and current are produced in the operation of the system due to the high voltage, there may be incompatibility within the legal limits. The important stages in this part are installation, commissioning, and operation of the plant. During the installation phase, electricity production begins with the placement of the panels and since the system does not work and is not connected to the grid, the electricity produced stops in the field environment. Therefore, employees are exposed to electric current and voltage. During the commissioning phase, the final tests of the plant are carried out. The most important of the tests is the grounding and leakage current protection test. When grounding and leakage current protection calculations are calculated incorrectly, excess current and voltage occur during the operation of the system. With the formation of excess current and voltage, the risk of passing over the workers is high. During the operation of the system, the annual maintenance of the plant and its control are provided by the remote monitoring system. There is also the possibility that workers or maintenance people may be exposed to high current and voltage during the cleaning of electricity generating panels. Occupational health and safety apply occupational health and safety rules, explains the purpose and importance of occupational health and safety, takes necessary precautions by listing the methods of protection from work accidents and occupational diseases, takes necessary precautions against risks arising from hazards and takes necessary measures in emergencies. Measuring physical sizes in renewable energy systems measures physical dimensions in accordance with the nature of the size by taking occupational health and safety measures. It measures the

length, area, and volume values by using a measuring device suitable for the nature of the quantity to be measured. It measures temperature with temperature measuring instruments and measures cross-section and diameter using diameter measuring tools. Measures resistance with a resistance measuring instrument and measures the inductance value with the LCR meter. Makes capacity measurement using measuring instruments, current meter with the help of ammeter and voltage meter with the help of voltmeter, frequency measures with frequency meter measuring instrument. Work and power meter with the help of counter and wattmeter. Basic operations in energy mechanics performs basic operations in energy mechanics in accordance with its technique by taking occupational health and safety measures and uses control and screw tightening tools suitable for the work piece. Uses simple cutting and shaping tools according to occupational health and safety rules. Performs surface and angle control according to the given size, using tools suitable for the job. Hand operations in energy mechanics takes occupational health and safety measures and performs hand operations in accordance with the technical drawing of the work piece. Files to bring the plane surface to the desired size and files for profile surface cleaning. Performs measurement and control in accordance with technical drawing dimensions. It makes marking to do basic operations on the work piece and performs the cutting process in accordance with the given dimensions. Drilling and screwing in energy mechanics, by taking occupational health and safety measures, performs drilling and screw operations in accordance with the given dimensions and makes hole drilling operations according to the given size by using appropriate apparatus and machine. It guides manually according to the material and the size on the work piece picture and draws a sheet by hand in accordance with the material and the size of the work piece picture and combines with screw-bolt. Mechanical parts and electrical-electronic diagram drawing, draws solar energy connection diagrams in accordance with standards by taking occupational health and safety measures. It draws panel electrical wiring diagrams in accordance with national and international standards and the mechanical parts of the panels in accordance with the different types of establishments. Fundamentals of electricity in renewable energy makes basic applications about electric current with generation and effects by taking occupational health and safety measures and uses electrical energy and resources. Makes calculations about electric current according to OHM's law. Benefit from the effects of electric current by taking occupational health and safety measures. It produces voltage according to

voltage generation methods by taking occupational health and safety measures. Fundamentals of direct current generated in cells makes circuit solutions and connections for the direct current produced in the cells by taking occupational health and safety measures. It takes the occupational health and safety measures and makes the cable connections of the GaSb batteries in accordance with the connection diagram and performs measurement and calculation processes in direct current (DA-DC) circuits. By taking occupational health and safety precautions, it makes direct current source cable connections in accordance with the Indoor Installation Regulation. Panel systems establish in accordance with the project by taking occupational health and safety measures and determines the radiation angle at the place of use with suitable measuring instruments according to the geographical location. It ensures the assembly of metal components according to the dimensions determined in the project and places the panels on the construction according to the sequence determined in the project. It makes panel cable transitions in accordance with its technique in accordance with the project and connects inter-panel and system grounding transition conductors using connection apparatus. By taking occupational health and safety measures, panel maintenance maintains the panels without interrupting the production and according to the technical specifications of the manufacturer. Controls the mounting bolts of the panel by taking occupational health and safety measures. It cleans the surface of the panels by taking occupational health and safety measures and controls the cable connections between the panels by taking occupational health and safety measures (Occupational Health and Safety Law No. 6331, 2012; Occupational Health and Safety Risk Assessment Regulation No. 28512, 2012; Regulation on Occupational Health and Safety Boards No. 28532, 2013; National Occupational Health and Safety Board Regulation No. 28550, 2013; Regulation No. 28861 on Supporting Occupational Health and Safety Services, 2013; Koçali, 2018; Koçali, 2021).

Experimental Setup

The experimental setup in the laboratory environment within the scope of the study consists of voltmeter (a), datalogger (b), GaSb cell (c) and heat source (d). Hot wire was used as a heat source in the experimental setup. As a result of opening the experimental set (f), open flame (e) was produced at the heat source (d). The temperature produced was also controlled with a thermal camera (f) to control the experimental temperature. When the desired temperature was reached, the values obtained with the voltmeter (a) and

datalogger (b) connected to the GaSb cell (c) were recorded. Dataloggers are devices that record the temperature and voltage values measured on the GaSb cell for a certain period. Figure 2 shows the entire experimental set.

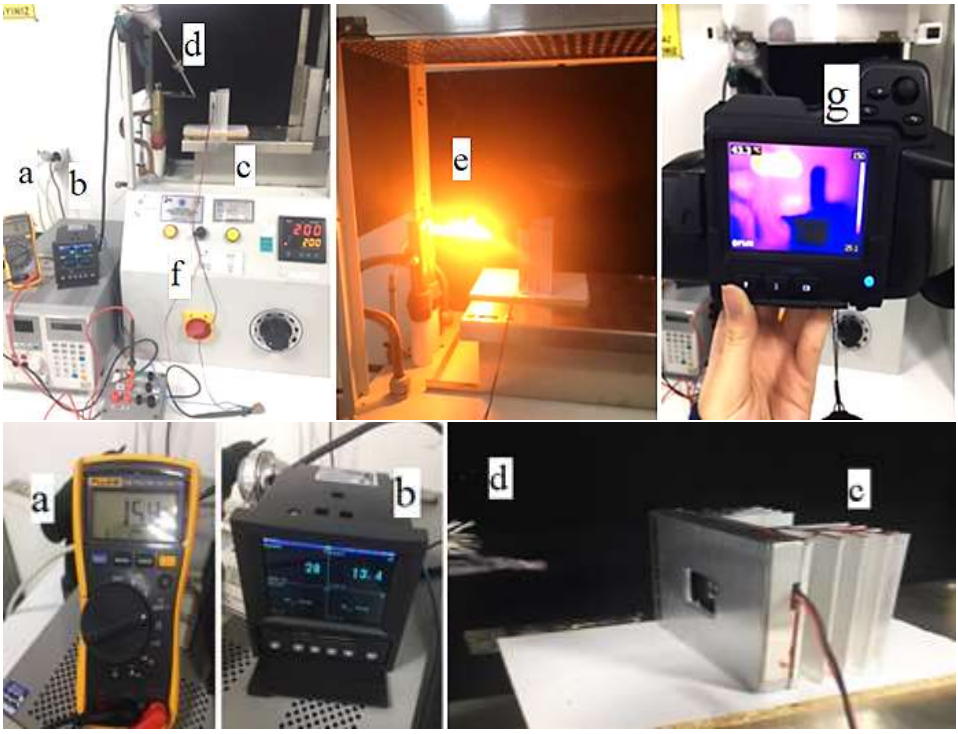

Figure 2: Experimental Study Setup

In the experimental study, a thermal camera was used as another measuring device. Thermal cameras are imaging devices that make use of infrared radiation, which cannot be seen but expresses itself as heat in the form of colors and forms that express the general structure of the image. Thermal cameras, which are non-contact measuring devices, detect the invisible infrared energy emitted by objects and display it as a thermal image on the camera screen. As seen in Figure 3, In the experiment, the highest temperatures on the hot wire were measured using a thermal camera.

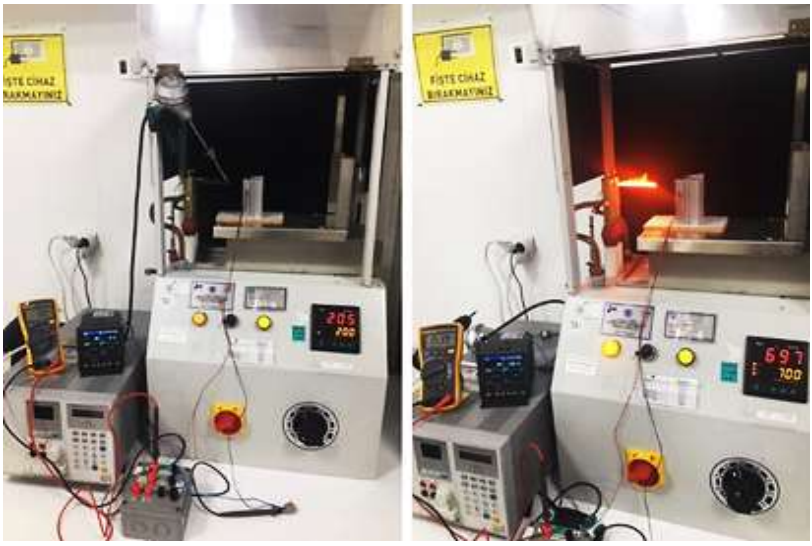

Figure 3: Voltage Values and Cell Temperature at 205 and 697 °C Source Temperature

RESULTS

As shown in Figure 3, the effect of voltage levels and varying source temperature on cell temperature was investigated using the GaSb cell type. Values for the source temperature ranged from 200°C to 1000°C. Additionally, as shown in Figure 2, the hot wire's maximum temperature values were measured using a thermal camera.

GaSb cell was used as the cell type in the thermophotovoltaic system which theoretically modeled by using high temperature waste heat. The temperature values applied on the cell are between 1000 K and 3000 K. As seen in Table 2, the optimum energy conversion efficiency value for an ideal GaSb TPV cell has been calculated as 33.15% in the analysis performed. This value is an optimal value. Table 3 and Figure 4 show the statistical results of cell efficiency (%) values obtained depending on radiation and cell temperature at theoretical analysis.

Table 2: Cell Efficiency (%) Values Obtained as Depend on Radiation and Cell Temperature of Thermophotovoltaic Systems at Theoretical Analysis

Cell temperature Radiation temperature	300 K	325 K	350 K	375 K	400 K
1000 K	24.02	18.27	12.74	7.73	3.80
1250 K	28.41	23.15	17.89	12.86	8.25
1500 K	30.89	25.99	21.11	16.30	11.72
1750 K	32.25	27.68	23.11	18.58	14.16
2000 K	32.93	28.65	24.35	20.07	15.86

2250 K	**33.15**	29.13	25.08	21.03	17.03
2500 K	33.08	29.28	25.45	21.62	17.81
2750 K	32.81	29.21	25.58	21.94	18.32
3000 K	32.40	28.98	25.53	22.07	18.62

The correlation obtained as a result of the error analysis made with the OriginPro 2021 software is as follows:

$$y = Intercept \sum_{i=0}^{n} A_i . x^i \quad (13)$$

The correlation obtained when analyzing using five different cell temperatures is as follows:

$$y = A_0 + (A_1.x) + (A_2.x^2) + (A_3.x^3) + (A_4.x^4) + (A_5.x^5) \quad (14)$$

According to actual analysis, the relationship between energy efficiency and radiation temperature is demonstrated dependent on the fluctuating cell temperature. For instance, the energy efficiency is 9.68% when the radiation temperature is 2000 K and the cell temperature is 400 K. In the statistical calculations, in Table 3, it was calculated that the error rate at 300 K temperature was the lowest. It was found to be 99.99% related to 2250 K radiation temperature. It is demonstrated in this instance that energy efficiency rises as radiation temperature rises.

Table 3: Statistical Results of Cell Efficiency (%) Values Obtained Depending on Radiation and Cell Temperature (Theoretical Analysis)

Cell temperature	300 K	325 K	350 K	375 K	400 K
Number of points	9	9	9	9	9
Residual sum of residual	4.50E-04	9.62E-04	1.15E-04	3.90E-06	0.00168
R-Square (COD)	0.99999	0.99999	0.99999	0.99999	0.99999
Adj. R-square	0.99998	0.99998	0.99999	0.99999	0.99998
Sum of squares	0.03178	0.03538	0.03941	0.04459	0.04998
Mean square	0.00636	0.00708	0.00788	0.00892	0.01
F value	1136.25	1156.47	2158.39	3589.91	1593.2
Prob>F	4.11E-05	4.00E-05	1.57E-05	7.34E-06	2.47E-05

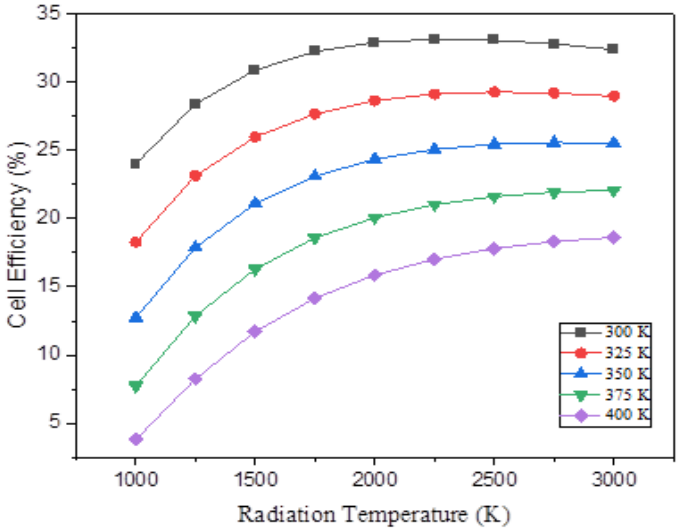

Figure 4: Cell Efficiency (%) Values Obtained as Depend on Radiation and Cell Temperature (Theoretical Analysis)

Table 4 shows that the optimal energy conversion efficiency of the GaSb solar cell structure has been determined to be 21.57%, according to the final design, in the real (lossy) analysis of the GaSb-cell TPV system installed on the final design. Table 5 and Figure 5 show the statistical results of cell efficiency (%) values obtained depending on radiation and cell temperature at real analysis. In the statistical calculations, in Table 5, it was calculated that the error rate at 300 K cell temperature was the lowest. It was found that there is a 99.99% correlation with 2500 K radiation temperature.

Table 4: Cell Efficiency (%) Values Obtained as Depend on Radiation and Cell Temperature of Thermophotovoltaic Systems at Real Analysis

Cell temperature Radiation temperature	300 K	325 K	350 K	375 K	400 K
1000 K	14.43	10.62	7.02	3.91	1.71
1250 K	17.62	14.05	10.57	7.29	4.40
1500 K	19.51	16.17	12.89	9.70	6.72
1750 K	20.61	17.49	14.39	11.36	8.44
2000 K	21.23	18.29	15.37	12.48	9.68
2250 K	21.51	18.74	15.98	13.24	10.57
2500 K	**21.57**	18.95	16.33	13.74	11.18
2750 K	21.48	19.00	16.51	14.04	11.61
3000 K	21.29	18.92	16.56	14.21	11.89

Table 5: Statistical Results of Cell Efficiency (%) Values Obtained Depending on Radiation and Cell Temperature (Real Analysis)

Cell temperature	300 K	325 K	350 K	375 K	400 K
Number of points	9	9	9	9	9
Residual sum of residual	9.90E-05	1.95E-04	7.94E-05	6.12E-04	0.0013
R-Square (COD)	0.99997	0.99999	0.99999	0.99999	0.99999
Adj. R-square	0.99999	0.99999	0.99999	0.99998	0.99997
Sum of squares	47.32012	66.45043	85.93328	99.13671	99.99875
Mean square	9.46402	13.29009	17.18666	20.02734	98041.77
F value	286761.6	204352.9	649133.5	20.01974	46257.46
Prob>F	1.03E-08	1.71E-08	3.02E-09	5.14E-08	1.59E-07

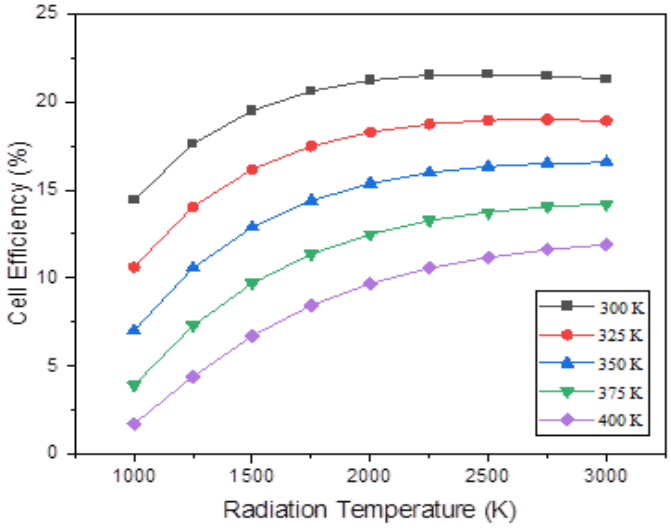

Figure 5: Cell efficiency (%) Values Obtained as Depend on Radiation and Cell Temperature (Real Analysis)

According to the shifting radiation temperature in the theoretical analysis, fill factor, short circuit current, open circuit voltage, and energy conversion efficiency values were determined and displayed in Table 11. According to Table 7, the real (lossy) analysis's highest open circuit voltage was 0.44 V at the 3000 K radiation temperature. In the statistical calculations in Table 8, the error rate at 300 K temperature was calculated to be the lowest. It was found to be 99.99% related to 3000 K radiation temperature. Table 8 and Figure 6 show the statistical results of temperature-dependent variation of open circuit voltage (v) values obtained in real (lossy) analysis.

Table 6: Variable Parameter Values Dependent on Radiation Temperature in Theoretical Analysis

Radiation temperature	V_{OC} (V)	J_{SC} (A/m^2)	FF (%)	η (%)
1000 K	0.28	0.16	71.00	24.02
1250 K	0.33	0.17	73.83	28.41
1500 K	0.33	4.52	75.53	30.89
1750 K	0.39	12.38	76.66	32.25
2000 K	0.41	27.21	77.52	32.93
2250 K	0.42	51.58	78.23	33.15
2500 K	0.44	87.99	79.03	33.08
2750 K	0.45	**138.87**	78.68	32.81
3000 K	0.46	206.53	79.39	32.40

Table 7: Temperature-dependent Variation of Open Circuit Voltage (V) Values Obtained in Real (Lossy) Analysis

Cell temperature Radiation temperature	300 K	325 K	350 K	375 K	400 K
1000 K	0.25	0.20	0.15	0.10	0.05
1250 K	0.31	0.26	0.21	0.16	0.11
1500 K	0.34	0.29	0.25	0.20	0.15
1750 K	0.37	0.32	0.28	0.23	0.19
2000 K	0.39	0.34	0.30	0.26	0.22
2250 K	0.41	0.36	0.32	0.28	0.24
2500 K	0.42	0.38	0.34	0.30	0.26
2750 K	0.43	0.39	0.35	0.31	0.27
3000 K	**0.44**	0.40	0.36	0.32	0.28

Table 8: Statistical Results of Temperature-Dependent Variation of Open Circuit Voltage (V) Values Obtained in Real (Lossy) Analysis

Cell temperature	300 K	325 K	350 K	375 K	400 K
Number of points	9	9	9	9	9
Residual sum of residual	1.67E-05	1.83E-05	1.09E-05	7.45E-06	1.88E-05
R-Square (COD)	0.99947	0.99948	0.99972	0.99983	0.99962
Adj. R-square	0.99859	0.99862	0.99926	0.99955	0.99999
Sum of squares	0.03178	0.03538	0.03941	0.04459	0.04998
Mean square	0.00636	0.00708	0.00788	0.00892	0.01
F value	1136.25	1156.474	2158.3957	3586.912	1593.208
Prob>F	4.11E-05	4.01E-05	1.57E-05	7.34E-06	2.48E-05

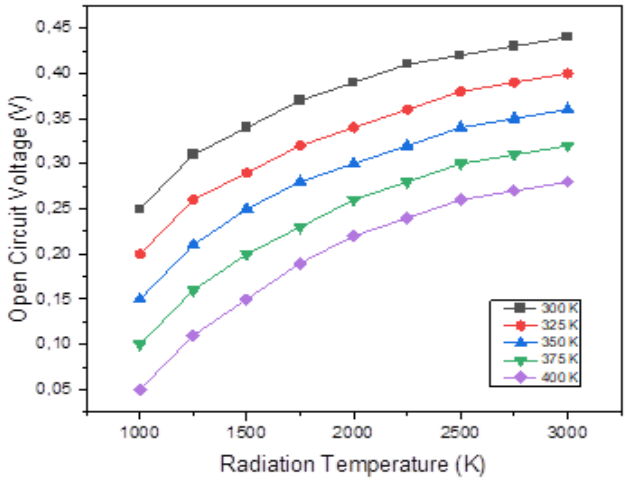

Figure 6: Temperature-dependent Variation of Open Circuit Voltage (V) Values Obtained in Real (Lossy) Analysis

Table 9 shows that the highest temperature dependent variation of filling factor value has been 78.77% at the 3000 K radiation temperature in the Real (Lossy) analysis. Table 10 and Figure 7 show the statistical results of temperature-dependent variation of filling factor (%) values obtained in real analysis. In the statistical calculations, in Table 9, it was calculated that the error rate at 300 K was the lowest. It was found to be 99.99% related to 3000 K radiation temperature.

Table 9: Temperature Dependent Variation of Filling Factor (%) Values Obtained in Real Analysis

Cell temperature Radiation temperature	300 K	325 K	350 K	375 K	400 K
1000 K	69.46	63.34	55.47	45.50	35.92
1250 K	72.88	68.22	62.43	55.22	46.53
1500 K	74.75	70.83	66.07	60.24	53.57
1750 K	75.89	72.30	68.30	63.45	57.61
2000 K	76.90	73.68	69.89	65.36	60.27
2250 K	77.41	74.40	70.84	66.96	62.33
2500 K	77.83	75.20	71.80	68.16	63.84
2750 K	78.30	75.69	72.64	69.08	64.89
3000 K	**78.77**	76.13	73.07	69.84	66.05

Table 10: Statistical Results of Temperature Dependent Variation of Filling Factor (%) Values Obtained in Real Analysis

Cell temperature	300 K	325 K	350 K	375 K	400 K
Number of points	9	9	9	9	9
Residual sum of residual	0.02184	0.03345	0.03597	0.02746	0.07083
R-Square (COD)	0.99977	0.99976	0.99986	0.99995	0.99991
Adj. R-square	0.99992	0.99936	0.99964	0.99986	0.99976
Sum of squares	72.80465	139.84884	264.87025	505.06917	795.65546
Mean square	14.56093	27.96977	52.97405	101.01383	159.13109
F value	2000.0765	2508.3901	4417.9727	11037.49	6740.2909
Prob>F	1.76E-05	1.26E-05	5.37E-06	1.36E-06	2.85E-06

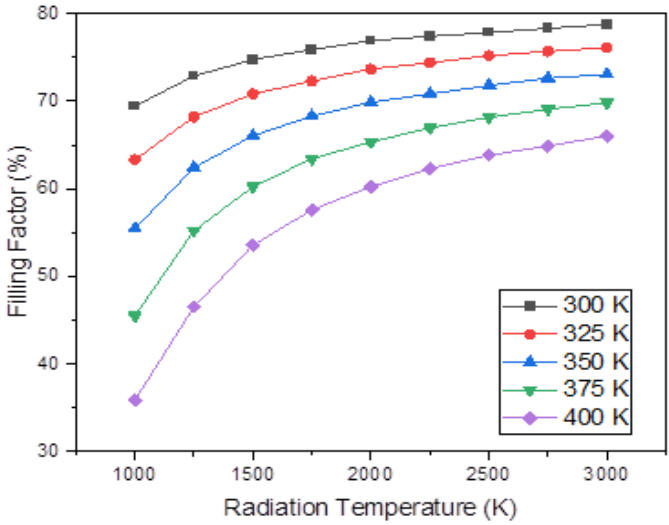

Figure 7: Temperature Dependent Variation of Filling Factor (%) in Real Analysis

Table 11 shows that the highest temperature dependent change of short circuit current value has been 151.90 A/m^2 at the 3000 K radiation temperature in the Real (Lossy) analysis. Table 12 and Figure 8 show the statistical results of temperature-dependent change of short circuit current (A/m^2) values obtained in real analysis. In the statistical calculations, in Table 12, it was calculated that the error rate at 400 K was the lowest. It was found to be 99.99% related to 3000 K radiation temperature.

Table 11. Temperature Dependent Change of Short Circuit Current (A/m^2) Values Obtained in Real Analysis

Cell temperature Radiation temperature	300 K	325 K	350 K	375 K	400 K
1000 K	0.10	0.11	0.12	0.13	0.14
1250 K	0.74	0.79	0.84	0.90	0.96
1500 K	2.94	3.09	3.25	3.42	3.59
1750 K	8.18	8.51	8.86	9.22	9.60
2000 K	18.17	18.73	19.44	20.08	20.76
2250 K	34.71	35.70	36.72	37.77	38.85
2500 K	59.57	61.03	62.53	64.07	65.63
2750 K	94.47	96.49	98.54	100.64	102.78
3000 K	141.05	143.69	146.38	149.12	151.90

Table 12: Temperature Dependent Change of Short Circuit Current (A/m^2) Values Obtained in Real Analysis

Cell temperature	300 K	325 K	350 K	375 K	400 K
Number of points	9	9	9	9	9
Residual sum of residual	2.80E-04	0.00255	3.24E-04	5.48E-04	2.44E-04
R-Square (COD)	0.99991	0.99976	0.99986	0.99995	0.99998
Adj. R-square	0.99976	0.99936	0.99964	0.99986	0.99992
Sum of squares	19584.91	20331.14	21097.97	21898.05	22724.08
Mean square	3916.9828	4066.2279	4219.5954	4379.6114	4544.8177
F value	4.19E+07	4.79E+07	3.90E+07	2.39E+07	5.58E+07
Prob>F	5.82E-12	1.50E-10	6.48E-12	1.35E-11	3.79E-12

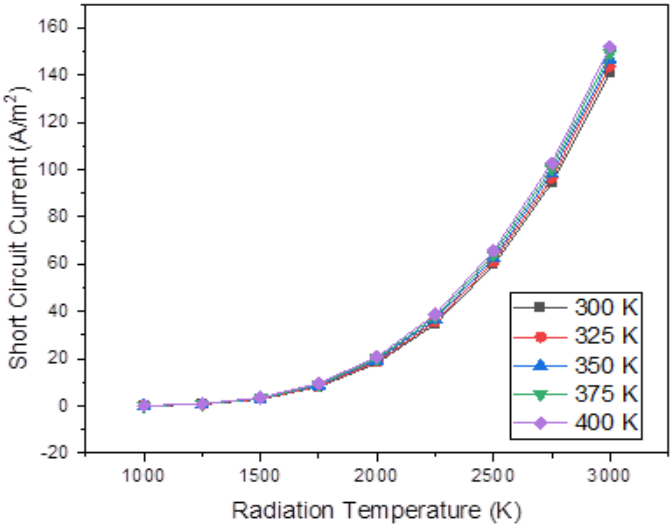

Figure 8: Temperature Dependent Change of Short Circuit Current (A/m^2) Values Obtained in Real Analysis

CONCLUSIONS

The usage areas of GaSb cells in Turkey are quite limited and theoretical studies are generally carried out. For this reason, besides the experimental and real application comparisons mentioned above, it is of great importance to specify the points to be considered during the installation of the system. The TPV system installation in our study was carried out within the scope of international standards and occupational health and safety. Not only national standards for system installation, but also seen that the experimental installation can be established within the framework of international standards accepted in this field. In addition, for researchers who plan to work in the field of thermophotovoltaics, guidance was provided on the installation of experimental setup. This system applied on high temperature GaSb cell was theoretically and really analyzed and compared in this study. In addition, statistical calculations were made for both analyzes using OriginPro software and the accuracy of the experiments was proved by obtaining the correlation covering the whole system.

This system applied on high temperature GaSb cell was theoretically and really analyzed and compared in this study. In addition, statistical calculations were made for both analyzes using OriginPro software and the accuracy of the experiments was proved by obtaining the correlation covering the whole system. The results obtained are as follows:

- While the optimum energy efficiency is 33.15% because of the theoretical modeling. The optimum energy efficiency obtained because of the real analysis is 21.57%. This difference happened as a result of lossless calculations under ideal conditions.
- The maximum energy efficiency is 33.15% at 2250 K radiation temperature. The minimum energy efficiency is 24.02% at 1000 K radiation temperature in theoretical analysis.
- When theoretical analysis is examined, as the tension rises, the current density drops. The lowest filling factor is 71.00% while the highest filling factor is 79.39%.
- The short circuit current reduces as the cell's temperature rises. As cell temperature increases, energy efficiency also decreases. As the cell's temperature drops, energy efficiency rises. The band gap closes as the cell's temperature rises, reducing the TPV cell's open circuit voltage.

Furthermore, higher cell temperature reduces filling factor and efficiency.

- According to the theoretical analysis, the maximum open circuit voltage was 0.46 V at 3000 K radiation temperature. However, this value dropped to 0.44 V at this temperature for the highest open circuit voltage.
- The short circuit current was 206.53 A/m^2 in the theoretical analysis at the highest radiation temperature of 3000 K, however it was only 151.90 A/m^2 in the real analysis.
- When the filling factor was examined, the maximum value in the theoretical analysis was 79.39%, however this value reduced to 78.77% in the real analysis.
- In the statistical calculations made with the OriginPro software, a correlation of 99.99% accuracy was obtained at the cell temperature of 300 K and the radiation temperature of 2500 K for real analysis. In the theoretical analysis, the same ratio was obtained at a cell temperature of 300 K and a radiation temperature of 2250 K.
- In general, it is shown that the real analyses' values are a little bit lower than the theoretical data. This is because the losses were not considered in the theoretical study. According to the real analysis, the thermophotovoltaic system may contribute to the present electricity production with an efficiency of about 21.57%.

Acknowledgements

This study is a combination of the authors MSc Thesis which are "*Development of Electrical Energy Production Technologies with Thermophotovoltaic Methods by Using Existing Waste Heat Potential in Thermal Systems*" (Thesis No:501488) at Department of Mechanical Engineering, Institute of Science of Istanbul Aydin University in 2017 and "*Investigation of Effects of Boron Compounds on Solar Energy Panels*" (Thesis No:424353) at Department of Mining Engineering, Institute of Graduate Studies in Science and Engineering of Istanbul University.

REFERENCES

Agyekum, E. B., Amjad, F., Mohsin, M., & Ansah, M. N. S. (2021). A bird's eye view of Ghana's renewable energy sector environment: A Multi-Criteria Decision-Making approach. *Utilities Policy*, *70*, 101219.

Aicher, T., Kästner, P., Gopinath, A., Gombert, A., Bett, A. W., Schlegl, T., ... & Luther, J. (2004, November). Development of a novel TPV power generator. In *AIP Conference Proceedings* (Vol. 738, No. 1, pp. 71-78). American Institute of Physics.

Aigrain, P. (1961). *The thermophotovoltaic converter*, unpublished lectures given at the Ecole Normale Superieure in 1956, and the Massachusetts Institute of Technology, Fall 1960 and Spring 1961.

Akhtar, S., Kurnia, J. C., & Shamim, T. (2015). A three-dimensional computational model of H2–air premixed combustion in non-circular micro-channels for a thermo-photovoltaic (TPV) application. *Applied Energy*, *152*, 47-57.

Amin, N. (2022). Principle of photovoltaics. In *Comprehensive Guide on Organic and Inorganic Solar Cells* (pp. 1-23). Academic Press.

Andreev, V. M., Grilikhes, V. A., Khvostikov, V. P., Khvostikova, O. A., Rumyantsev, V. D., Sadchikov, N. A., & Shvarts, M. Z. (2004). Concentrator PV modules and solar cells for TPV systems. *Solar energy materials and solar cells*, *84*(1-4), 3-17.

Andreev, V. M., Khvostikov, V. P., Khvostikova, O. A., Vlasov, A. S., Gazaryan, P. Y., Sadchikov, N. A., & Rumyantsev, V. D. (2005, January). Solar thermophotovoltaic system with high temperature tungsten emitter. In *Conference Record of the Thirty-first IEEE Photovoltaic Specialists Conference, 2005.* (pp. 671-674). IEEE.

Bauer, T., & Bauer, T. (2011). Applications of TPV generators. *Thermophotovoltaics: basic principles and critical aspects of system design*, 147-196.

Bauer, T., Forbes, I., Penlington, R., & Pearsall, N. (2003, January). The potential of thermophotovoltaic heat recovery for the glass industry. In *AIP conference proceedings* (Vol. 653, No. 1, pp. 101-110). American Institute of Physics.

Bianchi, M., Ferrari, C., Melino, F., & Peretto, A. (2012). Feasibility study of a Thermo-Photo-Voltaic system for CHP application in residential buildings. *Applied Energy*, *97*, 704-713.

Butcher, T. A., Hammonds, J. S., Horne, E., Kamath, B., Carpenter, J., & Woods, D. R. (2011). Heat transfer and thermophotovoltaic power generation in oil-fired heating systems. *Applied Energy*, *88*(5), 1543-1548.

Colangelo, G., De Risi, A., & Laforgia, D. (2003). New approaches to the design of the combustion system for thermophotovoltaic applications. *Semiconductor science and technology*, *18*(5), S262.

Coutts, T. J. (1999). A review of progress in thermophotovoltaic generation of electricity. *Renewable and Sustainable Energy Reviews*, 3(2-3), 77-184.

Coutts, T. J. (2001). An overview of thermophotovoltaic generation of electricity, *Sol. Energy Mater. Sol. Cells*, 66(1-4), 443-452.

Coutts, T. J. (2001). Thermophotovoltaic generation of electricity, Ch. 11 in Clean Electricity from Photovoltaics, MD, Archer and R. Hill, eds. Imperial College Press

Datas, A., & Algora, C. (2010). Detailed balance analysis of solar thermophotovoltaic systems made up of single junction photovoltaic cells and broadband thermal emitters. *Solar energy materials and solar cells*, *94*(12), 2137-2147.

Fentahun, D. A., Tyagi, A., & Kar, K. K. (2021). Numerically investigating the AZO/Cu2O heterojunction solar cell using ZnO/CdS buffer layer. *Optik*, *228*, 166228.

Ferrari, C., Melino, F., Pinelli, M., & Spina, P. R. (2014). Thermophotovoltaic energy conversion: Analytical aspects, prototypes and experiences. *Applied Energy*, *113*, 1717-1730.

Ferrari, C., Melino, F., Pinelli, M., Spina, P. R., & Venturini, M. (2014). Overview and status of thermophotovoltaic systems. *Energy Procedia*, *45*, 160-169.

Ferrari, C., Melino, F., Pinelli, M., Spina, P. R., & Venturini, M. (2014). Overview and status of thermophotovoltaic systems. *Energy Procedia*, *45*, 160-169.

Fraas, L. M., Avery, J. E., Huang, H. X., & Martinelli, R. U. (2003). Thermophotovoltaic system configurations and spectral control. *Semiconductor Science and Technology*, *18*(5), S165.

Fraas, L., Ballantyne, R., Hui, S., Ye, S. Z., Gregory, S., Keyes, J., ... & Daniels, B. (1999, March). Commercial GaSb cell and circuit development for the midnight sun® TPV stove. In *AIP Conference*

Proceedings (Vol. 460, No. 1, pp. 480-487). American Institute of Physics.

Green, M.A. (1981). Solar cell fill factors: general graph and empirical expressions. *Solid State Electronics*, 24(8), 788–789.

Guazzoni, G., Kittl, E., & Shapiro, S. (1968, October). Rare earth radiators for thermophotovoltaic energy conversion. In *1968 International Electron Devices Meeting* (pp. 130-130). IEEE.

Hasan, K., Yousuf, S. B., Tushar, M. S. H. K., Das, B. K., Das, P., & Islam, M. S. (2022). Effects of different environmental and operational factors on the PV performance: A comprehensive review. *Energy Science & Engineering*, *10*(2), 656-675.

Herterich, J., Baretzky, C., Unmüssig, M., Maheu, C., Glissmann, N., Gutekunst, J., ... & Würfel, U. (2022). Toward Understanding the Short-Circuit Current Loss in Perovskite Solar Cells with 2D Passivation Layers. *Solar RRL*, *6*(7), 2200195.

Horne, E., Morgan, M., & Butcher, T. (2000). Microcogeneration concepts using thermophotovoltaics. *Proceedings of ACEEE's 11th biennial summer study on energy efficiency in buildings*, *10*, 123-30. Washington, DC, USA.

Ishaq, H., Islam, S., Dincer, I., & Yilbas, B. S. (2020). Development and performance investigation of a biomass gasification based integrated system with thermoelectric generators. *Journal of Cleaner Production*, *256*, 120625.

Khaledi, P., Behboodnia, M., & Karimi, M. (2022). Simulation and optimization of temperature effect in solar cells CdTe with back connection Cu2O. *International Journal of Optics*, *2022*.

Koçali, K. (2016). *Investigation of effects of boron compounds on solar energy panels*. MSc Thesis, Institute of Graduate Studies in Science and Engineering, Istanbul University, Istanbul, Turkey (In Turkish).

Koçali, K. (2018). Investigation of occupational health and safety culture and applications in opet pit mines by using worker questionnaires. *Scientific Mining Journal*, 57(1), 15-24.

Koçali, K. (2021). *Maden Kazalarında Sorumluluklar ve Kusur Oranları*, Nobel Yayın Kitapevi (In Turkish).

Koçali, K., & Erçetin, R. (2021). Legal regulations regarding liabilities of workers and employers related to occupational health and safety in mining. 3. *Başkent Ulusal Disiplinler Arası Bilimsel Çalışmalar Kongresi*, 357-358. (In Turkish)

Kruger, J.S., Guazzoni, G., & Nawrocki, S.J. (1998). Army thermophotovoltaic reports, *4th NREL Conference Thermophotovoltaic Generation of Electricity*, (pages 30-35). Denver, CO.

Le, T. H., & Nguyen, C. P. (2019). Is energy security a driver for economic growth? Evidence from a global sample. *Energy policy*, *129*, 436-451.

Lee, C. C., Xing, W., & Lee, C. C. (2022). The impact of energy security on income inequality: The key role of economic development. *Energy*, *248*, 123564.

Lee, M. L., Fitzgerald, E. A., Bulsara, M. T., Currie, M. T., & Lochtefeld, A. (2005). Strained Si, SiGe, and Ge channels for high-mobility metal-oxide-semiconductor field-effect transistors. *Journal of applied physics*, *97*(1), 1.

Li, D., & Xuan, Y. (2022). Design and evaluation of a hybrid solar thermphotovoltaic-thermoelectric system. *Solar Energy*, *231*, 1025-1036.

Li, X., Li, Z., Jia, T., Yan, P., Wang, D., & Liu, G. (2021). The sense of community revisited in Hankow, China: Combining the impacts of perceptual factors and built environment attributes. *Cities*, *111*, 103108.

Lou, Y., & Li, Q. (2016). On energy utilization and structure of Sichuan province. *Journal of Tsinghua University (Sci & Tech)*, 43(2), 16-19.

Mustafa, K. F., Abdullah, S., Abdullah, M. Z., & Sopian, K. (2017). A review of combustion-driven thermoelectric (TE) and thermophotovoltaic (TPV) power systems. *Renewable and Sustainable Energy Reviews*, *71*, 572-584.

Nanotechnology Standards (2023). Statnano, Accessed: 10-April-2023. [Online]. Available: https://statnano.com/standards

National Occupational Health and Safety Board Regulation No. 28550. Official Gazette. Accessed: 11-April-2023. [Online]. Available: https://www.mevzuat.gov.tr/mevzuat?MevzuatNo=17095&MevzuatTur=7&MevzuatTertip=5 (In Turkish).

National Research Council. (2001). *Thermionics Quo Vadis?: An Assessment of the DTRA's Advanced Thermionics Research and Development Program*. National Academies Press.

Nelson, R. E. (2003). A brief history of thermophotovoltaic development. *Semiconductor Science and Technology*, *18*(5), S141.

Occupational Health and Safety Law No. 6331. Official Gazette, Accessed: 10-Apr-2023. [Online]. Available: https://www.resmigazete.gov.tr/eskiler/2012/06/20120630-1.htm (In Turkish).

Occupational Health and Safety Risk Assessment Regulation No. 28512. Official Gazette. Accessed: 10-April-2023. [Online]. Available: https://www.resmigazete.gov.tr/eskiler/2012/12/20121229-13.htm (In Turkish).

OHSAS 18001 Occupational Health and Safety Management Systems. Turkish Standardization Institute. Accessed: 10-April-2023. [Online]. Available: https://www.tse.org.tr/IcerikDetay?ID=88&ParentID=623 (In Turkish).

Önal, B. S., & Utlu, Z. (2017). Endüstriyel Sistemlerde Yüksek Sıcaklıklı Atık Isı Kazanım Amaçlı Termofotovoltaik Uygulamalarında Teorik Modelleme. 13. *Ulusal Tesisat Mühendisliği Kongresi*, pp. 181-191, Izmir, Turkey (In Turkish).

Önal, B.S. (2017). *Development of electrical energy production technologies with thermophotovoltaic methods by using existing waste heat potential in thermal systems*. MSc Thesis, Institute of Science, Istanbul Aydin University, Istanbul, Turkey. (In Turkish).

Ouremchi, M., El Mouzouade, S., El Khadiri, K., Tahiri, A., & Qjidaa, H. (2022). Integrated energy management converter based on maximum power point tracking for photovoltaic solar system. *International Journal of Electrical and Computer Engineering*, *12*(2), 1211.

Qiu, K., & Hayden, A. C. S. (2003). Thermophotovoltaic generation of electricity in a gas fired heater: influence of radiant burner configurations and combustion processes. *Energy conversion and management*, *44*(17), 2779-2789.

Qiu, K., & Hayden, A. C. S. (2006). Premixed gas combustion stabilized in fiber felt and its application to a novel radiant burner. *Fuel*, *85*(7-8), 1094-1100.

Qiu, K., & Hayden, A. C. S. (2012). Development of a novel cascading TPV and TE power generation system. *Applied Energy*, *91*(1), 304-308.

Regulation No. 28861 on Supporting Occupational Health and Safety Services. Official Gazette. Accessed: 11-April-2023. [Online]. Available: https://www.resmigazete.gov.tr/eskiler/2013/12/20131224-3.htm (In Turkish).

Regulation on Occupational Health and Safety Boards No. 28532. Official Gazette. Accessed: 11-April-2023. [Online]. Available: https://www.resmigazete.gov.tr/eskiler/2013/01/20130118-3.htm (In Turkish).

Salim, A. M., & Alsyouf, I. (2020). Development of renewable energy in the GCC region: status and challenges. *International Journal of Energy Sector Management*, *14*(6), 1049-1071.

Talbi, A., Khaaissa, Y., Nouneh, K., Feddi, E. M., & El Haouari, M. (2022). Effects of temperature, thickness, electron density and defect density on ZnS based solar cells: SCAPS-1D simulation. *Materials Today: Proceedings*, *66*, 116-121.

Tang, L., Xu, C., Liu, Z., Lu, Q., Marshall, A., & Krier, A. (2017). Suppression of the surface "dead region" for fabrication of GaInAsSb thermophotovoltaic cells. *Solar Energy Materials and Solar Cells*, *163*, 263-269.

Teofilo, V. L., Choong, P., Chen, W., Chang, J., & Tseng, Y. L. (2006), January). Thermophotovoltaic energy conversion for space applications. In *AIP Conference Proceedings* (Vol. 813, No. 1, pp. 552-559). American Institute of Physics.

Utlu, Z., & Önal, B. S. (2018). Thermodynamic analysis of thermophotovoltaic systems used in waste heat recovery systems: an application. *International Journal of Low-Carbon Technologies*, *13*(1), 52-60.

Utlu, Z., & Önal, B. S. (2018). Examination of thermophotovoltaic GaSb cell technology in low and medium temperatures waste heat. In *IOP Conference Series: Materials Science and Engineering* (Vol. 307, No. 1, p. 012074). IOP Publishing.

Utlu, Z., Kınacı, B., & Önal, B.S. (2017). Investigation of the use of waste heat in central heating systems in the thermophotovoltaic technology; GaSb cell application. In *12th Conference on Sustainable Development of Energy, Water and Environment Systems – SDEWES (*pages 774:1-16). Dubrovnik, Croatia, 2017.

Wedlock, B.D. (1963). Thermo-photo-voltaic energy conversion. *Proceedings of the IEEE*, *51*(5), 694-698.

Wen, H., Lee, C. C., & Song, Z. (2021). Digitalization and environment: how does ICT affect enterprise environmental performance?. *Environmental Science and Pollution Research*, *28*(39), 54826-54841..

White, D. C., & Hottel, H. C. (1994, January). Important factors in determining the efficiency of TPV systems. In *AIP conference Proceedings* (Vol. 321, No. 1, pp. 425-436). American Institute of Physics.

White, D. C., Wedlock, B. D., & Blair, J. (1961, May). Recent advances in thermal energy conversion. In *15th Annual Proceedings, Power Sources Conference* (pp. 125-132).

Xue, X., Yu, Y., & Ye, Z. (2022). Heat and mass transfer mechanism of micro-combustion system with dual-fuel at high environmental load. *Applied Thermal Engineering*, *200*, 117698.

Yamaguchi, H., & Yamaguchi, M. (1999, March). Thermophotovoltaic potential applications for civilian and industrial use in Japan. In *AIP Conference Proceedings* (Vol. 460, No. 1, pp. 17-29). American Institute of Physics.

Yerebakan, M. (2010). *Güneş Kollektörleri Uygulamaları*, 1st ed., Istanbul Ticaret Odası Yayınları, 2010 (In Turkish).

Zhang, L., Bai, W., Xiao, H., & Ren, J. (2021). Measuring and improving regional energy security: a methodological framework based on both quantitative and qualitative analysis. *Energy*, *227*, 120534.

CHAPTER 8

FUNDAMENTALS OF PHOTOCATALYTIC OXIDATION PROCESSES AND APPLICATIONS OF HYBRID-PHOTOCATALYTIC OXIDATION PROCESSES

Assist. Prof. Dr. Murat KIRANŞAN[1*]

[1]*University of Gumushane, Vocational School of Gumushane, Department of Chemistry and Chemical Processing Technologies, 29100-Gümüşhane, TURKEY.
*murat.kiransan@gumushane.edu.tr (*Corresponding Author), ORCID ID: 0000-0002-8520-6563

INTRODUCTION

Water is an indispensable resource for living things and although the amount of fresh water in the world is decreasing, it mainly consists of water resources that cannot be used directly by humans, such as ocean and sea salt waters and glaciers (Liang et al., 2012). Therefore, it is very important to develop effective and environmentally friendly methods to treatment wastewater and reduce or eliminate pollutants (Han et al., 2014). In recent years, water resources are gradually decreasing due to the rapid development of the pollution industries such as the pharmaceutical waste, distillation facility, textile, fertilizer, dye industries (Bessekhouad et al., 2004). In the future, our world there will be water crises due to increasing living standards, increasing human population and urbanization, toxic waste materials containing hazardous pollutants (Rivero et al., 2020; Wang et al., 2010).

Industrial wastes are an important factor for the environmental pollution. Available water resources are gradually decreasing with the industrialization, industrial waste, uncontrolled urbanization, and fast population growth (Deng et al., 2002). Reuse of the treatment wastewater has become an important parameter in the control, planning and development of countries water resources, especially due to the increase in the demand for water due to the development of the industry (Villegas et al., 2016; Strong and Burgess, 2008). Population growth and urbanization, climate change due to global warming and industrialization are among the causes of excessive water consumption and water pollution (Poyatos et al., 2010). A large part of the water is consumed for various purposes for industrial production and therefore large amounts of wastewater are formed. Wastewaters consists of different organic and inorganic components that are toxic and difficult to degradation (Esther et al., 2004; Oturan and Aaron, 2014). With the production of hydroxyl radicals, which are effective oxidizers in photocatalytic oxidation processes, toxic and harmful organic substances are transformed into harmless or less toxic structures (Li et al., 2013; Zango et al., 2020). In photocatalytic oxidation processes, organic pollutants interaction with the hydroxyl radical and transform into a carbon-centered biodegradable radical (Estrellan et al., 2010). These biodegradable intermediates are converted into CO_2 and H_2O or inorganic salts with mineralization as the last step and oxidation is completed (Zhu and Zhou, 2019). The efficiency of the system can be affected depending on the method of the advanced oxidation process selected, the physical and

chemical properties of the organic pollutant and the operating conditions (Feng et al., 2020; Jiang et al., 2021).

Photocatalytic oxidation processes include the use of photochemically generated reactive radicals to oxidize environmental pollutants. Light energy is one of the essential components of the photocatalytic oxidation process (Bahrudin and Nawi, 2019; Carvalho et al., 2010). Hybrid photocatalytic oxidation processes use either UV light (wavelength range 100-400 nm) or visible light to generate radicals, depending on the technology used (Lachheb et al., 2002). Ultraviolet radiation is commonly provided by mercury arc lamps in the photocatalytic oxidation methods. The radiation dose that UV lamps can provide depends on the UV light intensity and contact time (Franco et al., 2020; Sahu et al., 2018). The ultraviolet light intensity should be high enough in terms of efficiency and the solution should be homogeneously dispersed in the environment (Orooji et al., 2020). The intensity of the light emitted from the UV lamp decreases as it moves away from the UV source in the liquid medium. Another parameter, the longer the contact time, the greater the effect of UV light (Lee et al., 2015; Vaiano et al., 2017). Hybrid photocatalytic oxidation processes are basically divided into three parts. Photolytic and photocatalytic oxidation processes, photo-Fenton processes, photo-ozonation processes (Khataee et al., 2016).

1. FUNDAMENTALS OF THE PHOTOCATALYTIC OXIDATION PROCESS

Ultraviolet (UV) irradiation, which has an important effect on the degradation of organic and inorganic pollutants, constitutes the most important class of advanced oxidation processes (Ziarati et al., 2018). This process uses light of the appropriate wavelength to transmit photons of light to removal undesirable organic and inorganic pollutants (Tian et al., 2013). Generally, the UV spectrum has a wavelength range of 100 to 400 nm. In addition, ultraviolet irradiation can be examined in three groups: UV-A (315-380 nm), UV-B (280-315 nm) and UV-C (200-280 nm) (Shi et al., 2019; Tian et al., 2015). It is considered an effective wastewater treatment because it purifies strong organic pollutants in oxidation processes using UV light (Panwar et al., 2016). Therefore, ultraviolet irradiation is less affected by pH changes and chemical reagent addition is not required. Photochemical reactions are an application involving the interaction between organic pollution that cause chemical reactions by the interacting with UV light (Mou et al., 2012; Orooji et al., 2021). The photochemical oxidation process has

proven to be an effective removal method for the treatment of the organic pollution, which are particularly stubborn pollutants in the wastewater treatment plants (Mousavi et al., 2021). There are two types of the photochemical UV radiation, direct and indirect irradiation (Joo et al., 2016). Direct irradiation involves photon absorption by organic pollution before any photochemical reaction. This process is the described as photosensitized photodegradation (Hamadanian et al., 2017; Jang et al., 2017).

The pollutant excited by photons of light is converted into a higher energy excited molecule by direct irradiation. Organic pollutants stimulated with high energy can return to the basic state by releasing energy or can be transformed into radical intermediates by photo-oxidation reactions [Eqs. (1-3)] (Cao et al., 2017; Eskandarloo et al., 2015).

Pollutant + UV Light (A-B-C) → Pollutant* (1)
Pollutant* → Pollutant (2)
Pollutant* → Intermediates (Radicals) (3)
Intermediates → → Photodegradation products + CO_2 + H_2O (4)

Photochemical oxidation reactions it causes organic pollutants to decompose into basic and harmless products such as CO_2 and H_2O [Eq. (4)] (Chen et al., 2016).

The photocatalytic oxidation process is a photochemical reaction based on the absorption of visible or UV radiation energy directly or indirectly by a solid semiconductor material (Doan et al., 2021; Sun et al., 2018). In the interface between the excited semiconductor material and the solution, destruction or removal of the pollutants occurs without a chemical change in the catalyst (Dehkordi and Badiei, 2022). When a photocatalyst is exposed to light of the desired wavelength, the energy of the photons passes into the (e^-) conductivity band of the electrons in the valence band (Lei et al., 2020). In this process, an energy gap (h^+) is formed in the valence band This charge separation is one of the first important steps in the photocatalytic reaction. These pairs of the electrons and spaces come together again and give the energy to the environment as heat [Eqs.(5-6)] (Kayaci et al., 2014; Tiwari et al., 2022).

$$\text{Photocatalyst} \rightarrow e^-_{CB} + h^+_{VB} \quad (5)$$

$$e^-_{CB} + h^+_{VB} \rightarrow \text{Heat} \quad (6)$$

When semiconductor metal oxides come into contact with water, hydroxyl ions are formed. The holes formed by the continuation of the radiation move against the photocatalyst surface, and the electrons against the inner surface of the particle (Liu et al., 2014; Park et al., 2020). Thus, the risk of losing their activity by reuniting the electron/hole pair is the eliminated. Hydroxyl radicals (OH•) are formed as a result of the photocatalytic and photochemical reactions on the semiconductor surface [Eqs.(7-8)] (Qiu et al., 2018; Raja et al., 2021). The schematic of the photocatalytic oxidation process as shown in Fig. 1.

$$h^+_{VB} + H_2O \rightarrow OH^\bullet + H^+ \quad (7)$$

$$h^+_{VB} + OH^- \rightarrow OH^\bullet \quad (8)$$

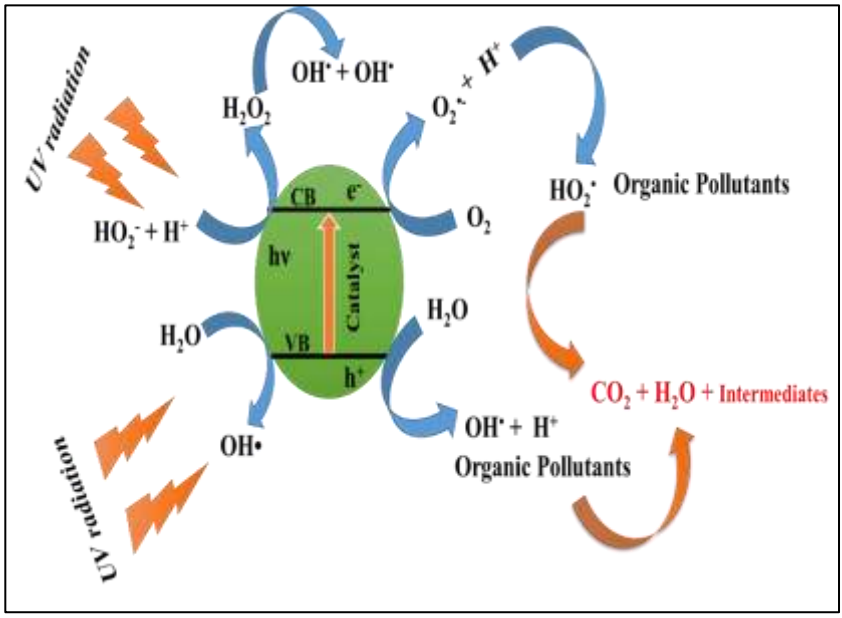

Figure 1. Schematic mechanism of the photocatalytic oxidation process (Raja et al., 2021; Sun et al., 2017; Tiwari et al., 2022).

Superoxide ion radical also reactions with water and molecules such as $O_2^{\bullet-}$, $HO_2^\bullet$, HO_2^-, O_2 and H_2O_2 are formed in the solution medium [Eqs.(9-14)] (Ren et al., 2019; Sun et al., 2017).

$$H^+ + O_2^{\bullet-} \rightarrow HO_2^\bullet \quad (9)$$

$$HO_2^\bullet \rightarrow H_2O_2 + O_2 \quad (10)$$

$$HO_2^{\bullet} + O_2^{\bullet-} \rightarrow O_2 + HO_2^- \quad (11)$$

$$HO_2^- + H^+ \rightarrow H_2O_2 \quad (12)$$

$$H_2O_2 \rightarrow H_2 + O_2 \quad (13)$$

$$H_2O_2 + HO_2^{\bullet} \rightarrow OH^{\bullet} + H_2O + O_2 \quad (14)$$

2. PROCESSES OF HYBRID-PHOTOCATALYTIC OXIDATION

Advanced oxidation processes with ultraviolet radiation consist of different hybrid processes. Hybrid photocatalytic oxidation processes are effective methods for removal organic pollutants from industrial wastewater. Ultraviolet radiation is converted into more effective processes with different hybrid techniques. These hybrid techniques are; photocatalytic-ozonation, sono-photocatalytic and photo-Fenton processes.

2.1. Photocatalytic-Ozonation Processes (UV/Catalytic/O_3)

The synergistic effect of ozone and ultraviolet radiation with the support of the catalyst is called the photocatalytic-ozonation process (Biglari et al., 2017). The photocatalytic-ozonation process is initiated by the photolysis of the ozone molecule. Photodegradation of the ozone molecule causes the formation of hydrogen peroxide and hydroxyl radical in the ultraviolet radiation of 310 nm wavelength (Fathinia et al., 2020; Gomes et al., 2017). The interaction of the ozone molecule with hydrogen peroxide occurs as a slow reaction. Photolysis of the hydrogen peroxide molecule with ultraviolet radiation produces two hydroxyl radicals (Solis et al., 2016; Xiao et al., 2015). However an acid-base equilibrium reaction become by forming hydrogen peroxide, a hydronium ion and a hydroperoxyl anion [Eqs.(15-18)] (Quinones et al., 2015).

$$H_2O + O_3 + h\nu \rightarrow H_2O_2 + O_2 \quad (15)$$

$$H_2O_2 + O_3 \rightarrow HO_2^{\bullet} + OH^{\bullet} + O_2 \quad (16)$$

$$H_2O_2 + h\nu \rightarrow 2\ OH^{\bullet} \quad (17)$$

$$H_2O_2 + H_2O \rightarrow H_3O^+ + HO_2^- \quad (18)$$

The hydroxyl radical react with ozone and hydrogen peroxide to produce the hydroperoxyl radical ($HO_2^{\bullet}$) and superoxide radicals ($O_2^{\bullet-}$) respectively. The superoxide radical reacts with the hydroxyl radical to give the hydroxyl ion [Eqs.(19-21)] (Mecha and Chollom, 2020; Mena et al., 2012).

$$OH^{\bullet} + O_3 \rightarrow O_2 + HO_2^{\bullet} \quad (19)$$

$$OH^{\bullet} + H_2O_2 \rightarrow O_2^{\bullet-} + H_2O + H^+ \quad (20)$$

$$OH^{\bullet} + O_2^{\bullet-} \rightarrow OH^- + O_2 \quad (21)$$

It contains three components to formation hydroxyl radicals ($OH^{\bullet}$) in the photo-ozonation hybrid system or to oxidize contaminants for the subsequent reactions. These components are UV radiation, Ozone (O_3) and hydrogen peroxide (H_2O_2) (Huang et al., 2016; Yin et al., 2016).

The use of photocatalysts with ozonation in the oxidation medium and the adsorption occurring on the surface of the catalyst create different oxidation mechanisms (Rey et al., 2014). Photocatalytic ozonation process is different from ozonation in the absence of the photocatalyst. The reactions formed by the synergistic effect of photocatalyst and ozonation are as follows [Eqs. (22-25)] (Liao et al., 2016; Orge et al., 2017).

$$\text{Photocatalyst} + h\nu \rightarrow \text{Photocatalyst} + e^- + h^+ \quad (22)$$

$$\text{Photocatalyst} + O_3 \rightarrow O_2 + O^{\bullet} \quad (23)$$

$$O_3 + h\nu \rightarrow O_2 + O^{\bullet} \quad (24)$$

$$H_2O_2 + h\nu \rightarrow 2\,OH^{\bullet} \quad (25)$$

A schematic representation of the effects of photocatalyst and ozonation processes on organic pollutants, respectively is given in Figure 2 (Anandan et al., 2010; Mehrjouei et al., 2015).

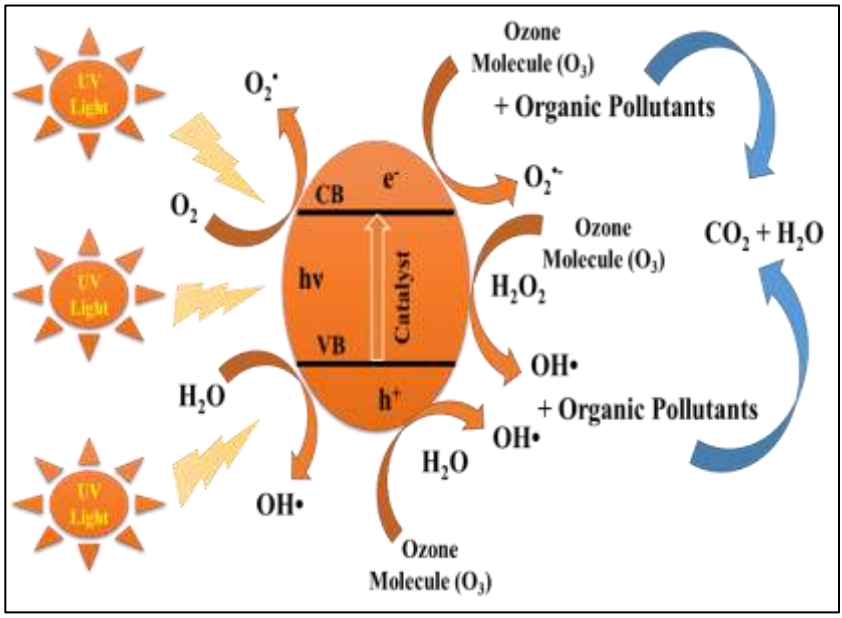

Figure 2. Schematic mechanism of the photocatalytic-ozonation process (Anandan et al., 2010; Niu et al., 2018; Orge et al., 2017).

In the treatment of wastewater, it is seen in the literature studies that the efficiency of the two oxidation systems for ozonation and photocatalysis, respectively increased due to the synergistic effect compared to the total oxidation yields (Ardizzone et al., 2011; Niu et al., 2018).

2.2. Photo-Fenton Oxidation Processes ($UV/H_2O_2/Fe^{2+}$)

The catalytic reaction formed by Fe^{2+} ions with H_2O_2 in the acidic conditions is known as the Fenton process. The decomposition of H_2O_2 in acid solution and in the dark, catalyzed by Fe^{2+} in the solution, leads to the generation of the hydroxyl radicals according to the well known thermal Fenton reaction (Zhou et al., 2018). The combination of H_2O_2 and Fe^{2+} reaction as the follows by the give hydroxyl radicals (•OH) stoichiometrically as shown in the equation [Eqs. (26-28)] (Qian et al., 2018; Zhao et al., 2020).

$$Fe^{2+} + H_2O_2 \rightarrow Fe^{3+} + \bullet OH + OH^- \quad (26)$$

$$Fe^{3+} + H_2O + UV \rightarrow Fe^{2+} + \bullet OH + H^+ \quad (27)$$

$$H_2O_2 + UV \rightarrow 2\ \bullet OH \quad (28)$$

The Fenton process, which takes place in the presence of UV light is called the photo-Fenton process. A Fenton system can achieve higher removal efficiencies in most cases when irradiated with ultraviolet light (Punzi et al., 2012; Sharmila et al., 2019). The rate of the disintegration in the photo-Fenton reaction is much greater than the classical Fenton reaction and also the volume of the sludge formed is the less (Kumar, 2011). The operating cost and chemical consumption in the photo-Fenton process is much lower than the classical Fenton process (Jiang et al., 2019). For all these reasons, the photo-Fenton process is a more advantageous method than the classical Fenton process (Zhang et al., 2019).

2.3. Sono-Photocatalytic Processes (US/UV/Catalytic)

The hybrid sono-photocatalytic oxidation process is an effective catalyst assisted process to increase the removal efficiency of organic pollutants in wastewater (Malika and Sonawane, 2021). The primary purpose of the sono-photocatalytic oxidation process is to reduce the treatment costs of industrial wastes and separation organic wastes into smaller molecules (Patidar and Srivastava, 2021).

To make the sono-photocatalytic oxidation process more effective, there are three factors that affect the mass transfer of organic wastes in the liquid phase. These factors are increased hydroxyl radical (·OH) production, formation of cavitation bubbles with the support of catalyst particles and catalyst surface (Selvamani et al., 2021). The reaction rate increases with the combination of the dual effect of ultraviolet and ultrasound radiation. Hydrogen peroxide is produced by the combination of sonolysis and photocatalytic oxidation [Eqs. (29-32)] (Matafonova and Batoev, 2019; Torres et al., 2008).

$$H_2O \rightarrow))))) \rightarrow OH^{\bullet} + H^{\bullet} \quad (29)$$

$$H_2O_2 + H^{\bullet} \rightarrow H_2O + {}^{\bullet}OH \quad (30)$$

$$H_2O_2 + hv \rightarrow 2\ {}^{\bullet}OH \quad (31)$$

$$H_2O_2 + O_2^{\bullet-} \rightarrow {}^{\bullet}OH + OH^- + O_2 \quad (32)$$

Adsorption of organic pollutants to specific centers on the catalyst surface will result in important increase in the number of ultrasonically active centers as a result of sono-photocatalytic oxidation reactions resulting in the reaction rate (Chachvalvutikul and Kaowphong, 2020). The schematic of the sono-photocatalytic oxidation process as shown in Fig. 3.

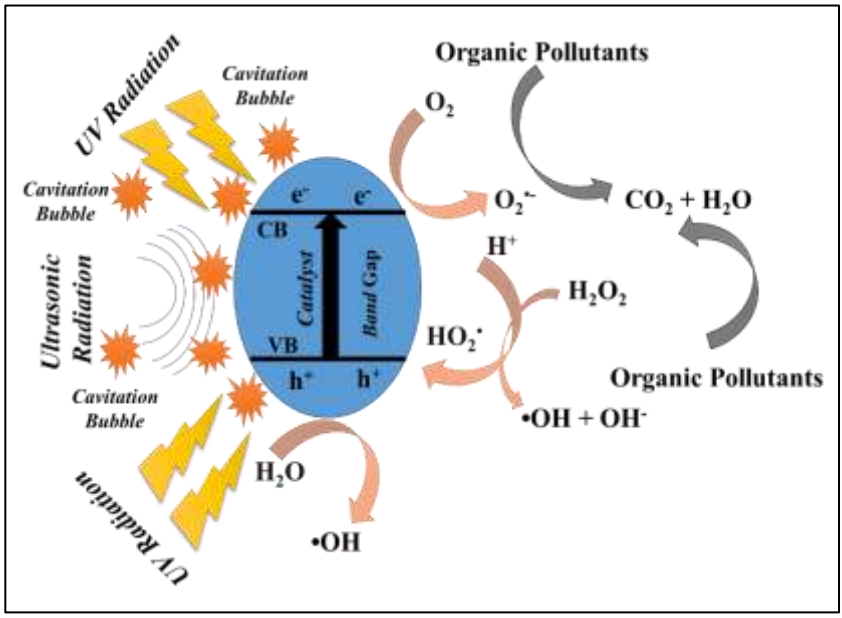

Figure 3. Schematic mechanism of the sono-photocatalytic process (Chachvalvutikul and Kaowphong, 2020; Maroudas et al., 2021; Torres et al., 2008).

Under the conditions resulting from sono-photocatalytic oxidation, suitable surface areas are formed due to the catalyst effect and the diffusion rates of organic wastes increase (Maroudas et al., 2021; Panda and Manickam, 2017).

3. APPLICATIONS OF PROCESSES

Hybrid photocatalytic oxidation processes are among the effective methods for the treatment of pollutants with complex molecules and difficult to decompose, such as organic wastes from wastewater (Meng et al., 2012; Oros-Ruiz et al., 2012). The processes that provide the highest efficiency in the removing organic pollutants from wastewater are photocatalytic-ozonation, photo-Fenton and sono-photocatalytic oxidation processes (Ebrahiem et al., 2017; Lashuk and Yargeau, 2021; Minella et al., 2014). As a result of the synergistic effect of hybrid photocatalytic oxidation processes, it provides effective removal of organic pollutants as a result of intense hydroxyl radical production (Yu et al., 2017). The technology is used sustainable as a result of efficient mass transfer and the use of advanced hybrid photocatalytic processes (Bozzi et al., 2004). Removal of organic

pollutants in the aquatic medium by photocatalytic oxidation processes is both an economical and effective process (Charanpahari et al., 2013).

Photocatalytic-ozonation processes are processes that increase the production of hydroxyl radicals (Fernandes et al., 2020). In the Photo-Fenton oxidation studies in the literature, it has been reported that as the ultraviolet power energy increases, the amount of degradation of organic pollutants in the aquatic medium increases as a result of the synergistic effect of the Fenton process (Giri and Golder, 2019). In the sono-photocatalytic oxidation hybrid process on the other hand, the positive effects of the sonolytic process increase the production of hydroxyl radicals as a result of the formation of bubbles in the solution due to ultrasonic cavitation (Al-Musawi et al., 2021; Eshaq and ElMetwally, 2019). As a result of the combination of ultrasonic radiation and ultraviolet radiation, the sono-photocatalytic process is an effective process used for the removal of organic pollutants in wastewater (Bezzerrouk et al., 2021).

4. CONCLUSION

It has been reported in the literature that it is an effective process in the degradation of organic and inorganic pollutants by photocatalytic oxidation processes. Hybrid photocatalytic oxidation processes are a process that increases the formation of hydroxyl radicals (OH•) under the influence of UV radiation. Hydroxyl radicals (OH•) are molecules that degradation organic pollutants. Hybrid photocatalytic oxidation processes have effective advantages over other advanced oxidation processes. Photocatalytic oxidation processes occur quickly and in a very short time. They are effective in removal all kinds of industrial wastewater. They are effective processes for different concentrations of organic and inorganic pollutants.

Hybrid photocatalytic oxidation processes have the potential to reduce toxic substances to life and fully mineralize organic pollutants. These processes are very effective in removal most micropollutants and also oxidize odor-causing compounds from drinking water. Hybrid photocatalytic oxidation reactions are very fast and contact times start from a few seconds. While reducing the pollution in wastewater it also provides microbial cleaning.

ACKNOWLEDGEMENTS

The authors would like to express special thanks to the University of Gumushane for supports.

REFERENCES

Al-Musawi, T. J., Mengelizadeh, N., Sathishkumar, K., Mohebi, S. and Balarak, D. (2021). Preparation of $CuFe_2O_4$/montmorillonite nanocomposite and explaining its performance in the sonophotocatalytic degradation process for ciprofloxacin. *Colloid and Interface Science Communications*, Vol. 45, pp 100532.

Anandan, S., Lee, G. L., Chen, P. K., Fan, C. and Wu, J. J. (2010). Removal of orange II dye in water by visible light assisted photocatalytic ozonation using Bi_2O_3 and Au/Bi_2O_3 nanorods. *Industrial & Engineering Chemistry Research*, Vol. 49, pp 9729-9737.

Ardizzone, S., Cappelletti, G., Meroni, D. and Spadavecchia, F. (2011). Tailored TiO_2 layers for the photocatalytic ozonation of cumylphenol, a refractory pollutant exerting hormonal activity. *Chemical Communications*, Vol. 47, No. 9, pp 2640-2642.

Bahrudin, N. N. and Nawi, M. A. (2019). Mechanistic of photocatalytic decolorization and mineralization of methyl orange dye by immobilized TiO_2/chitosan-montmorillonite. *Journal of Water Process Engineering*, Vol. 31, pp 100843.

Bessekhouad, Y., Robert, D. and Weber, J. V. (2004). Bi_2S_3/TiO_2 and CdS/TiO_2 heterojunctions as an available configuration for photocatalytic degradation of organic pollutant. *Journal of Photochemistry and Photobiology A: Chemistry*, Vol. 163, No. 3, pp 569-580.

Bezzerrouk, M. A., Bousmaha, M., Hassan, M., Akriche, A., Kharroubi, B. and Naceur, R. (2021). Enhanced methylene blue removal efficiency of SnO_2 thin film using sono-photocatalytic processes. *Optical Materials*, Vol. 117, pp 111116.

Biglari, H., Afsharnia, M., Alipour, V., Khosravi, R., Sharafi, K. and Mahvi, A. H. (2017). A review and investigation of the effect of nanophotocatalytic ozonation process for phenolic compound removal from real effluent of pulp and paper industry. *Environmental Science and Pollution Research*, Vol. 24, pp 4105-4116.

Bozzi, A., Dhananjeyan, M., Guasaquillo, I., Parra, S., Pulgarin, C., Weins, C. and & Kiwi, J. (2004). Evolution of toxicity during melamine photocatalysis with TiO_2 suspensions. *Journal of Photochemistry and Photobiology A: Chemistry*, Vol. 162, No. 1, pp 179-185.

Cao, Y., Xing, Z., Hu, M., Li, Z., Wu, X., Zhao, T., Xiu, Z., Yang, S. and Zhou, W. (2017). Mesoporous black N-TiO_{2-x} hollow spheres as

efficient visible-light-driven photocatalysts. *J. Catal.*, Vol. 356, pp 246-254.

Carvalho, H. W., Batista, A. P., Hammer, P. and Ramalho, T. C. (2010). Photocatalytic degradation of methylene blue by TiO_2–Cu thin films: Theoretical and experimental study. *Journal of Hazardous Materials*, Vol. 184, No. 1-3, pp 273-280.

Chachvalvutikul, A. and Kaowphong, S. (2020). Direct Z-scheme $FeVO_4$/BiOCl heterojunction as a highly efficient visible-light-driven photocatalyst for photocatalytic dye degradation and Cr (VI) reduction. *Nanotechnology*, Vol. 31, No. 14, pp 145704.

Charanpahari, A., Umare, S. S. and Sasikala, R. (2013). Effect of Ce, N and S multi-doping on the photocatalytic activity of TiO_2. *Applied surface science*, Vol. 282, pp 408-414.

Chen, Q., Wu, S. and Xin, Y. (2016). Synthesis of Au–CuS–TiO_2 nanobelts photocatalyst for efficient photocatalytic degradation of antibiotic oxytetracycline. *Chemical Engineering Journal*, Vol. 302, pp 377-387.

Dehkordi, A. B. and Badiei, A. (2022). Insight into the activity of TiO_2@ nitrogen-doped hollow carbon spheres supported on g-C_3N_4 for robust photocatalytic performance. *Chemosphere*, Vol. 288, pp 132392.

Deng, X., Yue, Y. and Gao, Z. (2002). Gas-phase photo-oxidation of organic compounds over nanosized TiO_2 photocatalysts by various preparations. *J Applied Catalysis B: Environmental*, Vol. 39, No. 2, pp 135-147.

Doan, V. D., Huynh, B. A., Le Pham, H. A. and Vasseghian, Y. (2021). Cu_2O/Fe_3O_4/MIL-101 (Fe) nanocomposite as a highly efficient and recyclable visible-light-driven catalyst for degradation of ciprofloxacin. *Environmental Research*, Vol. 201, pp 111593.

Ebrahiem, E. E., Al-Maghrabi, M. N. and Mobarki, A. R. (2017). Removal of organic pollutants from industrial wastewater by applying photo-Fenton oxidation technology. *Arabian Journal of Chemistry*, Vol. 10, pp 1674-1679.

Eshaq, G. and ElMetwally, A. E. (2019). Bmim [OAc]-Cu_2O/g-C_3N_4 as a multi-function catalyst for sonophotocatalytic degradation of methylene blue. *Ultrasonics sonochemistry*, Vol. 53, pp 99-109.

Eskandarloo, H., Badiei, A., Behnajady, M. A. and Mohammadi Ziarani, G. (2015). Photo and Chemical Reduction of Copper onto Anatase-Type TiO_2 Nanoparticles with Enhanced Surface Hydroxyl Groups as

Efficient Visible Light Photocatalysts. *Photochemistry and photobiology*, Vol. 91, No. 4, pp 797-806.

Esther, F., Tibor, C. and Gyula, O. (2004). Removal of synthetic dyes from wastewaters: a review. *Environment international*, Vol. 30, No. 7, pp 953-971.

Estrellan, C. R., Salim, C. and Hinode, H. (2010). Photocatalytic decomposition of perfluorooctanoic acid by iron and niobium co-doped titanium dioxide. *J. Hazard Mater.*, Vol. 179, pp 79-83.

Fathinia, M., Khataee, A., Vahid, B. and Joo, S. W. (2020). Scrutinizing the vital role of various ultraviolet irradiations on the comparative photocatalytic ozonation of albendazole and metronidazole: Integration and synergistic reactions mechanism. *Journal of Environmental Management*, Vol. 272, pp 111044.

Feng, S., Chen, T., Liu, Z., Shi, J., Yue, X. and Li, Y. (2020). Z-scheme CdS/CQDs/g-C_3N_4 composites with visible-near-infrared light response for efficient photocatalytic organic pollutant degradation. *Science of The Total Environment*, Vol. 704, pp 135404.

Fernandes, E., Martins, R. C. and Gomes, J. (2020). Photocatalytic ozonation of parabens mixture using 10% N-TiO_2 and the effect of water matrix. *Science of The Total Environment*, Vol. 718, pp 137321.

Franco, P., Sacco, O., De Marco, I., Sannino, D. and Vaiano, V. (2020). Photocatalytic degradation of eriochrome black-T azo dye using Eu-doped ZnO prepared by supercritical antisolvent precipitation route: a preliminary investigation. *Topics in Catalysis*, Vol. 63, No. 11, pp 1193-1205.

Giri, A. S. and Golder, A. K. (2019). Ciprofloxacin degradation in photo-Fenton and photo-catalytic processes: Degradation mechanisms and iron chelation. *Journal of Environmental Sciences*, Vol. 80, pp 82-92.

Gomes, J., Leal, I., Bednarczyk, K., Gmurek, M., Stelmachowski, M., Diak, M., Emilia Quinta-Ferreira, M., Costa, R., Quinta-Ferreira, R. M. and Martins, R. C. (2017). Photocatalytic ozonation using doped TiO_2 catalysts for the removal of parabens in water. *Sci. Total Environ.*, Vol. 609, pp 329-340.

Hamadanian, M., Rostami, M. and Jabbari, V. (2017). Graphene-supported C–N–S tridoped TiO_2 photo-catalyst with improved band gap and charge transfer properties. *Journal of Materials Science: Materials in Electronics*, Vol. 28, pp 15637-15646.

Han, B. Q., Zhang, F., Feng, Z. P., Liu, S. Y., Deng, S. J., Wang, Y. and Wang, Y. D. (2014). A designed Mn_2O_3/MCM-41 nanoporous composite for methylene blue and rhodamine B removal with high efficiency. *Ceramics International*, Vol. 40, No. 6, pp 8093-8101.

Huang, J., Wang, X., Pan, Z., Li, X., Ling, Y. and Li, L. (2016). Efficient degradation of perfluorooctanoic acid (PFOA) by photocatalytic ozonation. *Chemical Engineering Journal*, Vol. 296, pp 329-334.

Jang, B., Hong, A., Kang, H. E., Alcantara, C., Charreyron, S., Mushtaq, F., & Pane, S. (2017). Multiwavelength light-responsive Au/B-TiO_2 janus micromotors. *ACS nano*, Vol. 11, No. 6, pp 6146-6154.

Jiang, J., Gao, J., Li, T., Chen, Y., Wu, Q., Xie, T. and Dong, S. (2019). Visible-light-driven photo-Fenton reaction with α-Fe_2O_3/BiOI at near neutral pH: Boosted photogenerated charge separation, optimum operating parameters and mechanism insight. *Journal of colloid and interface science*, Vol. 554, pp 531-543.

Jiang, H., Sun, J., Zang, S., et al., (2021). Constructing broad spectrum response ROQDs/Bi_2WO_6/CQDs heterojunction nanoplates: synergetic mechanism of boosting redox abilities for photocatalytic degradation pollutant. *J. Environ. Chem. Eng.*, Vol. 9, No. 4, pp 105674.

Joo, J. B., Liu, H., Lee, Y. J., Dahl, M., Yu, H., Zaera, F. and Yin, Y. (2016). Tailored synthesis of C@TiO_2 yolk–shell nanostructures for highly efficient photocatalysis. *Catalysis Today*, Vol. 264, pp 261-269.

Kayaci, F., Vempati, S., Ozgit-Akgun, C., Donmez, I., Biyikli, N. and Uyar, T. (2014). Selective isolation of the electron or hole in photocatalysis: ZnO–TiO_2 and TiO_2–ZnO core–shell structured heterojunction nanofibers via electrospinning and atomic layer deposition. *Nanoscale*, Vol. 6, No. 11, pp 5735-5745.

Khataee, A. R., Kıranşan, M., Karaca, S. and Arefi-Oskoui, S. (2016). Preparation and characterization of ZnO/MMT nanocomposite for photocatalytic ozonation of a disperse dye. *Turkish Journal of Chemistry*, Vol. 40, pp 546-564.

Kumar, S. M. (2011). Degradation and mineralization, of organic contaminants by Fenton and photo-Fenton processes: review of mechanisms and effects of organic and inorganic additives. *Research Journal of Chemistry and Environment*, Vol. 15, No. 2, pp 96-112.

Lachheb, H., Puzenat, E., Houas, A., Ksibi, M., Elaloui, E., Guillard, C. and Herrmann, J. M. (2002). Photocatalytic degradation of various types

of dyes (Alizarin S, Crocein Orange G, Methyl Red, Congo Red, Methylene Blue) in water by UV-irradiated titania. *Applied Catalysis B: Environmental*, Vol. 39, No. 1, pp 75-90.

Lashuk, B. and Yargeau, V. (2021). A review of ecotoxicity reduction in contaminated waters by heterogeneous photocatalytic ozonation. *Science of The Total Environment*, Vol. 787, pp 147645.

Lee, K. M., Hamid, S. B. A. and Lai, C. W. (2015). Multivariate analysis of photocatalytic-mineralization of Eriochrome Black T dye using ZnO catalyst and UV irradiation. *Materials Science in Semiconductor Processing*, Vol. 39, pp 40-48.

Lei, Y., Guo, P., Jia, M., Wang, W., Liu, J. and Zhai, J. (2020). One-step photodeposition synthesis of TiO_2 nanobelts/MoS_2 quantum dots/rGO ternary composite with remarkably enhanced photocatalytic activity. *Journal of Materials Science*, Vol. 55, pp 14773-14786.

Li, Z., Zhang, P., Shao, T., Wang, J., Jin, L. and Li, X. (2013). Different nanostructured In_2O_3 for photocatalytic decomposition of perfluorooctanoic acid (PFOA). *J. Hazard Mater.*, Vol. 260, pp 40-46.

Liang, S., Can, B. W., Min, J. and Fang, X. L. (2012). COD removal and biodegradability enhancement of pharmaceutical wastewater using a multilayer internal electrolysis reactor. *Asian Journal of Chemistry*, Vol. 24, pp 112-116.

Liao, G., Zhu, D., Zheng, J., Yin, J., Lan, B. and Li, L. (2016). Efficient mineralization of bisphenol A by photocatalytic ozonation with TiO_2–graphene hybrid. *Journal of the Taiwan Institute of Chemical Engineers*, Vol. 67, pp 300-305.

Liu, G., He, F., Zhang, J., Li, L., Li, F., Chen, L. and Huang, Y. (2014). Yolk–shell structured Fe_3O_4@C@F-TiO_2 microspheres with surface fluorinated as recyclable visible-light driven photocatalysts. *Applied Catalysis B: Environmental*, Vol. 150, pp 515-522.

Malika, M. and Sonawane, S. S. (2021). The sono-photocatalytic performance of a novel water based Ti^{4+} coated $Al(OH)_3$-MWCNT's hybrid nanofluid for dye fragmentation. *International Journal of Chemical Reactor Engineering*, Vol. 19, No. 9, pp 901-912.

Maroudas, A., Pandis, P. K., Chatzopoulou, A., Davellas, L. R., Sourkouni, G. and Argirusis, C. (2021). Synergetic decolorization of azo dyes using ultrasounds, photocatalysis and photo-Fenton reaction. *Ultrasonics Sonochemistry*, Vol. 71, pp 105367.

Matafonova, G. and Batoev, V. (2019). Review on low-and high-frequency sonolytic, sonophotolytic and sonophotochemical processes for inactivating pathogenic microorganisms in aqueous media. *Water Research*, Vol. 166, pp 115085.

Mecha, A.C. and Chollom, M.N. (2020). Photocatalytic ozonation of wastewater: a review. *Environmental Chemistry Letters*, Vol. 18, pp 1491-1507.

Mehrjouei, M., Müller, S. and Möller, D. (2015). A review on photocatalytic ozonation used for the treatment of water and wastewater. *Chemical Engineering Journal*, Vol. 263, pp 209-219.

Mena, E., Rey, A., Acedo, B., Beltran, F. J. and Malato, S. (2012). On ozone-photocatalysis synergism in black-light induced reactions: Oxidizing species production in photocatalytic ozonation versus heterogeneous photocatalysis. *Chemical engineering journal*, Vol. 204, pp 131-140.

Meng, H. L., Cui, C., Shen, H. L., Liang, D. Y., Xue, Y. Z., Li, P. G. and Tang, W. H. (2012). Synthesis and photocatalytic activity of TiO_2@CdS and CdS@TiO_2 double-shelled hollow spheres. *Journal of alloys and compounds*, Vol. 527, pp 30-35.

Minella, M., Marchetti, G., De Laurentiis, E., Malandrino, M., Maurino, V., Minero, C. and Hanna, K. (2014). Photo-Fenton oxidation of phenol with magnetite as iron source. *Applied Catalysis B: Environmental*, Vol. 154, pp 102-109.

Mou, F., Xu, L., Ma, H., Guan, J., Chen, D. R. and Wang, S. (2012). Facile preparation of magnetic γ-Fe_2O_3/TiO_2 Janus hollow bowls with efficient visible-light photocatalytic activities by asymmetric shrinkage. *Nanoscale*, Vol. 4, No. 15, 4650-4657.

Mousavi, M., Soleimani, M., Hamzehloo, M., Badiei, A. and Ghasemi, J. B. (2021). Photocatalytic degradation of different pollutants by the novel gCN-NS/Black-TiO_2 heterojunction photocatalyst under visible light: Introducing a photodegradation model and optimization by response surface methodology (RSM). *Materials Chemistry and Physics*, Vol. 258, pp 123912.

Niu, X., Yan, W., Zhao, H. and Yang, J. (2018). Synthesis of Nb doped TiO_2 nanotube/reduced graphene oxide heterostructure photocatalyst with high visible light photocatalytic activity. *Applied Surface Science*, Vol. 440, pp 804-813.

Orge, C. A., Soares, O. S. G., Faria, J. L. and Pereira, M. F. R. (2017). Synthesis of TiO_2-Carbon Nanotubes through ball-milling method for

mineralization of oxamic acid (OMA) by photocatalytic ozonation. *Journal of environmental chemical engineering*, Vol. 5, No. 6, pp 5599-5607.

Orooji, Y., Mohassel, R., Amiri, O., Sobhani, A. and Salavati-Niasari, M. (2020). Gd_2ZnMnO_6/ZnO nanocomposites: green sol-gel auto-combustion synthesis, characterization and photocatalytic degradation of different dye pollutants in water. *Journal of Alloys and Compounds*, Vol. 835, pp 155240.

Orooji, Y., Tanhaei, B., Ayati, A., Tabrizi, S. H., Alizadeh, M., Bamoharram, F. F. and Karimi-Maleh, H. (2021). Heterogeneous UV-Switchable Au nanoparticles decorated tungstophosphoric acid/TiO_2 for efficient photocatalytic degradation process. *Chemosphere*, Vol. 281, pp 130795.

Oros-Ruiz, S., Gomez, R., Lopez, R., Hernandez-Gordillo, A., Pedraza-Avella, J. A., Moctezuma, E. and Perez, E. (2012). Photocatalytic reduction of methyl orange on Au/TiO_2 semiconductors. *Catalysis Communications*, Vol. 21, pp 72-76.

Oturan, M. A. and Aaron, J. J. (2014). Advanced oxidation processes in water/wastewater treatment: Principles and applications. A review. *Critical Reviews in Environmental Science and Technology*, Vol. 44, No. 23, pp 2577-2641.

Panda, D. and Manickam, S. (2017). Recent advancements in the sono-photocatalysis (SPC) and doped-sonophotocatalysis (DSPC) for the treatment of recalcitrant hazardous organic water pollutants. *Ultrasonics sonochemistry*, Vol. 36, pp 481-496.

Panwar, K., Jassal, M. and Agrawal, A. K. (2016). TiO_2–SiO_2 Janus particles with highly enhanced photocatalytic activity. *RSC advances*, Vol. 6, No. 95, pp 92754-92764.

Park, Y. K., Kim, B. J., Jeong, S., Jeon, K. J., Chung, K. H. and Jung, S. C. (2020). Characteristics of hydrogen production by photocatalytic water splitting using liquid phase plasma over Ag-doped TiO_2 photocatalysts. *Environmental Research*, Vol. 188, pp 109630.

Patidar, R. and Srivastava, V. C. (2021). Mechanistic and kinetic insights of synergistic mineralization of ofloxacin using a sono-photo hybrid process. *Chemical Engineering Journal*, Vol. 403, pp 125736.

Poyatos, J. M., Munio, M. M., Almecija, M. C., Torres, J. C., Hontoria, E. and Osorio, F., (2010). Advanced Oxidation Processes for Wastewater

Treatment: State of the Art‖. *Water Air Soil Pollut*, Vol. 205, pp 187-204.

Punzi, M., Mattiasson, B. and Jonstrup, M. (2012). Treatment of synthetic textile wastewater by homogeneous and heterogeneous photo-Fenton oxidation. *Journal of Photochemistry and Photobiology A: Chemistry*, Vol. 248, pp 30-35.

Qian, X., Wu, Y., Kan, M., Fang, M., Yue, D., Zeng, J. and Zhao, Y. (2018). FeOOH quantum dots coupled g-C_3N_4 for visible light driving photo-Fenton degradation of organic pollutants. *Applied Catalysis B: Environmental*, Vol. 237, pp 513-520.

Qiu, S., Yin, Z., Chen, J., Chen, L. and Cao, S. (2018). A facile synthesis of hollow TiO_2 photocatalyst with high amount of carbon exhibiting efficient visible-light photocatalytic performance. *Journal of the Chinese Advanced Materials Society*, Vol. 6, No. 1, pp 81-90.

Quinones, D. H., Alvarez, P. M., Rey, A. and Beltran, F. J. (2015). Removal of emerging contaminants from municipal WWTP secondary effluents by solar photocatalytic ozonation. A pilot-scale study. *Separation and Purification Technology*, Vol. 149, pp 132-139.

Raja, A., Son, N. and Kang, M. (2021). Construction of visible-light driven Bi_2MoO_6-rGO-TiO_2 photocatalyst for effective ofloxacin degradation. *Environmental Research*, Vol. 199, pp 111261.

Ren, L., Zhou, W., Sun, B., Li, H., Qiao, P., Xu, Y. and Fu, H. (2019). Defects-engineering of magnetic γ-Fe_2O_3 ultrathin nanosheets/mesoporous black TiO2 hollow sphere heterojunctions for efficient charge separation and the solar-driven photocatalytic mechanism of tetracycline degradation. *Applied Catalysis B: Environmental*, Vol. 240, pp 319-328.

Rey, A., Garcia-Munoz, P., Hernandez-Alonso, M. D., Mena, E., Garcia-Rodriguez, S., Beltran, F. J. (2014). WO_3–TiO_2 based catalysts for the simulated solar radiation assisted photocatalytic ozonation of emerging contaminants in a municipal wastewater treatment plant effluent. *Appl. Catal. B Environ.*, Vol. 154-155, pp 274-284.

Rivero, M. J., Ribao, P., Gomez-Ruiz, B., Urtiaga, A. and Ortiz, I. (2020). Comparative performance of TiO_2-rGO photocatalyst in the degradation of dichloroacetic and perfluorooctanoic acids. *Separ. Purif. Technol.*, Vol. 240, pp 116637.

Sahu, K., Singh, J., Satpati, B. and Mohapatra, S. (2018). Facile synthesis of ZnO nanoplates and nanoparticle aggregates for highly efficient

photocatalytic degradation of organic dyes. *Journal of Physics and Chemistry of Solids*, Vol. 121, pp 186-195.

Selvamani, P. S., Vijaya, J. J., Kennedy, L. J., Mustafa, A., Bououdina, M., Sophia, P. J. and Ramalingam, R. J. (2021). Synergic effect of Cu_2O/MoS_2/rGO for the sonophotocatalytic degradation of tetracycline and ciprofloxacin antibiotics. *Ceramics International*, Vol. 47, No. 3, pp 4226-4237.

Sharmila, V. G., Kumar, S. A., Banu, J. R., Yeom, I. T. and Saratale, G. D. (2019). Feasibility analysis of homogenizer coupled solar photo Fenton process for waste activated sludge reduction. *Journal of environmental management*, Vol. 238, pp 251-256.

Shi, Y., Zhang, Q., Liu, Y., Chang, J. and Guo, J. (2019). Preparation of amphiphilic TiO_2 Janus particles with highly enhanced photocatalytic activity. *Chin. J. Catal.*, Vol. 40, pp 786-794.

Solis, R. R., Rivas, F. J., Martinez-Piernas, A. and Aguera, A. (2016). Ozonation, photocatalysis and photocatalytic ozonation of diuron. Intermediates identification. *Chemical Engineering Journal*, Vol. 292, pp 72-81.

Strong, P. J. and Burgess, J. E. (2008). Treatment methods for wine-related and distillery wastewaters: A review. *Bioremediation journal*, Vol. 12, No. 2, pp 70-87.

Sun, H., He, Q., She, P., Zeng, S., Xu, K., Li, J. and Liu, Z. (2017). One-pot synthesis of $Au@TiO_2$ yolk-shell nanoparticles with enhanced photocatalytic activity under visible light. *Journal of colloid and interface science*, Vol. 505, pp 884-891.

Sun, Y., Lin, H., Wang, C., Wu, Q., Wang, X. and Yang, M. (2018). Morphology-controlled synthesis of TiO_2/MoS_2 nanocomposites with enhanced visible-light photocatalytic activity. *Inorganic Chemistry Frontiers*, Vol. 5, No. 1, pp 145-152.

Tian, J., Leng, Y., Zhao, Z., Xia, Y., Sang, Y., Hao, P., Zhan, J., Li, M. and Liu, H. (2015). Carbon quantum dots/hydrogenated TiO_2 nanobelt heterostructures and their broad spectrum photocatalytic properties under UV, visible, and near-infrared irradiation. *Nano Energy*, Vol. 11, pp 419-427.

Tian, J., Sang, Y., Zhao, Z., Zhou, W., Wang, D., Kang, X., Liu, H., Wang, J., Chen, S. and Cai, H. (2013). Enhanced photocatalytic performances of CeO_2/TiO_2 nanobelt heterostructures. *Small* Vol. 9, pp 3864-3872.

Tiwari, D., Lee, S. M. and Kim, D. J. (2022). Photocatalytic degradation of amoxicillin and tetracycline by template synthesized nano-structured Ce^{3+}@ TiO_2 thin film catalyst. *Environmental Research*, Vol. 210, pp 112914.

Torres, R. A., Nieto, J. I., Combet, E., Petrier, C. and Pulgarin, C. (2008). Influence of TiO_2 concentration on the synergistic effect between photocatalysis and high-frequency ultrasound for organic pollutant mineralization in water. *Applied Catalysis B: Environmental*, Vol. 80, No. 1-2, pp 168-175.

Vaiano, V., Matarangolo, M., Sacco, O. and Sannino, D. (2017). Photocatalytic treatment of aqueous solutions at high dye concentration using praseodymium-doped ZnO catalysts. *Applied Catalysis B: Environmental*, Vol. 209, pp 621-630.

Villegas, L. G. C., Mashhadi, N., Chen, M., Mukherjee, D., Taylor, K. E. and Biswas, N. (2016). A short review of techniques for phenol removal from wastewater. *J Current Pollution Reports*, Vol. 2, No. 3, pp 157-167.

Wang, B. B., Cao, M. H., Tan, Z. J., Wang, L. L., Yuan, S. H., Chen, J. (2010). Photochemical decomposition of perfluorodecanoic acid in aqueous solution with VUV light irradiation. *J. Hazard Mater.*, Vol. 181, pp 187-192.

Xiao, J., Xie, Y. and Cao, H. (2015). Organic pollutants removal in wastewater by heterogeneous photocatalytic ozonation. *Chemosphere*, Vol. 121, pp 1-17.

Yin, J., Liao, G., Zhu, D., Lu, P. and Li, L. (2016). Photocatalytic ozonation of oxalic acid by g-C_3N_4/graphene composites under simulated solar irradiation. *Journal of Photochemistry and Photobiology A: Chemistry*, Vol. 315, pp 138-144.

Yu, Y., Wen, W., Qian, X. Y., Liu, J. B. and Wu, J. M. (2017). UV and visible light photocatalytic activity of Au/TiO_2 nanoforests with Anatase/Rutile phase junctions and controlled Au locations. *Scientific reports*, Vol. 7, No. 1, pp 41253.

Zango, Z. U., Jumbri, K., Sambudi, N. S., Ramli, A., Bakar, N. H. H. A., Saad, B., Rozaini, M. N. H., Isiyaka, H. A., Jagaba, A. H., Aldaghri, O. and Sulieman, A. (2020). A critical review on metal-organic frameworks and their composites as advanced materials for adsorption and photocatalytic degradation of emerging organic pollutants from wastewater. *Polymers*, Vol. 12, pp 1-42.

Zhang, Y., Zhang, N., Wang, T., Huang, H., Chen, Y., Li, Z. and Zou, Z. (2019). Heterogeneous degradation of organic contaminants in the photo-Fenton reaction employing pure cubic β-Fe_2O_3. *Applied Catalysis B: Environmental*, Vol. 245, pp 410-419.

Zhao, J., Ji, M., Di, J., Zhang, Y., He, M., Li, H. and Xia, J. (2020). Novel Z-scheme heterogeneous photo-Fenton-like g-C_3N_4/FeOCl for the pollutants degradation under visible light irradiation. *Journal of Photochemistry and Photobiology A: Chemistry*, Vol. 391, pp 112343.

Zhou, L., Lei, J., Wang, L., Liu, Y. and Zhang, J. (2018). Highly efficient photo-Fenton degradation of methyl orange facilitated by slow light effect and hierarchical porous structure of Fe_2O_3-SiO_2 photonic crystals. *Applied Catalysis B: Environmental*, Vol. 237, pp 1160-1167.

Zhu, D. and Zhou, Q. (2019). Action and mechanism of semiconductor photocatalysis on degradation of organic pollutants in water treatment: a review. *Environ. Nanotechnol. Monit. Manag.*, Vol. 12, pp 100255.

Ziarati, A., Badiei, A. and Luque, R. (2018). Black hollow TiO_2 nanocubes: advanced nanoarchitectures for efficient visible light photocatalytic applications. *Appl. Catal. B Environ.*, Vol. 238, pp 177-183.

CHAPTER 9

ULTRASOUND EXTRACTION in FOOD INDUSTRY

Assoc. Prof. Cem BALTACIOĞLU[1*], Betül TEMİZSOY

[1] *Niğde Ömer Halisdemir University, Engineering Faulty, Food Engineering Department, Niğde, Türkiye.cembaltacioglu@ohu..edu.tr https://orcid.org/0000-0001-8308-5991

1 INTRODUCTION

Extraction is generally the process of selectively separating a compound from a mixture using a solvent. Extraction processes are applied in two different ways as liquid-liquid and solid-liquid extraction processes. Solid-liquid extraction is the process of taking the components in a solid matrix into a solvent in contact with the matrix. Solid-liquid extraction methods used in recent years include microwave-assisted extraction, supercritical fluid extraction, pressurized liquid extraction, emphasized electric field assisted extraction, enzyme assisted extraction and include ultrasonically assisted extraction (Tomaz et al., 2019; Cheetangdee, 2019).

The extraction process generally involves the extraction of the target components in the solid or liquid phase from the solvent. phase extraction. Liquid-liquid and solid-liquid extraction There are two different application methods (Aguilera, 2003). Solid-liquid extraction; solid a mass in which the components contained in the solid are taken into the solvent in contact with the solid transfer process. To extract the desired solute component from the solid phase or a solid is brought into contact with a liquid phase to remove an unwanted component. Solute

components diffuse from the solid to the liquid phase, resulting in the components initially present in the solid they separate. In this event, diffusion coefficients, changes in the boundary layer and Many factors such as concentration gradient play a role (Corrales et al., 2009). The extraction process consists of three basic steps. In the first step, the selected the extraction solvent penetrates into the solid matrix and the components dissolves. The dissolved components are then transported out of the solid matrix. Last but not least in this stage, the extracted components are separated from the solvent phase (Tomaz et al., 2019). In the extraction process, extraction temperature, extraction time, solvent type and Factors such as solvent/solid ratio are parameters that affect extraction efficiency. This parameters, as well as the particle size of the material to be extracted, the extraction affects the yield. The surface area is increased by size reduction and thus the extraction efficiency can be increased by shortening the diffusion pathway. However, particle reducing the size too much may cause blockages in the equipment and/or undesirable components are also extracted, leading to a decrease in yield (Bosiljkov et al., 2017).

1.1 Extraction

The first step in the quantitative and qualitative analysis of components in foods is the extraction process. Extraction is the process of taking the components in the solid or liquid phase into the liquid phase with the help of different solubility properties. Extraction is one of the processes widely used in food engineering to separate a compound from a mixture with a suitable solvent. Extraction is the basic process step both in the recovery of food components and in obtaining some food products (sugar, fat, protein), and in particular, the isolation of some desired products (antioxidants and flavorings), as well as the removal of some contaminants and undesirable components (for example, alkaloids, cholesterol, etc.). is used to remove from food (Tizia, 2003). It is often appropriate to use a liquid for a separation process. The extraction process, which is encountered in various forms in many branches of the industry, is generally the process of separating a solid or liquid component from other solid or liquid components using a suitable solvent.

In extraction, one of the phases can be solid and the other liquid, and both phases can be liquid. According to these situations, liquid-liquid and solid-liquid extractions can be mentioned, respectively. Both extractions are of great importance in the chemical industry.

1.1.1 Liquid-Liquid Extraction

The method of removing one or more components in a liquid solution from the solution by bringing this solution into contact with a suitable solvent is called liquid liquid extraction. By simply making use of the density difference of two liquids that do not mix with each other, the principle of the denser liquid coming to the bottom and the less dense liquid to the top is applied in the separation funnel.

Although liquid liquid extraction is not as widely used as distillation, this process has important applications. It has gained great importance especially in the petroleum industry, and it has been started to be used in the refining of these lubricants to improve the viscosity characteristics of lubricants. It is also used in the extraction of vegetable oils using furfurol as a solvent (Banchero and Badger, 1986). In the separation of aconitic acid from cane molasses (Azzam and Radwan, 1986), in the recovery of tartaric acid (Faizal and Smagghe, 1991) and malic acid (Duarte et al., 1989) from wine factory wastewater, in the recovery of acetic acid from vinegar using high-

boiling solvents (Tatlı et al. ., 1987) utilizing liquid liquid extraction. The products obtained from liquid liquid extraction are mostly separated again by distillation or evaporation (Treybal, 1980). Examples of the use of classical solvent extraction in the food industry are given in Table 1 (Llyod and Wyk, 2011).

Table 1. Usage areas of classical solvent extraction in food field

SOLVENT	FEED	PRODUCT	COMPONENT
Water	Malted barley	Fermented barley	Sugar, grain solution
Acidic water	Citrus peel	Pectin	Pectin
Alkaline water	Fat-free soy flour	Soy protein	
Ethanol	Black carrot	Betalain	Betalain
Methylene chloride	Green coffee beans	Decaffeinated coffee	Caffeine
hexane	Soy	Soy oil	
Methyl ethyl ketone	Spices	Spice oleoracins	
Tributyl phosphate	Phosphoric acid	Food grade phosphoric acid	

1.1.2 Solid-Liquid Extraction

By treating the ground solid sample with a liquid solvent, the solid matrix is transferred to the liquid solvent. In solid and liquid extraction, which is based on the principle of obtaining one or a part of the components of a solid substance using a suitable solvent, the yield is affected by factors such as solvent type, pH, solid-liquid ratios, particle size, temperature, and time (İlbay, 2016).

The main stages of solid-liquid extraction are as follows:

- Entry of the solvent into the solid matrix
- Dissolution or decomposition of components
- Transfer of dissolved components out of the solid matrix
- Passage of the extracted soluble components from the outer surface of the solid matrix into the solution

- Movement of extract relative to solid
- Separation of extract and solid (Aguilera, 2003).

Solid-liquid extraction is one of the methods used for many years in the extraction of antioxidants and phenolic substances from products. Two of these studies are summarized below.

Alberti et al. (2014) carried out an optimization study of phenolic extraction from apples using the response surface method. In the study, BoxBenhken experimental design was used, time (10-20 minutes), temperature (10-40˚C) and solvent concentration (70-99.9% methanol and 50-80% acetone) were chosen as independent variables. They looked at total phenolic substance, total flavonoid and antioxidant capacity (with DPPH and FRAP methods). The optimum extraction conditions were determined as 15 minutes with 84.5% methanol at 28 ˚C and 20 minutes with 65% acetone at 10 ˚C. In most of the extractions carried out with acetone, more bioactive components could be extracted, thus higher antioxidant capacity was determined.

Vazquez et al. (2012) carried out an optimization study of antioxidant extraction from chestnut seed shell by response surface method. Two solvents, ethanol and methanol, were chosen as solvents. Temperature (25-75˚C), time (30-120 minutes) and solvent concentration (50-90%) were chosen as independent variables in the study, which was carried out using a 33 factorial design. Extraction yield, total phenolic substance, antioxidant activity (with FRAP, DPPH, ABTS methods) and average molecular weights were examined. They found that temperature and solvent concentrations had an effect on all measurements, but the effect of time was negligible. Optimum extraction conditions were determined as 50% ethanol at 75˚C for 30 minutes in experiments where methanol was used as a solvent and 50% methanol concentration was carried out for 75 minutes at 75˚C and ethanol was used as solvent. In these conditions, 18.95% yield was obtained in the extractions performed with methanol, and the total amount of phenolic substance was determined as 36.32 g GAE/100 g extract. In the extractions carried out with ethanol under optimum conditions, a yield of 17.95% was obtained, and the total amount of phenolic substance was found to be 26.11 g GAE / 100 g extract.

1.1.3 Classical Extraction Methods

It has negative aspects such as long extraction times, large amount of solvent requirement, low extraction selectivity, high cost and necessity of evaporation of large amounts of solvent. For this reason, the development of green and modern extraction methods has been increasing in recent years in order to obtain biomolecules effectively and to bring all the negative aspects of classical methods into a positive shape.

In the researches, generally methanol, acetone, ethanol, hexane, water or mixtures of these solvents in different ratios and classical extraction methods; distillation, holding, crushing, maceration, boiling, mixing, extraction under pressure methods are generally used in research. (Jayasinghe et al., 2003; Diaz-Maroto et al., 2004; Chiang et al., 2005; Lee et al., 2005; Cruz-Vega et al. 2009; Kwee and Niemeyer, 2011; El-Beshbishy and Bahashwan, 2012; Wongsa et al., 2012; Carro et al., 2013; Benedec et al., 2015; Zlotek et al., 2016).

1.1.4 Modern Extraction Methods

It is a known fact that there has been an increase in the use of these techniques in recent years due to many advantages such as being suitable for automation, low solvent consumption, short extraction time, low sample preparation cost (Wan and Wong, 1996; Eskilsson and Björklund, 2000).

From modern extraction methods, ultrasound assisted extraction, enzyme assisted extraction, microwave assisted extraction, pulsed electric field assisted extraction, supercritical flow extraction and pressurized liquid extraction have been developed as modern extraction methods, some of which are 'green extraction' as they comply with the standards set by the US Environmental Protection Agency. techniques' (EPA, 2017).

The basic properties sought in extraction methods developed today are use of more reliable chemicals, energy efficiency design, use of renewable raw materials, prevention of pollution, shortened extraction time, low cost and prevention of accidents (Wen et al., 2018).

Biomolecules obtained in extraction should be obtained without loss and degradation and without additional purification (Demir, 2015). Extraction of biomolecules from plant materials is of particular interest to the cosmetics, herbal medicine, and food industries (Vinatoru et al., 2017).

1.1.5 Extraction Rate

The dissolution process can be considered within the framework of the general velocity equation. Well;

Dissolution rate = (driving force)/resistance

In this case, the driving force is the difference between the concentration of the exchanged component at the solid material interface and the concentration of the solid material in the solvent liquid.

To obtain a melt from a solid material, the following equation can be written:

$dw/d\theta=K_1 A(y_s-y)$

In the formula:

$dw/d\theta$= dissolution rate

K_1= mass transmission coefficient

A = contact surface area

y = the concentration of the soluble component in the liquid mass

y_s= the concentration of the soluble component at the contact (overlap) surface

2 MODERN EXTRACTION METHODS

Parallel to the development of new technologies, the basic understanding of extraction principles has advanced. This progress has led to new directions in sample preparation. These include microextraction, miniaturization and integration of sampling, separation and quantitation steps used in analytical processes. Therefore In sample preparation, classical extraction techniques have been replaced by techniques such as microwave-assisted extraction, supercritical fluid extraction, pressurized liquid extraction (or accelerated solvent extraction), sonication-assisted liquid extraction. The similarity between these techniques is the possibility of working at high temperature and pressure, which significantly increases the speed of the extraction event (Büyüktuncel, 2012).

Conventional extraction is characterized by long extraction times, high costs, the need for high purity solvents, the necessity to evaporate large quantities of solvents, low extraction selectivity and the thermal

degradation (Chemat, 2017) have led to the development of new extraction techniques (Azmir et al., 2013). Ultrasound-assisted extraction,

enzyme-assisted extraction, microwave-assisted extraction, emphasized electric field assisted extraction, pressurized liquid by supercritical flow extraction extraction methods such as modern extraction methods have been developed and among these techniques some of which have been recognized by the U.S. Environmental Protection Agency 'green techniques' because they comply with set standards (EPA, 2017). Today The basic principles sought in the extraction techniques developed features; use of more reliable chemicals, energy efficiency design, renewable raw materials utilization, pollution prevention, shortened extraction time, low cost and reduced risk of accidents prevention (Wen et al, 2018; Şengül et al., 2019).

2.1 Emphatic Electric Field Assisted Extraction

Stressed electric field (VEA) has been recognized as a useful method for improving pressing, drying, extraction and diffusion processes in the last decade (Barsotti and Cheftel, 1998; Angersbach et al., 2000; Vorobiev et al., 2005; Vorobiev and Lebovka, 2006). The basic principle of VEA is to break down the structure of the cell membrane and increase the efficiency of extraction by applying electric pulses to the product placed between a series of electrodes, with durations varying between 1100 μs. In the cell exposed to VEA, molecules accumulate on both sides of the membrane surface according to their charge in the cell based on their dipole properties. Accumulated surface charges increase the transmembrane potential and electromechanical stress. When the transmembrane potential exceeds a critical value of about 1 Volt, repulsion occurs between the charge carrier molecules in the weak areas of the membrane and pores are formed. This situation causes an increase in the severity of permeability (Azmir et al., 2013). Depending on the design of the treatment room, VEA works continuously or intermittently (Puertolas et al., 2010). effectiveness of VEA implementation; The specific energy input varies depending on factors such as the number of highlights, application temperature, and the properties of the material to be extracted (Heinz et al., 2003). With the application of VEA, the membrane structure of the plant material can be broken down and destroyed, thus shortening the extraction time and increasing the mass transfer. Cup et al. (2004) suggest that the VEA process used for betanin extraction from beet roots performs more efficient extraction than processes such as freezing and mechanical pressing. Corralesa et al. (2008) reported that among the many methods used to extract anthocyanins from grape waste (stems, seeds and skins), VEA gave the best

results. Similarly, Delsart et al. (2012) reported that VEA treatment enhanced the extraction of polyphenols and anthocyanins (Figure 1).

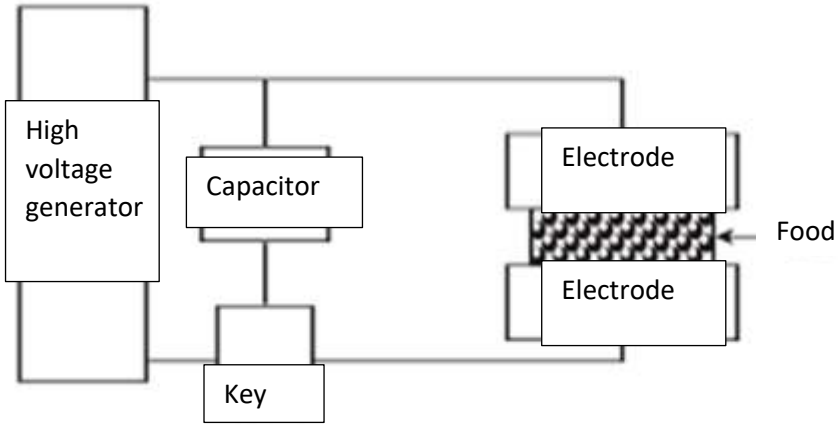

Figure 1. Emphatic Electric Field Assisted Extraction

2.2 Enzyme Assisted Extraction

Some phytochemicals in the plant matrix are dispersed in the cell cytoplasm, and some compounds are retained in the polysaccharide-lignin network by hydrogen bonds or hydrophobic bonds inaccessible to a solvent in a routine extraction process (Azmir et al., 2013). Enzymatic pretreatment is seen as an effective way to release bound compounds or increase yields in general (Rosenthal et al., 1996). The addition of specific enzymes such as cellulase, α-amylase and pectinase during the extraction ensures the degradation of the cell wall and increases the hydrolysis of polysaccharides and lipid components (Rosenthal et al., 1996; Singh et al., 1999). For enzyme assisted extraction; There are two different applications, enzyme-assisted aqueous extraction and enzyme-assisted cold pressing (Latif and Anwar, 2009). Enzyme assisted aqueous extraction has been developed for use in the extraction of oils from various seeds (Hanmoungjai et al., 2001; Rosenthal et al., 1996, 2001; Sharma et al., 2002). In the enzyme-assisted cold pressing system, enzymes are used in the hydrolysis of the cell wall of seeds, since there is no polysaccharide-protein colloid (Concha et al., 2004). Besides the moisture content of the plant (Dominguez et al., 1995); Parameters such as enzyme composition and concentration, particle size of plant material, solid-liquid ratio and hydrolysis time are key factors for enzyme assisted extraction (Niranjan and Hanmoungjai, 2004). Bhattacharjee et al. (2006) characterizes

this extraction method as an ideal alternative for the extraction of bioactive compounds from oilseeds since the enzymes are non-toxic and non-flammable. Since this method uses water as a solvent instead of organic chemicals, it is considered an environmentally friendly technology (Puri et al., 2012). Maier et al. (2008) extracted phenolic acids, non-anthocyanin flavonoids and anthocyanins using a 2:1 mixture of pectinolytic and cellulolytic enzymes from grape pomace and stated that higher yields were obtained compared to sulfide assisted extraction. In a study conducted for the recovery of phenolic antioxidants from raspberry pulp, it was reported that the addition of enzyme to hydro-alcoholic extraction gave better results compared to the non-enzymatic control (Laroze et al., 2010).

2.3 Microwave Assisted Extraction

It is considered as a new method that can be used in the extraction of liquid-soluble components from the material using microwave energy (Figure 2) (Azmir et al., 2013). Microwaves are electromagnetic fields in the range of 300 MHz to 300 GHz. Microwave assisted extraction is basically based on the effect of microwaves on polar molecules (Letellier and Budzinski, 1999). Electromagnetic energy is converted into heat by following the ionic conduction and dipole return mechanisms (Jain, 2009). During ionic conductivity, heat is generated as a result of the resistance of the medium to the flow ion. On the other hand, ions determine their directions according to frequently changing field signs, and the constant change of directives causes intermolecular collisions, resulting in heat production (Azmir et al., 2013). As stated by Alupului (2012), the microwave assisted extraction mechanism includes three consecutive steps. The first step involves the separation of the dissolved components from the active parts of the material matrix by the effect of increasing temperature and pressure. The second and third steps are respectively; diffusion of the solvent through the sample matrix and the release of soluble components from the material matrix to the solvent. The advantages of the system are faster heating, increased extraction efficiency and smaller equipment compared to conventional methods for the extraction of bioactive components from plant material (Cravottoa et al., 2008). In addition, microwave assisted extraction method is described as an environmentally friendly technology as it reduces the use of organic solvents (Alupului, 2012). Pan et al. (2003) stated that in the microwave assisted extraction process they applied for the extraction of polyphenols and caffeine from green tea leaves, they obtained higher yields than other extraction

methods applied in 20 hours at room temperature. Asghari et al. (2011) reported that some bioactive components, including cinnamaldehyde and tannin, from various plants are extracted more quickly and easily by microwave assisted extraction method compared to conventional methods. In a study comparing microwave assisted extraction and ultrasound assisted extraction methods, in the extraction of natural phenolic compounds from lime (*Citrus aurantiifolia*) peels; It has been shown that ultrasound assisted extraction is more effective in obtaining natural antioxidant extracts compared to microwave assisted extraction (Rodsamran and Sothornvit, 2019).

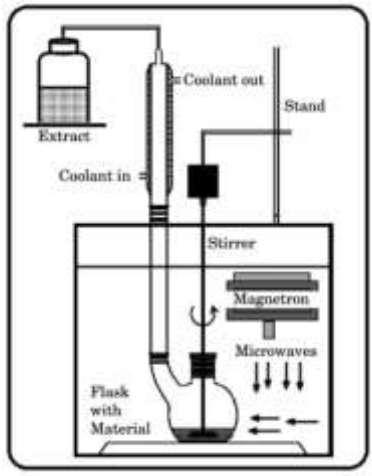

Figure 2. Microwave Assisted Extraction (Shahid et al., 2016)

2.4 Pressurized Liquid Extraction

The method, which was discovered by Richter et al. in 1996, is now known as accelerated liquid extraction, advanced solvent extraction or high-pressure solvent extraction (Nieto et al., 2010). Pressurized liquid extraction is the application of high pressure to keep the solvent well above the boiling point of the solvent (Azmir et al., 2013). The high pressure applied facilitates the extraction (Figure 3). Thanks to the combination of high pressure and temperature, this technique provides a fast extraction as well as requiring a small amount of solvent. While high extraction temperature increases solubility and mass transfer, it provides higher analyte solubility by lowering the viscosities and surface tensions of solvents, thus increasing the extraction efficiency (Ibanez et al., 2012). Compared to the classical soxhlet extraction, the method has been found to significantly reduce the use of solvent and time (Richter et al., 1996). According to Wang and Weller (2006), the pressurized

liquid extraction technique is also used effectively to remove organic pollutants that are stable at high temperatures from environmental matrices. Ibanez et al. (2012) used the pressurized liquid extraction method for the extraction of bioactive components from sea sponges and reported effective results. In addition, the same researchers stated that the method is an environmentally friendly extraction application since the use of organic solvents is quite low. Pressurized liquid extraction is a method that has been successfully applied in the extraction of bioactive components. Extraction of isoflavones from soybean with this method under optimized conditions was carried out without degradation (Rostagno et al., 2004). Shen and Shao (2005) performed the extraction of terpenoids and sterols from tobacco using pressurized liquid extraction as well as soxhlet extraction and ultrasound assisted extraction methods. Researchers reported that pressurized liquid extraction is less effective than ultrasound assisted extraction method, but it can be a good alternative to classical extraction methods, considering yield, reproducibility, extraction time and solvent usage. Contrary to this research; Mroczek and Mazurek (2009) optimized the pressurized liquid extraction conditions for the extraction of lycorine and galanthamine alkaloids and emphasized that the results were more efficient than hot solvent extraction, microwave assisted extraction and ultrasound assisted extraction methods. Luthria (2008) determined that parameters such as temperature, pressure, particle size, time, and sample: solvent ratio are highly effective on pressurized liquid assisted extraction of phenolic compounds from parsley plant.

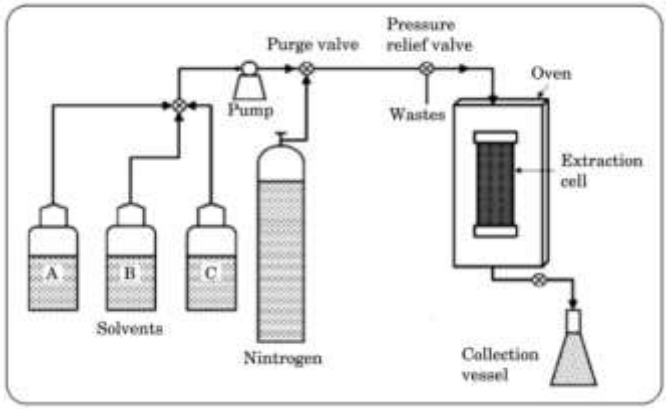

Figure 3. Pressurized Liquid Extraction (Shahid et al., 2016)

2.5 Supercritical Fluid Extraction

Substances in nature exist in the form of solid, liquid or gas. The supercritical state is a distinctive state and can only be achieved by keeping a substance under temperature and pressure above the critical point. The critical point is the point above the characteristic temperature and pressure values and where the distinctive gas and liquid phases of the substance do not exist (Inczedy et al., 1998). Since the specific properties of the gas and/or liquid disappear in the supercritical state, the supercritical fluid can never be liquefied by changing the temperature and pressure (Azmir et al., 2013). Supercritical fluid with gas-like diffusion, viscosity and surface tension properties; It has liquid-like density and dissolving power properties. These properties enable the compounds to be extracted with higher efficiency (Sihvonen et al., 1999). A simple supercritical fluid extraction system that consists of a mobile phase tank, usually CO_2 as a fluid, a pump for pressurizing the gas, auxiliary solvent, solvent vessel and pump, an oven into which the extraction vessel will be placed, a control device for measuring and maintaining the high pressure inside, and a capture unit (Figure 4). Generally, different types of meters such as dry/wet gas meters can be connected to the system (Azmir et al., 2013). Carbon dioxide is the ideal solvent used in supercritical fluid extraction. Although the critical temperature for this solvent is close to room temperature (31°C) and the low critical pressure is 74 bar, the system generally offers the opportunity to operate at moderate pressures between 100-450 bar (Temelli and Güçlü-Üstündag, 2005). The only disadvantage of carbon dioxide is that although it is ideal for non-polar substances such as lipids and oils, it is not suitable for most pharmaceuticals and drug samples due to its low polarity. This negative situation is eliminated by the use of chemical modifiers (Lang and Wai, 2001; Ghafoor et al., 2010). The main variables affecting the yield in the extraction of bioactive components from plants with the help of supercritical fluid; temperature, pressure, particle size, moisture content of the feed material, extraction time, CO_2 flow rate and solvent: sample ratio (Temelli and Güçlü-Üstündag, 2005; Ibanez et al., 2012). Supercritical fluid extraction, which has become popular in the last 10 years, is frequently used for the extraction of active ingredients from materials such as leaves, flowers, seeds, and fruits. Supercritical fluid extraction has many advantages over conventional extraction methods: Since supercritical fluid has a higher diffusion coefficient and lower viscosity and surface tension than other liquid solutions, it penetrates the sample matrix more and significantly reduces the extraction time compared to conventional methods. A complete extraction is achieved by returning the supercritical

fluid back to the sample. In classical extraction methods, separation of the solute from the solvent is a very time-consuming process. In supercritical fluid extraction, the separation process can be shortened easily by lowering the fluid pressure. Since supercritical flow extraction works at room temperature, it is an ideal method for the extraction of temperature sensitive components. Compared to classical extraction methods, it can be studied with less samples. Since a small amount of organic solvent is used, the method can be described as environmentally friendly. Recovery of supercritical fluid is possible and thus waste generation is minimized (Lang and Wai, 2001). The biggest disadvantage of supercritical fluid extraction is the high investment cost of the system as it operates at high pressure above 80 atm. Another disadvantage is that even in CO_2 tubes, which are considered pure, 1-2% of oxygen reacts with components such as antioxidants sensitive to oxidation, causing them to decompose, albeit in a low amount (Cocero et al., 2000). One of the studies using supercritical fluid extraction is on the extraction of caffeine from tea stem and fiber wastes by İçen and Gürü (2010). Researchers reported the maximum caffeine yield as 14.95 mg/g tea stalk waste and 18.92 mg/g tea fiber waste. Kavoura et al. (2019) reported that in the supercritical carbon dioxide extraction of sage (Salvia fruticosa), the pressure applied between 100 bar and 280 bar at 60°C changed the extraction efficiency between 5.2% and 10.3%, and the extraction efficiency increased as the pressure increased.

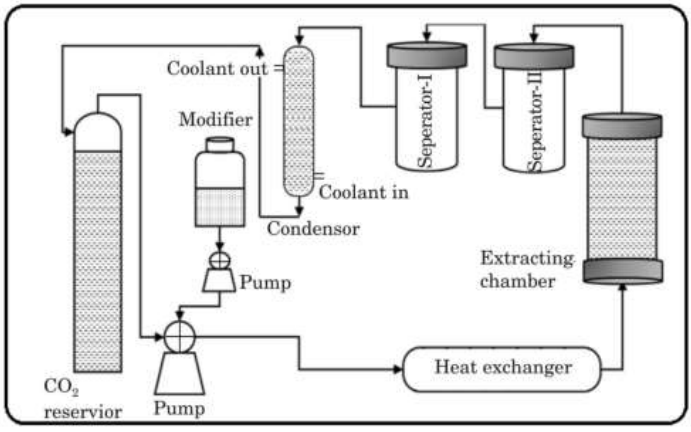

Figure 4. Supercritical Fluid Extraction (Shahid et al., 2016)

3 ULTRASOUND ASSISTED EXTRACTION

Ultrasound assisted extraction method is a method that uses ultrasonic waves, which are mechanical waves propagating in an elastic environment, which provides degradation in the plant cell wall and accelerates mass transfer, enabling the desired biomolecules to be obtained in a shorter time and with higher efficiency compared to classical methods (Figure 5). In addition, it is an environmentally friendly technology with lower energy consumption and less solvent use (Figure 8) (Vilkhu et al., 2008; Jadhav et al., 2009). Ultrasound assisted extraction method, which has gained popularity since 2010, is still frequently used today (Poongothai et al., 2010; Dabre et al., 2011; Marquez-Sillero et al., 2013; Gliszczy´nska-Swiglo et al., 2015; Benkerrou et al., 2018; Kurek et al., 2018).

There is an increasing demand for an alternative technology, ultrasound assisted extraction. Cavitation created by ultrasound facilitates the extraction process by creating physical and chemical changes in raw materials. Since cell walls are destroyed by ultrasound, it is a faster method than other extraction methods.

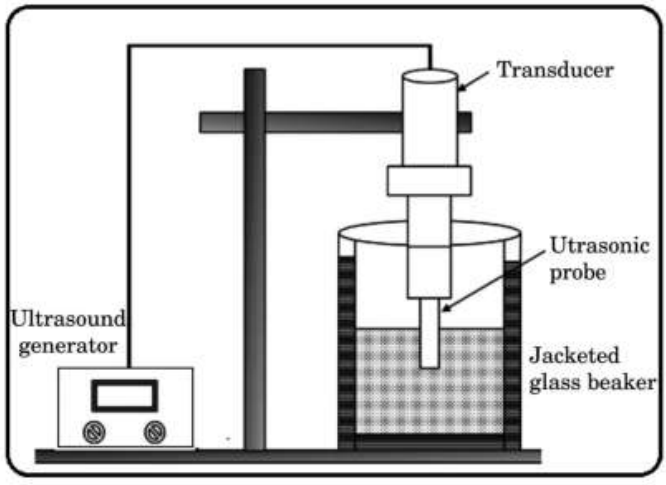

Figure 5. Ultrasound Assisted Extraction (Shahid et al., 2016)

3.1 History of Ultrasound

Ultrasonic waves were first produced in 1881 by the piezoelectric effect obtained by applying an alternating voltage to a certain plane of the sodium potassium tartrate tetrahydrate crystal and generating vibration (Mackersie et al., 2005).

3.2 Ultrasound General Information

The mechanical vibrations of the particles in equilibrium are called sound, and the number of these vibrations per second is called frequency. The unit of sound frequency is Hertz (Hz). Sound waves cannot be transmitted in a vacuum, they need a molecular medium for their transmission. The diffusivity of sound and the compressibility of the medium are inversely proportional to each other. Therefore, sound travels slowest in gases and fastest in solids. Sound vibrations propagate in the medium as waves, as shown in Figure 6.

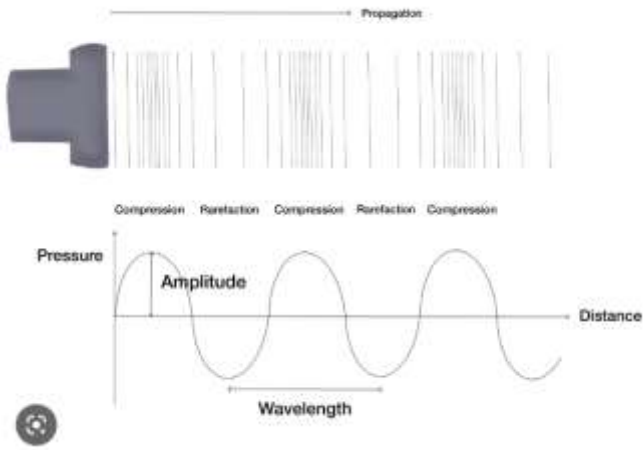

Figure 6. Propagation of Sound Vibrations in the Medium as Waves

UltrasSound is defined as sound waves with frequencies (~ 20 kHz) beyond the range of human hearing (Awad et al., 2012). The human hearing range is determined as 20 Hz-20 kHz, and sounds in the 20 kHz–1 MHz range give the commercially studied ultrasound frequency range (Mason and Lomier, 2002).

Ultrasound is an acoustic energy and is divided into three groups:

- Low Frequency-High Power (20kHz–100 kHz)
- High Frequency-Medium Power (100 kHz-1MHz)
- High Frequency–Low Power (1MHz–10MHz)

Ultrasound creates many effects while passing through a medium. The most important of these effects is cavitation; During the passage of the sound wave through a liquid, the pressure drops and the distance between the

molecules rises above the normal, forming bubbles. These bubbles are gradually enlarged, and when they reach a volume that will become more difficult to oscillate and absorb more energy, they are damped inward. This damping phenomenon is called cavitation (Kantaş, 2007; Uzunoğlu, 2012). Cavitation formation is shown in Figure 7.

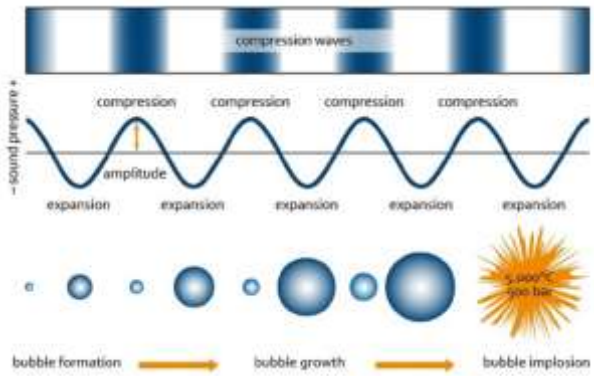

Figure 7. Cavitation Formation

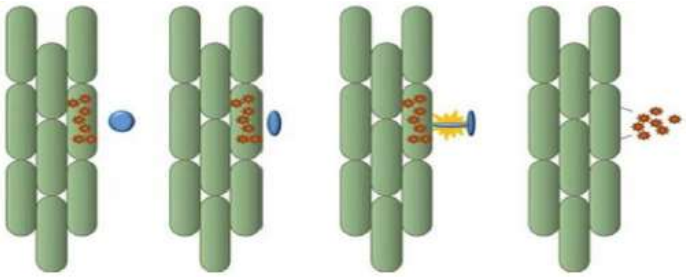

Figure 8. Illustration of the Effect Mechanism of Ultrasound Assisted Extraction

3.3 Equipment Used in Ultrasound Assisted Extraction

Ultrasound affects the samples in two different ways, directly and indirectly, according to different treatment methods (Kek et al., 2013). While the direct effect is seen when the sound wave acts directly on the sample; The indirect effect occurs when the sound wave reaches the containers in the environment before it reaches the sample (Figure 9-12). Ultrasonic probes are devices commonly used in laboratories (Santos et al., 2007). Some studies have shown an increase in mass transfer when the ultrasonic probe is used (Legay et al., 2011). This increase is due to the direct contact of ultrasonic waves with the sample without encountering any obstacles during the

propagation process (Capelo-Martínez, 2009). However, corrosion of the ultrasonic probe as a result of long-term use (Wibetoe et al., 1999) and loss of volatile components in case the system is open are the biggest disadvantages of the system. Apart from the probe system, ultrasonic baths provide an indirect effect of ultrasound on the samples (Santos et al., 2007). A transducer is used as the ultrasonic power source in both the probe ultrasound device and the ultrasonic baths. The piezoelectric transducer is the most widely used type in ultrasonic reactors. Ultrasonic bath is the most known and used type of ultrasonic device. It usually consists of a stainless steel tank with one or more ultrasonic transducers. Ultrasonic baths generally operate at a frequency of around 40 kHz and are equipped with a temperature control mechanism. In addition to being very cheap and easily accessible, they offer the opportunity to work with many samples at the same time. However, when compared with the probe system; The disadvantage of the system is the low ultrasound power sent directly to the sample. The ultrasonic intensity supplied to the system is weakened by the water and the glass materials used in the analysis.

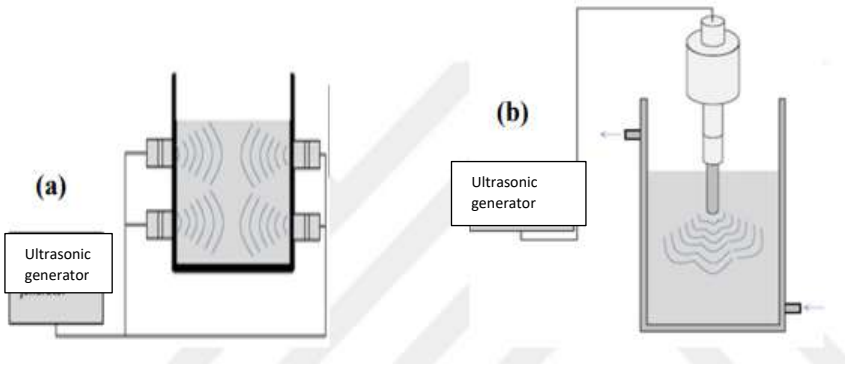

Figure 9. Ultrasonic Bath (a), Ultrasonic Probe (b)

Figure 10. Ultrasonic Bath

Figure 11. Ultrasonic Probe

Recently, new bath systems operating at 25 kHz have been developed for extraction applications, where these disadvantages are limited. These baths consist of a stainless steel reactor equipped with a double-layer mantle that provides temperature control with water circulation through cooling/heating systems. The system is less efficient than the probe ultrasound system, but it is widely used due to the ease of use of the device and the possibility of processing more than one sample at the same time (Chemat et al., 2017). Ultrasonic probes are often preferred systems in small volume extraction applications. The probe system is more powerful than ultrasonic baths because the transmitted ultrasonic intensity is transmitted over a small surface. It generally operates at around 20 kHz and is connected to a probe immersed in the transducer reactor. Thus, direct transmission of ultrasound to the extraction medium is ensured with minimum energy losses. A variety of probes are available with different lengths, diameters, and tip shapes. Probe

selection is made according to the application and sample volume. The ultrasonic intensity transmitted by the probe to the liquid medium causes a rapid temperature rise in the reactor. Cooling of the reactor with a double jacketed cooling system is required for extraction. This is a disadvantage for the probe system (Vinatoru, 2015). In recent years, innovative technologies that combine ultrasonic extraction technique with classical extraction methods such as soxhlet extraction and distillation have been developed rapidly (Chemat et al., 2017).

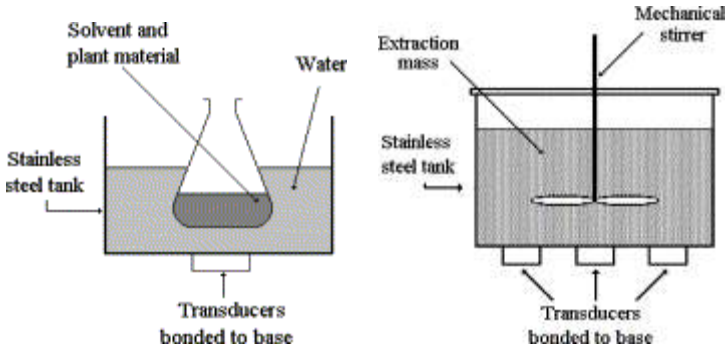

Figure 12. Illustration of Indirect (a) and Direct (b) Ultrasound Applications (Vinatoru, 2001).

3.4 Parameters Affecting Ultrasound Assisted Extraction

Properties of ultrasonic waves such as frequency, wavelength and amplitude affect acoustic cavitation and therefore extraction. In addition to the power input, reactor design and probe shape are among the factors affecting the process (Pingret et al., 2013). The parameters affecting the ultrasound assisted extraction are discussed under two categories as physical parameters and environmental parameters.

3.4.1 Physical Parameters

Since ultrasound application is a mechanical wave, its characteristics such as frequency, wavelength and amplitude affect acoustic cavitation and thus extraction. Besides power, the reactor design and the shape of the probe can also influence the process (Palma et al., 2013). Studies show that high ultrasonic power induces significant changes in the material (depending on the

nature and properties of the medium) by inducing larger shear forces. However, food industry, this parameter is usually used to achieve the best result. is optimized using minimum power for (Bermúdez-Aguirre et al., 2011). General as extraction efficiency in ultrasound-assisted extraction and ultrasound power is increased to improve efficiency, solvent-solid The humidity of food matrices is reduced to increase contact. In these applications, temperature is increased to shorten the extraction time can also be optimized (Dedebaş et al., 2021).

3.4.1.1 Power and temperature

Although the acoustic power energy is not always reported in a process where ultrasound is applied to chemical reactions and processes; There are some physical methods that allow it to be measured directly or indirectly. These methods estimate the increased energy by measuring the physical and chemical changes in the environment following the application of ultrasonic waves. The most commonly used physical methods for measuring acoustic pressure are the aluminum foil method using hydrophones and optical microscopes, and the colorimetric method (Margulis and Margulis, 2003). Indirect measurement of OH radicals formed after the collapse of cavitation bubbles is also a chemical method used (Suslick et al., 2011). Many studies show that high ultrasonic power increases the cutting force and causes large changes in the material. However, in the food industry, this parameter has been optimized to achieve the best results and use minimum power (Bermudez-Aguirre et al., 2011). In general, the highest efficiency in ultrasound assisted extraction is achieved by increasing the ultrasound power, reducing the moisture content of the food to increase the solvent-solid contact and adjusting the temperature to shorten the extraction time (Chemat et al., 2017). The selected ultrasound frequency is also among the factors affecting the extraction process. Frequency affects bubble resonance size. The most commonly used frequency range is between 20 kHz and 100 kHz. The use of higher frequencies in ultrasound assisted extraction has only been studied in a few studies. Toma et al. (2001) reported that other high frequency ranges they applied compared to 20 kHz reduced the physical effects of ultrasound on the structure of Calendula officinale leaves. Interestingly, Chukwumah et al. (2009) reported in a study on peanuts that the extracted phenolic components changed according to the applied frequency, while daidzein and genistein were obtained at 25 kHz, while biochanin A and trans-resveratrol were extracted at 80 kHz. However, it was noted that the

required extraction time was prolonged at 80 kHz frequency. Gonzalez-Centeno et al. (2014) applied 3 different frequencies, 40, 80 and 120 kHz, for the extraction of phenolics from grape pomace and reported that the most effective frequency was 40 kHz. As the frequency of ultrasound increases, the production of cavitation in the liquid and therefore the cavitation density decreases (Mason and Lorimer, 2002). Acoustic cavitation at high frequency is very difficult to achieve. Because the cavitation bubbles need some time to return to their original state during the relaxation cycle, and this time will decrease at high frequency and the cavitation bubbles will not be able to grow sufficiently. The duration of the relaxation phase is inversely proportional to the ultrasonic frequency. Therefore, larger amplitude values are required to generate cavitation at high frequency (Mason and Lorimer, 2002). At low frequencies, the temporary cavitation bubbles are relatively few in number, but the bubble diameters are large and their physical rather than chemical effects are greater (Leong et al., 2011, Mason et al., 2011).

3.4.1.2 Density

Ultrasonic intensity is defined as the energy transmitted per square meter emission surface per second (Tiwari et al., 2015). This parameter is directly related to the transducer amplitude and therefore the pressure amplitude of the sound wave (Santos et al., 2009). Increasing the pressure amplitude increases the severity of bubble collapse. A minimum value of ultrasonic intensity is required to exceed the cavitation threshold. Ultrasound intensity is one of the important factors affecting the extraction efficiency. The increase in density causes an increase in sonochemical effects (Mason and Lorimer, 2002). Increasing the amplitude can increase the intensity of the ultrasound and cause the liquid to mix instead of cavitation, thus causing the ultrasonic transducer to deteriorate rapidly, causing poor ultrasound transmission. However, the amplitude value should be increased when working with high viscosity liquids such as oil (Santos et al., 2009). Wang et al. (2015) determined the ultrasonic intensity value at 20 kHz frequency as 10.18-14.26 W/cm2 in their study on the extraction of pectin by ultrasound assisted extraction. However, Chemat et al. (2017) reported that this intensity value should be optimized because increasing ultrasonic intensity does not mean that the extraction efficiency will increase much. Shape and size of ultrasonic reactors: In case of using ultrasonic bath, since ultrasonic waves are reflected on solid surfaces, the shape of the reaction vessel is very important. For the lowest reflection of waves, the best choice is to work with glass

sample cups with a flat conical bottom (Lorimer and Mason, 1987). The wall thickness of the sample container should be as minimal as possible in order not to weaken the ultrasound transmission (Santos et al., 2009). The position of the transmitter relative to the transducer should be determined in order to calculate the reactor dimensions, achieve maximum efficiency and ensure maximum energy transfer to the environment (Sun et al., 2011). It is observed that the density decreases rapidly both circularly and axially when ultrasonic probes are used. Therefore, a minimum gap should be left between the ultrasonic probe and the vessel wall so that they do not touch each other (Santos et al., 2009). It is thought that the shape and diameter of the probe may have an effect on the extraction if the ultrasonic probe is used in the extraction. Most of the probes are made of titanium alloy due to their resistance to heat and corrosion. However, the use of probes that wear out over time causes the passage of metal parts into the extraction medium. It is thought that the use of pyrex and quartz materials can solve the problem of metal transmission to the environment (Cravottoa et al., 2008).

3.4.2 Environment Related Parameters

Ultrasonic extraction is widely used in food processes is used (Table 2). Environment influences the success of ultrasound-assisted extraction is one of the most important parameters. Ultrasound application solvent to be used is based on the solubility of the target metabolites. vapor pressure, surface tension and vapor pressure of the solvent viscosity is also important. These physical parameters acoustic cavitation and more specifically the cavitation threshold (Mason et al., 2002). Viscosity or surface tension increase, leading to an increase in molecular interactions. significantly increases the cavitation threshold. For example resistance to movement of the ultrasound device with increased viscosity increases when working with samples with high viscosity. It is recommended to work with high power (amplitude) (Capelo-Martinez, 2009). Ultrasound extraction usually uses low solvents with vapor pressure are preferred. Because this aggregation of cavitation bubbles in type solvents, better than solvents with high vapor pressure (Flannigan et al., 2010). Temperature is another parameter affecting solvent properties. While increasing temperature decreases viscosity and surface amplitude, vapor increases the vapor pressure. The higher the vapor pressure, the more causing solvent vapor to enter the cavitation bubble reduces the effects of sonication (Capelo-Martinez, 2009). Generally, increasing the temperature increases the extraction efficiency (Palma et al.,

2013). The absence of gas in the medium causes cavitation bubbles makes it difficult to form, because cavitation bubbles can cause ultrasound consists of gases (vapor) dissolved in the applied liquid (Petrier et al., 2008; Dedebaş et al., 2021).

3.4.2.1 Solvent

In addition to the solubility of the target metabolites, physical parameters such as solvent viscosity, surface tension and vapor pressure have an effect on the extraction efficiency in ultrasound assisted extraction. These physical parameters are effective on acoustic cavitation (Mason and Lorimer, 2002). In order for cavitation to begin in a liquid, the negative pressure in the relaxation cycle must overcome the cohesive forces between the molecules that make up the liquid. An increase in viscosity or surface tension causes an increase in molecular interactions, raising the cavitation threshold significantly. Therefore, the amplitude value should be increased when working with high viscous liquids. Because as the sample viscosity increases, the resistance of the sample against ultrasonic device movement (eg. probe tip) increases. Therefore, high intensity (or high amplitude) is recommended to obtain the necessary mechanical vibrations to result in cavitation. In ultrasound assisted extraction, solvents with low vapor pressure are preferred because the collapse of cavitation bubbles is more intense compared to solvents with high vapor pressure (Santos et al., 2009). The vapor pressure also depends on the temperature of the liquid medium.

3.4.2.2 Temperature

One of the most important factors affecting solvent properties is temperature. While temperature increase causes a decrease in viscosity and surface tension; increases the vapor pressure. The increase in vapor pressure, on the other hand, will cause more solvent vapor to enter the bubbles, resulting in the formation of many bubbles that will collapse with less intensity, and thus the sonication effect will decrease at higher temperatures (Santos et al., 2009). For this reason, low temperatures are preferred, and temperature control is generally used to limit the temperature increase (Salisova et al., 1997). Generally, it is known that the temperature increases up to a certain level increases the extraction efficiency (Palma et al., 2013). It has been reported by some researchers that the temperature increase between 20 and 70°C increases the extraction efficiency when compared to the samples without sonication (Shirsath et al., 2012; Chemat et al., 2017). This

effect causes an increase in the number of cavitation bubbles, a larger solvent-solid contact area, an increase in solvent diffusion, and thus an increase in the outflow and solubility of the desired compounds from the cell. However, it was determined that this effect decreased when the temperature was close to the boiling point of the solvent; most researchers report the beneficial effect of low temperature below 30°C on productivity (Palma and Barroso, 2002, Zhang et al., 2008; Esclapez et al., 2011). It is important to choose the temperature according to the target compound (Zhang et al., 2009). Therefore, temperature control is required to prevent deterioration of temperature sensitive compounds.

3.4.2.3 Presence of dissolved gases and external pressure

The absence of gases in the environment makes it difficult to form cavitation bubbles. Because cavitation bubbles consist of gases dissolved in the liquid (Petrier et al., 2008). The dissolved gases are almost drawn to form new cavitation bubbles in the solvent.

Table 2. The use of ultrasound in food processing (Patist and Bates, 2008).

Applicaiton	Advantage
Extraction	Increasing the efficiency of extraction yield
Emulsification/homogenization	Economical emulsion generation, micro flow with high shear stress
Crystallization	More uniform and small crystal formation, modification of crystals
Filtration	Increasing flow rate, reducing contamination
Separation	Improvement of chemical separation techniques, collection of particles
Defoaming	Reducing the use of defoamer, protecting pipelines
Inactivation (enzyme)	Direct effect on microbial cell membrane by increase in heat transfer, low temperature enzyme inactivation, cavitation
Fermentation	Accelerate fermentation, stimulate living tissue, increase metabolite production, improve substrate transfer
Heat transfer	Ability to work at low temperatures, facilitating heating and drying processes, increasing heat transfer

In general, some pretreatment treatments are used to reduce the initial moisture content, change the texture of the fruit, or reduce the overall drying process time. Ultrasonic application is an alternative way to reduce energy

consumption and drying time. The advantage of using ultrasound is that the process can be performed at ambient temperature and no heating is required.

In the food industry, the use of ultrasound as a pretreatment method is new and there are not many studies on this pretreatment method (Fabiano et al., 2008). The amplitude of the ultrasound wave used, the duration of the application, the composition of the food, the temperature and the volume where the application is made are effective on the effectiveness of the ultrasound application (Vercet et al., 1997).

Today's food industry aims at maximum quality and safety production with minimum energy consumption. Ultrasound application is a technology that is used for different purposes in the food industry and continues its development. It offers advantages such as reducing processing time, reducing operating and maintenance costs, increasing efficiency, quality, and safety (Alexandre et al., 2012; Amirante et al., 2017). Table 3 shows example applications where ultrasound is used in the food industry.

Table 3. Some studies in the literature

Material	**Extracted Substance**	**Used Equipment**	**Results**	**Referance**
Grape	Amino acid	Ultrasonic bath	The extraction application by ultrasonic extraction at 70°C for 6 minutes was compared with the maceration method. Ultrasonic extraction has been shown to provide higher yields.	Carrera vd., 2015
Red rice	Melatonin	Ultrasonic probe	Optimum extraction conditions were determined using 50% methanol at 18.5 °C in 10 minutes, extraction with 2.5:1 solvent-sample ratio. The ultrasonic extraction method proposed in this study is a reliable, inexpensive and simple technique for the determination of melatonin in rice grains. It is clear from	Setyanings-ilh vd., 2016

			the results.	
Pomegranate waste	Antioxidant-rich oil	Ultrasonic probe	Ultrasound assisted extraction was carried out at an ultrasound power of 130 W and a frequency of 20 kHz, and it has been proven that the ultrasound method reduces energy consumption and the amount of solvent, and allows the use of renewable natural products.	Goula vd., 2017
Corn tassel	Flavonoid	Ultrasonic bath	When the extraction is optimized, the most suitable extraction time is 20 minutes, the solid-liquid ratio is 1:20. The ethanol concentration increased by 30%. As a result of extraction with ultrasonic extraction, 467.59 μmol/L flavonoid was obtained.	Zheng vd., 2016

In recent years, there are many studies on the use of ultrasound assisted extraction method in the extraction of bioactive compounds that are important for the food, cosmetic and pharmaceutical industries. Rawson et al. (2011) ultrasonic pretreatment was applied to carrot samples at 20 kHz frequency for 3, 10 minutes and 25°C. Following the application, the preservation of carotenoids was investigated by applying hot air assisted drying and freeze drying. For control purposes, the withering was done at 80°C for 3 minutes with air-assisted drying without applying ultrasonic treatment. As a result of the research, it was found that the samples that were freeze-dried after ultrasonic pretreatment were better in terms of carotenoid preservation (in both 3 and 10 minutes) than the samples that were dried with hot air after ultrasonic pretreatment. Among the freeze-dried samples after ultrasonic pretreatment, the highest carotenoid preservation was achieved in both applications (3, 10 min) at the lowest ultrasonic wave (24.4 μm).

Ma et al. (2009) and Salar Bashi et al. (2012) report that ultrasound assisted extraction is cheaper and easier to apply than modern methods, microwave assisted extraction and supercritical fluid extraction. Ma et al. (2008) and Hossain et al. (2012) reported that antioxidant activity was high in phenolic-rich extracts obtained by ultrasound assisted extraction. The study, in which the ultrasound assisted extraction method used in the extraction of lignans and some phenolic substances from flax seeds decreased mucilage formation and increased the extraction efficiency, also shows that ultrasound application accelerates mass transfer (Corbin et al., 2015). Hammi et al. (2015) reported the extraction condition providing the best antioxidant activity for Zizyphus lotus fruit as ultrasound assisted extraction at 63°C, 50% ethyl alcohol concentration, 25 minutes, with 67 ml/g solvent/solid material ratio.

Yang et al. (2018), on the other hand, used ultrasound assisted extraction for protein extraction from rice and reported that ultrasound increased yield, product purity and modifying properties. In addition to the bioactive compounds mentioned from plants, ultrasound assisted extraction also contains aroma substances (Caldeira et al., 2004; Xia et al., 2006; Canales et al., 2017; Santos et al., 2019), mineral substances (Santos et al. 2017), and especially natural color substances (Shen et al., 2014; Joaquin-Cruz et al., 2015; Zhang and Wang, 2017; Machado et al., 2017; Pinela et al., 2019) are also widely used in extraction.

4 CONCLUSION

When choosing the technique to be used to extract a desired compound from a product, parameters such as extraction efficiency and reproducibility, ease of the procedure applied, time, cost and safety should all be considered. On the other hand, the increasing economic value of biomolecules and functional foods enriched with these compounds will enable the development of more advanced extraction methods in the future. Ultrasound assisted extraction method, which is widely used in the recovery of bioactive compounds, which is especially important for the food, cosmetic and pharmaceutical industries; It is an application that ensures the degradation of the plant cell wall with the help of ultrasonic waves and accelerates the mass transfer, enabling the desired bioactive components to be obtained in a shorter time and with higher efficiency compared to classical techniques. In addition, it is an environmentally friendly technology with lower energy consumption and less solvent usage. In recent years, besides ultrasound

assisted extraction, effective methods such as enzyme assisted extraction, microwave assisted extraction, accentuated electric field assisted extraction, supercritical flow extraction and pressurized liquid extraction, as well as combinations of these methods with classical extraction methods have been used. Thanks to the 'green extraction techniques', which are supported by the restrictions and regulations brought by national and international organizations within the framework of environmental regulations and are developed more and more each day, new alternative technologies will be developed that use more reliable chemicals with less energy consumption, cost and time can be used in different fields.

ACKNOWLEDGEMENT

I would like to thank Gökhan Can Gökalp for her valuable contributions in this study.

REFERENCES

Aguleira, J. M. (2003). Solid–Liquid Extraction. In: Extraction optimization in food engineering. CRC Press, pp: 35-55.

Alberti, A., Zielinski, A. A. F., Zardo, D. M., Demiate, I. V., Nogueira, A. ve Mafra, L. I. (2014). Optimisation of the extraction of phenolic compounds from apples using response surface methodology. Food Chemistry, 149: 151- 158.

Alexandre, E.M.C., Brandão, T.R.S. ve Silva, C.L.M., 2012. Efficacy of non-thermal technologies and sanitizer solutions on microbial load reduction and quality retention of strawberries. Journal of Food Engineering, 108 (3), 417-426.

Alupului, A., 2012. Microwave Extraction of Active Principles From Medicinal Plants. U.P.B. Science Bulletin, Series B, 74 (2).

Amirante, R., Distaso, E., Tamburrano, P., Paduano, A., Pettinicchio, D. ve Clodoveo, M.L., 2017. Acoustic cavitation by means ultrasounds in the extra virgin olive oil extraction process. Energy Procedia, 126 (201709), 82-90.

Angersbach, A., Heinz, V., Knorr, D., 2000. Effects of Pulsed Electric Fields on Cell Membranes in Real Food Systems. Innovative Food Science and Emerging Technologies,1 (2): 135-149.

Asghari, J., Ondruschka, B., Mazaheritehrani, M., 2011. Extraction of Bioactive Chemical Compounds From the Medicinal Asian Plants by Microwave Irradiation. Journal of Medicinal Plants Research, 5 (4): 495-50.

Awad, T.S., Moharram, H.A., Shaltout, O.E., Asker, D., Youssef, M.M., 2012. Applications of Ultrasound İn Analysis, Processing and Quality Control of Food: A review. Food Research International, 48: 410-427.

Azmir, J., Zaidul, I.S.M., Rahman, M.M., Sharif, K. M., Mohamed, A., Sahena, F., Jahurul, M.H.A., Ghafoor, K., Norulaini, N.A.N., Omar, A.K.M., 2013. Techniques for Extraction of Bioactive Compounds From Plant Materials: A Review. J. Food Eng., 117 (4): 426-436.

Azzam, A.M. ve Radwan, M.H. (1986). Separation Of Aconitic Acid From Molasses By Solvent Extraction, Fette, Seifen, Anstrichmittel, 88, 3, 97-99.

Banchero, J. ve Badger, W.L. (1986). Kimya Mühendisliğine Giriş. Çataltaş, İ. (Çev.), 3. Baskı, İnkilap Kitapevi, İstanbul, 885 s.

Barsotti, L., Cheftel, J.C., 1998. Traitement Des Aliments Par Champs Electriques Pulses. Science Des Aliments, 18: 584-601.

Benedec, D., Hanganu D., Oniga I., Tiperciuc B., Olah N. K., Raita, O., Bischin, C., Silaghi-Dumitrescu, R., Laurian, V., 2015. Assessment of rosmarinic acid content in six lamiaceae species extracts and their antioxidant and antimicrobial potential. Pakistan Jaurnal of Pharmaceutical Sciences, 28(6), 2297–2303.

Benkerrou, F., Bey, M.B., Amrane, M., Louaileche, H., 2018. Ultrasonic-Assisted Extraction of Total Phenolic Contents from Phoenix dactylifera and Evaluation of Antioxidant Activity: Statistical Optimization of Extraction Process Parameters. Journal of Food Measurement and Characterization, 12 (3): 1910-1916.

Bermudez-Aguirre, D., Mobbs, T., Barbosa-Cánovas, G., 2011. Ultrasound applications in food processing, In Ultrasound Technologies for Food and Bioprocessing. Feng, H., Barbosa-Canovas, G., Weiss, J. (eds). Springer, New York, USA, pp. 65–105.

Bhattacharjee, P., Singhal, R.S., Tiwari, S.R., 2006. Supercritical Carbon Dioxide Extraction of Cottonseed Oil. Journal of Food Engineering, 79 (3): 892–989.

Bosiljkov, T., Dujmić, F., Bubalo, M. C., Hribar, J., Vidrih, R., Brnčić, M. ve Jokić, S., 2017. Natural deep eutectic solvents and ultrasound-assisted extraction: Green approaches for extraction of wine lees anthocyanins. Food and Bioproducts Processing, 102, 195-203.

Büyüktuncel, E., 2012. Gelişmiş Ekstraksiyon Teknikleri. Hacettepe Üniversitesi Eczacılık Fakültesi Dergisi Cilt 32 / Sayı 2 / Temmuz 2012 / ss. 209-242

Caldeira, I., Pereira, R., Clímaco, M.C., Belchior, A. and Bruno De Sousa, R., 2004. Improved Method for Extraction of Aroma Compounds in Aged Brandies and Aqueous Alcoholic Wood Extracts Using Ultrasound. Analytica Chimica Acta, 513: 125-134.

Canales, R., Guiñez, M., Bazán, C., Reta, M., Cerutti, S., 2017. Determining Heterocyclic Aromatic Amines in Aqueous Samples: A Novel Dispersive Liquid-Liquid Micro-Extraction Method Based on Solidification of Floating Organic Drop and Ultrasound Assisted Back Extraction Followed by UPLC-MS/MS. Talanta, 174: 548-555.

Capelo-Martínez, J.L., 2009. Ultrasound in Chemistry: Analytical Applications, JohnWiley & Sons.

Carrera, C., Ruiz-Rodríguez, A., Palma, M., and Barroso, C.G., 2015, Ultrasound-assisted extraction of amino acids from grapes, Ultrasonics sonochemistry, 22:499-505pp.

Carro, M.D., Lanni, C., Magi, E., 2013. Determination of terpenoids in plant leaves by GC-MS: Development of the method and application to Ocimum basilicum and Nicotiana langsdorfi. Analytical Letters, 46(4), 630–39.

Cheetangdee, N., 2019. Rice Phenolic: Extraction, Characterization and Utilization in Foods. Polyphenols in Plants, Ed: Watson, R.R. Academic Press, Cambridge, 217- 242.

Chemat, F., Rombaut, N., Sicaire, A.G., Meullemiestre, A., Fabiano-Tixier, A.S., AbertVian, M., 2017. Ultrasound Assisted Extraction of Food and Natural Products. Mechanisms, Techniques, Combinations, Protocols and Applications. A review. Ultrasonics Sonochemistry, 34: 540-560.

Chiang, L. C., Cheng P.W., Chiang W., Lin C.C., 2005. Antiviral activities of extracts and selected pure constituents of Ocimum basilicum. Clinical and Experimental Pharmacology and Physiology, 32(10), 811–16.

Chukwumah, Y.C., Walker, L.T., Verghese, M., Ogutu, S., 2009. Effect of Frequency and Duration of Ultrasonication on the Extraction Efficiency of Selected Isoflavones and TransResveratrol From Peanuts (Arachis hypogaea). Ultrasonic Sonochemistry, 16: 293-299.

Cocero, M.J., Gonzalez, S., Perez, S., Alonso, E., 2000. Supercritical Extraction of Unsaturated Products: Degradation of Beta Carotene Supercritical Extraction Processes, Journal of Supercritical Fluids, 19: 39-44.

Concha, J., Soto, C., Chamy, R., Zuniga, M.E., 2004. Enzymatic Pretreatment on Rosehip Oil Extraction: Hydrolysis and Pressing Conditions. Journal of American Oil Chemist's Society, 81 (6): 549-552.

Corbin, C., Fidel, T., Leclerc, E.A., Barakzoy, E., Sagot, N., Falguieres, A., Renouard, S., Blondeau, J.P., Ferroud, C., Doussot, J., Laine, E., Hano, C., 2015. Development and Validation of An Efficient Ultrasound Assisted Extraction of Phenolic Compounds from Flax (Linum usitatissimum L.) Seeds. Ultrasonic Sonochemistry, 26: 176-185.

Corrales, M., García, A.F., Butz, P. ve Tauscher, B., 2009. Extraction of anthocyanins from grape skins assisted by high hydrostatic pressure. Journal of Food Engineering, 90(4), 415-421.

Corralesa, M., Toepflb, S., Butza, P., Knorrc, D., Tauschera, B., 2008. Extraction of Anthocyanins From Grape By-Products Assisted by Ultrasonics, High Hydrostatic Pressure or Pulsed Electric Fields: A

Comparison. Innovative Food Science and Emerging Technologies, 9 (1): 8591.

Cravottoa, G., Boffaa, L., Mantegnaa, S., Peregob, P., Avogadrob, M., Cintasc, P., 2008. Improved Extraction of Vegetable Oils Under HighİntensityUltrasound and/or Microwaves. Ultrasonics Sonochemistry, 15 (5): 898-902.

Cruz-Vega, D., Verge-Star, M., Salinas-Gonzales, N., 2009. Determination of antioxidant and radical scavenging activity of basil (*Ocimum basilicum* L. family lamiaceae) assayed by different methodologies. China Journal of Chinese Materia Medica, 22(4), 557–59.

Dabre, R., Azad, N., Schwämmle, A., Lämmerhofer, M., Lindner, W., 2011. Simultaneous Separation and Analysis of Water-and Fat-Soluble Vitamins on Multi-Modal Reversed-Phase Weak Anion Exchange Material by HPLC-UV. J. Sep. Sci., 34: 761-772.

Dedebaş, T., Capar, T. D., Ekici, L., Yalçın, H., 2021. Yağlı Tohumlarda Ultrasonik-Destekli Ekstraksiyon Yöntemi ve Avantajları. Avrupa Bilim ve Teknoloji Dergisi, (21), 313-322.

Delsart, C., Ghidossi, R., Poupot, C., Cholet, C., Grimi, N., Vorobiev, E., Milisic, V., Peuchot, M.M., 2012. Enhanced Extraction of Phenolic Compounds From Merlot Grapes By Pulsed Electric Field Treatment. American Journal of Enology and Viticulture, 63 (2): 205-211.

Demir, E, Serdar, G., Sökmen, M., 2015. Comparison of Some Extraction Methods for Isolation of Catechins and Caffeine From Turkish Green Tea. International Journal of Secondary Metabolite, 2 (2): 16-25.

Díaz-Maroto, M. C., Paloma, E. S., Castro, L., Gonzales-Vinas, M. L., Perrez-Cello, M., S., 2004. Changes produced in the aroma compounds and structural integrity of basil (*Ocimum basilicum* L.) during drying. Journal of the Science of Food and Agriculture, 84(15), 2070–7

Dominguez, H., Ntiiiez, M.J., Lema, J.M., 1995. Enzyme-Assisted Hexane Extraction of Soybean Oil. Food Chemistry, 54 (2): 223-231.

Duarte, M.M.L., Lozar, J., Malmary, G. ve Molinier, J. (1989). Equilibrium diagrams at 19°C of water-malic acid-2-methyl-1-propanol, watermalic acid-1-propanol, and water-malic acid-3-methyl-1-butanol ternary systems Journal of Chemical & Engineering Data, 34, 1, 43-45.

El-Beshbishy, H.A., Bahashwan, S.A., 2012. Hypoglycemic effect of basil (Ocimum basilicum) aqueous extract is mediated through inhibition

of αglucosidase and α-amylase activities: an in vitro study. Toxicology and Industrial Health, 28(1), 42–50.

EPA, 2017. http://www.epa.gov/greenchemistry/ pubs/about_gc.html. (Erişim Tarihi: 21 Aralık 2017).

Esclapez, M.D., García-Pérez, J.V., Mulet, A., Cárcel, J.A., 2011. Ultrasound-Assisted Extraction of Natural Products, Food Engineering Reviews, 3: 108-120.

Eskilsson, C.S., Björklund, E., 2000. Analytical-scale microwave-assisted extraction. Journal of Chromatography A, 902(1), 227–50.

Fabiano, A.N.F., Francisca, I.P.O. ve Sueli, R., 2008. Use of ultrasound for dehydration of papayas. Food and Bioprocess Technology, 1 (4), 339-345.

Faizal, M. ve Smagghe, F. (1991). Equilibrium diagrams at 20°C of water-tartaric acid-2-methyl-1-proponal, water-tartaric acid-1-propanol, and watertartaric acid-3-methyl-1-butanol ternary systems, Journal of Chemical & Engineering Data, 36, 1, 43-45.

Fincan, M., De Vito, F., Dejmek, P., 2004. Pulsed Electric Field Treatment for Solid– Liquid Extraction of Red Beetroot Pigment. Journal of Food Engineering, 64 (3): 381-388.

Flannigan, D.J., Suslick, K.S., 2010. Inertially confined plasma in an imploding bubble. Nature Physics, 6(8), 598.

Ghafoor, K., Park, J., Choi, Y.H., 2010. Optimization of Supercritical Carbon Dioxide Extraction of Bioactive Compounds From Grape Peel (Vitis labrusca B.) by Using Response Surface Methodology. Innovative Food Science and Emerging Technologies, 11 (3): 485-490.

Gliszczy´nska-Swiglo, A., Rybicka, I., 2015. Simultaneous Determination of Caffeine and Water-Soluble Vitamins ´ In Energy Drinks by HPLC With Photodiode Array and Fluorescence Detection. Food Anal. Methods, 8: 139-146.

Gonzalez-Centeno, M.R., Knoerzer, K., Sabarez, H., Simal, S., Rosselló, C., Femenia, A., 2014. Effect of Acoustic Frequency and Power Density on the Aqueous Ultrasonic-Assisted Extraction of Grape Pomace (Vitis vinifera L.). A Response Surface Approach, Ultrason. Sonochem., 21: 2176-2184.

Goula, A. M., Ververi, M., Adamopoulou, A. and Kaderides, K., 2017, Green ultrasound-assisted extraction of carotenoids from pomegranate wastes using vegetable oils, Ultrasonics Sonochemistry, 34:821–830pp.

Hammi, K.M., Jdey, A., Abdelly, C., Majdoub, H., Ksouri, R., 2015. Optimization of UltrasoundAssisted Extraction of Antioxidant Compounds From Tunisian Zizyphus lotus Fruits Using Response Surface Methodology. Food Chemistry, 184: 80-89.

Hanmoungjai, P., Pyle, D.L., Niranjan, K., 2001. Enzymatic Process for Extracting Oil and Protein From Rice Bran. Journal of The American Oil Chemists Society, 78 (8): 817-821.

Heinz, V., Toepfl, S., Knorr, D., 2003. Impact of Temperature on Lethality and Energy Efficiency of Apple Juice Pasteurization by Pulsed Electric Fields Treatment. Innovative Food Science and Emerging Technologies, 4 (2): 167-175.

Hossain, M.B., Brunton, N.P., Patras, A., Tiwari, B., O'donnell, C.P., Martindiana, A.B., Barry-Ryan, C., 2012. Optimization of Ultrasound Assisted Extraction of Antioxidant Compounds From Marjoram (Origanum majorana L.) Using Response Surface Methodology. Ultrasonic Sonochemistry, 19 (3): 582-590.

Ibanez, E., Herrero, M., Mendiola, J.A., CastroPuyana, M., 2012. Extraction and Characterization of Bioactive Compounds With Health Benefits From Marine Resources: Macro and Micro Algae, Cyanobacteria, and İnvertebrates. In: Hayes, M. (Ed.), Marine Bioactive Compounds: Sources, Characterization and Applications. Springer, pp. 55-98.

Inczedy, J., Lengyel, T., Ure, A.M., 1998. Supercritical Fluid Chromatography and Extraction. Compendium of Analytical Nomenclature (Definitive Rules 1997), Third Ed. Blackwell Science.

İçen, H., Gürü, M., 2010. Effect of Ethanol Content on Supercritical Carbon Dioxide Extraction of Caffeine From Tea Stalk and Fiber Wastes. Journal of Supercritical Fluids, 55 (1): 156-160.

İlbay, Z., 2016. Turunçgil Meyve ve Yapraklarının Farklı Ekstraksiyon Yöntemleriyle Ekstraksiyonu ve Matematik Modellemesi. İstanbul Üniversitesi, Fen Bilimleri Enstitüsü, Kimya Mühendisliği Anabilim Dalı, Temel İşlemler ve Termodinamik Bilim Dalı. Doktora Tezi, 168 s.

Jadhav, D., Rekha, B.N., Parag, R.G., Virendra, K.R., 2009. Extraction of Vanillin From Vanilla Pods: A Comparison Study of Conventional Soxhlet and Ultrasound Assisted Extraction. Journal of Food Engineering, 93: 421-426.

Jain, T., 2009. Microwave Assisted Extraction for Phytoconstituents – An Overview. Asian Journal of Research in Chemistry, 2 (1): 19-25.

Jayasinghe, C., Goto, N., Aoki, T., Wada, S., 2003. Phenolics composition and antioxidant activity of sweet basil (Ocimum basilicum L.). Journal of Agricultural and Food Chemistry, 51(15), 4442–49.

Joaquín-Cruz, E., Dueñas, M., García-Cruz, L., Salinas-Moreno, Y., Santos-Buelga, C., GarcíaSalinas, C., 2015. Anthocyanin and Phenolic Characterization, Chemical Composition and Antioxidant Activity of Chagalapoli (Ardisia compressak) Fruit: A Tropical Source of Natural Pigments. Food Research International, 70: 151-157.

Kantaş, Y., 2007. Effect of Ultrasound on Drying Rate of Selected Produce. (Doktora Tezi), Ortadoğu Teknik Üniversitesi, Ankara.

Kavoura, D., Kyriakopoulou, K., Papaefstathiou, G., Spanidi, E., Gardikis, K., Loulia, V., Aligiannis, N., Krokida, M., Magoulasa, K., 2019. Supercritical CO2 extraction of Salvia fruticosa. The Journal of Supercritical Fluids 146: 159-164.

Kek, S., Chin, N., Yusof, Y., 2013. Direct and Indirect Power Ultrasound Assisted PreOsmotictreatments In Convective Drying of Guava Slices. Food Bioprod. Process., 91: 495-506.

Kurek, M.A., Karp, S., Wyrwisz, J., Niu, Y.G., 2018. Physicochemical Properties of Dietary Fibers Extracted From Gluten-Free Sources: Quinoa (Chenopodium quinoa), Amaranth (Amaranthus caudatus) and Millet (Panicum miliaceum). Food Hydrocolloids, 85: 321-330.

Kwee, E.M., Niemeyer, E.D., 2011. Variations in phenolic composition and antioxidant properties among 15 basil (Ocimum basilicum L.) cultivars. Food Chemistry, 128(4),1044–50.

Lang, Q., Wai, C.M., 2001. Supercritical Fluid Extraction in Herbal and Natural Product Studies A Practical Review. Talanta, 53 (4): 771-782.

Laroze, L., Soto, C., Zúñiga, M.E., 2010. Phenolic Antioxidants Extraction From Raspberry Wastes Assisted by-Enzymes. Electronic Journal of Biotechnology, 13 (6): 1-11.

Latif, S., Anwar, F., 2009. Physicochemical Studies of Hemp (Cannabis sativa) Seed Oil Using Enzyme-Assisted Cold-Pressing. European Journal of Lipid Science and Technology, 111 (10): 1042-1048.

Lee, S.J., Umano, K., Shibamoto, T., Lee, K.G., 2005. Identification of volatile components in basil (Ocimum basilicum L.) and Thyme leaves (Thymus vulgaris L.) and their antioxidant properties. Food Chemistry, 91(1), 131– 37.

Legay, M., Gondrexon, N., Le Person, S., Boldo, P., Bontemps, A., 2011. Enhancement of Heat Transfer by Ultrasound: Review and Recent Advances, Int. J. Chem. Eng.

Leong T., Ashokkumar M.S., 2011. Kentish, The Fundamentals of Power Ultrasound: A Review, Acoust. Aust., 39: 54-63.

Letellier, M., Budzinski, H., 1999. Microwave Assisted Extraction of Organic Compounds. Analusis, 27 (3): 259-270.

Llyod, P. J. Ve Wyk, J. (2011). Introduction to extraction in food prosessing. In: Enhancing Extraction Processes in Food Industry. CRC Press, pp:1-24.

Lorimer, J.P., Mason, T.J., 1987. Sonochemistry. Part 1 – The Physical Aspects. Chem. Soc. Rev. 16: 239-74.

Luthria, D.L., 2008. Influence of Experimental Conditions on the Extraction of Phenolic Compounds From Parsley (Petroselinum crispum) Flakes Using a Pressurized Liquid Extractor. Food Chemistry, 107 (2): 745-752.

Ma, Y. Q., Chen, J. C., Liu, D. H., Ye, X.Q., 2009. Simultaneous Extraction of Phenolic Compounds of Citrus Peel Extracts, Effect of Ultrasound. Ultrasonics Sonochemistry, 16: 57– 62.

Machado, A.P.F, Pereira A., Barbero, G.F., Martínez, J., 2017. Recovery of Anthocyanins From Residues of Rubus fruticosus, Vaccinium myrtillus and Eugenia brasiliensis By Ultrasoundassisted Extraction, Pressurized Liquid Extraction and Their Combination. Food Chemistry, 231: 1-10.

Mackersie, J.W., Timoshkin, I.V., MacGregor, S.J., 2005. Generation of High-Power Ultrasound by Spark Discharges in Water. IEEE Trans. Plasma Sci., 33 (5): 1715-1724.

Maier, T., Göppert, A., Kammerer, D.R., Schieber, A., Carle, R., 2008. Optimization of a Process for Enzyme-Assisted Pigment Extraction From Grape (Vitis vinifera L.) pomace. European Food Research and Technology, 227 (1): 267-275.

Margulis, M.A., Margulis, I.M., 2003. Calorimetric Method for Measurement of Acoustic Power Absorbed in A Volume of A Liquid. Ultrasonic Sonochemistry, 10: 343-345.

Márquez-Sillero, I., Cárdenas, S., Valcárcel, M., 2013. Determination of Water-Soluble Vitamins in Infant Milk and Dietary Supplement Using a Liquid Chromatography On-Line Coupled to A Corona-Charged Aerosol Detector. J. Chromatogr. A, 1313: 253-258.

Mason, T.J., Cobley, A.J., Graves, J.E., Morgan, D., 2011. New Evidence for the Inverse Dependence of Mechanical and Chemical Effects on the Frequency of Ultrasound, Ultrasonic Sonochemistry, 18: 226-230.

Mason, T.J., Lorimer, J.P., 2002. General principles, In Applied Sonochemistry: Uses of Power Ultrasound in Chemistry and Processing, Mason, T.J., Lorimer J.P. (eds), Wiley-Vch Verlag, Germany, pp. 25-74.

Mroczek, T., Mazurek, J., 2009. Pressurized Liquid Extraction and Anticholinesterase ActivityBased Thin-Layer Chromatography With Bioautography of Amaryllidaceae Alkaloids. Analytica Chimica Acta, 633 (2): 188-196.

Nieto, A., Borrull, F., Pocurull, E., Marcé, R.M., 2010. Pressurized Liquid Extraction: A Useful Technique to Extract Pharmaceuticals and Personal-Care Products From Sewage Sludge. Trac Trends In Analytical Chemistry, 29 (7): 752-764.

Niranjan, K., Hanmoungjai, P., 2004. Enzyme-aided aquous extraction. In Nutritionally Enhanced Edible Oil Processing. Dunford, N.T., Dunford, H.B. (eds), Aocs Publishing.

Palma, M., Barbero, G.F., Pineiro, Z., Liazid, A., Barroso, C.G., Rostagno, M.A., Prado, J.M., Meireles, M.A.A., 2013. Natural Product Extraction: Principles and applications, Chapter 2: Extraction of natural products: principles and fundamental aspects, In: Rostagno, M.A., Prado, J.M. (eds), The Royal Society of Chemistry, UK, pp. 58-88.

Palma, M., Barroso, C.G., 2002. Ultrasound-Assisted Extraction and Determination of Tartaric and Malic Acids From Grapes and Winemaking byProducts. Analytica Chimica Acta, 458: 119-130.

Pan, X., Niu, G., Liu, H., 2003. Microwave-Assisted Extraction of Tea Polyphenols and Tea Caffeine From Green Tea Leaves. Chemical Engineering and Processing, 42 (2): 129-133.

Patist, A. ve Bates, D., 2008. Ultrasonic innovations in the food industry: From the laboratory to commercial production. Inno Food Sci Emerg Techno, 9 (2), 147– 154.

Petrier, C., Gondrexon, N., Boldo, P., 2008. Ultrasons Et Sonochimie, Techniques De L'ingénieur Chimie Verte: Optimisation Des Modes De Séparation. D'activation Et De Synthèse Base Documentaire: Tıb493duo.

Pinela, J., Prieto, M.A., Pereira, E., Jabeur, I., Barreiro, M.F., Barros, L., Ferreira, I.J.F.R., 2019. Optimization of Heat and UltrasoundAssisted Extraction of Anthocyanins from Hibiscus sabdariffa Calyces for Natural Food Colorants. Food Chemistry, 275: 309-321.

Pingret, D., Fabiano-Tixier, A.S., Chemat, F., 2013. Chapter 3: Ultrasound-Assisted Extraction. In natural product extraction: Principles and applications. Rostagno, M.A., Prado, J.M. (eds). The Royal Society of Chemistry, UK, pp. 89-112.

Poongothai, S., Ilavarasan, R., Karrunakaran, C.M., 2010. Simultaneous and Accurate Determination of Vitamins B1, B6, B12 and Alpha-Lipoic Acid in Multivitamin Capsule by Reverse-Phase High Performance Liquid Chromatographic Method. Int. J. Pharm. Pharm. Sci., 2: 133-139.

Puertolas, E., López, N., Saldaña, G., Álvarez, I., Raso, J., 2010. Evaluation of Phenolic Extraction During Fermentation of Red Grapes Treated by A Continuous Pulsed Electric Fields Process at Pilot-Plant Scale. Journal of Food Engineering, 119 (3): 1063-1070.

Puri, M., Sharma, D., Barrow, C.J., 2012. EnzymeAssisted Extraction of Bioactives From Plants. Trends in Biotechnology, 30 (1): 37–44.

Rawson, A., Tiwari, B.K., Tuohy, M.G., O'Donnell, C.P. ve Brunton, N., 2011. Effect of ultrasound and blanching pretreatments on polyacetylene and carotenoids content of hot air and freze dried carrot discs. Ultrasonics Sonochemistry, 18 (5), 1172–1179.

Richter, B.E., Jones, B.A., Ezzell, J.L., Porter, N.L., Avdalovic, N., Pohl, C., 1996. Accelerated Solvent Extraction: A Technology for Sample Preparation. Analytical Chemistry, 68 (6): 10331039.

Rodsamrana, P., Sothornvita, R., 2019. Extraction of Phenolic Compounds from Lime Peel Waste Using Ultrasonicassisted and MicrowaveAssisted Extractions. Food Bioscience, 28: 6673.

Rosenthal, A., Pyle, D.L., Niranjan, K., 1996. Aqueous and Enzymatic Processes for Edible Oil Extraction. Enzyme Microbial Technology, 19 (6): 402-420.

Rosenthal, A., Pyle, D.L., Niranjan, K., Gilmour, S., Trinca, L., 2001. Combined Effect of Operational Variables and Enzyme Activity on Aqueous Enzymatic Extraction of Oil and Protein From Soybean. Enzyme and Microbial Technology, 28 (6):499-509.

Rostagno, M.A., Palma, M., Barroso, C.G., 2004. Pressurized Liquid Extraction of İsoflavones From Soybeans. Analytica Chimica Acta, 522 (2): 169-177.

Salar Bashi, D., Mortazavi, S.A., Rezaei, K., Rajaei, A., Karimkhani, M.M., 2012. Optimization of Ultrasound-Assisted Extraction of Phenolic Compounds From Yarrow (Achillea beibrestinii) by Response Surface Methodology. Food Science and Biotechnology, 21 (4): 1005-1011.

Salisova, M., Toma, S., Mason, T.J., 1997. Comparison of Conventional and Ultrasonically Assisted Extractions of Pharmaceutically Active Compounds From Salvia officinalis, Ultrasonic Sonochemistry, 4: 131-134.

Santos, D.C.M.B., Carvalho, L.S.B., Lima, D.C., Leão, D.J., Teixeira, L.S.G., Gracas, M., 2017. Korndetermination of Micronutrient inerals in Coconut Milk by ICP-OES After UltrasoundAssisted Extraction Procedure. Journal of Food Composition and Analysis, 34(1): 75-80.

Santos, H.M., Capelo, J.L., 2007. Trends in Ultrasonic-Based Equipment for Analytical Sample Treatment. Talanta, 73: 795-802.

Santos, H.M., Lodeiro, C., Capelo-Martínez, J.L., 2009. The Power of Ultrasound, In: CapeloMartínez J. L. (Ed.), Ultrasound in chemistry: Analytical applications, Wiley-Vch Verlag, Germany, pp. 1-16.

Santos, K.A., Gonçalves, J.E., Cardozo-Filho, L., da Silva, E.A., 2019. Pressurized Liquid and Ultrasound-Assisted Extraction of A-Bisabolol from Candeia (Eremanthus erythropappus) Wood. Industrial Crops and Products, 130: 428-435.

Setyaningsih, W., Duros, E., Palma, M. and Barroso, C.G., 2016, Optimization of the ultrasound- assisted extraction of melatonin from red rice (Oryza sativa) grains through a response surface methodology, Applied Acoustics, 103:129-135pp.

Shahid, M., Yusuf, M., Mohammad, F. 2016. Plant Phenolics: A Review on Modern Extraction Techniques Recent Progress in Medicinal Plants: Vol. 41- Analytical and Processing TechniquesPublisher: Studium Press LLC, USA

Sharma, A., Khare, S.K., Gupta, M.N., 2002. EnzymeAssisted Aqueous Extraction of Peanut Oil. Journal of American Oil Chemist's Society, 79 (3): 215-218.

Shen, J., Shao, X., 2005. A Comparison of Accelerated Solvent Extraction, Soxhlet Extraction, and Ultrasonic-Assisted Extraction for Analysis

of Terpenoids and Sterols in Tobacco. Analytical and Bioanalytical Chemistry, 383 (6): 1003-1008.

Shen, Y., Zhang, X., Prinyawiwatkul, W., Xu, Z., 2014. Simultaneous Determination of Red and Yellow Artificial Food Colourants and Carotenoid Pigments in Food Products. Food Chemistry, 157: 553-558

Shirsath, S.R., Sonawane, S.H., Gogate, P.R., 2012. Intensification of Extraction of Natural Products Using Ultrasonic Irradiations-A Review of Current Status. Chemistry of Engineering Process, 53: 10-23.

Sihvonen, M., Järvenpää, E., Hietaniemi, V, Huopalahti, R., 1999. Advances in Supercritical Carbon Dioxide Technologies. Trends in Food Science and Technology, 10 (6-7): 217-222.

Singh, R.K., Sarker, B.C., Kumbhar, B.K., Agrawal, Y.C., Kulshreshtha, M.K., 1999. Response Surface Analysis of Enzyme-Assisted Oil Extraction Factors for Sesame, Groundnut, and Sunflower Seeds. Journal of Food Science and Technology, 36 (6): 511-514.

Sun, Y., Liu, D., Chen, J., Ye, X., Yu, D., 2011. Effects of Different Factors of Ultrasound Treatment on the Extraction Yield of the AllTrans-β-Carotene From Citrus Peels. Ultrasonic Sonochemistry, 18: 243-249.

Suslick, K.S., Eddingsaas, N.C., Flannigan, D.J., Hopkins, S.D., Xu, H., 2011. Extreme Conditions During Multibubble Cavitation: Sonoluminescence As A Spectroscopic Probe. Ultrasonic Sonochemistry, 18: 842-846.

Şengül, M., Topdaş, E.F., 2019. Katı-Sıvı Ekstraksiyonunda Kullanılan Modern Teknikler ve Bu Teknikler Arasında Ultrason Yardımlı Ekstraksiyonun Yeri. Atatürk Üniv. Ziraat Fak. Derg., 50 (2): 201-216.

Temelli, F., Güçlü-Üstündag, Ö., 2005. Supercritical Technologies for Further Processing of Edible Oils. Bailey's Industrial Oil and Fat Products. John Wiley & Sons, Inc.

Tiwari, B.K., 2015. Ultrasound: A Clean, Green Extraction Technology, TrAC Trends in Analytical Chemistry, 71: 100-109.

Tizia, C. and Liadakıs, G.(ed). 2003. Extraction Optimization in Food Engineering. Marcel Dekker Inc. New York, Basel, pp:442.

Toma, M., Vinatoru, M., Paniwnyk, L., Mason, T.J., 2001. Investigation of the Effects of Ultrasound on Vegetal Tissues During Solvent Extraction. Ultrasonic Sonochemistry, 8: 137-142.

Tomaz, I., Hazanic, N., Preiner, D., Stupic, D., Andabaka, Z., Maletic, E., Kontic, J., Asperger D., 2019. Extraction Methods of Polyphenol from Grapes. Extraction Of Grape Polyphenols, Ed: Watson, R.R. Polyphenol in Plants (secondedition), Academicpress, Cambridge, 151-167.

Treybal, R.E. (1980). Mass-Transfer Operations, Third Edition, McGraw-Hill Book Company, New York, 784 p. UK Food Standards Agency. Current EU

Uzunoğlu, T.P., 2012. Yüksek Güçlü Ultrases İşleminin Kısa ve Uzun Ömürlü Ayranın Mikrobiyolojik ve Duyusal Özelliklerine Etkisi. (Y. Lisans Tezi), İstanbul Teknik Üniversitesi, Fen Bilimleri Enstitüsü, İstanbul.

Vazquez, G., Agullo, F., Castro C. G., Freire, M. S., Antorrena, G., Alvarez J. G. (2012). Response surface optimization of antioxidants extraction from chestnut (Castanea sativa) bur. Industrial Crops and Products, 35(1):126-134.

Vercet, A., Lopez, P. ve Burgos, J., 1997. Inactivation of heat resistant lipase and protease from Pseudomonas fluores¬cens by manothermosonication. Journal of Dairy Research, 80 (1), 29-36.

Vilkhu, K., Manasseh, R., Mawson, R., Ashokkumar, M., 2011. Ultrasonic recovery and modification of food ingredients, In Ultrasound Technologies for Food and Bioprocessing. Feng, H., BarbosaCanovas, G., Weiss J. (eds). Springer, New York, USA, s. 345-368.

Vilkhu, K., Mawson, R., Simons, L., Bates, D., 2008. Applications and Opportunities for Ultrasound Assisted Extraction in the Food Industry-A Review. Innovative Food Science Emerging Technology, 9: 161-169.

Vinatoru, M., 2001. An Overview of Ultrasonically Assisted Extraction of Bioactive Principles From Herbs. Ultrasonic Sonochemistry, 8: 303-313.

Vinatoru, M., 2015. Ultrasonically Assisted Extraction (UAE) of Natural Products Some Guidelines for Good Practice and Reporting, Ultrason. Sonochem., 25: 94-95.

Vinatoru, M., Mason, T.J., Calinescu, I., 2017. Ultrasonically Assisted Extraction (UAE) and Microwave Assisted Extraction (MAE) of Functional Compounds From Plant Materials. Trends In Analytical Chemistry, 97: 159-178.

Vorobiev, E., Jemai, A.B., Bouzrara, H., Lebovka, N.I., Bazhal, M.I., 2005. Pulsed Electric Field Assisted Extraction of Juice from Food Plants. In Novel Food Processing Technologies. BarbosaCanovas, G., Tapia, M.S., Cano, M.P. (eds). Crc Press, New York, pp. 105-130.

Vorobiev, E., Lebovka, N.I., 2006. Extraction of ıntercellular components by pulsed electric fields. In: Pulsed Electric Field Technology for the Food Industry. Raso, J., Heinz, V. (eds). Fundamentals and Applications. Springer, New York, pp. 153-194.

Wan, H.B., Wong, M.K., 1996. Minimization of solvent consumption in pesticide residue analysis. Journal of Chromatography A, 754(1–2), 43–47.

Wang, L., Weller, C.L., 2006. Recent Advances in Extraction of Nutraceuticals From Plants. Trends In Food Science & Technology, 17 (6): 300–312.

Wang, W., Ma, X., Xu, Y., Cao, Y., Jiang, Z., Ding, T., Ye, X., Liu, F.X., 2015. Ultrasound Assisted Extraction of Pectin From Grapefruit Peel: Optimization and Comparison with the Conventional Method. Food Chemistry, 178: 106-114.

Wen, C., Zhang, J., Zhang, H., Dzah, C.S., Zandile, M., Duan, Y., Ma, H., Luo, X., 2018. Advances in Ultrasound Assisted Extraction of Bioactive Compounds From Cash Crops. UltrasonicsSonochemistry, 48: 538-549.

Wibetoe, G., Takuwa, D.T., Lund, W., Sawula, G., 1999. Coulter Particle Analysis Used Forstudying the Effect of Sample Treatment in Slurry Sampling Electrothermal Atomicabsorption Spectrometry. Fresenius' J. Anal. Chem., 363: 46-54.

Wongsa, P., Chaiwarit, J., Zamaludien, A., 2012. In vitro screening of phenolic compounds, potential inhibition against α-amylase and α-glucosidase of culinary herbs in Thailand. Food Chemistry, 131(3), 964-71.

Xia, T., Shi, S., Wan, X., 2006. Impact of UltrasonicAssisted Extraction on the Chemical and Sensory Quality of Tea İnfusion. Journal of Food Engineering, 74: 557-560.

Yang, X., Li, Y., Li, S., Oladejo, A.O., Wang, Y., Huang, S., Zhou, C., Ye, X., Ma, H., Duan, Y., 2018. Effects of Ultrasound-Assisted α-Amylase Degradation Treatment With Multiple Modes on the Extraction of Rice Protein. Ultrasonics Sonochemistry, 40: 890-899.

Zhang Q.A., Zhang Z.Q., Yue X.F., Fan X.H., Li T., Chen S.F., 2009. Response Surface Optimization of Ultrasound-Assisted Oil Extraction From Autoclaved Almond Powder. Food Chemistry, 116: 513-518.

Zhang Z.S., Wang L.J., Li, D., Jiao, S.S., Chen, X.D., Mao Z.H., 2008. Ultrasound Assisted Extraction of Oil From Flaxseed. Seperation and Purification Technology, 62: 192-198.

Zhang, Q.A., Wang, T.T., 2017. Effect of Ultrasound Irradiation on the Evolution of Color Properties and Major Phenolic Compounds In Wine During Storage. Food Chemistry, 234: 372-380.

Zheng, L.L., Wen, G., Yuan, M.Y. and Gao, F., 2016, Ultrasound-assisted extraction of total flavonoids from corn silk and their antioxidant activity, Journal of Chemistry, 2016:5p.

Zlotek, U., Szymanowska, U., Karaś, M., Świeca, M., 2016. Antioxidative and antiinflammatory potential of phenolics from purple basil (Ocimum basilicum L.) leaves induced by jasmonic, arachidonic and β-aminobutyric acid elicitation. International Journal of Food Science and Technology, 51(1), 163–70.

CHAPTER 10

FUZZY HD METHOD

Dr. Hasan DİLBAS[1]

[1] Van Yuzuncu Yil University, Engineering Faculty, Civil Engineering Department, Van, Türkiye. hasandilbas@yyu.edu.tr ORCID ID: 0000-0002-3780-8818

INTRODUCTION

Decision-making in consideration of multi-criteria is a crucial task in decision-making theory. In general, problems of multi-criteria decision-making (MCDM) are considered with two different classes according to solution steps, such as discrete and continuous. Here, multi-objective decision making (MODM) methods and multi-attribute decision-making (MADM) methods solve the continuous and discrete problems, respectively, and MADM is focus of the present study. MCDM, however, is generally utilized and discussed in the current papers and MCDM is employed in this study. Discrete MCDM problems generally have the following parts in matrix form (Eq. (1)):

$$D = \begin{array}{c} \\ t_1 \\ \vdots \\ t_n \end{array} \begin{array}{c} \begin{array}{ccc} x_1 & \dots & x_n \end{array} \\ \begin{bmatrix} m_{11} & \cdots & m_{1l} \\ \vdots & \ddots & \vdots \\ m_{k1} & \cdots & m_{kl} \end{bmatrix} \end{array} \quad (1)$$

where, $\{t_1, t_2, \dots, t_n\}$ is the alternatives (stimuli, actions), $\{x_1, x_2, \dots, x_n\}$ is the criterions for decision-making, and m_{kl} is the score of the k^{th} alternative relating to l^{th} criterion. The aim is to define/calculate the best alternative. With the other words, the aim is to select the best overall value. Many methods can be employed to determine the overall value of k^{th} alternative, V_k. Here, if the weight w_l -it is greater than 0 and sum of weights should be 1.00- are assigned to l^{th} criterion, V_k is able to be found as given in Eq. (2):

$$V_k = \sum_{l=1}^{n} w_l \times m_{kl} \quad (2)$$

In the recent past, the weights of the criterions have been determined in many ways subjectively and objectively. Also, some methods have been proposed in the literature. ENTROPY, CILOS and IDOCRIW are some of the weighting methods worked objectively and, however, SWARA, DEMATEL, SIMOS, CRITIC, LBWA and ROC are some of the weighting methods worked subjectively(Bardakçı, Arslan, Sel, Demir, & Haste, 2020). Besides, many studies involving MCDM have been suggested some methods and TOPSIS (Technique for Order of Preference by Similarity to Ideal Solution) (Çakır & Dilbas, 2021; Olson, 2004), AHP (Analytic Hierarchy Process) (Lin & Kou, 2021), ELECTRE (Elimination et choix traduisant la realite) (Liu & Wan, 2019) are some of the proposed methods. Also, for comparison and study purposes, we may refer to these as a MCDM methods such as CODAS, MACBETH, GRA, MABAC, ANP, VIKOR, COPRAS, SWARA, SMAA,

DEMATEL, PROMETHEE, ORESTE, TODIM, ARAS, MOORA, ENTROPI, WASPAS, EDAS (Ersöz & Kabak, 2010; Mi, Tang, Liao, Shen, & Lev, 2019; Rezaei, 2015; Yıldızbaşı et al., 2020).

MCDM methods ease to find the best alternative in consideration of all criterions of alternatives with their advantages and disadvantages. The theory of the MCDM methods usually include complex calculation steps compared to four basic operations (addition, subtraction, multiplication, and division), and the usefulness of the MCDM methods is generally related with the operations of the methods. Thus, preferences are shaped by common simplicity trends, ability of MCDM methods and their advantages/disadvantages.

1. FUZZY HD METHOD

"Fuzzy HD Method" (FHDM) is a new MCDM, proposed and developed inspiring HD Method (HDM) (Dilbas, 2021; Kabirova, Husem, Dilbas, Uysal, & Canpolat, 2022). FHDM includes basic operations with only few steps. In addition, consideration of weights for the criterions of alternatives is optional in FHDM. Thus, FHDM includes two ways to achieve the final score (K value) for the alternatives. The steps of the method, FHDM is detailed below.

1.1. Steps of Fuzzy HD Method

It is considered that m alternatives with m criterions are there. The matrix of alternatives is defined as (Eq. (3)):

$$M = \begin{bmatrix} m_{11} & \cdots & m_{1l} \\ \vdots & \ddots & \vdots \\ m_{k1} & \cdots & m_{kl} \end{bmatrix} \tag{3}$$

where m_{kl} is the l^{th} criterion of k^{th} alternative and M is the score matrix of alternatives.

The ideal alternative with criterions in FHDM and its inclusion in the score matrix M are obligation, and it should be located in the first row of the matrix M. Then, the criterions of the alternatives are divided by the criterions of the ideal alternative in consideration of the criterion types. Accordingly, each criterion is made as relative of the ideal alternative (Eq. (4)):

$$M_d = \begin{bmatrix} m_{11}/m_{11} & \cdots & m_{1l}/m_{1l} \\ \vdots & \ddots & \vdots \\ m_{k1}/m_{11} & \cdots & m_{kl}/m_{1l} \end{bmatrix} = \begin{bmatrix} 1 & \cdots & 1 \\ \vdots & \ddots & \vdots \\ d_{k1} & \cdots & d_{kl} \end{bmatrix} \quad (4)$$

where M_d is the matrix of the relative criterions of the alternatives and d_{kl} is the l^{th} relative criterion of k^{th} alternative. Hence, the relative values are obtained, and are considered in Eq. 5 for the calculation of the Alternative's Score Values (K value):

$$K = \frac{\prod_{i=1}^{n} dx_i}{\prod_{i=1}^{n} dy_i} \qquad \therefore \qquad 0 \leq K \leq 1 \quad (5)$$

here, K is the scores of the alternative's Score Value, dx_i and dy_i is the criterions of the alternative. dx_i and dy_i are affected by the condition/action employed in decision and formed the criterion of the alternative negatively, and positively, with another expression, decreases and increases the criterion value, respectively. It can be stated that the criterions can be thought as dx_i as while the determination/observation/prediction of impact of condition/action paid attention to making decision on criterion is impossible.

1.2. Fuzzy Weighting of Criterions of Alternatives

The weights are able to be ensured to the criterions of the alternatives as given in Eq. 6.:

$$M^* = \begin{matrix} w \\ \vdots \\ w_n \end{matrix} \begin{bmatrix} m_{11} & \cdots & m_{1l} \\ \vdots & \ddots & \vdots \\ m_{k1} & \cdots & m_{kl} \end{bmatrix} = \begin{bmatrix} m_{11}^* & \cdots & m_{1l}^* \\ \vdots & \ddots & \vdots \\ m_{k1}^* & \cdots & m_{kl}^* \end{bmatrix} \quad (6)$$

where M^* is the alternatives' score matrix, and m_{kl} is the l^{th} weighted criterion of k^{th} alternative.

While obtaining the score matrix of M* alternatives, the weights used will be transferred to the HD method as fuzzy. At this point, membership operations in blurring are triangular, trapezoidal, etc. can be introduced to the method. For example, for the triangular membership function (Eq. (7-9)):

$$a = (a_1, a_2, a_3) \quad (7)$$

$$f_a(x) = \begin{cases} \frac{x-a_1}{a_2-a_1} \text{for } a_1 \leq x \leq a_2 \\ \frac{x-a_2}{a_3-a_2} \text{ for } a_3 \leq x \leq a_2 \\ 0 \text{ for } x < a_1 \text{ and } x > a_3 \end{cases} \quad (8)$$

Here, a_i is a rational number, $f_a(x)$ is the triangular membership function and is used for determination of fuzzy weights, X is the independent variable of function $f_a(x)$. The fuzzy values obtained as a result of defining the weight values with membership functions, the values of the weighted alternatives can be found with the help of the vertex method and distance (*D*) calculation (Eq. (9)).

$$D = \sqrt{(\frac{1}{3}(a_1 - b_1)^2 + (a_2 - b_2)^2 + (a_3 - b_3)^2)} \quad (9)$$

1.3. Acceptability Levels for K Values of Alternatives

The Acceptability Levels (ALs) are the classification of the results as excellent, very good, good, acceptable and extreme to ease the making decision. ALs are, in other words, the notations given to the results and forms the verbal meaning of numerical results (K values). ALs are listed below and are the notations resulting from relative evaluation compared to ideal alternative:

- **Acceptable**, for $0.75 \leq K \leq 1.00$
- **Good**, for $0.50 \leq K < 0.75$, the alternative is,
- **Very good**, for $0.25 \leq K < 0.50$, the alternative is
- **Excellent**, for $0 \leq K < 0.25$, the alternative is,
- **Extreme**, for $K > 1.00$. The alternative cannot be used in the decision-making.

By using the results of FHDM, many comparisons can be made. ***First***, FHDM ensures to compare the alternatives in consideration of K values and, ***second*** it eases the selection of the best alternative. The lowest K value shows the best choice, and it is found after only few steps. ***Third***, FHDM eases classification of the alternatives according to the acceptability levels. It can be noted that four divisions of the acceptability levels are firstly proposed for FHDM in the literature according to author's experiences and can be revised

for different conditions. This approach opens a topic in the literature, and it needs improvement with a lot of research.

CONCLUSION

In this chapter, a MCDM (Fuzzy HD Method (FHDM)) developed from HD Method is proposed. The positive and the negative sides of HDM is examined and detailed in the study are concluded as given below:

- FHDM shows a great success with low number calculation steps. Thus, FHDM saves time.
- Alternatives can be classified in consideration of Acceptability Levels (ALs). The levels are formed according to the author experience. However, ALs can be updated for different conditions/applications. This opens a path in the literature.
- FHDM can be applied to the real-world problems with/without weighting process.
- However, if all criterions are accepted as "d_{xi}" for the determination of K value of the alternative due to the rule, weights have no effect on K value of the alternative. This is the disadvantage of FHDM and requires improvement with advanced new calculation step/steps.

REFRENCES

Bardakçı, S., Arslan, R., Sel, A., Demir, G., & Haste, H. (2020). Kriter Ağırlıklandırma Yöntemleri. (H. Bircan, Ed.) (1st ed.). Ankara Turkey: Nobel Akademik Yayıncılık.

Çakır, Ö., & Dilbas, H. (2021). Durability properties of treated recycled aggregate concrete: Effect of optimized ball mill method. Construction and Building Materials, 268, 121776. https://doi.org/10.1016/j.conbuildmat.2020.121776

Dilbas, H. (2021). A New Decision Support System Proposal For Evaluating Concrete Test Results: HD Method. In 2nd International Conference on Access to Recent Advances in Engineering and Digitalization (ARANCONF 2021) (pp. 28–29). Kayseri.

Ersöz, F., & Kabak, M. (2010). Savunma Sanayi Uygulamalarında Çok Kriterli Karar Verme Yöntemlerinin Literatür Araştırması. Savunma Bilimleri Dergisi, 1(9), 97–125. https://doi.org/10.17134/sbd.85950

Kabirova, A., Husem, M., Dilbas, H., Uysal, M., & Canpolat, O. (2022). Metakaolin-Based and Blast Furnace Slag-Activated Geopolymer Cement with Waste Powders. Iranian Journal of Science and Technology, Transactions of Civil Engineering. https://doi.org/10.1007/s40996-022-00954-2

Lin, C., & Kou, G. (2021). A heuristic method to rank the alternatives in the AHP synthesis. Applied Soft Computing, 100, 106916. https://doi.org/10.1016/j.asoc.2020.106916

Liu, X., & Wan, S. (2019). A method to calculate the ranges of criteria weights in ELECTRE I and II methods. Computers & Industrial Engineering, 137, 106067. https://doi.org/10.1016/j.cie.2019.106067

Mi, X., Tang, M., Liao, H., Shen, W., & Lev, B. (2019). The state-of-the-art survey on integrations and applications of the best worst method in decision making: Why, what, what for and what's next? Omega (United Kingdom), 87, 205–225. https://doi.org/10.1016/j.omega.2019.01.009

Olson, D. (2004). Comparison of weights in TOPSIS models. Mathematical and Computer Modelling, 40, 721–727.

Rezaei, J. (2015). Best-worst multi-criteria decision-making method. Omega (United Kingdom), 53, 49–57. https://doi.org/10.1016/j.omega.2014.11.009

Yıldızbaşı, A., Aktaş, A., Çalık, A., Çalış, A. B., Adem, A., Erdebilli, B., … İç, Y. T. (2020). ÇOK KRİTERLİ KARAR VERME YÖNTEMLERİ: MS Excel Çözümlü Uygulamalar. (M. Kabak & Y. Çınar, Eds.) (1st ed.). Ankara Turkey: Nobel Akademik Yayıncılık.

ISBN: 978-625-367-156-3